New confined metal complexes built from hemicryptophane ligands for catalysis in confined space and predictable chirality control at the metal core

Gege Qiu

École Doctorale des Sciences Chimiques (ED250)

L'Institut des Sciences Moléculaires de Marseille (iSm2)

THÈSE DE DOCTORAT

pour obtenir le grade de

DOCTEUR de l'ÉCOLE CENTRALE de MARSEILLE

Discipline : Chimie

Nouveaux complexes métalliques confinés au sein de ligands hémicryptophanes pour la catalyse en milieux confiné et le contrôle de la chiralité autour du centre métallique

Par

Monsieur **Gege QIU**

Directeur de thèse : Pr. MARTINEZ Alexandre

Soutenue le 22 octobre 2020

devant le jury composé de :

M. Sebastien GOEB, *Chargé de recherche CNRS à,l'Université d'Angers*	Rapporteur
M. Matthieu RAYNAL, Chargé de recherche CNRS à *Sorbonne Université*	Rapporteur
Mme Jalila SIMAAN, *Directeur de recherche CNRS à L'Université d'Aix Marseille*	Examinatrice
M. Alexander SOROKIN, *Directeur de recherche CNRS à l'IRCELYON*	Examinateur
M. Cedric COLOMBAN, CNRS à l'*Université Aix Marseille*	Membre invité
Mme Paola NAVA, *Maître de conferences* à l'Université *Aix-Marseille*	Co-directrice de thèse
M. MARTINEZ Alexandre, *Professeur de l' École Centrale de Marseille*	Directeur de thèse

Acknowledgements

First of all, I would like to thank my PhD supervisor Pr. Alexandre Martinez for his supervision and direction. He is so knowledgeable in a wide range of disciplines that I benefit a lot every time when we discussed together. And meanwhile, he is such a nice and patient person. As the director of group, he gets along very well with everyone, but he never behaves like a boss, with whom you have to speak in a very gentle way, so it's always a pleasant talk with him. Despite his strong academic background, he is also a person who works so hard. All of this has impressed and inspired me a lot, that I will appreciate forever.

I would like to thank Dr. Paola NAVA, who is my co-supervisor. At the beginning, I didn't know anything about computational chemistry, but she was very patient and taught me a lot of computational chemistry.

I also have to thank Cedric COLOMBAN. He is very knowledgeable and helpful, and I can always get useful suggestions from him when I encounter some problems in chemistry.He is also a very careful person, who could pick up some minor details, which leaves me very deep impression. Besides, he provided me with some technical support which facilitated my research a lot. He gave me a lot of patient guidance about chemistry and many experimental techniques. I would also like to thank Dr. Bastien Chatelet, an associate professor of Centrale Marseille in our group. He will always explain to you some synthesis problems very tirelessly.

Next, I would like to send my sincere thanks to Dr. Sabine Chevallier-Michaud for Mass; Dr. Roseline Rosas for liquid NMR; Dr. Christophe Chendo and Valérie Monnier for HRMS; Dr. Michel Giorgi for single crystal X-ray diffraction; Dr. Nicolas Vanthuyne and Marion Jean for HPLC.

I would also like to thank jury members of my PhD defense: M. Sebastien GOEB, Chargé de recherche, Université d'Angers ; M. Matthieu RAYNAL, Chargé de recherche, Sorbonne Université ; Mme Jalila SIMAAN, Directeur de recherche, Université Aix-Marseille ， M. Alexander SOROKIN, Directeur de recherche, IRCELYON, for their examination and comments on my PhD work, that I appreciate so much.

I passed three years full of joy in Marseille which is definitely attributed to my friends and colleagues. They helped me so much especially in my life, and I spent very

pleasant time with them. I want to express my sincere gratitude to you from the bottom of my heart: Damien, Hervé, Didier, Laurent, Xiaotong, Magalie, Lingyu, Augustin, Marc, Romain, Chunyang, Donglin, Peng, Xuru……

I would also like to address my gratitude to China Scholarship Council for financial support during my three years of PhD study in Marseille.

In the end, I would like to express my greatest gratitude to my parents and my wife Fangfang for their unconditional love and support, which motivates me forward. No more words could express my gratitude, but I still want to say thank you, I love you!

List of abbreviations

Ac = acetyl

aq = aqueous

Ar = aryle

Bn = benzyl

cat. = catalyst

CTV = cyclotriveratrylene

CuAAC = copper(I)-catalyzed alkyne-azide cycloaddition

d = doublet

DBU = diazabicycloundecene

DCC = dynamic covalent chemistry

DCM = dichloromethane

DFT = density functional theory

DHP = dihydropyranne

DMF = *N*, *N*-dimethylformamide

δ = chemical shift

ECD = electronic circular dichroism

ee = enantiomeric excess

Et = ethyl

ESI = electrospray ionization

h = hour

Hz = hertz

HPLC = High Performance Liquid Chromatography

HRMS = High Resolution Mass Spectroscopy

IR = infrared spectroscopy

J = coupling constant in hertz

m = multiplet

Me = methyl

NMR = Nuclear Magnetic Resonance spectroscopy

Otf = triflate

Ph = phenyl

ppm = parties per million

rt = room temperature

s = singlet

t = triplet

t-Bu = tertbutyl

THF = tetrahydrofuran

THP = tetrahydropyranne

TLC = thin film chromatography

TON = turnover number

TOF = turnover frequency

TPA = tris(2-pyridylmethyl)amine

tren = tris(2-aminoethyl)amine

Table of contents

General Introduction

In the fields of host-guest chemistry and supramolecular catalysis, hemicryptophanes are molecular cages that have attracted an increasing attention over the last years. This organic capsules combine a cyclotriveratrylene (CTV) group and another C_3 symmetrical unit, that could be, for example, a ligand for metal-ions complexation. In this line, hemicryptophane-based complexes have been recently reported as more selective and efficient catalysts compared to they parent models devoid of cavity. This is why we are focusing on the developement of new hemicryptophane-based catalysts.

The main goal of this thesis was to design, prepare and apply new hemicryptophane cages as supramolecular ligand for metal coordination in confined space. In particular, this work aimed at developping new methods to obtain (*i*) enantiopure complexes with controlled helicity, and (*ii*) new confined catalyst with enhanced efficiency and selectivity.

First par of the Chapter I of the thesis consist in an overview of the recent progresses in the synthesis of hemicryptophanes. This chapter also consists in a comprehensive literature review about (*i*) history of the development of such cage compounds, as well as their applications in recognition and catalysis in confined space; and (*ii*) recent examples of control and transfer of chirality within tripodal cages.

The second Chapter describes the study of a novel small molecular hemicryptophane (**1**), which is directly composed of one CTV part and one tris(2-pyridylmethyl)amine (TPA) ligand, connected by three methylene $–CH_2-$ bridges. We explain how chirality transfer in this new hemicryptophane can control the propeller arrangement of the TPA ligand and its corresponding copper-complex. Besides, related computational simulations have been used to study, understand, and explain this transfer of chirality.

In Chapter III we have proposed the design and synthesis of two new hemicryptophane cages built from the TBTA ligand, which is a common ligand for

copper-catalyzed azide alkyne cycloaddition (CuAAC) reaction. We have studied these new TBTA-based hemicryptophane cages as new ligands for CuAAC reactions in confined space aiming at improving the stability and selectivity of the catalyst.

In Chapter IV, new hemicryptophane cages displaying two metal binding-sites in a single cavity have been developed aiming at reproducing the key structure of methane monooxygenases enzymes. This new cage has been studied as ligand for the coordination of Cu^{II} and Zn^{II} metal ions.

Finally, we have designed and synthesized three novel CTV derivatives, which have the potential to form new supramolecular metalla-cages through self-assembly processes (chapter V). Such CTV ligands, substituted by pyridine derivatives, have been sent to the group of Prof. M. Hardie (University of Leeds, UK), to engage the first self-assembly tests. We indeed believe that such CTV-based ligands might be used to build novel self-assembled capsules.

Chapter I: Bibliography

Part I: Synthesis and applications of hemicryptophane organic cages

Part II: Chirality transfer in tripodal supramolecular cages

I.1: Synthesis and applications of hemicryptophane organic cages

I.1.1 Introduction

Molecular cages holding a three-dimensional cavity are attracting considerable attention in modern supramolecular chemistry due to their potential applications in molecular recognition, catalysis, drug delivery, biosensing, separation, and storage. [1-5] Among these different cages, hemicryptophanes, which are combining a cyclotriveratrylene (CTV) unit with another different C_3-symmetrical moiety, have recently received a growing interest. The chemistry of hemicryptophane has been developed quite slowly before 2005.[6] In 1982, Lehn and Collet described the first two members of a new type of molecular cages called speleands (Figure 1.1a), which associated a CTV and a crown ether unit, showing potential recognition properties toward methylammonium cations.[7] However, it was not before 2005 that the first synthesis of an enantiopure hemicryptophane was described by Crassous and Dutasta (Figure 1.1b)[8]

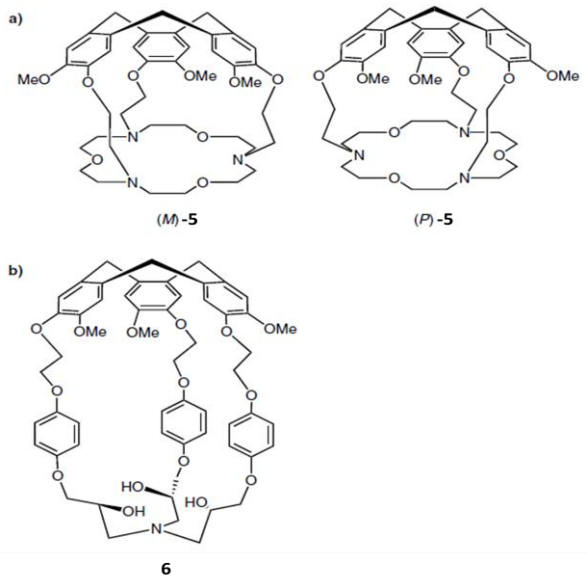

Figure 1.1 (a) Representation of the racemic mixture of the first hemicryptophane **5** reported in 1982; (b) representation of the first enantiopure hemicryptophane **6** reported in 2005.

After 2005, hemicryptophanes have received a growing interest leading to a

blossoming field of research, particularly for molecular recognition. A series of sophisticated enantiopure hemicryptophanes has been synthesized benefiting from the inherent chirality of the CTV unit. These receptors could be interestingly used for stereoselective recognition of chiral guest molecules.[9] An important aspect of hemicryptophanes is indeed their inherent chirality arising from the CTV unit (*M* or *P* configuration), whereas their southern part commonly aims at introducing inner functionalities.

Due to the growing demand for artificial hosts, the preparation of hemicryptophanes could be considered as a significant breakthrough for applications in recognition or catalysis. On this basis, the first part of this chapter will first focus on the different strategies that has been developed to prepare, purify and characterize this emergent class of molecular capsules. We will then turn to the recent examples of their applications in recognition and catalysis in confined space.

I.1.2 Synthesis of hemicryptophanes

There are two main routes for designing and synthesizing hemicryptophanes: (*i*) by connecting the CTV and the other unit with covalent bonds (organic cages) or (*ii*) through a self-assembly process involving metal-ligand linkage (metalla-cage). Altrough self-assembled hemicryptophane capsules are currently attracting some attention due to the developments of self-assembling strategies[10], this section will only focus on the first strategy (covalent cages), as it is the approach developed in the team of A. Martinez. The preparation of covalent hemicryptophanes usually needs multistep synthesis, and often the main drawback of these syntheses is a low to modest overall yield. Covalent hemicryptophanes could be obtained following two main methods: (*i*) by intramolecular macrocyclization reaction (template approach, Figure 1.2a) and (ii) by connecting directly the CTV part and the southern part ([1+1] coupling strategy (Figure 1.2b).

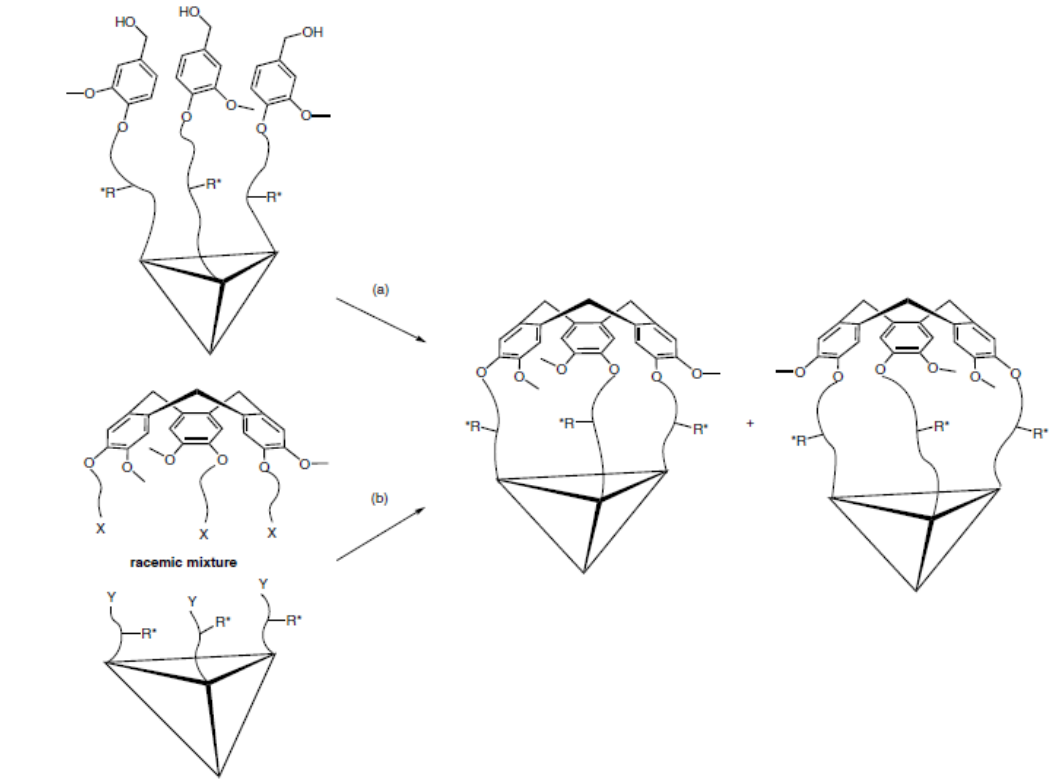

Figure 1.2 Representation of the two different strategies usually used for the synthesis of hemicryptophane hosts: (a) formation of the CTV unit as the final step; (b) [1 + 1] coupling of two parts.

The first way to prepare hemicryptophanes consists in the building the CTV unit at the end of the synthesis by using the "template method" previously reported for the synthesis of cryptophanes.[11] Indeed, the Friedel−Crafts alkylation is a common approach for the synthesis of CTV and therefore cryptophanes and hemicryptophanes. This acid-catalyzed cyclization reaction usually needs Bronsted (HCOOH) or Lewis acid ($Sc(OTf)_3$) catalysts. This intramolecular cyclodehydration closes the hemicryptophane by three final Friedel–Crafts alkylations to generate the CTV at the last step (Figure 1.3I).[12] Yields and difficulty in purification usually depend on the structures of the hemicryptophane precursors.

The second way ([1+1] coupling) is very effective in many cases and is particularly well suited for the preparation of enantiopure hemicryptophanes (starting from enantiopure CTV precursors, Figure 1.3 II). [13] It should be noted that another feasible way to introduce the southern unit to the functionalized CTV scaffold exists. In this way hemicryptophanes are formed by an intramolecular cyclization that

generate the southern part .[14] This approach has been seldom used compared to strategies based on the cage closure reaction at the north part or the [1 + 1] coupling presented above.

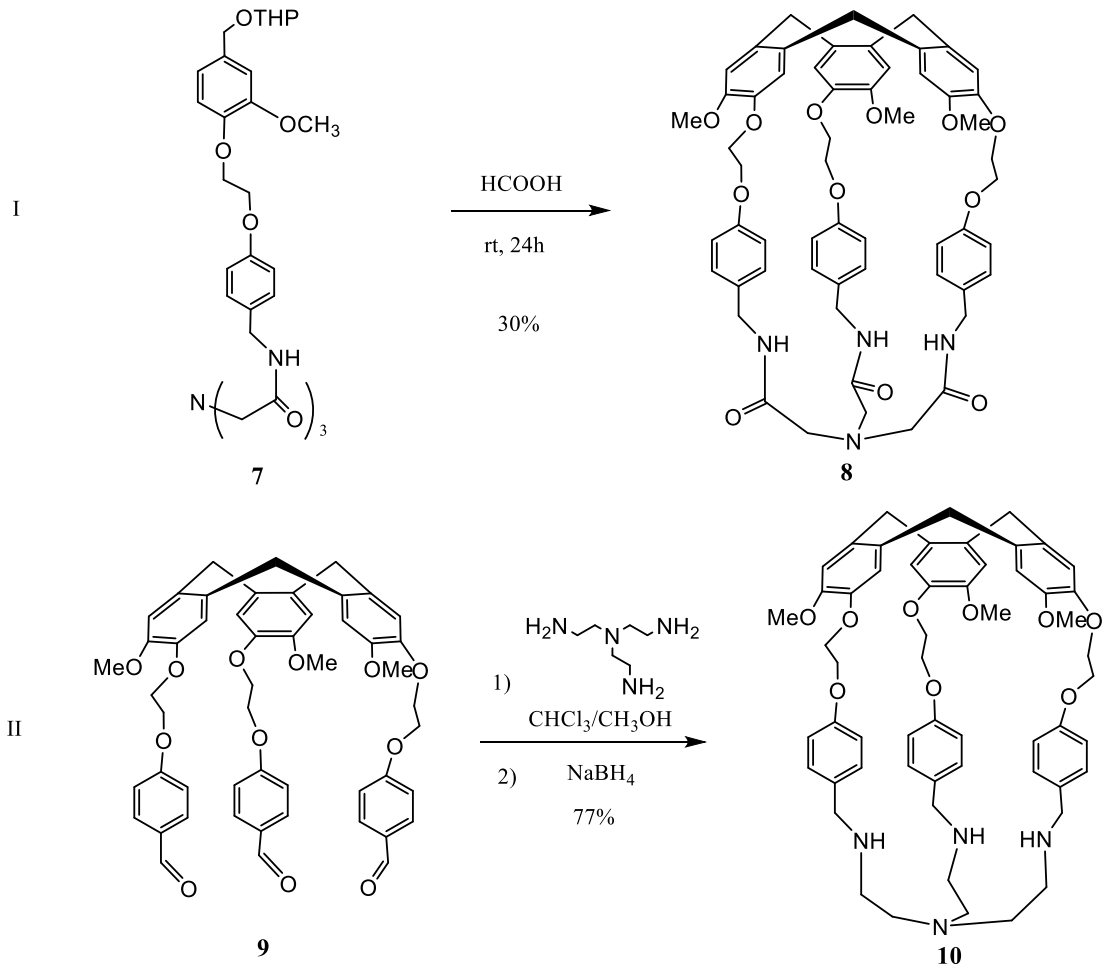

Figure 1.3 (I) formation of the CTV by HCOOH-catalyzed macrocyclization as the last step. (II) [1 + 1] coupling between one aldehyde based CTV part and the tris(2-aminoethyl)amine unit.

I.1.3 Enantiopure hemicryptophanes obtained by means of chiral HPLC resolution

Enantiopure compounds are very important in chemical sciences, especially in the fields of molecular recognition and host-guest systems. Furthermore, chiral molecular receptors are the basis of many biorecognition processes and have important implications for biochemistry or pharmacology. The design, preparation

and purification of synthetic chiral hosts, such as molecular cages, is however a very difficult task. In order to separate two enantiomers of one chiral cage, the chiral semi-preparative high-performance liquid chromatography (HPLC) technique plays an important role for the resolution of racemic mixtures. Using this purification method, enantiopure hemicryptophane cages can be obtained by (*i*) resolution of CTV-based precursors first, or (*ii*) resolution of the final hemicryptophane racemate. In 2010, the first example of the resolution of a racemic mixture of hemicryptophane molecular cages using the chiral semipreparative HPLC purification technique was reported by Martinez, Dutasta and co-workers.[15] Through injections (8.0 mg/mL solutions in $CDCl_3$) of the racemic mixture on a (*S*,*S*) Whelk-O1 chiral column, they successfully separated the two enantiomers of the following cage (*M*-**8** and *P*-**8** in Figure 1.4). The excellent enantiomeric excess values obtained for the *M*- and *P*- enantiomers of **8** (up to 96% and 99%) demonstrate the efficiency of the separation. However, this resolution of hemicryptophane enantiomers only stayed at the hundred of milligram scale, and the efficiency of the chiral HPLC separation is highly sensitive to the structure of the desired capsules. The efficiency of the chiral HPLC-separation could be significantly improved by the initial resolution of a CTV-based precursor racemate followed by its functionalization to form the enantiopure cage. In 2016, Martinez and co-workers have successfully separated 2 grams of each *M*- and *P*-enantiomers of the precursor CTV(CH_2CH_2Br)$_3$ (*M*-**11** and *P*-**11** in Figure 1.4) with an enantiomeric excess >99.5%.

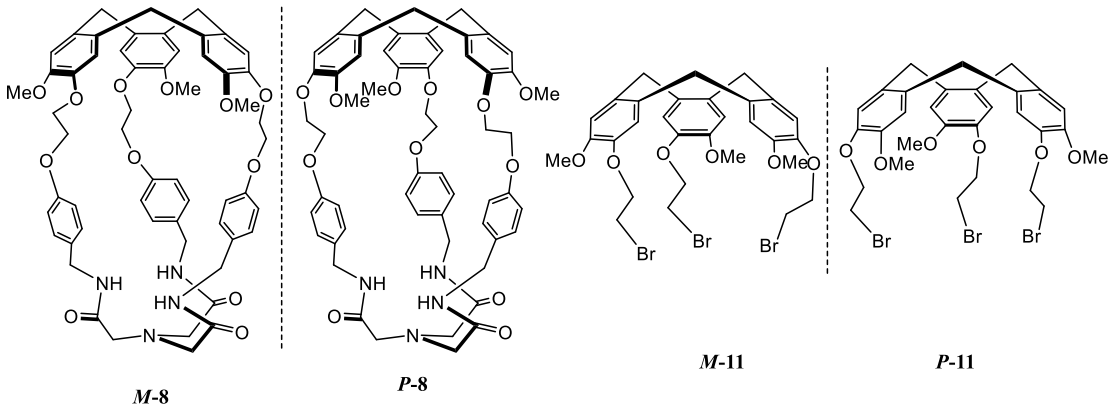

Figure 1.4 Structrures of the enantiopure hemicryptophanes *M*-**8** and *P*-**8** (left) and CTVs *M*-**11** and *P*-**11** (right), obtained by chiral HPLC-resolution.

I.1.4 Host-guest chemistry

Host–guest chemistry is one of the defining concepts of supramolecular chemistry that describes the formation of unique complexes between two or more molecules, via non-covalent interactions. A host molecule has an internal space (the so-called 'cavity') in which another molecule, the guest molecule, can be incorporated. Since Pedersen, Lehn and Cram proposed the concept of host-guest chemistry, it has opened the way to the construction of supramolecular (inclusion) complexes. Several types of host molecules have been reported, including crown ethers, cryptands, spherands, carcerands and cyclodextrins (Figure 1.5). The guest molecule can be incorporated in the cavity of host molecule.

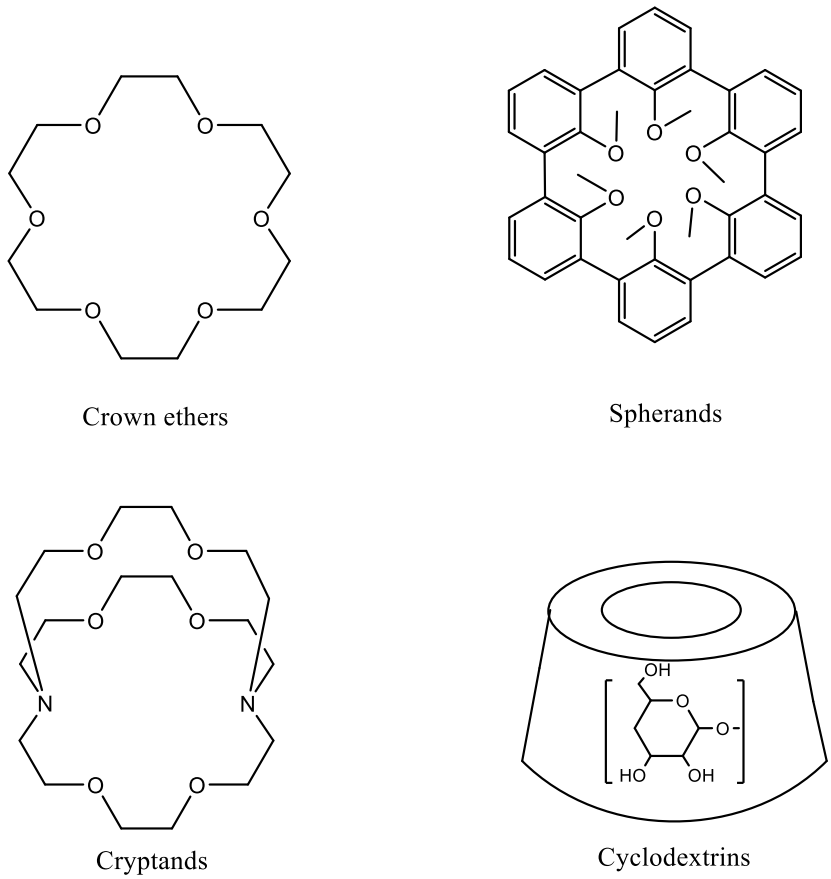

Figure 1.5 Structures of some host molecules.

The hemicryptophanes can work as excellent receptors due to some advantages : (*i*) their rigid CTV scaffolds can provide cavities of variable shape and size, (*ii*) different kind of southern groups that offer special recognition capabilities can be incorporated,

and (*iii*) the chirality of the CTV itself. For examples, hemicryptophanes have shown good complexation properties with ammoniums, ion pairs,[16-21] and fullerenes[22].

Among the possible non-covalent interactions between one hemicryptophane host and a guest, most of them are hydrogen bonds or interactions with charged species (ammonium, ion pairs, zwitterions). For instance, the first hemicryptophane, (**1** in Figure 1.1) can interact strongly with ammonium ions through cation-π interactions with its CTV unit[7]. Hemicryptophanes can also encapsulate ion-pairs. The host–guest interactions between Me_4N^+Cl and cage **8** have been studied using a DFT approach (Figure 1.6a).[23] In 2008, another heteroditopic hemicryptophane cage was reported by Jabin et al.. This host interacts with the anion (chloride ion) and the cation (ammonium ion) simultaneously. [21] Interestingly, hemicryptophanes could also perform partial encapsulations. Makita and cowokers indeed reported in 2016 the partial encapsulation of acetylcholine within a hemicryptophane host : the X-ray structure indicates that the ammonium unit of the acethylcholine (Ach^+) is inside the cavity (due to the cation-π interactions), while the acetyl unit and chloride counterions are outside the cavity (Figure 1.6b).[24] Finally, in 2011, Zhanting Li's group developed a new (CTV)-based capsule that can strongly encapsulate C60 and C70 fullerenes by combining hydrogen bonding[22].

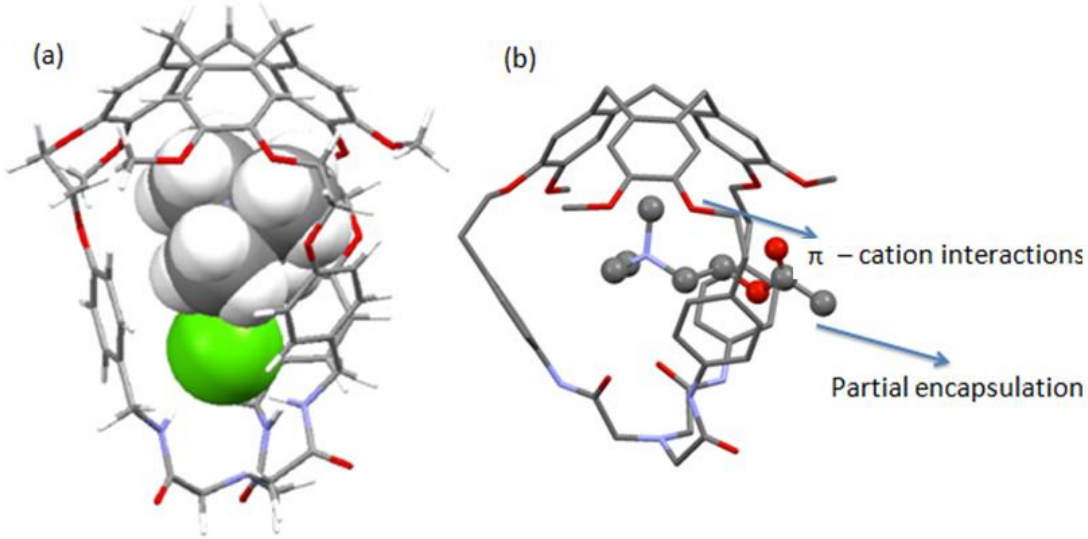

Figure 1.6. Examples of hemicryptophane-based host-guest complexes (a) DFT-optimized structure of Me_4N^+Cl@**8**; (b)X-ray crystal structure of Me_4N^+Cl@**10**

I.1.5 Catalysis in confined space

Catalysis plays an important role in the development of the chemical industry and society. A large number of materials and chemical intermediates are synthesized directly and indirectly with catalysts. In nature, many chemical reaction processes require enzymatic catalysis, usually with the advantages of high efficiency and high selectivity. However, the enzymes are not so easy to mimic, because the structure of enzymes is complicated, and some reactions are performed in specific confined spaces displaying multiple functionalities.

Advances in transition state theory and computer technology have made possible the simulation and understanding of the enzyme's active-sites [25]. In order to mimic the efficient chemistry found in enzymes, the catalysis in confined space aims at reproducing the second coordination sphere of enzymes. In the past decades, metal-organic cages, metal-organic frameworks, organic hosts, and nanoreactors have therefore attracted a growing interest.[26] In the following, some related research examples of homogeneous catalysis in confined spaces, will illustrate the effect of constrained mediums on catalytic selectivity and efficiency. Among the various examples of supramolecular catalysis, we will particularly focus on the examples where catalysis takes place inside the cavity of hemicryptophanes cages.

Inspired by enzymes, chemists have tried to mimic their confined environment through the development of organic architectures, such as cyclodextrins or calixarenes,[27] which contain well-defined cavities. Similarly, the hemicryptophanes show potential to work as ligand for complexing metal ion. Because the hemicryptophane cavity can be modified and adapted to different substrates, selective transformations could be envisioned. In 2009, Martinez and co-workers have shown, for the first time, that hemicryptophane-based transition metal complexes are efficient supramolecular catalysts (Figure 1.7).[28] The diastereomeric hemicryptophane−oxidovanadium(V) complexe **12** successfully oxidized the sulfide substrates to sulfoxide with 10 mol% catalyst and cumene hydroperoxide (CHP) as oxygen source. It was found to be an efficient supramolecular catalyst in the oxidation of thioanisol with yields up to 95%. Comparing with its parent model ligand, devoid of cavity, the hemicryptophane catalyst show higher yield due to the role of

hemicryptophane hydrophobic cavity (protect the metal-active site).

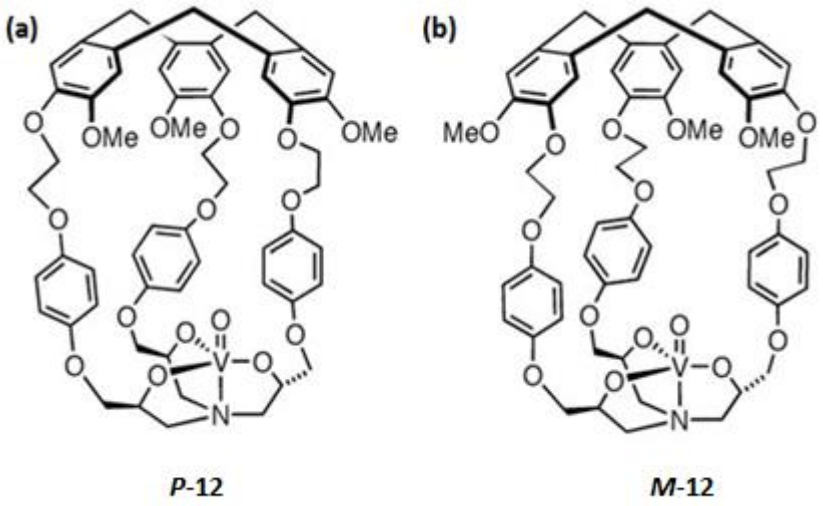

Figure 1.7 Structures of the *P*- (a) and *M*- (b) enantiomers of the hemicryptophane – oxidovanadium(V) complexe **12**.

In 2013, the group of Alexandre Martinez used a Copper-Hemicryptophane (**13**) complex as a catalyst for the oxidation of cycloalkane by H_2O_2 (Figure 1.8).[29] By comparing with the open model complex (Figure 1.8b) and the Cu(II) salt $Cu(ClO_4)_2(H_2O)_6$, the reaction with the Cu(II)-hemicryptophane complex shows better yield (28% and 15%, respectively) demonstrating the great potential of such an approach for the C-H oxidation. The stability of the catalyst is improved by encapsulating the active site in the molecular cavity. Other reasons may be the preferential encapsulation of the alkane substrate in the hydrophobic cavity and the ejection of the first oxidation product (alcohol).

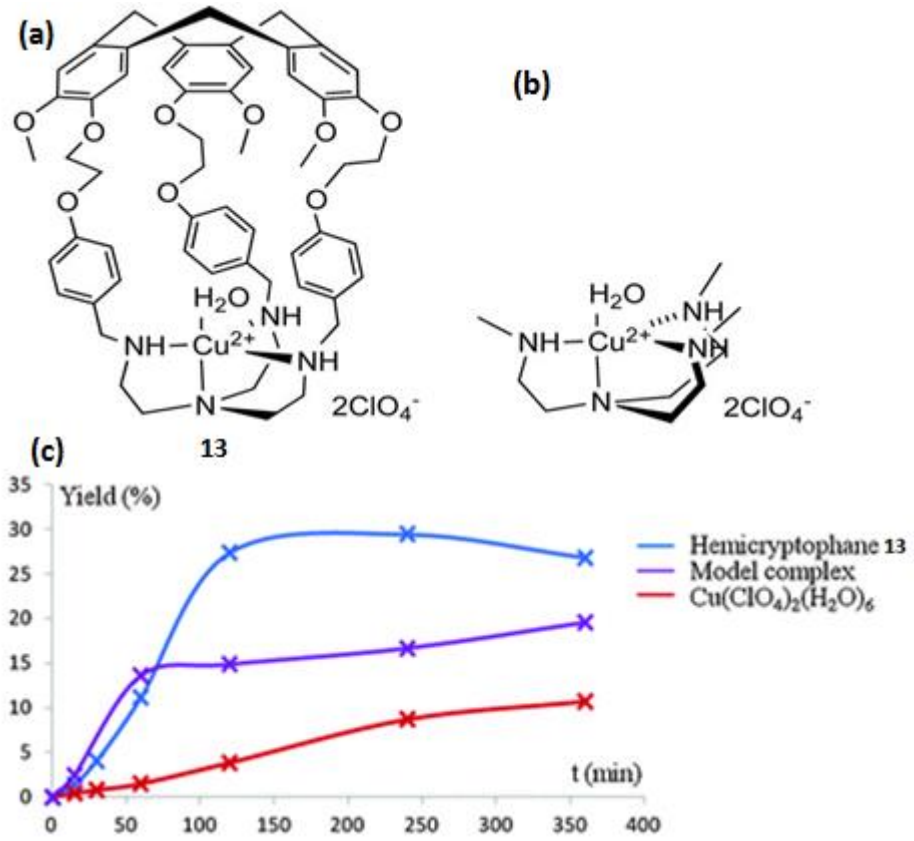

Figure 1.8 Structure of (a) Hemicryptophane-copper(Cu) complexes **13**, and (b) the open model catalyst. (c) GC-monitored oxidation of cyclohexane catalyzed by hemicryptophane-copper(Cu) complexes, the model catalyst, and $Cu(ClO_4)_2(H_2O)_6$.

In addition, the group of Martinez reported a new functionalized cage in 2018, which contains a Verkade's superbase motif and can be used as a tool to create frustrated Lewis pairs.[30] They tested the reaction between *p*-chlorobenzaldehyde and cyclopentenone with the cage **14** and the model Verkade's superbase **15** lacking cavity (Figure 1.9). Performances are improved with the cage system. The cage **14** was more efficient due to confinement of the Verkade's superbase in the cavity of the hemicryptophane host. The key role of the cavity has been highlighted: the acid-base reaction with the Lewis acidic partner ($TiCl_4$) cannot take place due to the confinement of the Verkade's superbase in the cavity of the hemicryptophane host, thus providing an effective system for the reaction.

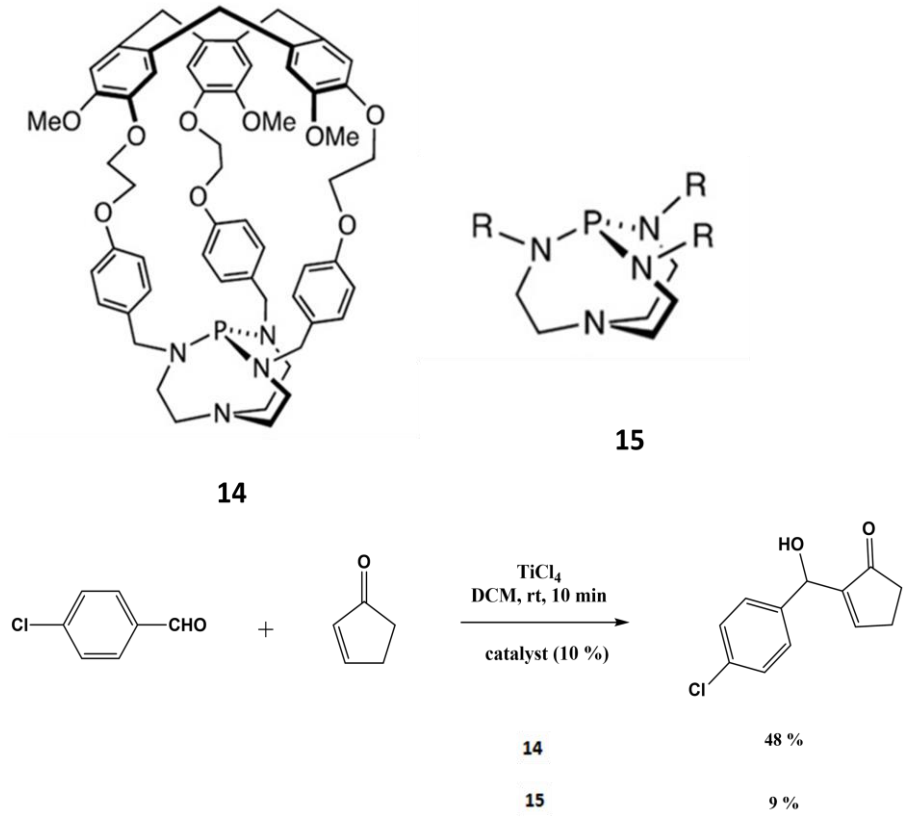

Figure 1.9 The Morita Baylis Hillman reaction catalyzed by **14** and model superbase **15**

Hemicryptophane ligands have also been used for the oxidation of methane: Sorokin, Martinez, and co-workers have compared the iron cage-complex **Fe^{II}(Hm-TPA)** with the model **Fe^{II}(TPA)** for this reaction (shown in Figure 1.10).[31] The cage-complex shows better results in terms of efficiency (total turnover number TON are double) and selectivity in the mono-oxidized methanol product (multiplied by a factor 2). This improvement results from several factors: (*i*) the hemicryptophane acts as an efficient receptors for CH_4, (*ii*) the confined iron catalyst is more stable and therefore more efficient, and (*iii*) the over-oxidation of the polar CH_3OH product is limited due to its ejection from the cage's cavity .

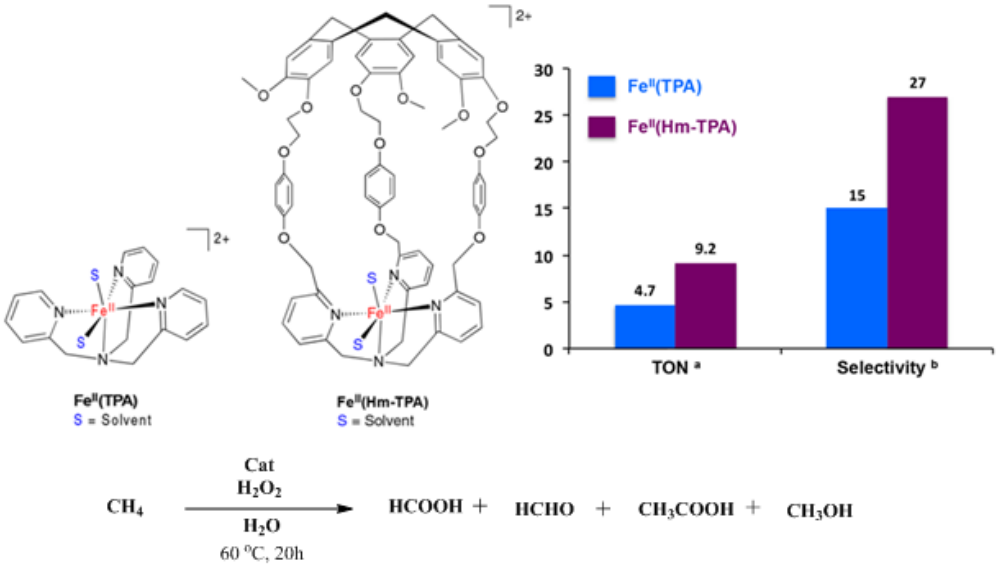

Figure 1.10 The result of oxidation of CH_4 by H_2O_2 using **Fe^{II}(TPA)** and **Fe^{II}(Hm-TPA**). Structure of the hemicryptophane catalysts **Fe^{II}(Hm-TPA)** and its corresponding model **Fe^{II}(TPA)** (top left). Comparison of the turnover numbers (TON) and selectivity in methanol observed during the oxidation of CH_4 by H_2O_2 catalyzed by **Fe^{II}(TPA)** (blue) and **Fe^{II}(Hm-TPA)** (purple).

Finally, it should be noted that organic cages are not only supramolecular structures, which could be used to achieve confined catalysis. Numerous self-assembled cages and coordination cages have been used as nano-reactors. These molecular capsules are structured by weaker interactions than covalent bonds, such as metal coordination or hydrogen bonding. They have different geometric shapes, which may induce unexpected regioselectivity or stereoselectivity. For instance, Fujita and coworkers compared an organopalladium cage (**16** in Figure 1.11) to a bowl system, for the stoichiometric Diels-Alder reaction between anthracene and phthalimide guests. The Diels-Alder reaction of anthracenes in the presence of the bowl **17** yields the expected product **19** (9,10-position ring). On the contrary, the use of the cage leads to an unusual isomer, the 1,4-adduct **18** (Figure 1.11).[32] When a reaction is performed in such a capsule, different selectivities might be observed due to the existence of the confined space.

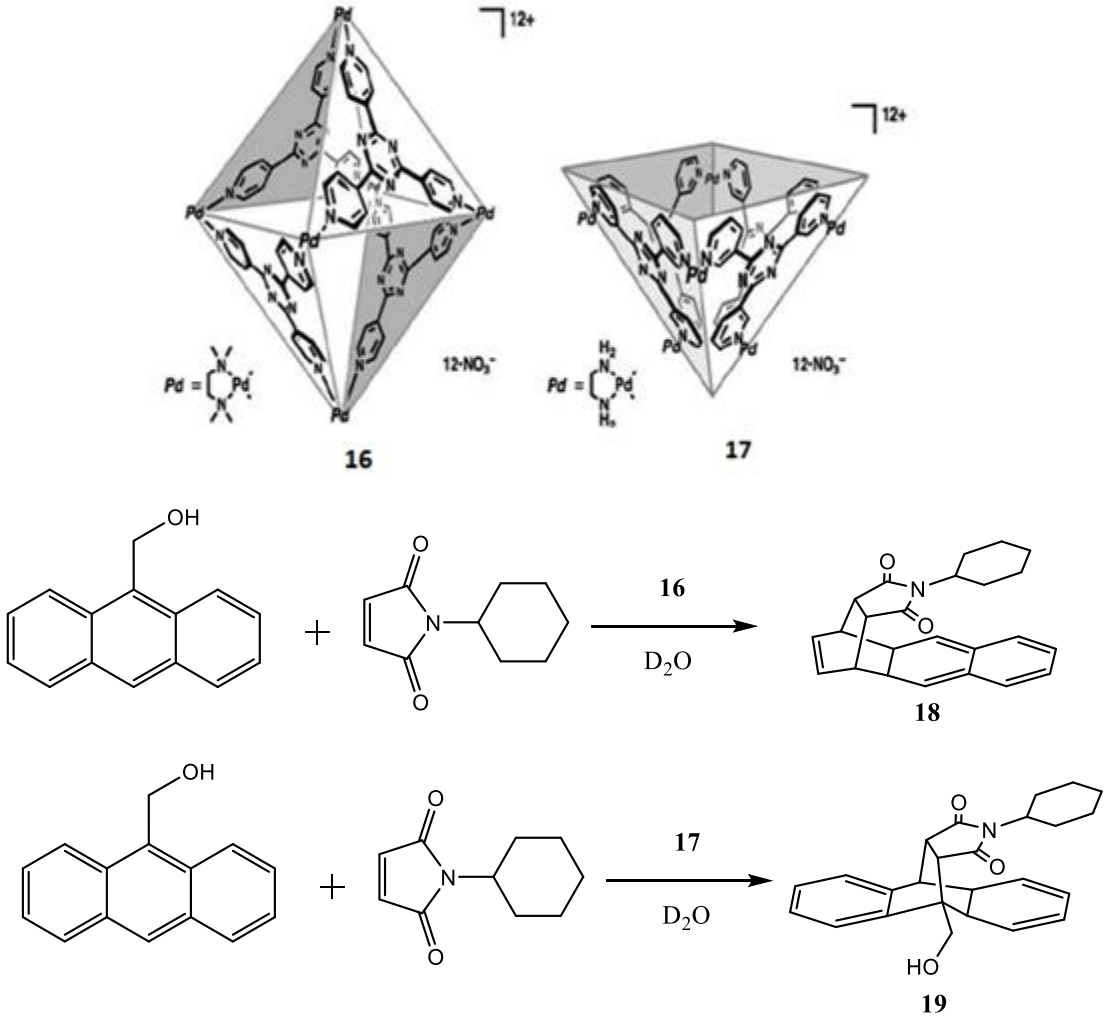

Figure 1.11 Diels-Alder reaction between 9-hydroxymethylanthrancene and N-cyclohexylphthalimide, in the presence of the self-assembled hosts **16** and **17**, leading to unusual regioisomer **18** within the cavity of cage **16,** and the normal product **19** with the presence of the bowl **17**

I.1.6 Conclusions

In this part, the synthesis of hemicryptophane organic cages has been described. In terms of molecular recognition and restricted-space catalysis, hemicryptophanes have great potential, because their CTV part can bring unique chirality and help structuring the three-dimensional cavity of the cage. Furthermore hemicryptophanes have been reported as particularly useful scaffold for homogeneous catalysis in confined space often yielding to stable, efficient, and more selective catalysts. By comparing with

some model catalysts, it has been proved that the catalytic process occurred inside the hemicryptophane cavity. Importantly, no inhibition of the catalysis by the product has been observed by using this kind of capsules. These results therefore demonstrate that hemicryptophanes are flexible structures that allow for the ejection of the products that is not blocked inside the cage.

More new hemicryptophane cages need to be designed for host-guest chemistry or for enantioselective catalysis. Such hemicryptophane cages can be tested and applied in various catalytic reactions that are presently under consideration in our laboratory. It is also very interesting to study if the chirality of the CTV could be transferred to the bottom part to prepare new chiral cage-ligands with controlled chirality.[32]

I.1.7 References

1. Ajami, D., L. Liu, and J. Rebek, Jr., *Soft templates in encapsulation complexes.* Chem Soc Rev, 2015. **44**(2): p. 490-9.
2. Jin, Y., et al., *Dynamic covalent chemistry approaches toward macrocycles, molecular cages, and polymers.* Acc Chem Res, 2014. **47**(5): p. 1575-86.
3. Durot, S., J. Taesch, and V. Heitz, *Multiporphyrinic cages: architectures and functions.* Chem Rev, 2014. **114**(17): p. 8542-78.
4. Yu, G., K. Jie, and F. Huang, *Supramolecular Amphiphiles Based on Host-Guest Molecular Recognition Motifs.* Chem Rev, 2015. **115**(15): p. 7240-303.
5. Zarra, S., et al., *Molecular containers in complex chemical systems.* Chemical Society Reviews, 2015. **44**(2): p. 419-432.
6. J. L. Atwood, J.E.D.D., D. D. MacNicol, F. Vögtle und J. ‐ M. Lehn. , *Comprehensive Supramolecular Chemistry.* Angewandte Chemie International Edition, 1996. **109**(9): p. 2.
7. Canceill, J., et al., *Speleands. Macropolycyclic receptor cages based on binding and shaping sub-units. Synthesis and properties of macrocycle cyclotriveratrylene combinations. Preliminary communication.* Helvetica Chimica Acta, 1982. **65**(6): p. 1894-1897.
8. Gautier, A., et al., *Chiral Trialkanolamine-Based Hemicryptophanes: Synthesis and Oxovanadium Complex.* Organic Letters, 2005. **7**(7): p. 1207-1210.
9. Wei, J., et al., *Versatile syntheses of hemi-cryptophanes and a metallo-cryptophane from a hexa-functionalized C3v -symmetrical tribenzotriquinacene (TBTQ) derivative.* Chem Asian J, 2015. **10**(5): p. 1150-8.
10. Hardie, M.J., *Self-assembled Cages and Capsules Using Cyclotriveratrylene-type Scaffolds.* Chemistry Letters, 2016. **45**(12): p. 1336-1346.
11. Brotin, T. and J.-P. Dutasta, *Cryptophanes and Their Complexes—Present and Future.* Chemical Reviews, 2009. **109**(1): p. 88-130.

12. Raytchev, P.D., et al., *A new class of C3-symmetrical hemicryptophane hosts: triamide- and tren-hemicryptophanes.* J Org Chem, 2010. **75**(6): p. 2099-102.

13. *<Chatelet et al. - 2011 - Shorter and Modular Synthesis of Hemicryptophane-t.pdf>*.

14. Gosse, I., et al., *A thiophosphorylated hemicryptophane: structure of the toluene inclusion complex.* New Journal of Chemistry, 1999. **23**(5): p. 545-548.

15. Perraud, O., et al., *Resolution and absolute configuration assignment of a chiral hemicryptophane molecular cage.* Chirality, 2010. **22**(10): p. 885-888.

16. Kataoka, K., et al., *Amine-triggered molecular capsules using dynamic boronate esterification.* Chemical Communications, 2009(13): p. 1682-1684.

17. Schmitt, A., et al., *Synthesis of the First Water-Soluble Hemicryptophane Host: Selective Recognition of Choline in Aqueous Medium.* Organic Letters, 2014. **16**(9): p. 2374-2377.

18. Schmitt, A., et al., *Chiral Discrimination of Ammonium Neurotransmitters by C3-Symmetric Enantiopure Hemicryptophane Hosts.* Chirality, 2013. **25**(8): p. 475-479.

19. Perraud, O., et al., *Hemicryptophane host as efficient primary alkylammonium ion receptor.* Organic & Biomolecular Chemistry, 2012. **10**(5): p. 1056-1059.

20. Zhang, D., et al., *Insights into the Complexity of Weak Intermolecular Interactions Interfering in Host–Guest Systems.* ChemPhysChem, 2015. **16**(14): p. 2931-2935.

21. Le Gac, S. and I. Jabin, *Synthesis and Study of Calix[6]cryptamides: A New Class of Heteroditopic Receptors that Display Versatile Host–Guest Properties Toward Neutral Species and Organic Associated Ion-Pair Salts.* Chemistry – A European Journal, 2008. **14**(2): p. 548-557.

22. Wang, L., et al., *Hydrogen Bonding-Directed Quantitative Self-Assembly of Cyclotriveratrylene Capsules and Their Encapsulation of C60 and C70.* The Journal of Organic Chemistry, 2011. **76**(9): p. 3531-3535.

23. Perraud, O., et al., *The cooperative effect in ion-pair recognition by a ditopic hemicryptophane host.* Chemistry, 2011. **17**(15): p. 4177-82.

24. Makita, Y., et al., *A tri-aromatic amide hemicryptophane host: synthesis and acetylcholine binding.* Tetrahedron Letters, 2016. **57**(46): p. 5112-5115.

25. Garcia-Viloca, M., et al., *How Enzymes Work: Analysis by Modern Rate Theory and Computer Simulations.* Science, 2004. **303**(5655): p. 186.

26. Crini, G., *Review: a history of cyclodextrins.* Chem Rev, 2014. **114**(21): p. 10940-75.

27. Dai, Y., et al., *8.14 Chromatographic Separations and Analysis: New Stationary Phases.* 2012: p. 286-310.

28. Martinez, A. and J.-P. Dutasta, *Hemicryptophane–oxidovanadium(V) complexes: Lead of a new class of efficient supramolecular catalysts.* Journal of Catalysis, 2009. **267**(2): p. 188-192.

29. Perraud, O., et al., *Oxidation of cycloalkanes by H2O2 using a copper-hemicryptophane complex as a catalyst.* Chem Commun (Camb), 2013. **49**(13): p. 1288-90.

30. Yang, J., et al., *Endohedral Functionalized Cage as a Tool to Create Frustrated Lewis Pairs.* Angewandte Chemie International Edition, 2018. **57**(43): p. 14212-14215.

31. Ikbal, S.A., et al., *Bioinspired Oxidation of Methane in the Confined Spaces of Molecular Cages.* Inorg Chem, 2019. **58**(11): p. 7220-7228.

32. Qiu, G., et al., *Chirality transfer in a cage controls the clockwise/anticlockwise propeller arrangement of the tris(2-pyridylmethyl)amine ligand.* Chem Commun (Camb), 2019. **55**(94): p. 14158-14161.

I.2 Chirality transfer in tripodal supramolecular cages

This part consist in a mini review article that has been submitted to the journal "*Frontiers in Chemistry*", in August 2020, for publication in an article collection on *Supramolecular Chirogenesis in Chemical and Related Sciences*.

Control and transfer of chirality within well-defined tripodal cages

Gege Qiu, Paola Nava, Cédric Colomban*, and Alexandre Martinez*

I.2.1 Abstract

The development of new strategies to turn achiral artificial hosts into highly desirable chiral receptors is a crucial challenge in order to advance the fields of asymmetric transformations and enantioselective sensing. Over the past few years, C_3 symmetrical cages have emerged as interesting class of supramolecular hosts that has been reported as efficient scaffolds for chirality dynamics (such as generation, control, and transfer). On this basis, this mini review, which summarizes the existing examples of chirality control and propagation in tripodal supramolecular cages, aims at discussing the benefits and perspectives of each approach.

I.2.2 Introduction

Stereoselective bindings are essential events for biochemical functions such as enzymatic catalysis and recognition of natural metabolites. In order to reproduce the efficiency of the stereoselective receptors found in the biological world, the synthesis of chiral artificial hosts has attracted considerable attention over the past few decades. In this context, the development of new strategies for preparation of chiral receptors as well as the discovery of the factors that govern both chirality genesis and selective binding events are of particular interest. In this context, the supramolecular approach appears as particularly promising as it allows for the construction of tridimensional hosts that could, for example, mimic enzymes cavities.[1] Among supramolecular hosts, organic or self-assembled cages built from chiral building blocks are of particular interest due to their ability to bind guests within their interior. A variety of chiral organic, [2] or metallo-cages [3,4] have been constructed over the past years, via covalent bond or coordination driven assembly processes respectively.

However, being able to induce, control, and transfer chirality within supramolecular cages (and their related host-guest complexes), remains a highly challenging task. In this line, C_3 symmetrical cages have recently emerged as particularly interesting scaffolds because of their tendency to form triple-stranded helix or propeller-like structures. Aiming at providing a general view about recent progress in the preparation of chiral tripodal cages displaying control and/or transfer of chirality, this mini-review summarizes current knowledge on how the chiral information can (*i*) propagate along tridimensional architectures, and (*ii*) can be controlled upon chiral sorting, or guest binding.

The first part of the review will be devoted to examples of propagation of the stereochemical information from one chiral unit to another part of the C_3 symmetrical architectures. Its second part will described how chiral-sorting events could lead to the preferential formation of enantiopure tripodal hosts. Finally, the last part will focus on the highly challenging on-demand control of the host-chirality dictated by binding of external guests.

I.2.3 Propagation of the chirality in tripodal cages

A straightforward strategy to generate chiral hosts consists in the covalent substitution of a chiral precursor, aiming at creating an inner cavity. In particular, chiral C_3 symmetrical cages have been obtained by connecting one chiral moiety with another tripodal unit, by three linkers. The presence of three identical linkers connected to one chiral component represents an interesting structural motif as it allows for the formation of a triple-stranded helical structure with controlled orientation. It has been indeed observed that the stereochemical information of the chiral unit could propagate along the structure to (*i*) induce a controlled propeller-like arrangement of the linkers and (*ii*) turn another linked achiral part into a chiral structure. Chirality transfer events within tripodal hosts were firstly evidenced between the chiral unit and its nearest linkers, resulting in a remote control of their helical arrangement (**Figure 1.12**). For example, Badjić et al. reported the preparation and characterization of the gated stereoisomeric basket (**20**).[5] Such C_3 symmetrical cavitand was built from a basket unit owning a *P*- or *M*- twisted structure, decorated by three aminopyridines gates at its rim. The authors demonstrated, through a

combination of $^{1}H/^{13}C$-NMR analysis and computational results, that the aminopyridine substituents display a right- or left-handed propeller like arrangement maintained by an intramolecular N-H···N hydrogen-bond network. Interestingly, the unidirectional orientation of the gates folding is dictated by the chirality (*P*- or *M*-) of the southern twisted chiral basket. By mean of computational studies, the authors indeed suggests that the *P*- basket framework imposes an anti-clockwise orientation while a clockwise orientation of the gate is predicted for the *M*- basket.

By replacing aminopyridine by quinolone gates, the same team reported, one year later, the enantiopure basket (**21**), that displays a solvent dependent transfer of the stereochemical information of the basket to the rim.[6] By comparison with **20**, **21** exhibits π–stacked gates instead of hydrogen-bonded ones. 2D ^{1}H-NMR characterizations, exciton-coupled circular dichroism (ECD) analysis, and computational modeling, reveal that the clockwise and/or anticlockwise orientations of the quinolone gates exist in acetonitrile, while the three substituents remains randomly oriented in the non-polar dichloromethane solvent.

In the same vein, hemicryptophanes are organic cages built from a northern bowl-shaped, and C_3 symmetrical cyclotriveratrylene (CTV) unit, connected to another tripodal moiety by three spacers.[7] Due to the inherent chirality of the CTV unit, hemicryptophanes are chiral cages with *M* or *P* configuration. Enantiopure versions of this kind of hosts are commonly obtained following two main strategies: (*i*) the chiral HPLC resolution of a racemic mixture of *P* and *M* structures and (*ii*) the addition of another chiral moiety and separation of the resulting diastereoisomers.[8] A hemicryptophane (**22**), which connects a CTV unit and a phophotrihydrazone moiety, through three butylene (-C_4H_8-) linkers, was reported in 2016 as ligand for Ga^{III} and Fe^{III} octahedral metal ions.[9] The authors observed, trough XRD analysis, that the butylene linkers of **22** displayed a clockwise/anticlockwise helical orientation (α or β helicity): interestingly, for both **22** and its corresponding metal complexes Ga^{III}(**22**) and Fe^{III}(**22**), such solid state helical arrangement of the linkers (α or β) was imposed by the configuration of the CTV unit. Indeed only (*M*-)CTV-(β-)helix and (*P*-)CTV-(α-)helix pairs of enantiomiers were observed. In 2018, the group of Martinez reported a new example of a hemicryptophane cage displaying a remote control of the linkers helical arrangement, dictated by the CTV unit.[10] The hemicryptophane (**23**),

which displays linkers constituted of both amine and amide groups, was prepared. Analysis of its X-ray molecular structure reveals H-bond interactions between the amide and the amine functions of each arm resulting in a triple-stranded helical arrangement of the linkers (**Figure 1.12, D**). Interestingly, the chirality of such triple helices was dictated by the chirality of the CTV unit (*P*- or *M*-). The hemicryptophane **(*P*)-23**, indeed displayed a Δ propeller-like arrangement of the linkers while the **(*M*)-23** revealed a Δ orientation. Moreover, careful ^{1}H-NMR analyses allow the authors to suggest that the controlled arrangement observed in the solid state, may be retained in solution. This example highlights the remarkable flexibility of the whole organic structure that is strongly twisted and displays a propagation of the CTV's chirality over nine bonds.

Based on theses interesting examples of chirality transfer between chiral unit and linkers, the supramolecular chemists asked themselves: could this phenomenon be extended in order to control the helical arrangement of another achiral C_3 symmetrical unit? The remote control of the helical arrangement by some tripodal units is indeed of particular interest, as it might allow to turn an achiral artificial ligand into an enantiomerically-pure binding site. For example, the control of the helicity of the C_3 symmetrical tris(2-pyridylmehyl)amine (TPA) ligand has attracted considerable attention due to its versatile applications, ranging from bio-inspired models,[11] catalysts,[12] to chiral sensors.[13] This ligand could display a propeller-like arrangement of its pyridine units that rapidly interconvert between clockwise and anticlockwise enantiomeric conformations. Therefore, by controlling the sense of its pyridines twist, the achiral TPA could be switched into a highly desirable chiral coordinating structures. In 2019, the X-ray structure of the TPA-based hemicryptophane **24** was reported during the study of this cage-ligand for selective metal-based methane oxidation.[14] This solid-state structure reveals a CTV-dictated triple-stranded helical arrangement of the phenyl linkers of **24**, but no orientation of the southern TPA part was observed. On this basis, Colomban, Martinez and co-wokers have designed the structurally contracted cage **1** [15] where the phenyl linkers are replaced by single methylene –CH_2- (**Figure 1.12, F**). The authors resonated that a closer proximity between the chiral northern CTV cap and the southern TPA ligand would result on the propagation of the chirality of the CTV to the TPA ligand allowing for a predictable control of its helicity. These expectations turn out to be

accurate since the organic cage **1**, which represents the smallest hemicryptophane ever reported, remarkably displayed a controlled clockwise / anticlockwise propeller arrangement of the TPA unit dictated by the chirality of the CTV unit (*M*- or *P*-). The covalent capping with a *M*-CTV unit indeed results in a left-handed propeller arrangement of the TPA (while *P*-CTV lead to a right-handed propeller arrangement). It should be noted that enantiopure version of (*M)*-**1** and (*P)*-**1** were obtained in an highly efficient purification step based on the chiral-HPLC resolution of the racemic mixture **(+/-)1** (ee values >99.5%). Importantly, this strong chirality transfer is maintained upon metallation of the TPA moiety with Cu(I) metal ion. The resulting complex **Cu^{I}(1)(Cl)**, (**Figure 1.12, F**) display a rare T-shaped coordination geometry along with a controlled helicity of the TPA unit that is maintained in both the solution and the solid state (XRD, ^{1}H-NMR, ECD analysis). To the best of our knowledge this approach was the first, and to date unique, example of a predictable and robust control of the TPA helicity, achieved through its covalent substitution with a chiral C_3 symmetrical unit. Furthermore, in sharp contrast with other chiral TPA-based cages found in the literature, which often display structural studies of the helicity based on computational methods, the chirality transfer in **1** and **Cu^{I}(1)(Cl)** were unambiguously evidenced through XRD analysis. Finally the design of the cage-ligand **1**, that allows the authors to report an unprecedented Cu(I) complex with a controlled helicity of the TPA-Cu(I) core, highlight the promises of the approach for the preparation of novel optically pure metal-based catalysts and receptors.

This strategy, combining chiral CTV cap and short spacers to control the chirality of another C_3 symmetrical unit, has been further exemplified by Martinez and his team through the preparation of the hemicryptophane **25.**[16] Due to its ability to engage strong hydrogen-bonds, the benzene-1,3,5-tricarboxamide (BTA) unit has been widely reported as a useful building block for the preparation of supramolecular assemblies. [17,18] Therefore, methods able to tune and control its structural properties are of particular interest. With such considerations in mind, the nanosized cage **25** was built aiming at controlling the sense of rotation of the three amides of the BTA unit. Hemicryptophane **25**, consists in a southern BTA covalently linked to a chiral CTV cap by three ethylene $–C_2H_4$- linkers (**Figure 1.12, G**). Interestingly, the close proximity between CTV and BTA units in this cage, allows for a remote control of the Λ/Δ orientation of the three amides of the south part dictated by the chirality of

the CTV cap. It was indeed demonstrated, though XRD analysis of single crystal of the racemic mixture of **(+/-)25**, that the BTA unit capped with a *M*-CTV displays a Λ orientation of their amides, while the cage built from a *P* cap result in an Δ arrangement of the chiral conformation. It was shown that the enantiopure cages (M-Λ)-**25** and (P-Δ)-**25** could be easily obtained, with excellent ee values (*ee >97.5 %,)* through straightforward chiral-HPLC resolution of the racemic mixture followed by ECD-based assignment of the absolute configurations. Finally, the authors proposed, based on ^{1}H-NMR observations, that the chirality transfer observed in the solid states might be retained in solution.

Another remarkable strategy to achieve a predictable control of the chirality of a tripodal ligand consists in its non-covalent capping with a chiral concave open-cage structure, through intermolecular ionic contacts. This so-called "Russian nesting doll" approach have been reported in 2016 by Badjic and coworkers, which used the chiral molecular baskets developed by this team to create and control a propeller-like arrangement of a TPA-based Zinc complex.[19] The self-assembled architecture **Zn^{II}(27)(Cl)** is based on supramolecular ionic interactions between a zinc complex substituted with three positively charged ammonium groups **$Zn^{II}(TPA^{NH3})Cl$**, and the chiral molecular nest **26** (displaying three negatively charged carboxylates at its rim). Formation of the entrapped Zn complex **Zn^{II}(27)(Cl)** in its nesting form, without appearance of intermolecular aggregates, was evidenced by ^{1}H-NMR titration, ESI-MS analysis, and computational simulations. The preferential formation of the Russian nesting dolls conformation of **Zn^{II}(27)(Cl)** was explained by both hydrophobic effect and nonpolar interactions between the two hydrophobic shell of **26** and **$Zn^{II}(TPA^{NH3})$**. It was interestingly observed that the chirality of the anionic basket **26**, which display (S)-alanine amino acids groups at its rim, is efficiently transferred to the cationic **$Zn^{II}(TPA^{NH3})Cl$** moiety, resulting in a controlled propeller-like arrangement of the TPA's pyridines. It was indeed proven through careful analysis of computed structures and circular dichroism (CD) spectrum, that the supramolecular interactions between the three carboxylates of **26** and the ammoniums of **$Zn^{II}(TPA^{NH3})Cl$** were responsibles for the exclusive formation of a left-handed (*M*) Zn-TPA core. Interestingly, this study allows the authors to demonstrate, for the first time, that a predictable control of the helical arrangement of TPA-based complexes, could be achieve by an ionic contract-based transfer of chirality within tripodal cages.

In 2017, the same group further exemplified the approach by studying the capture of several metallated and non-metallated TPA derivatives by both anionic and cationic molecular baskets.[20] Molecular dynamic computational simulations and ^{1}H NMR / ITC experimental analysis were performed to better understand the formation of the nesting complexes, which was found to be driven by hydrophobic effects and assisted by ionic host/guest contracts.

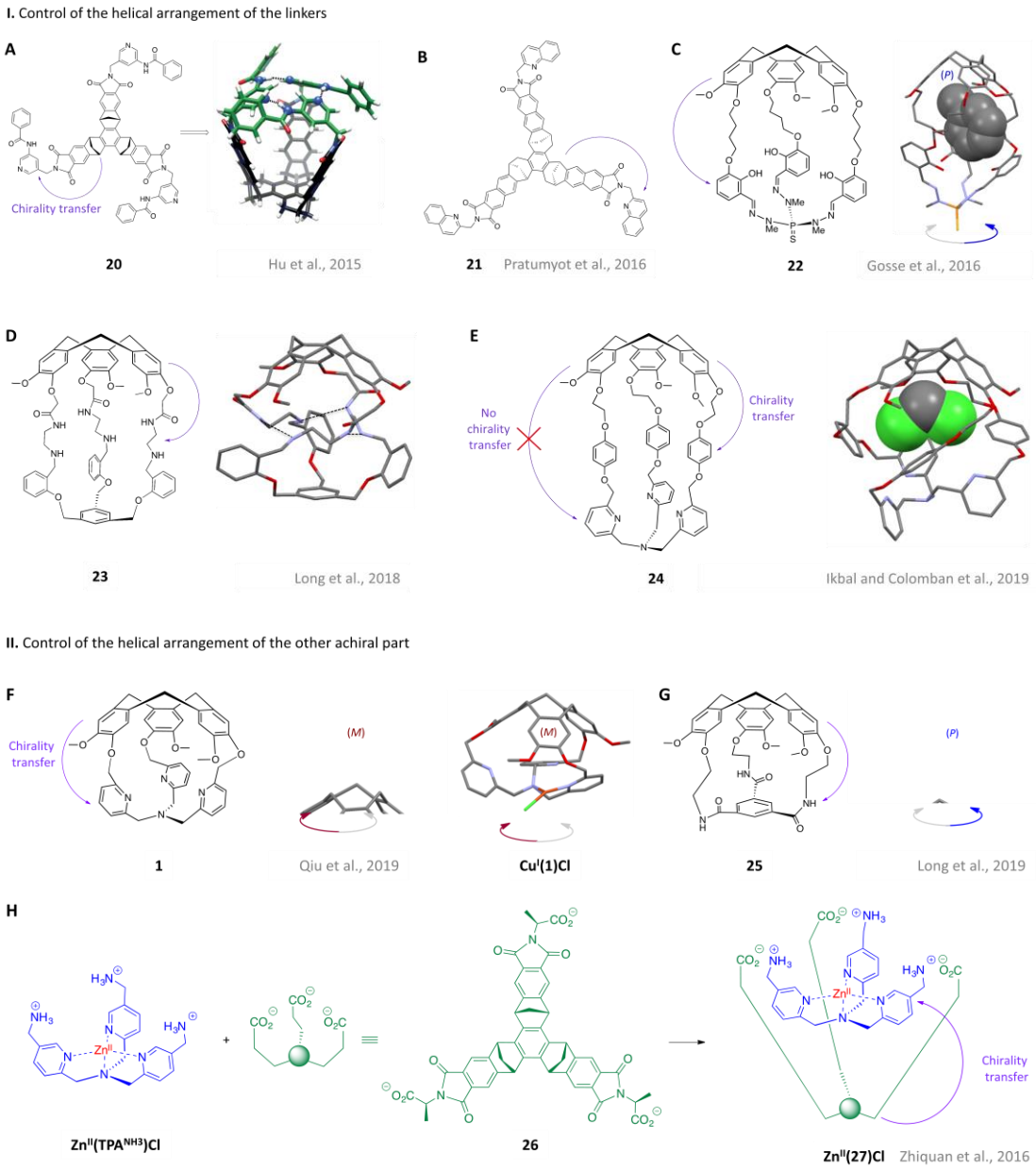

Figure 1.12 Examples of tripodal cages displaying a transfer of chirality between a chiral unit and its side arms. Schematic representation and computed structures of open cages **20** (**A**) and **21** (**B**) together with the schematic representation and XRD structures of hemicryptophanes **22** (**C**), **23** (**D**) and **24** (**E**) (the XRD structure of **22** and **24** displays an entrapped molecule of toluene and CH_2Cl_2 respectively). (II.)

Examples of C_3 symmetrical cages showing a propagation of the stereogenic information from a chiral unit to another tripodal ligand. Schematic representation and XRD structures of hemicryptophane **1** and its corresponding CuCl complex (**F**) and hemicryptophane **25** (**G**), along with the chemical structures of the nesting complex **Zn^{II}(27)(Cl)** and its precursors **26** and **$Zn^{II}(TPA^{NH3})Cl$** (**H**). Purple arrows depicts the observed chirality transfers.

I.2.4 Chiral-sorting in tripodal cages

This second part of the mini-review aims at describing how the chirality of one coupling partner could influence the chirality of a second precursor during the formation of chiral tripodal cages. Could the thermodynamic resolution of a racemic mixture of precursors by its coupling with another enantiopure unit, result in the exclusive formation of optically pure C_3 symmetrical cage ? To answer this question Martinez and coworkers studied in 2015 the [1+1] coupling reaction between a racemic mixture of an aldehyde-based CTV derivative **(+/-)28** (*M*- and *P*-) and a chiral TREN unit **(S,S,S)-29.**[21] Thanks to this novel chiral-sorting based strategy, the synthesis of the enantiopure cage ***M*-(*S*,*S*,*S*)30** was successfully reported. Enantiopure *(S,S,S)*-TREN precursors displaying methyl, isopropyl, and phenyl substituent were tested and, in all cases, the reductive amination results in the exclusive formation of a single diastereomer *M*-(S,S,S) of the tripodal cage **30** in a 15% average yield. The high diastereoselectivity of the cage formation was indeed evidenced through ^{1}H-NMR, XRD diffraction, and ECD analysis in both solid-state and solution. It was clearly demonstrated that the reaction between the chiral TREN unit and the two enantiomers of the CTV unit provides two different products: while the condensation with *M*-CTV gives a well defined cage ***M*-(S,S,S)30,** the reaction involving *P*-CTV results in the formation of insoluble polymeric species. As highlighted by the authors, such thermodynamic resolution could be seen as a transfer of the stereochemical information of the CTV unit through a remarkable ten-bonds distance (10 Å).

As part of chiral discriminations, the self-sorting phenomenon, in which a racemic mixture of cage-precursor is spontaneously sorted in narcissistic or social assemblies, is particularly challenging since homo- and heterochiral structures only differ from

the spatial orientations of the enantiomers. Interesting examples of chiral self-sorting events have been reported during the formation of supramolecular architectures.[22,23] This strategy has been recently applied to access enantiomerically pure C_3-symmetric cages built from two identical cofacial chiral units. Within the few examples of chiral self sorting achieved through dynamic covalent chemistry (**DCC)**, Mastalerz and coworkers reported, in 2017, the preparation of an enantiopure tripodal cage build from two cofacial triaminotribenzotriquinacene chiral units **31** assembled by three bis(salicyaldehyde) linkers **32**.[24] The reaction between a racemic mixture of **31** (*M* and *P*) and the linkers leads to the preferential formation of the narcissic self-sorted products **(*M/M*)-33** and **(*P/P*)-33** rather that the social one **(*M/P*)-33**. Therefore, a remarkable control of the chirality of the two partners, resulting in to the selective formation of chiral salicyimine based-cages was achieved, no matter the nature of the organic solvent. Based on experimental observations, the authors were able to explain such preferential self-sorting event by the rather low solubility of the social self-sorting product (***M/P*)-33**, both product formations being in thermodynamic equilibrium during the condensation process. A combination of semi-empirical calculations and variable temperature (VT) ^{1}H NMR analysis allow the authors to conclude that enthalpy favors the social self-sorting product **(*M/P*)-33** (by 6.5 +/- 3.4 kJmol^{-1}) while entropy favors the formation of the narcissic self-sorting product (*M/M* or *P/P*)-**33** (by 38 +/- 11JK^{-1}mol^{-1}). This work demonstrates that a selective preparation of chiral covalent tripodal cage could be achieved following a chiral self-sorting strategy taking advantage from (*i*) the favorable entropy of homochiral architecture and (*ii*) the difference in solubility between homo- and heterochiral compounds.

In the same line, enantiopure self-assembled metallacages have been constructed through the spontaneous chiral self-sorting of racemic mixtures of ligands, upon metal coordination.[25,26]. Although several reports of chiral metal-based assemblies, obtained by chiral self-sorting events, can be found in the literature, examples of C_3 symmetrical self-assembled cages, constructed from two cofacial tripodal ligand, are more rare. Goeb, Sallé and co-workers very recently reported the preparation of a tripodal self-assembled metallacage **36** constituted of two cofacial truxene units **34** assembled by the diruthenium bridging complexes **35**.[27] The truxene building block **34**, which includes three pyridines binding sites, was obtained by the two steps

derivatisation of the hexabutyl truxene. The achiral **34** is described as a face-rotating ligand meaning that it displays two different faces with opposite directionalities. The rotation of the methylene bridges of **34** indeed results in one clockwise (C) and one anti-clockwise (A) face (**Figure 1.13**). As consequence, cages resulting from the cofacial assembly of **34** could either lead to hetero-chiral assembly **(*C/A*)-36** or homochiral stereoisomers **(*C/C*)-36 or (*A/A*)-36**. The self-assembled cage **36** was prepared by reacting the truxene building block **34** (1 equiv.) with 1.5 equivalent of diruthenium complexe $\mathbf{35^{Napth}}$, which act as the three wall of the C_3-symmetrical cages. Interestingly, the self-assembly leads in the exclusive formation of a mixture of $[M_6L_2]$ chiral cages **(*C/C*)-36** and **(*A/A*)-36**. ^{1}H NMR, 2D COSY and DOSY NMR analysis, and XRD solid-state characterizations indeed allow the authors to conclude that the self-assembly is dictated by an homo-chiral self-sorting event. Such remarkable behavior, where homo-chiral cages emerges from a mixture of achiral building blocks, was found to be dictated by (*i*) the through-space interactions between the alkyl substituants of both cofacial units and (*ii*) the tilt value of the ruthenium-based wall.

To summarize, these examples highlight the fact that chiral tripodal cages, constructed from dynamic covalent bonds or metal-ligand linkages, could be effectively obtained following a chiral-sorting approach. This strategy, that could involve two different chiral coupling partners,[21] two enantiomers of the same building blocks,[24] or two identical achiral ligands,[27] displays crucial benefits regarding the desired straightforward preparation of enantiopures hosts avoiding tremendous purifications steps.

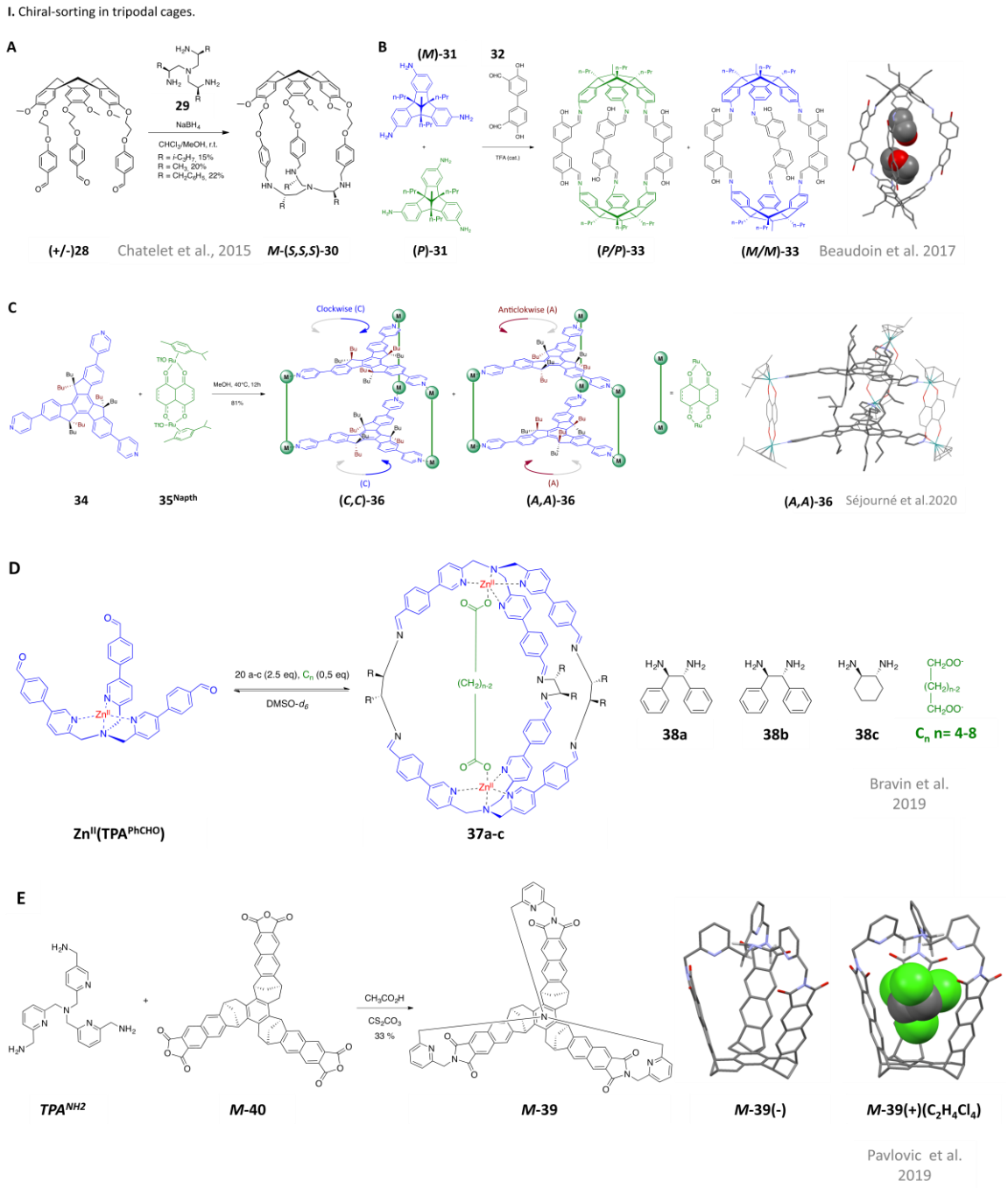

Figure 1.13 Examples of tripodal chiral cages obtained by chiral sorting. (**A**) Preparation of the enantiopure hemicryptophane **30**. (**B**) Chiral sorting of the homo-chiral covalent cage **33** together with the XRD structure of **(*M*,*M*)-15** displaying two encapsulated molecules of THF. (**C**) Sorting of the homochiral metallacage **36** and XRD structure of **(*A*-*A*)36**. (II) Examples of guest-dictated control of the chirality in tripodal cages. (**D**) Schematic representation of the preparation of TPA-cages **37a-c**. (**E**) Schematic representation of the capsule **(*M*)-39** along with XRD structures of (***M*)39(-)** (contain a disordered CH_2Cl_2 molecule, not represented) and **(*M*)39(+)($C_2H_4Cl_4$)**.

I.2.5 Control of the host chirality through guest binding

The on-demand control of the chirality of an artificial receptor is a particularly challenging goal for chemists aiming at reproducing the allosteric recognition processes found in the biological world. Therefore, the discovery of systems that allow for a switch of chirality dictated by an external stimulus is of particular interest.[28,29]. On this basis, tripodal cages displaying helical arrangements and able to encapsulate guests within their inner space, appear as promising systems since a guest-dictated control of the host chirality might arise from specific binding events.

As highlighted in the first part of this mini-review, the control of the propeller arrangement of Zn^{II} and Cu^{II} complexes made from the TPA derivatives is of particular interest for the development of chiral molecular sensors with characteristic CD absorption features.[30] With such considerations in mind, the team of Zonta has explored the possibility of constructing flexible TPA-based cages able to switch between a clockwise (*P*) or anticlockwise (*M*) orientation of the pyridine's propeller arrangement, depending on the nature of the encapsulated guest. Their indeed report, in 2019, the preparation and characterizations of the chiral tripodal cages **37** based on two cofacial **TPA** coordinating units connected through chiral diamines linkers (**38a, 38b and 38c**).[31] The host-guest adducts were formed in situ through the addition of 5 equivalents of the diamine linkers **38a-c** to a mixture of the $\mathbf{Zn^{II}(TPA^{PhCHO})}$ complex (2 equiv.) and dicarboxylate guest $\mathbf{C_n}$ (1 equiv.), (**Figure 1.13**). This template approach allows for the complete formation of cage with entrapped dicarboxylate guests ranging from $\mathbf{C_4}$ to $\mathbf{C_8}$ (while uncomplete cage formation are reported for the longer C_9 and C_{10} guests). The authors characterized the resulting supramolecular architectures in solution by mean of ^{1}H-NMR, 2D-NMR and MS techniques and determined their chiroptical properties through electronic circular dichroism (ECD) analysis. It was observed that an unexpected change in the ECD spectra of the Zn^{II}(TPA)–based cage **37a**, occureed upon moving along the $\mathbf{C_{4\text{-}8}}$ guest series. Upon increasing the molecular length of the guest, a gradual negative to positive switch of the ECD signal, accompanied with a red shift of the maximum of absorbance, was indeed reported (in the case of cage **37a**, that display di-aryl linkers). The authors ruled out the hypothesis that the observed inversion of ECD spectra

might result from modifications in the guests chiroptical properties or binding behaviors as (*i*) the alkyl-based guests do not absorb in this region and (*ii*) the observed ECD absorption were founded to be concentration independent. Based on these observation, it was postulated that the changes in the chiroptical properties of the host-guest system (ECD spectra), upon changes of the length of the guest, arouse from structural modification of the tripodal host that displays two stereodynamic TPA ligands and six stereogenic centers. As previously shown for this kind of host, the cavity size in **37a** (Zn-Zn distance) is indeed dictated by the size of the entrapped guest.[32] This assumption was supported by calculated CD spectra, which confirmed that changes in the helicity of the TPA units induce an inversion of the CDs. Although no XRD structures of the hosts were reported, the mechanism of the guest lenght-dependent ECD changes was further elucidate by mean of DFT calculations of the cage conformation for each host-guest complexes. The guest-dependent breathing ability of the host arises from an increase or decrease of the dihedral angle between the vicinal amine that results in a switch in the helicity of the TPA ligand.

Another interesting example of guest-dependent control of the TPA's dynamic chirality has been reported, the same year, by Badjic and coworkers.[33] The organic cage **39**, constituted of a TPA-based ligand (**TPA^{NH2}**) covalently linked to a chiral molecular basket **40** (*M*- or *P*-), derived from a previous work on switchable chiral host for the on-demand accommodation and release of small guests upon protonation/deprotonation of the TPA unit.[34] As an extension of this work, the authors reported, in 2019, a detailed structural study demonstrating that the rapid interconversion of the arrangement of the cage's TPA (between clockwise(+) and anticlockwise(-) orientations) could be frozen upon encapsulation of haloalkane guests. The structural modifications of the tripodal host (*M*)-**39**, upon encapsulation of chlorinated or brominated guests, have been experimentally evidenced in both solution (NMR spectroscopy) and solid-state (XRD) (**Figure 1.13**). Furthermore the relative stability, upon guest binding, of the two diastereomeric forms of the capsule displaying clockwise (*M*)-**39**(+) or anticlockwise (*M*)-**39**(-) arrangements of the TPA, was computationally determined (DFT). While the encapsulation of the small CH_2Cl_2 did not influence the (+) or (-) orientation of the pyridines, these results remarkably demonstrate that the accommodation of larger guests such as CCl_4, $C_2H_4Cl_4$, or CBr_4 leads to the formation of a (*M*)-**39**(-) / (*M*)-**39**(+) mixture with a 3:1 ratio. In other

world, upon guest binding, both CX···π halogen-bonding and CX···HC hydrogen-bonding interactions between the haloalkane guests (X= Cl or Br) and **39** (respectively involving the benzene ring of the basket and the -CH_2- of the TPA), slow-down the interconversion of the TPA unit, and favor the counterclockwise propeller-like orientation. Therefore, this work interestingly demonstrates that dynamic chirality of a host and stereoselective encapsulation processes might be closely related be mean of weak supramolecular contacts.

I.2.6 Conclusion and discussion

To summarize, this mini-review highlights recent advances related to the induction, control, and transfer of chirality within tripodal supramolecular cages (and their related host-guest complexes). Various cages of C_3 symmetrical type, displaying a predictable and robust control of the chirality, have been recently prepared. These enantiopure cages are usually obtained following three main synthetical approaches. Firstly, the tendency of C_3 symmetrical cages to form triple-stranded helix or propeller-like structures has been exploited to prepared architectures displaying a transfer of the stereogenic information from one chiral unit to *i*) its nearest linkers or *ii*) another C_3 symmetrical unit. This predictable control on the chirality of other linked units, was found to arise from noncovalent interactions such as hydrogen bonding or steric repulsion. Interestingly, this approach have been used to turn achiral ligand into highly valuable coordinating structures leading to metal complexes with controlled helicity, advancing the field of asymmetric transformations and enantioselective sensing.

A second way to obtain enantiopure tripodal cages is based on chiral-sorting event occurring during the final formation step. Following this approach, both organic and metal-based chiral cages have been obtained through [1+1] coupling reactions between *i*) one chiral unit and a racemic mixture of another achiral moiety, or *ii*) two chiral coupling partners. The different factors that govern the observed preferential formations of one stereoisomers, social dimeric structures, or narcissistic assemblies, have been identified. The selective formation of such thermodynamically favored products was indeed found to result from difference of solubility between the possible

chiral assemblies, or through-space interactions between bulky substituents of the coupling partners.

Finally, a new kind of on-demand control of the chirality of supramolecular hosts has recently emerged through interesting examples of tripodal hosts presenting guest-dictated helicity. This promising approach, based on a preferential arrangement of the host-guest complex compared to the empty host, open new opportunities toward the development of hosts that could mimic the allosteric properties found in some biological receptors.

Altogether, these examples of preparation of enantiopure chiral C_3 symmetrical supramolecular cages have led to the discovery and understanding of the mechanisms that result in chirality induction and control. It is therefore reasonable to expect that such way of generating, controlling, and propagate chirality will be further applied to other class of supramolecular architectures, and will result in the preparation of highly demanded stereoselectives receptors and catalysts.

I.2.7 References

1. Liu, M., Zhang L., and Wang, T. (2015). Supramolecular Chirality in Self-Assembled Systems. *Chem. Rev.*, **115**, 7304–7397. doi: 10.1021/cr500671p
2. Brotin T., Guy L., Martinez A., Dutasta J.-P. (2013). Enantiopure supramolecular cages: synthesis and chiral recognition properties. *Top Curr Chem.* **341**, 177-230. doi:10.1007/128_2013_487
3. Chen, L. J., Yang, H. B., and Shionoya, M. (2017). Chiral metallosupramolecular architectures. *Chem. Soc. Rev.*, **46**, 2555
4. Hardie M. J. (2016), Self-assembled Cages and Capsules Using Cyclotriveratrylene-type Scaffolds. Chem. Lett. **45**, 1336–1346 | doi:10.1246/cl.160780
5. Hu, L., Polen, S., Hardin, A. M., Pratumyot, Y., Hadad, C. M., and Badjić, J. D. (2015). On the Transfer of Chirality, Thermodynamic Stability, and Folding Characteristics of Stereoisomeric Gated Baskets. *Eur. J. Org. Chem.* 6832–6840. doi: 10.1002/ejoc.201501071]
6. Pratumyot, Y., Chen, S., Hu, L., Polen, S. M., Hadad, C. M., and Badjić J. D. (2016). Assembly and Folding of Twisted Baskets in Organic Solvents. *Org. Lett.*, **18**, 4238−424. doi: 10.1021/acs.orglett.6b01976.
7. Zhang, D., Martinez, A. and Dutasta, J.-P. (2017). Emergence of Hemicryptophanes: From Synthesis to Applications for Recognition, Molecular Machines, and Supramolecular Catalysis. *Chem. Rev.*, **117**, 4900−4942.
8. Colomban, C., Châtelet, B., and Martinez A. (2019). Different Strategies for Obtaining Enantiopure Hemicryptophanes. *Synthesis*. **51**, 2081-2099. doi: 10.1055/s-0037-1612420
9. Gosse, I., Robeyns, K., Bougault, C., Martinez, A., Tinant, B., and Dutasta, J. P. (2016). Synthesis and Structural Studies of Gallium(III) and Iron(III) Hemicryptophane Complexes. *Inorg. Chem.* **55**, 1011−1013. doi: 10.1021/acs.inorgchem.5b02750
10. Long, A., Perraud, O., Jeanneau, E., Aronica, C., Dutasta, J. P., and Martinez, A. (2018). A hemicryptophane with a triple-stranded helical structure. *Beilstein J. Org. Chem.* 14, 1885–1889. doi:10.3762/bjoc.14.162.
11. M. Borrell, E. Andris, R. Navrátil, J. Roithová and M. Costas, Nat. Commun., 2019, **10**, 901

12. R. L. Peterson, R. A. Himes, H. Kotani, T. Suenobu, L. Tian, M. A. Siegler, E. I. Solomon, S. Fukuzumi and K. D. Karlin, J. Am. Chem. Soc., 2011, **133**, 1702–1705
13. L. You, J. S. Berman and E. V. Anslyn, Nat. Chem., 2011, **3**, 943
14. Ikbal, S. A., Colomban, C., Zhang, D., Delecluse, M., Brotin, T., Dufaud, V., Dutasta, J. P., Sorokin A. B., and Martinez, A. (2019). Bioinspired Oxidation of Methane in the Confined Spaces of Molecular Cages. *Inorg. Chem.*, **58**, 7220–7228. doi: 10.1021/acs.inorgchem.9b00199.
15. Qiu, G., Colomban, C., Vanthuyne, N., Giorgi M., and Martinez, A. (2019). Chirality transfer in a cage controls the clockwise/anticlockwise propeller arrangement of the tris(2-pyridylmethyl)amine ligand. *Chem. Commun.* **55**, 14158-14161. doi: 10.1039/c9cc07244f.
16. Long, A., Jean, M., Albalat, M., Vanthuyne, N., Giorgi, M., Górecki, M., Dutasta, J.P, Martinez, A. (2019). Synthesis, resolution, and chiroptical properties of hemicryptophane cage controlling the chirality of propeller arrangement of a C3 triamide unit. *Chirality*, **31**, 910-916. doi:10.1002/chir.23131.
17. Kulkarni, C.; Meijer, E. W., and Palmans, A. R. A. (2017). Cooperativity Scale: A Structure–Mechanism Correlation in the Self-Assembly of Benzene-1,3,5-tricarboxamides. *Acc Chem Res*, **50**, 1928-1936.
18. Zimbron, J. M., Caumes, X., Li, Y., Thomas, C. M.; Raynal M.; and Bouteiller L. (2017). Real-time control of the enantioselectivity of a supramolecular catalyst allows selecting the configuration of consecutively formed stereogenic centres. *Angew. Chem.*, **56**, 14016-14019.
19. Zhiquan, L., Polen, S., M. Hadad, C., RajanBabu, T. V., and Badjić, J. D. (2016). Russian Nesting Doll Complexes of Molecular Baskets and Zinc Containing TPA Ligands. *J. Am. Chem. Soc.* **138**, 8253−8258. doi: 10.1021/jacs.6b04436.
20. Zhiquan, L., Polen, S. M., Hadad, C. M., RajanBabu, T. V., and Badjić, J. D. (2017). Examining the Scope and Thermodynamics of Assembly in Nesting Complexes Comprising Molecular Baskets and TPA Ligands. *Org. Lett.*, **19**, 4932−4935. doi: 10.1021/acs.orglett.7b02391
21. Chatelet, B.; Joucla, L.; Padula, D.; Di Bari, L.; Pilet, G.; Robert, V.; Dufaud, V.; Dutasta, J.-P.; and Martinez, A. (2015). Remote Control of Helical Chirality: Thermodynamic Resolution of a Racemic Mixture of CTV Units by Remote Stereogenic Centers. *Org. Lett.* **17**, 500−503

22. W. Makiguchi, J. Tanabe, H. Yamada, H. Iida, D. Taura, N. Ousaka, E. Yashima (2015). Chirality- and sequence-selective successive self-sorting via specific homo- and complementary-duplex formations. *Nat. Commun*. **6**, 7236. Doi: 10.1038/ncomms8236
23. Tateishi, T., Kojima, T., Hiraoka S. (2018). Chiral self-sorting process in the self-assembly of homochiral coordination cages from axially chiral ligands. *Commun. Chemistry*. *Doi: 10.1038/s42004-018-0020-4*
24. Beaudoin, D.; Rominger, F.; and Mastalerz, M. (2017). Chiral Self-Sorting of [2+3] Salicylimine Cage Compounds. *Angew. Chem. Int. Ed.* **56**, 1244 –1248. doi: 10.1002/anie.201610782.
25. Weilandt, T., Kiehne, U., Schnakenburgband, G., Lützen. A. (2009). Diastereoselective self-assembly of dinuclear heterochiralmetallosupramolecular rhombs in a self-discriminating process. *Chem. Commun.* **17**, 2320–2322. Doi: 10.1039/b819335e
26. Schulte, T. R., Holstein, J. J., and Clever, G. H. (2019) Chiral Self-Discrimination and Guest Recognition in Helicene-Based Coordination Cages. Angew. Chem. Int. Ed. 2019, **58**, 5562 –5566. Doi: 10.1002/anie.201812926
27. Séjourné, S.; Labrunie, A.; Dalinot, C.; Benchohra, A.; Carré, V.; Aubriet, F.; Allain, M.; Sallé, M., and Goeb, S. (2020). Chiral Self-Sorting in Truxene-Based Metallacages. *Inorganics,* 2020, **8**, 1. doi:10.3390/inorganics8010001.
28. Martinez, A.; Guy, L. and Dutasta J.-P. (2010). Reversible, Solvent-Induced Chirality Switch in Atrane Structure: Control of the Unidirectional Motion of the Molecular Propeller. *J. Am. Chem. Soc*., **132**, 16733–16734. DOI : 10.1021/ja10287
29. Zhao, D.; Neubauer T. M.; Feringa B. L. (2015) Dynamic control of chirality in phosphine ligands for enantioselective catalysis, *Nat. Commun.*, DOI: 10.1038/ncomms7652
30. You, L.; Pescitelli, G.; Anslyn, E. V.; Di Bari, L. (2012). An Exciton-Coupled Circular Dichroism Protocol for the Determination of Identity, Chirality, and Enantiomeric Excess of Chiral Secondary Alcohols. *J. Am. Chem. Soc.* **134**, 7117-7125. DOI: 10.1021/ja301252h
31. Bravin, C., Mason, G., Licini, G., and Zonta C. (2019). A Diastereodynamic Probe Transducing Molecular Length into Chiroptical Readout. *J. Am. Chem. Soc.* **141**, 11963−11969. doi: 10.1021/jacs.9b04151.

32. Bravin, C.; Badetti, E.; Scaramuzzo, F. A.; Licini, G.; Zonta, C. Triggering Assembly and Disassembly of a Supramolecular Cage. *J. Am. Chem. Soc.* 2017, **139** (18), 6456−6460.)
33. Pavlovic, R. Z., Zhiquan ,L., Güney, M., Lalisse, R. F., Hopf, R. G., Gallucci, J., Moore, C., Xie, H., Hadad, C. M., and Badjic´, J. D. (2019). Multivalent C-H···Cl/Br-C Interactions Directing the Resolution of Dynamic and Twisted Capsules. *Chem. Eur. J.* doi: 10.1002/chem.201903006
34. Zhiquan, L., Xie, H., Border, S. E., Gallucci, J., Pavlović, R. Z., and Badjić J. D. (2018). A Stimuli Responsive Molecular Capsule with Switchable Dynamics, Chirality, and Encapsulation Characteristics. *J. Am. Chem. Soc.* **35**, 11091-11100. doi: 10.1021/jacs.8b06190

Chapter II: New small tris(2-pyridylmethyl)amine-based hemicryptophane for predictable control of the ligand's helicity by chirality transfer

This second chapter will describe the study of a novel small molecular cage (**1**), which is directly composed of one CTV part and one tris(2-pyridylmethyl)amine (TPA) ligand, connected by three methylene –CH_2- bridges. At the beginning, we designed this small cage for the oxidation of methane. Indeed, previous works of our group, have demonstrated that hemicryptophane ligands can improve the catalytic efficiency and selectivity of the methane oxidation to methanol catalyzed by iron complexes (See chapter I). We therefore hoped that a structurally contracted cage, displaying a small cavity, might increase the capture of the methane molecule. But we found that the cage's cavity was too small to encapsulate the methane molecule (because of the self-encapsulation of one of the three methylene –CH_2N of the TPA unit). Interestingly, the crystal structure of **1** reveals that the inherent chirality of the CTV cap was transmitted to the TPA part (helical arrangement). Due to the coordination ability of the pyridines and the tertiary amine of the TPA ligand, we also tried to prepare new metal complexes with controlled helicity. The corresponding results will be presented in the following section under the form of an article that has been published in 2019 in the journal *Chemical Communications.* In order to facilitate the reading of the article, the corresponding experimental characterizations (Supplementary informations) have been incorporated in the annex n°1, which follows the article.

The second section of this chapter will present the preliminary catalytic tests that have been preformed in order to evaluate if this new enantiopure cage-ligand could bring positive effect on copper-catalyzed enantioselective transformations. Finally, we will present DFT (density functional theory) calculations of the molecular cage configuration in the last section of this chapter, which can help to rationalize the peculiar structural properties of **1**, further explaining the chirality transfer from its CTV to its bottom part (the formation of propeller arrangement).

II.1 Chirality Transfer in a Cage Controls the Clockwise / Anticlockwise Propeller-like Arrangement of the tris(2 pyridylmethyl)amine Ligand

*A predictable control of the propeller arrangement of the tris(2-pyridyl-methyl)amine (TPA) ligand was achieved through the preparation of the smallest hemicryptophane **1**. This novel designed cage displays a chirality transfer from its northern unit to the TPA ligand. **1** can coordinate Cu(I), yielding in a rare T-shaped complex with controlled helicity of the TPA-Cu(I) core.*

The tris(2-pyridylmethyl)amine (TPA) ligand has been widely reported as a convenient and efficient scaffold for the development of metal-based complexes, catalysts and sensors. In particular, structural and functional models of Iron(II),[1-3] and Copper(I),[4-6] mono-oxygenases based on the TPA unit have been developed. TPA derivatives have also been involved in the preparation of stereodynamic metal complexes applied in chiral sensing and enantiomeric excess determination.[7-11] Furthermore, this tripodal ligand has recently aroused a growing interest in the field of supramolecular architectures. It has been indeed successfully incorporated into supramolecular cages, aiming at developing switchable dynamic architectures,[12] or at providing new scaffold for coordination, and host-guest chemistry in confined spaces.[13, 14]

Due to its broad interest, its versatility, and its conformational dynamic nature, the control of the chirality of this C_3 symmetrical ligand is highly desirable. Because of the propeller-like arrangement of its pyridine units, the TPA ligand rapidly interconvert between two enantiomeric conformations. Controlling the sense of the pyridines twist is therefore key to access new organic chiral architectures with potential application in sensing of biological molecules, enantioselective catalysis, or preparation of optically pure materials. The control of the dynamic of the propeller arrangement of the TPA ligand (left- or right-handed) has been initially achieved through synthetic modification of the TPA core such as incorporation of an alkyl group at one of the benzylic position.[15] Such modified ligands result in a shift of the equilibrium toward one of the two (right or left-handed) stereoisomers. More recently, Badjić and coworkers reported an elegant strategy based on the supramolecular functionalization of a cationic TPA derivative with an anionic C_3 symmetrical concave basket.[16] The static chirality of the basket results in the exclusive formation of left-handed Zn-TPA supramolecular complex via intermolecular ionic contact. Very lately, Zonta and coworkers observed a length-dependent inversion of the TPA helicity upon guest-binding in a supramolecular cage.[17]

We present herein a new approach to build TPA-based architectures displaying predictable and controlled arrangement of the propeller-like arrangement of the pyridines through its capping with a chiral C_3 symmetrical unit.

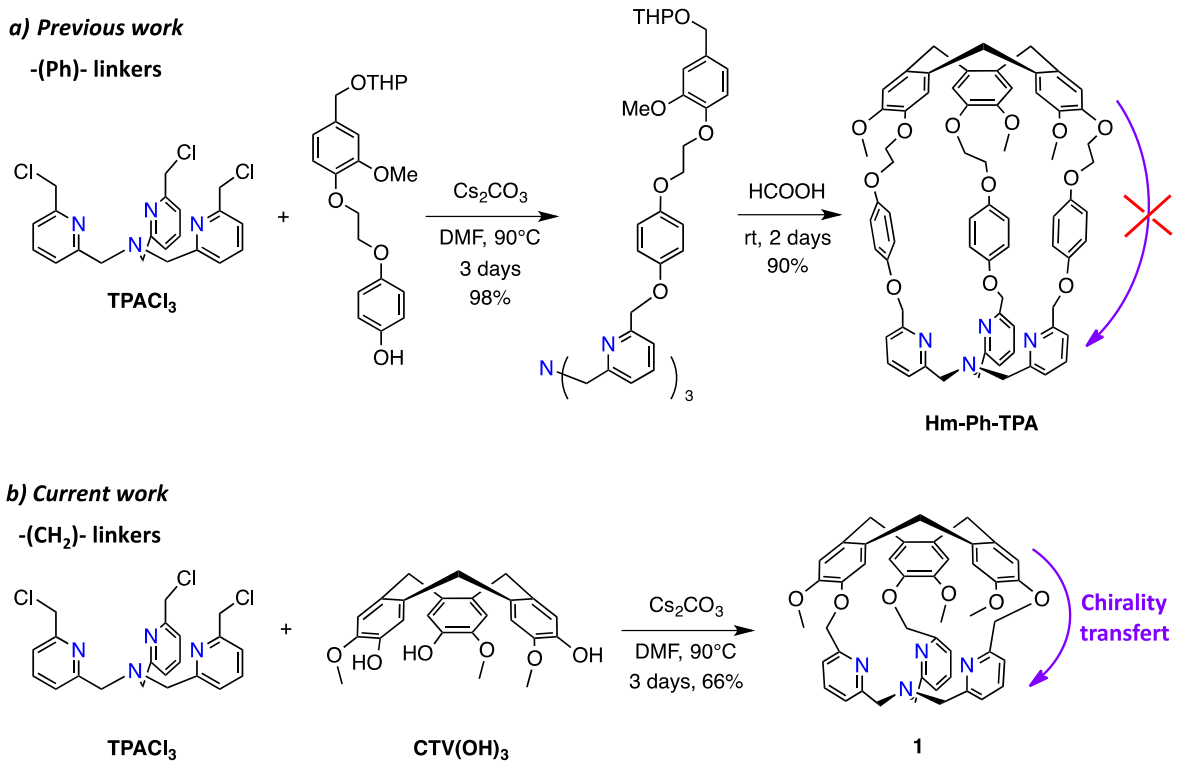

Figure 2.1 (a) Previously reported synthesis of Hemicryptophane **Hm-Ph-TPA**. (b) "1+1 coupling" strategy used for the synthesis of **1**.

Our group has recently incorporated a TPA ligand into an optically pure hemicryptophane organic cage **Hm-Ph-TPA** (Figure 2.1a).[18] **Hm-Ph-TPA** displays a chiral C_3 symmetrical cyclotriveratrylene (CTV) unit covalently linked to a TPA moiety through phenyl spacers. The corresponding iron(II) complex has been reported has an efficient bio-inspired catalyst for the oxidation of methane in confined space.[19] A careful look at its XRD structure indicates the formation of a triple-stranded helical arrangement of the phenyl linkers dictated by the chirality of the CTV unit (*P*- or *M*- configuration). However, no orientation of the three southern pyridines could be observed (See annex

page 25, Figure S12 and S13). Clearly, in **Hm-Ph-TPA**, the chiral CTV is situated too far from the southern TPA unit to induce any chirality transfer. On this basis, we envisioned that the building of hemicryptophane displaying shorter linkers might result in an efficient chirality transfer from the CTV to the TPA unit. We therefore design the new hemicryptohane **1**, which displays a CTV unit linked to a TPA moiety by simple methylene -CH_2- linkers, representing the smallest hemicryptophane ever reported.[20, 21] **1** was obtained in a 66% yield via the direct coupling of the CTV intermediate **CTV(OH)$_3$** and the TPA-trichloride precursor **TPACl$_3$** (Figure 2.1b). Compared to **Hm-Ph-TPA**, which was obtained following a "template approach",[20] the one step synthesis of **1** represents an alternative and more straightforward access to TPA-based capsules. Due to the chiral nature of its northern CTV unit, **1** is obtained as a racemate **(±)-1** that could be optically resolved using chiral HPLC (see annex page13). Enantiopure **(-)-(*M*)-1** and **(+)-(*P*)-1** hosts have been indeed efficiently separated with ee values > 99.5% and their absolute configuration determined through electronic circular dichroism (ECD) analysis (Figure 2.2a).[22, 23]

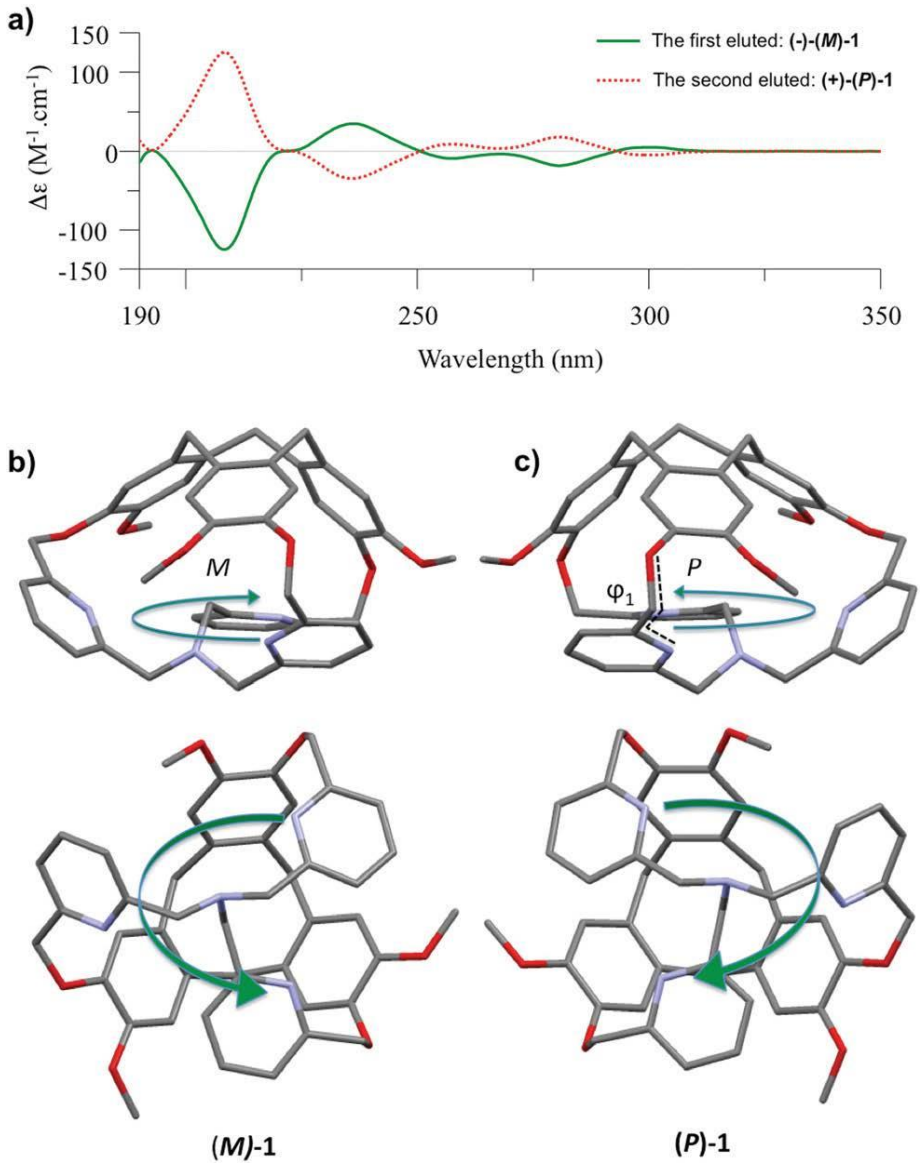

Figure 2.2 (a) ECD spectra of **(-)-(*M*)-1** (green) and **(+)-(*P*)-1** (red), in CH_3CN at 298K. Diagram of the X-ray crystal structure of **(±)-1** : (b) **(*M*)-1** and (c) **(*P*)-1**. Green arrow: orientation of the arrangement of the pyridine moiety. Twist of the pyridines, reflected by the O-C-C-N torsion φ (φ = (φ1 + φ2 + φ3) /3), have been estimated from these structures: φ= -68.6° for **(*M*)-1** and φ= +68.6° for **(*P*)-1** (**(*M*)-1** : φ1 = -8,5° φ2 = -106,4° φ3 = -90,75°, and (P)-1 : φ1 = +8,5° φ2 = +106,4° φ3 = +90,75°).

Single crystals of **1**, suitable for X-ray diffraction, were obtained by slow diffusion of Et_2O to a solution of cage in CH_2Cl_2. **1** crystalizes with an asymmetric unit containing four molecules with two of each enantiomers corresponding to CTV with *M*- and *P*-configuration (Figure S2, annex page 3). The resulting XRD structure confirms the

functionalization of the TPA ligand by the bowl-shaped CTV unit, which describes a well-defined cavity. Contrary to **Hm-Ph-TPA**, no CH_2Cl_2 molecule is observed inside the cavity of **1**, which appears to be too small for encapsulation of exogenous organic solvent molecules. Instead, one of the three methylene –**CH₂**-N of the TPA unit resides inside the hydrophobic cavity of **1** with the two C-H bonds pointing toward the inner space. The two other -CH_2- are pointing outward (Figure 2.2). Such "self-encapsulation of one –**CH₂**-N therefore results in a C_1 symmetrical conformation of **1**. Interestingly, a remarkable propeller-like arrangement of the three pyridine of the southern unit, imposed by the chirality of the northern CTV, is clearly observed. The hemicryptophane **(*M*)-1** bearing a *M*- CTV unit, indeed imposes a left-handed (*M*) propeller-like arrangement of the TPA's pyridines while the **(*P*)-1** counterpart displays a right-handed (*P*) helicity (Figure 2.2). Importantly, such propeller-like arrangement of the pyridine units could not be observed in the previously reported hemicryptophane **Hm-Ph-TPA**. In solution, the ^{1}H NMR spectrum of **1** displays identical, sharp and well-defined signals for the protons belonging to the pyridine (H_b, H_c, H_d), the -CH_2- linkers ($H_{e,e'}$) and CTV unit (H_h, H_g, H_f, $H_{i,i'}$), indicating that **1** presents, on average, a C_3 symmetrical structure in $CDCl_3$, at room temperature (Figure 2.3a). The assignment of these resonances was achieved through 2D-NMR experiments (See annex page 4). Contrary to **Hm-Ph-TPA**,[18, 19] and other reported TPA-based cages,[12] **1** displays clearly distinct signals for the methylene protons (-**CH₂**-N) at the alpha position of the tertiary amine ($H_{a/a'}$, $\Delta\delta$ = 0,66 ppm) revealing their diastereotopic character. It should be noted that the highly symmetrical ^{1}H-NMR spectrum observed for **1** in solution, at 298K, contrasts with the C_1 symmetrical structure observed in the solid-state. This is easily explained by a fast conformational exchange between the inward and outward orientations of the -**CH₂**-N methylene groups at 298K in solution. Interestingly, 2D-NMR NOESY experiment reveals through-space correlations between methylene proton $H_{a,a'}$ and aromatic protons $H_{f,g}$ belonging to the northern CTV unit as well as between signal corresponding to the protons H_b, H_c of the pyridines and the one corresponding to the -O**CH₃** of the CTV, H_h (Figure S3, annex page 4). The latter imply a close proximity between the "southern" pyridines and the CTV unit that confirm that the *C1* symmetrical form of **1** (observed in solid state) is also adopted in solution (but with a dynamic exchange between the inner and the outer -**CH₂**-N) (Figure S4, annex page 4). Variable temperature (VT) ^{1}H-NMR analysis of **1**, indicates a particularly fast motion as broadening but no complete decoalescence of the signals was observed in the 298-220K temperature range (Figure S5, annex page 5).

Could this dynamic behaviour be slow down to observed the C_1 symmetrical conformation of **1** by VT ^{1}H-NMR studies? Badjić and co-workers have recently shown that the protonation of the tertiary amine of covalent TPA-based capsule with HCl, result in less dynamic and more preorganized receptors. In this vein, we assumed that the protonation of the TPA moiety of **1** might slow down the dynamic –**CH$_2$**-N exchange motion observed from 298 to 220K. Our attempts lead to success as the VT-NMR study of the protonated racemate **[1.H]-Cl** (See annex page 8), displays a progressive appearance of a new set of signals, with more complex pattern, upon decreasing the temperature to 250K-215K (Figure S7, see annex page 6). Compared to the effective 3-fold symmetry (on average) observed for **[1.H]-Cl** at 298K, these new signals appear split, indicating a loss of the cage symmetry (Figure S8, annex page 8). Clearly, at lower temperature, the –**CH$_2$**-N exchange become slower on the NMR time scale allowing for the observation of the C_1 symmetrical configuration of **[1.H]-Cl**. Like **1**, the self-encapsulation of one methylene **CH$_2$**-N group in the hydrophobic cavity of **[1.H]-Cl** was observed in its XRD structure (Figure 2.3b).

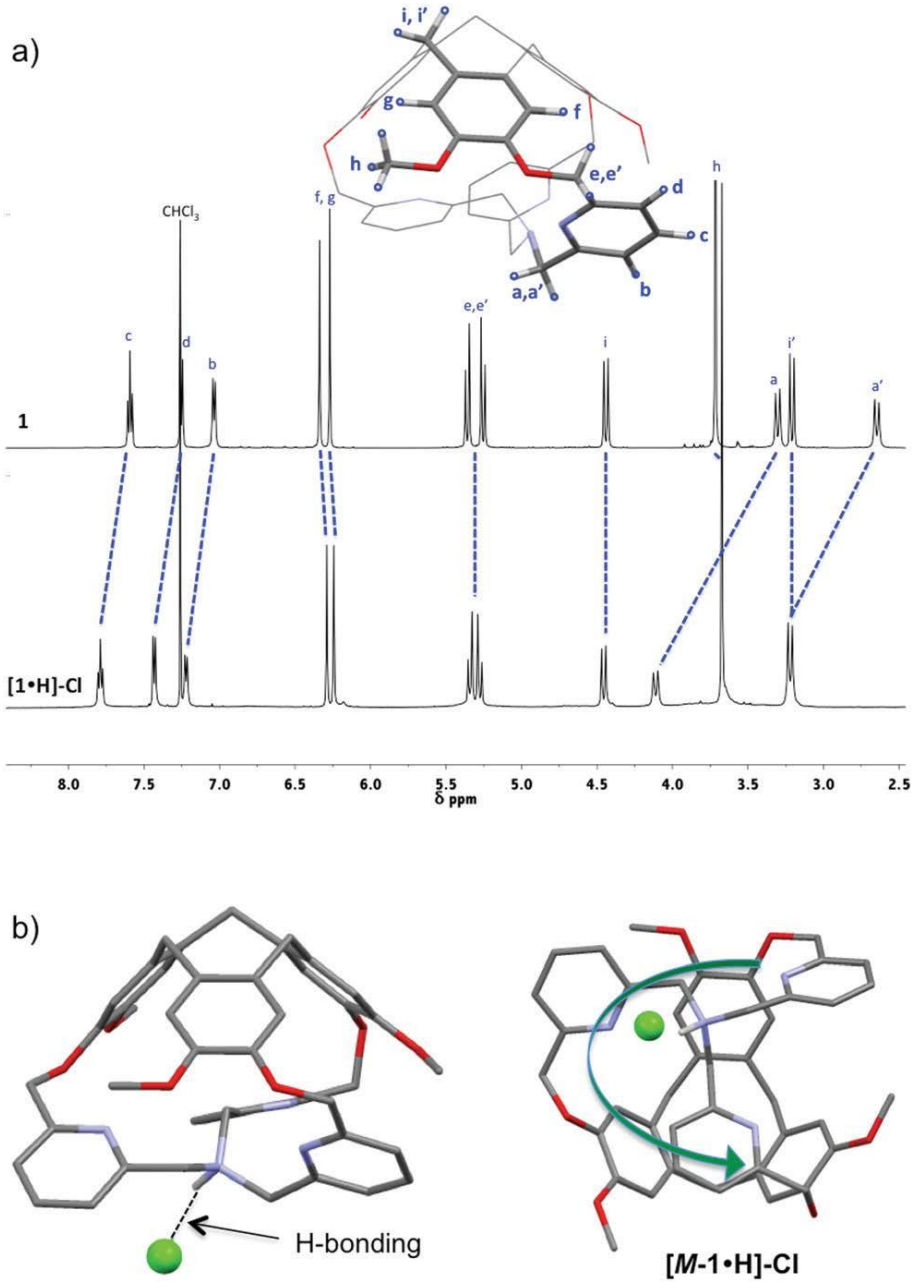

Figure 2.3 (a) Partial ^{1}H NMR spectra (500 MHz, CDCl3, 298 K) of **1** (top) and **[1·H]-Cl** (bottom). (b) Side (left) and south (right) views of the X-ray crystal structure of the protonated capsule **[(M)-1·H]-Cl**. Only the hydrogen atom belonging to the protonated tertiary amine has been included for clarity.

Importantly, this structure confirms a propeller-like organization of the three pyridine of the TPA unit that is imposed by the chirality of the northern CTV. The hemicryptophane bearing a *M*-CTV leads to the anticlockwise propeller-like arrangement of the TPA

(Figure 2.3b), while the *P*-CTV induces the clockwise configuration (Figure S9, annex page 9). Altogether, these results demonstrate that (*i*) the C_1 symmetrical form of **1** (observed in the solid state) is involved in the conformational exchange observed in solution and (*ii*) the chirality transfer from the CTV to the TPA unit is maintained in the protonated form of **1**.

On this basis, we then explore the possibility of performing metal-complexation at the propeller-shaped TPA unit of **1**. Such coordination might indeed results in (*i*) the breaking of the propeller-like arrangement of the pyridines or, more interestingly, (*ii*) to the formation of a new kind of enantiopure metal complex with a controlled chirality at the TPA coordination unit. To demonstrate the ability of **1** to form metallo-complexes, we studied its complexation properties toward copper(I) chloride salt. Various CuCl complexes of TPA derivatives have been reported over the past decade as structural model for copper containing oxygenase enzyme,[24, 25] or atom transfert catalyst.[26, 27] Although dissociation of one pyridyl moiety have been reported for **Cu^{I}(TPA)(Cl)** in solution, the corresponding solid state structures always displayed a pentacoordinated copper in an achiral trigonal-bipyramidal (TBP) coordination geometry.[27] The **Cu^{I}(1)(Cl)** complex, prepared by reacting **1** with 1 equivalent of copper(I) chloride in THF (See annex page 7), affords single crystals suitable for X-ray diffraction (Figure 2.4a). Interestingly, while XRD structures of hemicryptophanes **1** and [**1.H]-Cl** displayed racemic crystals of co-crystallized *M*- and *P*- enantiomers, **Cu^{I}(1)(Cl)** affords an enantiopure crystal which solely displayed the *M*-enantiomer in its asymmetric unit. The latter suggests an unusual narcissistic conglomerate of **Cu^{I}(1)(Cl)** in the crystalline-state. Remarkably, the left-handed (*M*-) propeller-like configuration of the TPA, imposed by the *M*-CTV cap, remains unchanged upon binding of CuCl. **Cu^{I}(1)(Cl)** therefore displays an helical asymmetry dictated by the chirality of the northern CTV unit. The copper center in **Cu^{I}(1)(Cl)**, displays a highly unusual trigonal planar T-shaped coordination mode. A tri-coordinated mononuclear copper(I) centre, in a distorted trigonal plane that comprises the tertiary amine, one pyridine, and chlorine ion in *trans* to the pyridine ligand, is indeed observed (Figure 2.4a). Cu-N bond lengths of 2.543 Å and 1.939 Å were respectively found for the tertiary amine and the pyridine ligands, along with a 2.123 Å long Cu-Cl bond. Angles of 76°, 112° and 158° were respectively found for N-Cu-Pyridine, N-Cu-Cl and Pyridine-Cu-Cl, attesting for a distorted T-shaped coordination mode. Importantly ^{1}H-NMR analysis confirms that such C_1 symmetrical structure is

retained in solution (Figure S10, annex page 23). Indeed, compared to the *C*$_3$ symmetrical (on average) spectra of **1**, all signals of **Cu^{I}(1)(Cl)** split, indicating a loss of the cage symmetry. For instance, the signal belonging to the O-**CH$_3$** protons (H$_h$), resonating as a single singlet in **1** (at 3.72 ppm), are resonating as three distinct singlets in the case of **Cu^{I}(1)(Cl)** (at 3.93, 3.78 and 3.55 ppm, Figure 2.4b). To the best of your knowledge, the latter represents a totally unprecedented geometry for TPA-based copper(I) complexes. Such coordination-mode interestingly resembles the one of some enzymatic active sites which display Cu(I) center in a T-Shaped geometry such as lytic polysaccharide monooxygenases LPMOs (displaying Cu(I)-N(His) bond lengths of 1.9 Å).[28]

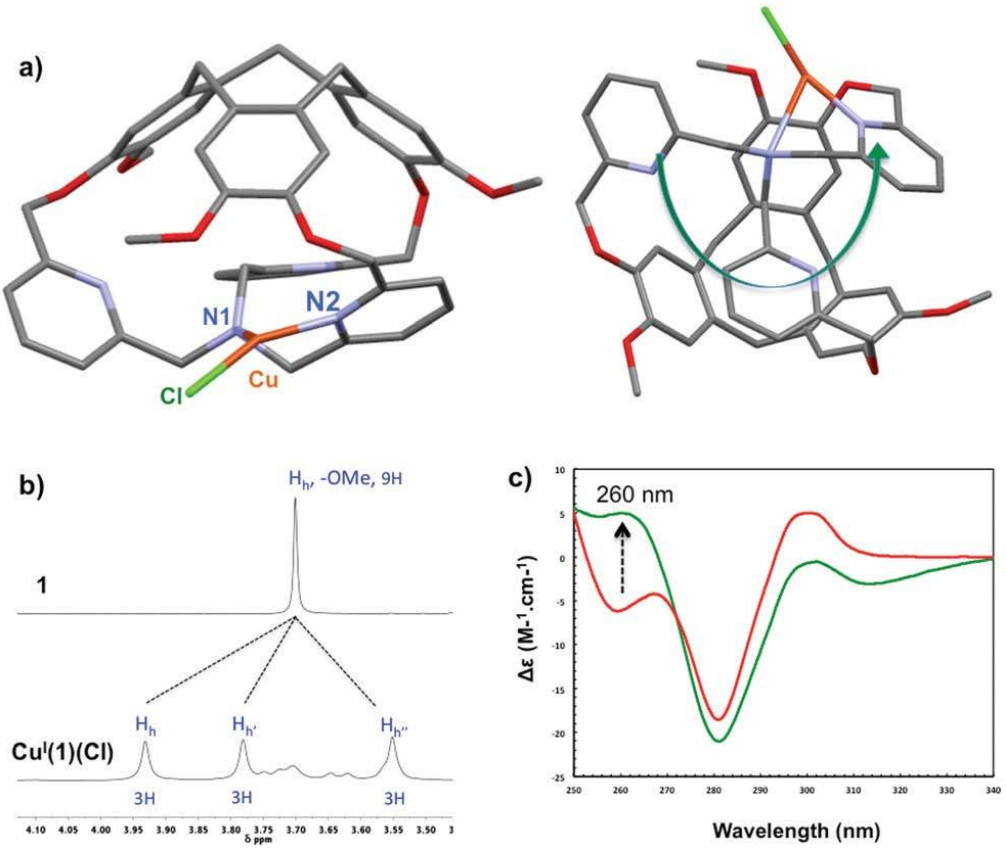

Figure 2.4 (a) Side (left) and south (right) views of the X-ray crystal structure of the copper(I) complex **(*M*)-Cu^{I}(1)(Cl)** displaying a ***M*-CTV** unit that imposes a ***M***-propeller like arrangement of the TPA ligand. (b) Comparison of the partial ^{1}H NMR spectra (500MHz, 260 K, $CDCl_3$) of **1** and **Cu^{I}(1)(Cl)**. Comparison of the ECD spectra of the enantiopure (***M*)-1** ligand (0.57 mM, red) and its corresponding CuCl complex **(*M*)-Cu^{I}(1)Cl** (0.51 mM, green), in CH_2Cl_2 at 298 K.

Finally, the enantiopure **(*M*)-Cu^{I}(1)(Cl)** complex, prepared form the optically resolved **(*M*)-1** ligand, was analysed by ECD spectroscopy. Compared to **(*M*)-1**, the metallated **(*M*)-Cu^{I}(1)(Cl)** displayed a positive ECD couplet at 260 nm characteristic for the electronic π-π* transition of the TPA-metal chromophore.[16, 29] Along with XRD and ^{1}H-NMR studies, the ECD analysis therefore confirms that a transfer of chirality from the CTV unit to the (TPA)Cu^{I}(Cl) core occurs in both solid state and solution.

In conclusion, a novel variation on the TPA ligand is described incorporating a chiral CTV unit that imposes and controls the propeller arrangement of the pyridine moeties. Such remote control of the TPA helicity was unambiguously demonstrated (through XRD analysis), in hemicryptophane **1** as well as in its protonated **[1.H]-Cl** and metallated **Cu^{I}(1)(Cl)** forms. Importantly, the predictable chiral arrangement of the TPA ligand was maintained upon metallation of the hemicryptophane ligand, leading to novel chiral metal centre with highly unusual coordination mode in both solid state and solution. We envisioned that this new approach should find applications in the field of asymmetric catalysis and enantioselective recognition. Future work will indeed be devoted to the use of such metal-complexes as asymmetric catalysts and molecular receptors.

II.2 **Annex N°1:**

Experimental procedures and characterizations corresponding to the article:

Chirality Transfer in a Cage Controls the Clockwise/Anticlockwise Propeller-like Arrangement of the tris(2-pyridylmethyl)amine Ligand

1. Chemical and instrumentation

All reagents were commercial reagent grade and were used without further purification. **$TPACl_3$,**[S1] and **$CTV(OH)_3$,** [S2] (were obtained according to reported protocols.

Instrumentation

^1H NMR and ^{13}C NMR were recorded on a Bruker Avance III HD 300 MHz and 500MHz spectrometers. ^1H NMR and ^{13}C NMR chemical shifts δ are reported in ppm referenced to the protonated residual solvent signal. ESI-HRMS were performed on a SYNAPT G2 HDMS (Waters) mass spectrometer with API and spectra were obtained with TOF analysis. Measurements were realized with two internal standards. Electronic Circular Dichroism. ECD and UV spectra were measured on a JASCO J-815 spectrometer equipped with a JASCO Peltier cell holder PTC-423 to maintain the temperature at 25.0 ± 0.2°C. A CD quartz cell of 1 mm of optical pathlength was used. The CD spectrometer was purged with nitrogen before recording each spectrum, which was baseline subtracted.The baseline was always measured for the same solvent and in the same cell as the samples.The spectra are presented without smoothing and further data processing

2. Experimental procedure and characterisation

Synthetic procedure for 1

To a solution of **$CTV(OH)_3$** (408 mg, 1 mmol) and **$TPA(Cl)_3$** (440mg, 1.03 eq) in DMF(350 mL), Cs_2CO_3 (500 mg) was added in one portion. Then the solution was stirred overnight at 90°C under argon. The mixture was then allowed to return to room temperature, evaporated and water was added (200 mL). The aqueous mixture was extracted with CH_2Cl_2 (3x 100 mL). The combined organic phases were washed with 1M aqueous NaOH (100 mL), washed with brine (100 mL), dried over Na_2SO_4, filtered and evaporated to dryness. The residue was purified purified by column chromatography on silica (eluent : CH_2Cl_2 / CH_3OH; 12:1) to afford a white solid. Yield: 66%. ^1H NMR (300 MHz, $CDCl_3$) δ ppm: 7.59 (t, J = 7.6 Hz, 3H, PyH), 7.26 (s, 3H, PyH), 7.04 (d, J = 7.6 Hz, 3H, PyH), 6.34 (s, 3H, ArH), 6.27 (s, 3H, ArH), 5.36 (d, J = 12.8 Hz, 3H,OCH_2Py), 5.25 (d, J = 12.8 Hz, 3H,OCH_2Py), 4.44 (d, J = 13.7 Hz, 3H, $ArCH_2Ar$), 3.72 (s, 9H, OCH_3), 3.30 (d, J = 14.0 Hz, 3H, $PyCH_2N$), 3.21 (d, J = 13.8 Hz, 3H, $ArCH_2Ar$), 2.64 (d, J = 14.1 Hz, 3H, $PyCH_2N$). HRMS (ESI, [M + H]+): m/z: calcd for for $C_{45}H_{42}N_4O_6$ 735.3104, found 735.3165. ^{13}C NMR (101 MHz, 298K, $CDCl_3$): δ ppm: 159.14, 154.47, 149.63, 144.80, 136.11, 133.72, 131.29, 124.00, 120.52, 120.44, 113.63, 71.80, 57.00, 56.22, 36.26.

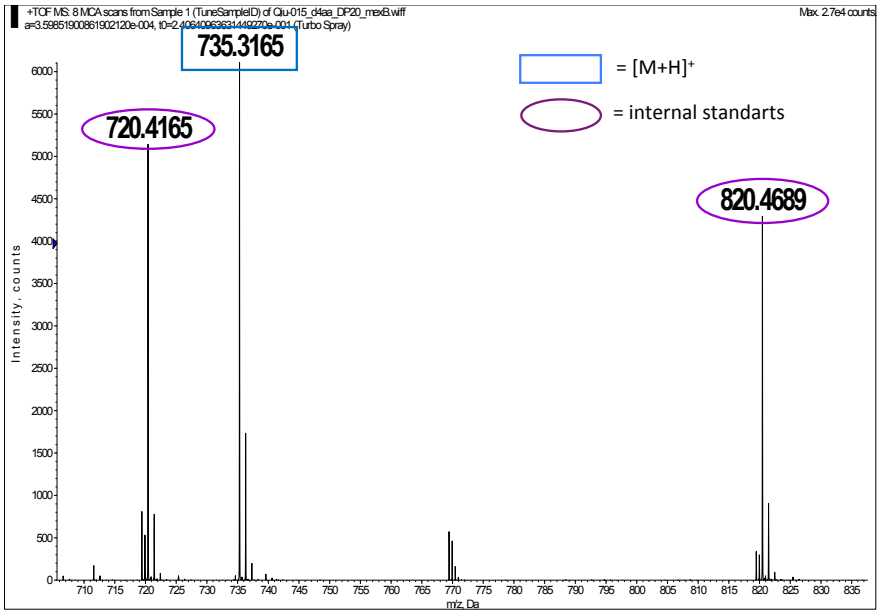

Spectra S1. ESI-HRMS spectra of **1** in CH_2Cl_2 / MeOH. The isotopic pattern at m/z = 735.3165 can be attributed to **1**.H+ ($m/z_{\text{calculated}}$ = 735.3104).

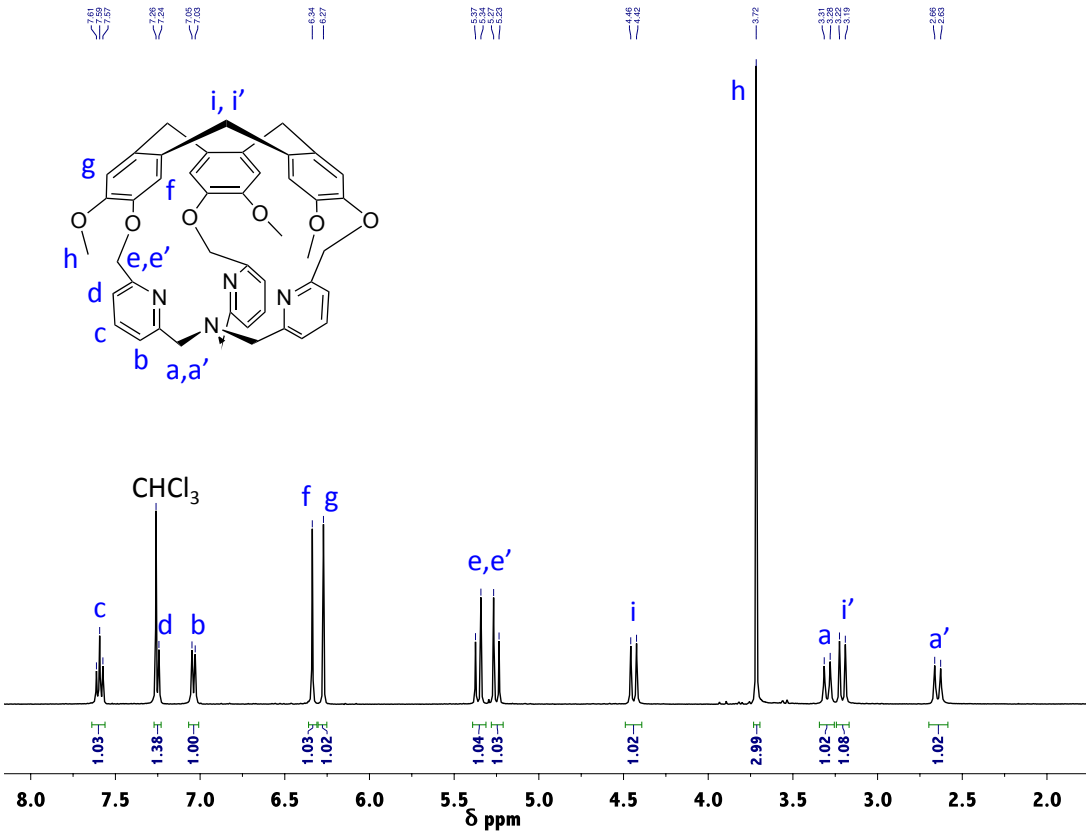

Spectra S2. ^{1}H-NMR spectra ($CDCl_3$, 300 MHz) of hemicryptophane **1**, at 298K

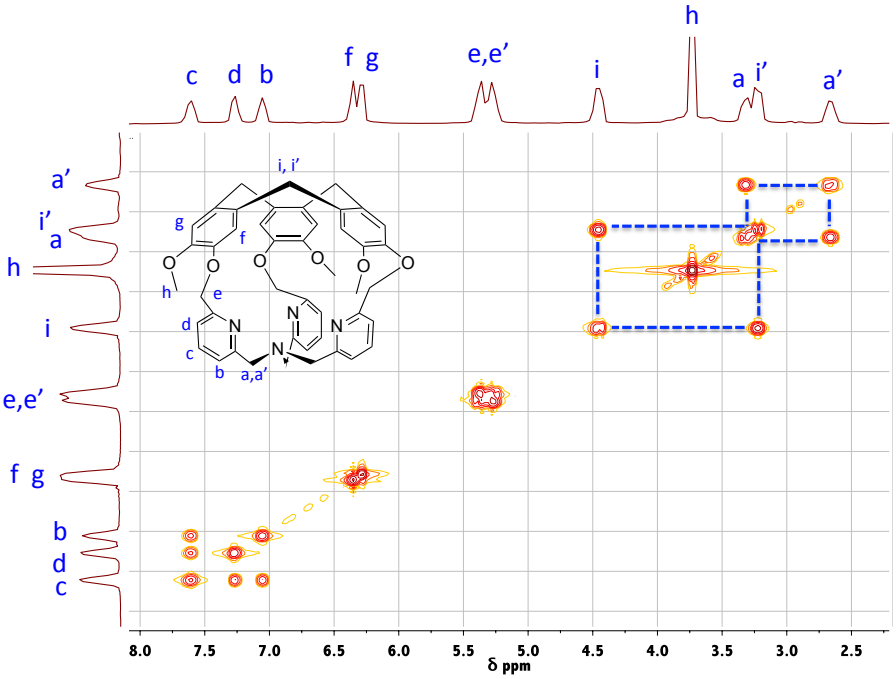

Spectra S3. 2D COSY-NMR spectra ($CDCl_3$, 300MHz) of **1** in $CDCl_3$, at 298K

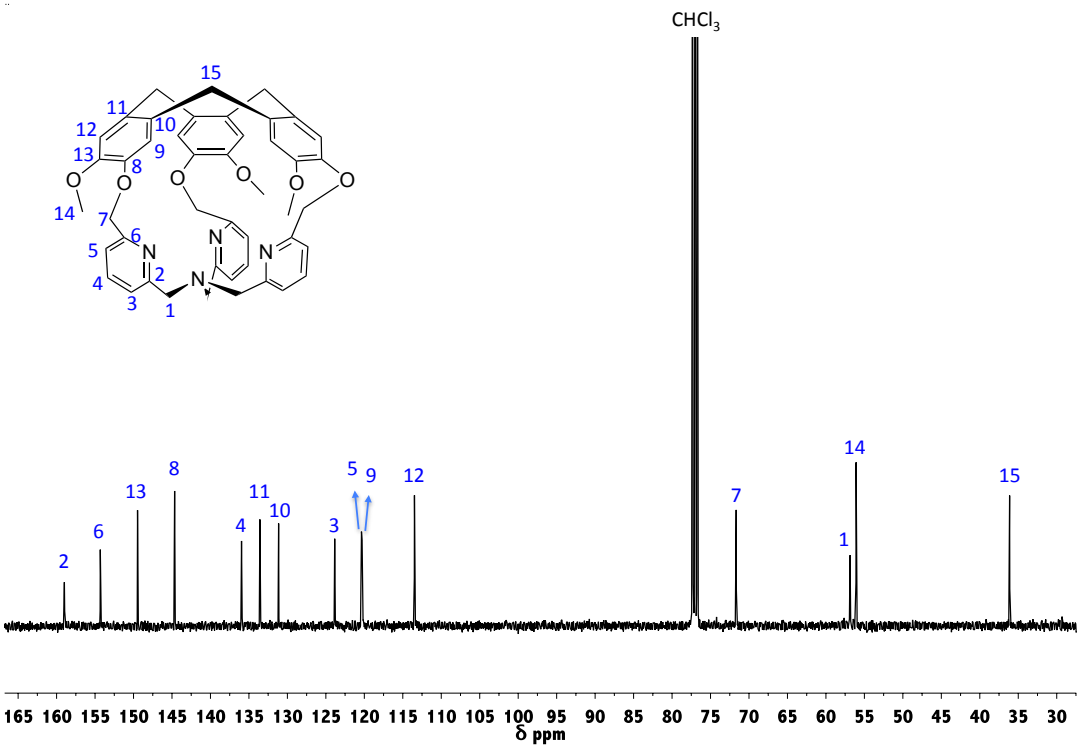

Spectra S4. ^{13}C-NMR spectra ($CDCl_3$, 101 MHz) of **1** in $CDCl_3$, at 298K.

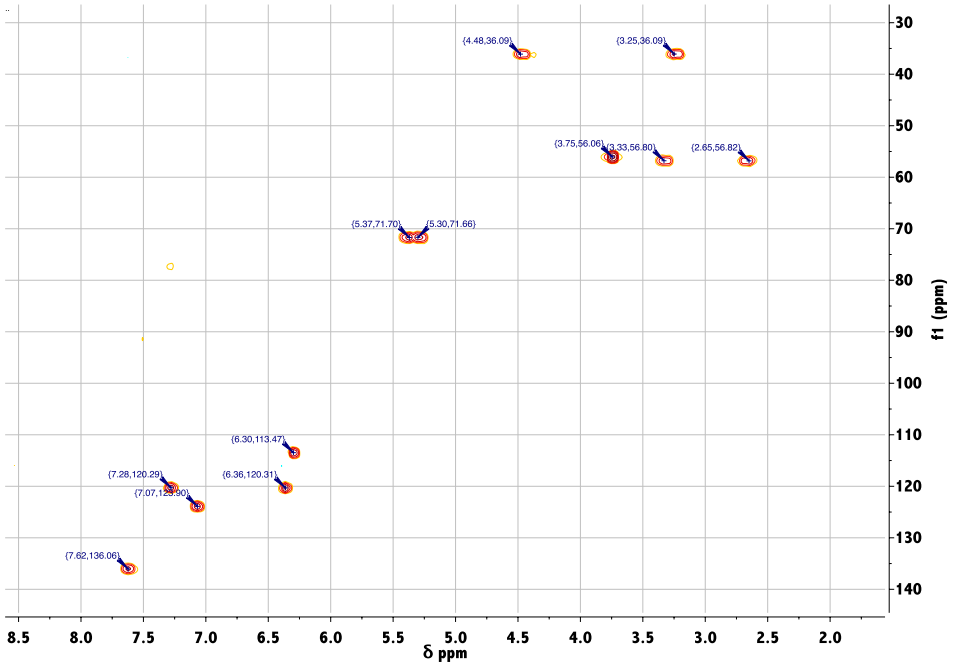

Spectra S5. ^{1}H-^{13}C HSQC-NMR spectra ($CDCl_3$, 300MHz) of **1** in $CDCl_3$, at 298K

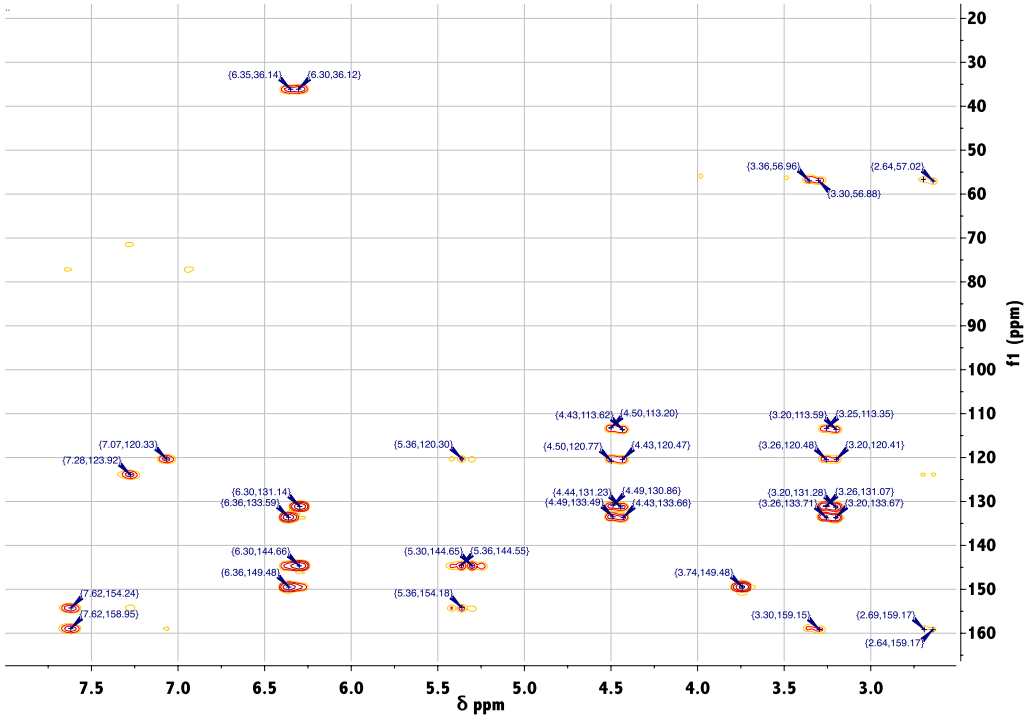

Spectra S6. ^{1}H-^{13}C HMBC-NMR spectra ($CDCl_3$, 300MHz) of **1** in $CDCl_3$, at 298K

Synthetic procedure for [1.H]-Cl

Protonation of the tertiary amine of **1** was achieved through its treatment with concentrated HCl in a CH_2Cl_2/CH_3OH solvent mixture, resulting in the formation of the protonated racemate **[1.H]-Cl**. Purity of the resulting adduct was further confirmed through ^{1}H-NMR and X-Ray diffraction studies. The ^{1}H-NMR spectrum of **[1.H]-Cl** (298K, $CDCl_3$) display, on average, a C_3 symmetrical structure with the characteristic signal of the quaternary H-N+ resonating at 12.00 ppm (Spectra S5). Compared to **1**, **[1.H]-Cl** display downfield shifted signal for the proton belonging to the pyridine (Hb, Hc, Hd) and the methylene HN+-CH_2 (Ha,a'). Proton belonging to the CTV unit (Hh, Hg, Hf, Hi,i') were less affected, confirming that the protonation takes place at the southern part of the molecule. Interestingly, the methylene protons (-CH_2-) at the alpha position of the quaternary amine of TPA (Ha/a' resonating at 4.11 and 3.21 ppm) remain diastereotopic with a gap of 0.9 ppm.

Single crystals of **[1.H]-Cl**, suitable for X-ray diffraction, were obtained by slow diffusion of Et_2O to a solution of cage in CH_2Cl_2 / MeOH. It display an asymmetric unit containing two of each *M*- and *P*- enantiomers of **[1.H]-Cl** (Fig. S9). For both enantiomers identical distances between the quaternary ammonium proton N+-H and the chlorine atom are observed (DN-H--Cl= 2.104 Å, ΘN-H—Cl = 153.29°), indicating for H-bonding interactions. It should be noted that, in both cases, the chlorine anion is engaged in a second hydrogen bond with an exogeneous molecule of methanol (DO-H--Cl = 2.440 Å, ΘO-H—Cl = 159.47°, see Figure S9).

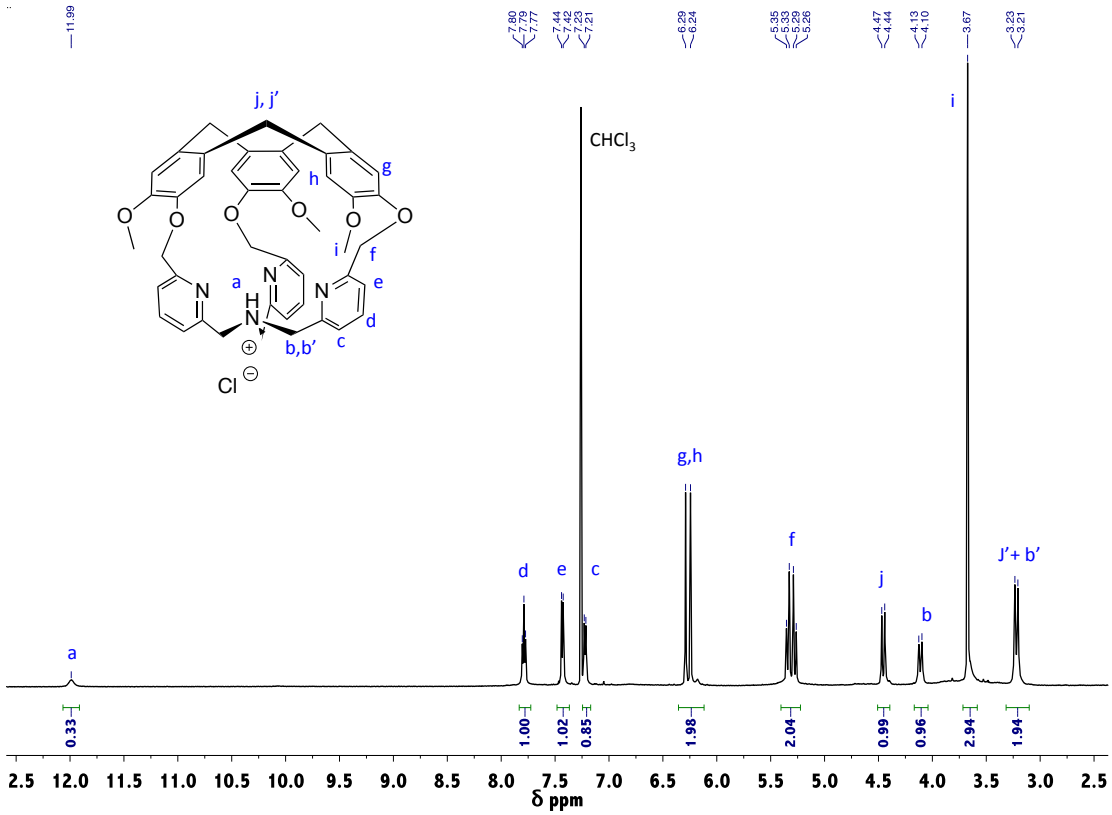

Spectra S7. ^{1}H-NMR spectra ($CDCl_3$, 300 MHz) of [**1.H]-Cl**, at 298K

Synthetic procedure for $Cu^{I}(1)(Cl)$

CuCl (1.35 mg, 0,0136 mol, 1.0 equiv.) was added, at room temperature to a stirred solution of **1** (10 mg, 0.0136 mmol, 1.0 equiv.) in THF (2 mL). The metallation occurred immediately and a pale yellow solid precipitated within minutes. The resulting pale yellow solid was isolated by filtration, washed with THF and dried in vacuo to give **$Cu^{I}(1)(Cl)$** in a 88% yield. ^{1}H-NMR spectrum of **$Cu^{I}(1)(Cl)$** at 298K display broad signals while its spectrum recorded at 260K gives well-defined and sharp signals (Spectra S6, figure S10). HRMS (ESI, $[M + Na]^{+}$): m/z calcd for $C_{45}H_{42}N_4O_6CuClNa$ 855.1981 found 855.1985. ^{1}H NMR (500 MHz, $CDCl_3$, 260K) δ ppm: 8.47 (d, 1H, PyH), 7.91 (m, 1H, PyH), 7.82 (t, 1H, PyH), 7,60 (t, 1H, PyH), 7,54 (d, 1H, PyH), 7,35 (d, 1H, PyH), 7.30 (d, 1H, PyH), 7.06 (broad, 1H, PyH), 6.94 (d, 1H, PyH), 6.45 (s, 1H, ArH), 6.36 (s, 1H, ArH), 6.12 (s, 1H, ArH), 6.01 (s, 1H, ArH), 5.88 (d, 1H, OCH_2Py), 5.76 (s, 1H, ArH), 5.72 (d, 1H, OCH_2Py), 5.47 (d, 1H, OCH_2Py), 5.35 (d, 1H, OCH_2Py), 5.31 (s, 1H, ArH), 4.98 (d, 1H, OCH_2Py), 4.84 (d, 1H, OCH_2Py), 4,45 (d, 1H, $ArCH_2Ar$), 4,30 (t, 2H, $ArCH_2Ar$), 3.93 (s, 3H, OCH_3), 3.78 (s, 3H, OCH_3), 3.73 (d, 1H, $PyCH_2N$), 3.71 (br s, 1H, $PyCH_2N$), 3.63 (d, 1H, $PyCH_2N$), 3.55 (s, 3H, OCH_3), 3.22 (m, 2H, $ArCH_2Ar$), 2.99 (d, 1H, $ArCH_2Ar$), 2.79 (d, 1H, $PyCH_2N$), 2.34 (d, 1H, $PyCH_2N$), 0.30 (d, 1H, $PyCH_2N$).

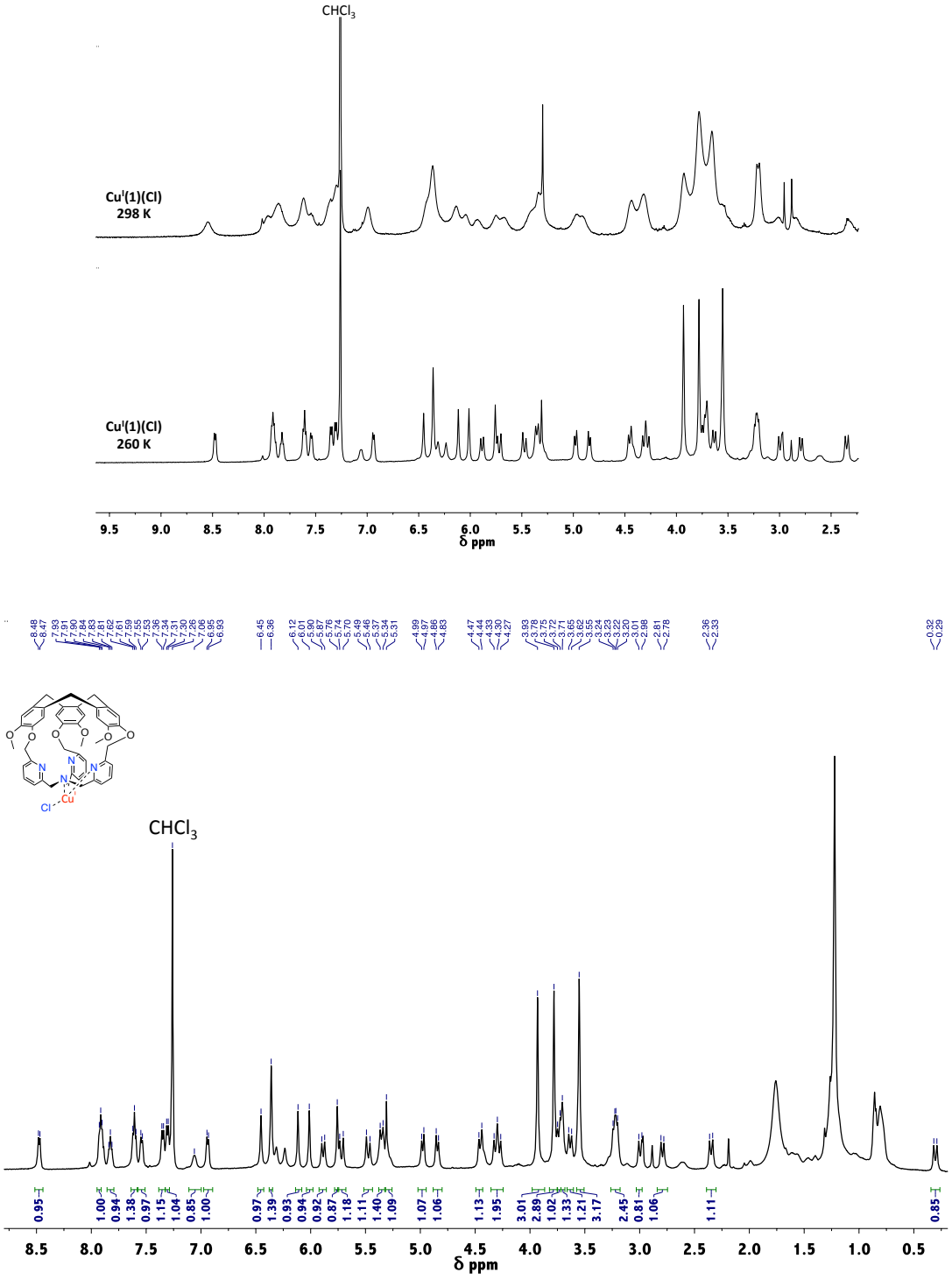

Spectra S8. Comparison of the ^{1}H-NMR spectra of **Cu^{I}(1)(Cl)**, at 298k and 260K. (Top). ^{1}H-NMR spectra ($CDCl_3$, 500 MHz) of **Cu^{I}(1)(Cl)**, at 260K (bottom), all signals corresponding to protons of **Cu^{I}(1)(Cl)** (integrated signals), have been assigned accordingly to the 2D COSY NMR experiment (spectra S9).

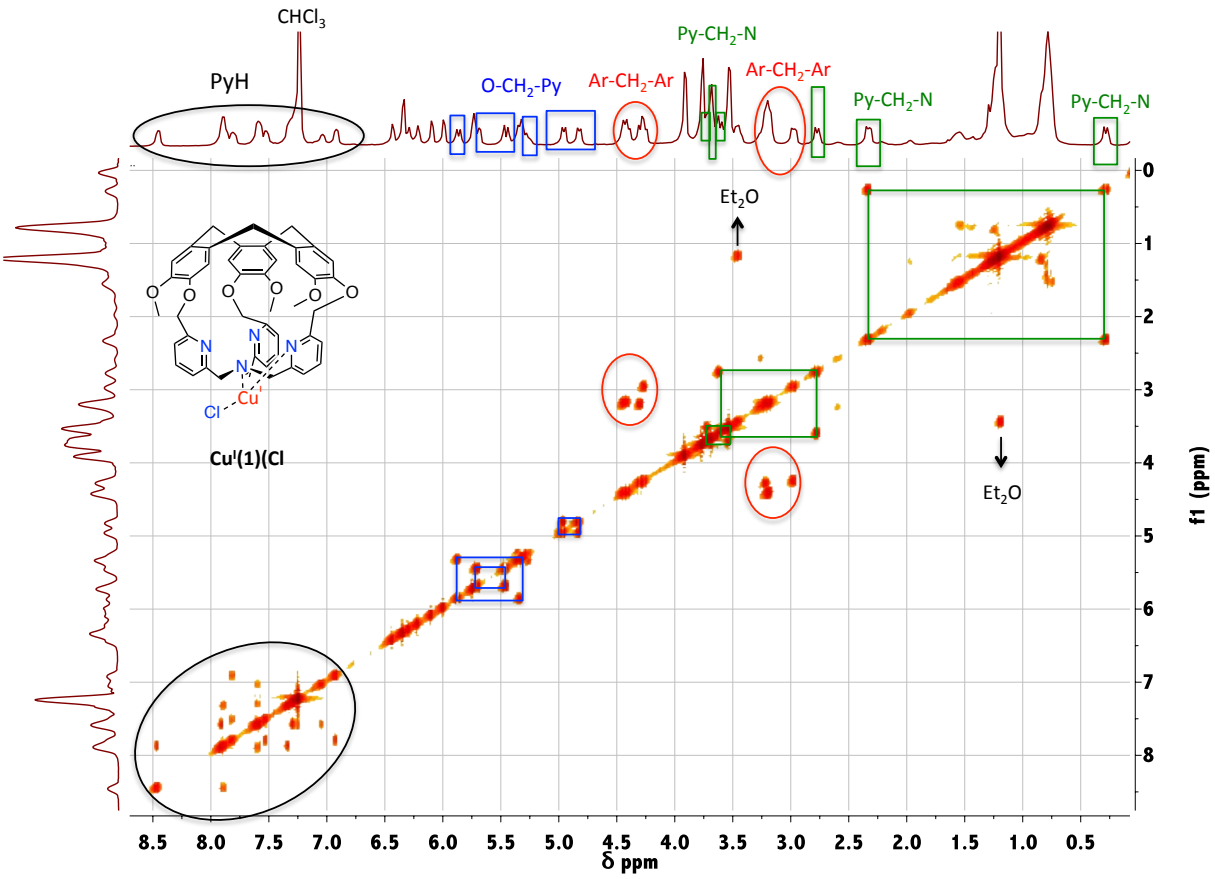

Spectra S9. 2D COSY-NMR spectra ($CDCl_3$, 300MHz) of **Cu^{I}(1)(Cl)** in $CDCl_3$, at 260K.

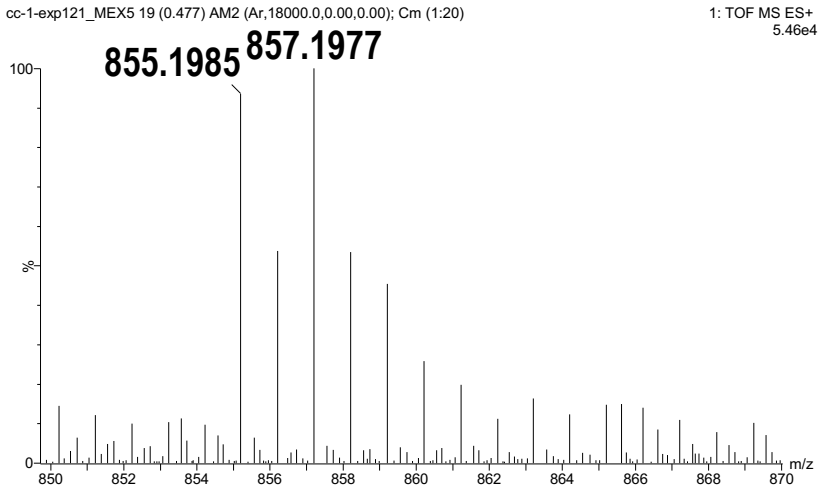

Spectra S10. ESI-HRMS spectra of **Cu^{I}(1)(Cl)** in CH_2Cl_2 / MeOH. The istopic pattern at m/z = 855.1985 can be attributed to **Cu^{I}(1)(Cl)**.Na+ ($m/z_{\text{calculated}}$ = 855.1981).

Single crystal X-ray Diffraction Data

- **1** (CCDC 1951499)

Single crystals of $C_{45}H_{42}N_4O_6$ (**1**) were crystallized by slow diffusion of Et_2O in a CH_2Cl_2 solution of the compound. A suitable crystal was selected and mounted on a SuperNova, Dual, Cu at home/near, AtlasS2 diffractometer. The crystal was kept at 253.00(10) K during data collection. Using Olex2, [S3] the structure was solved with the ShelXT, [S4] structure solution program using Intrinsic Phasing and refined with the ShelXL, [S5] refinement package using Least Squares minimisation.

Empirical formula	C45H42N4O6
Formula weight	734.82
Temperature/K	253.00(10)
Crystal system	monoclinic
Space group	$P2_1/c$
a/Å	10.02810(10)
b/Å	18.2669(2)
c/Å	20.2604(2)
β/°	98.4730(10)
Volume/Å3	3670.84(7)
Z	4
ρcalcg/cm3	1.330
μ/mm-1	0.718
F(000)	1552.0
Crystal size/mm3	0.14 × 0.12 × 0.06
Radiation	CuKα (λ = 1.54184)
2Θ range for data collection/°	6.548 to 142.092
Index ranges	-12 ≤ h ≤ 11, -22 ≤ k ≤ 21, -24 ≤ l ≤ 23
Reflections collected	34483
Independent reflections	7044 [Rint = 0.0231, Rsigma = 0.0159]
Data/restraints/parameters	7044/0/499
Goodness-of-fit on F2	1.041
Final R indexes [I>=2σ (I)]	R1 = 0.0468, wR2 = 0.1246
Final R indexes [all data]	R1 = 0.0530, wR2 = 0.1302
Largest diff. peak/hole / e Å-3	0.41/-0.29

- **[1.H]-Cl** (CCDC 1951501)

Single crystals of $C_{46}H_{47}ClN_4O_7$ **([1.H]-Cl**) were crystallized by slow diffusion of Et_2O in a CH_2Cl_2 / MeOH solution of the compound. A suitable crystal was selected and mounted on a SuperNova, Dual, Cu at home/near, AtlasS2 diffractometer. The crystal was kept at 295 K during data collection. Using Olex2, [S3] the structure was solved with the ShelXT, [S4] structure solution program using Intrinsic Phasing and refined with the ShelXL, [S5] refinement package using Least Squares minimisation.

Empirical formula	$C_{46}H_{47}ClN_4O_7$
Formula weight	803.32
Temperature/K	295
Crystal system	monoclinic
Space group	$P2_1/c$
a/Å	20.7019(2)
b/Å	10.84040(10)
c/Å	17.9416(2)
β/°	101.3700(10)
Volume/Å3	3947.38(7)
Z	4
ρcalcg/cm3	1.352
μ/mm-1	1.340
F(000)	1696.0
Crystal size/mm3	0.22 × 0.18 × 0.12
Radiation	CuKα (λ = 1.54184)
2Θ range for data collection/°	8.714 to 141.928
Index ranges	-25 ≤ h ≤ 25, -13 ≤ k ≤ 13, -21 ≤ l ≤ 15
Reflections collected	28096
Independent reflections	7529 [Rint = 0.0345, Rsigma = 0.0264]
Data/restraints/parameters	7529/0/527
Goodness-of-fit on F2	1.017
Final R indexes [I>=2σ (I)]	R1 = 0.0470, wR2 = 0.1270
Final R indexes [all data]	R1 = 0.0519, wR2 = 0.1332
Largest diff. peak/hole / e Å-3	0.39/-0.40

- **Cu^{I}(1)(Cl)** (CCDC 1951500)

Single crystals of $C_{45}H_{42}ClCuN_4O_6$ (**Cu^{I}(1)(Cl)**) were crystallized by slow diffusion of Et_2O in a CH_2Cl_2 solution of the compound. A suitable crystal was selected and mounted on a SuperNova, Dual, Cu at home/near, AtlasS2 diffractometer. The crystal was kept at 293 K during data collection. Using Olex2, [SX3] the structure was solved with the ShelXT, [SX4] structure solution program using Intrinsic Phasing and refined with the ShelXL, [SX5] refinement package using Least Squares minimisation.

Empirical formula	$C_{45}H_{42}ClCuN_4O_6$
Formula weight	833.81
Temperature/K	293
Crystal system	orthorhombic
Space group	$P2_12_12_1$
a/Å	11.7718(7)
b/Å	15.1157(8)
c/Å	21.9868(14)
Volume/Å3	3912.3(4)
Z	4

ρcalcg/cm3	1.416
μ/mm-1	0.682
F(000)	1736.0
Crystal size/mm3	0.44 × 0.3 × 0.14
Radiation	MoKα (λ = 0.71073)
2Θ range for data collection/°	5.742 to 55.724
Index ranges	-15 ≤ h ≤ 9, -18 ≤ k ≤ 17, -28 ≤ l ≤ 18
Reflections collected	12359
Independent reflections	7513 [Rint = 0.0261, Rsigma = 0.0720]
Data/restraints/parameters	7513/0/518
Goodness-of-fit on F2	1.076
Final R indexes [I>=2σ (I)]	R1 = 0.0645, wR2 = 0.1423
Final R indexes [all data]	R1 = 0.1155, wR2 = 0.1658
Largest diff. peak/hole / e Å-3	0.93/-0.45
Flack parameter	0.48(3)

Chiral HPLC resolution of (±)-1

• The sample is dissolved in chloroform, injected on the chiral column, and detected with an UV detector at 254 nm and circular dichroism detector at 254 nm. The flow-rate is 1 mL/min.

Column	Mobile Phase	t1	k1	t2	k2	α	Rs
Chiralpak ID	Heptane / ethanol and triethylamine / dichloromethane (30/30/40)	5.36 (-)	0.82	6.76 (+)	1.29	1.58	4.40

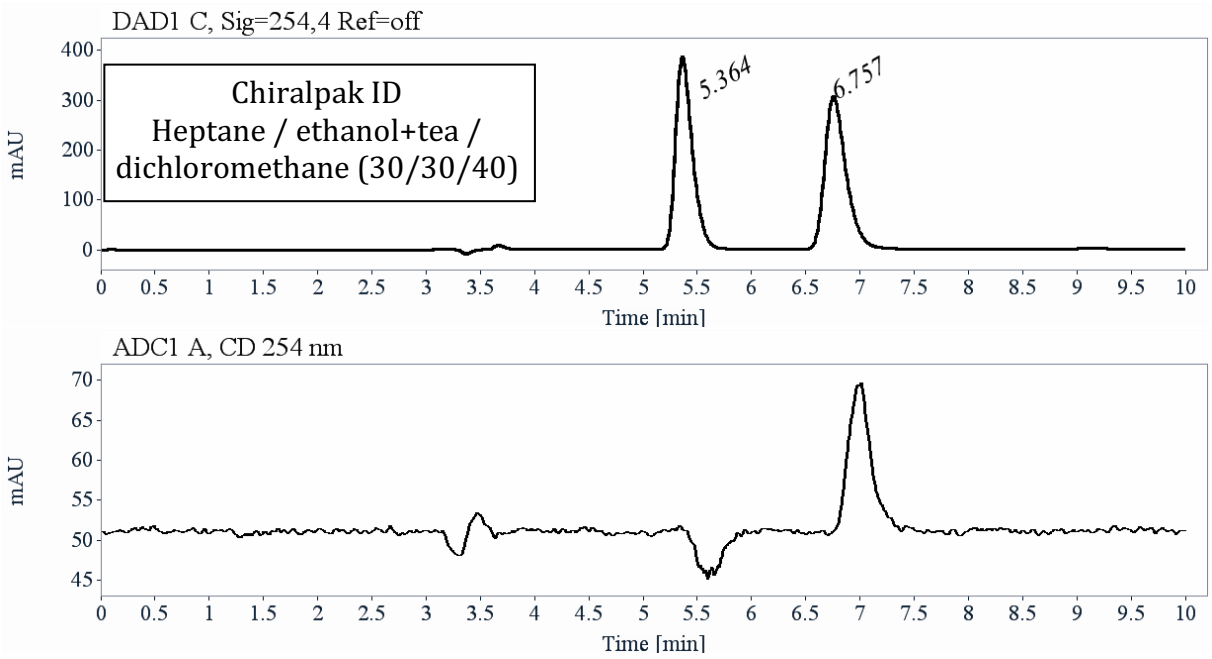

RT [min]	Area	Area%	Capacity Factor	Enantioselectivity	Resolution (USP)
5.36	4183	50.08	0.82		
6.76	4169	49.92	1.29	1.58	4.40
Sum	8352	100.00			

Preparative separation for **1** :

• Sample preparation: About 38 mg of **1** are dissolved in 2 mL of dichloromethane.

• Chromatographic conditions: Chiralpak ID (250 x 10 mm), hexane / ethanol and triethylamine / dichloromethane (30/30/40) as mobile phase, flow-rate = 5 mL/min, UV detection at 254 nm.

• Injections (stacked): 4 times 500 µL, every 7.2 minutes.

• First fraction: 13 mg of the first eluted with ee > 99.5 %

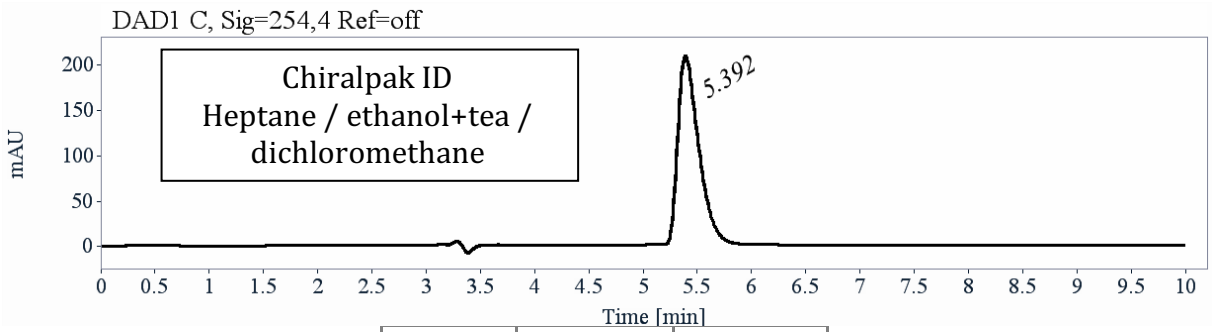

RT [min]	Area	Area%
5.39	2785	100.00
Sum	2785	100.00

• Second fraction: 13 mg of the second eluted with ee > 99.5%

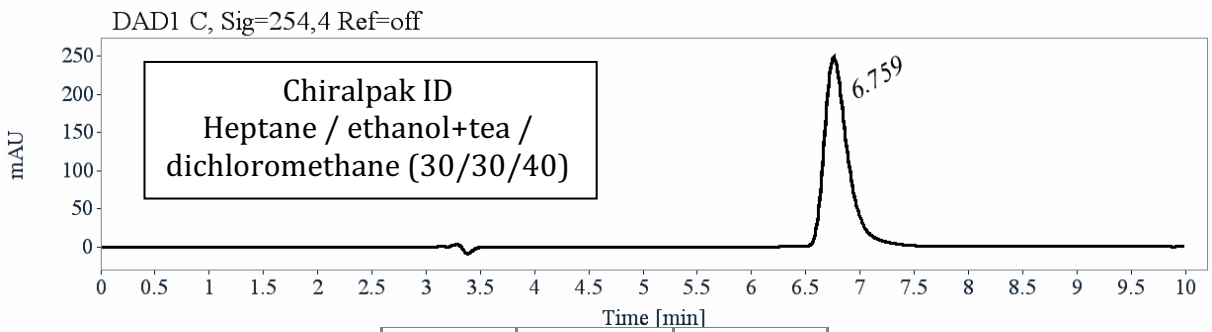

RT [min]	Area	Area%
6.76	3605	100.00
Sum	3605	100.00

Optical rotations

Optical rotations were measured on a Jasco P-2000 polarimeter with a halogen lamp (589, 578, 546, 436, 405 and 365 nm), in a 10 cm cell, thermostated at 25°C with a Peltier controlled cell holder.

λ (nm)	**1** first eluted on Chiralpak ID $[\alpha]_\lambda^{25}$ (CH_2Cl_2, c = 0.170)	**1** second eluted on Chiralpak ID $[\alpha]_\lambda^{25}$ (CH_2Cl_2, c = 0.171)
589	- 168	+ 168
578	-176	+ 176
546	- 205	+ 205
436	- 364	+ 363
405	- 455	+ 456
365	- 657	+ 656

Supplementary figures

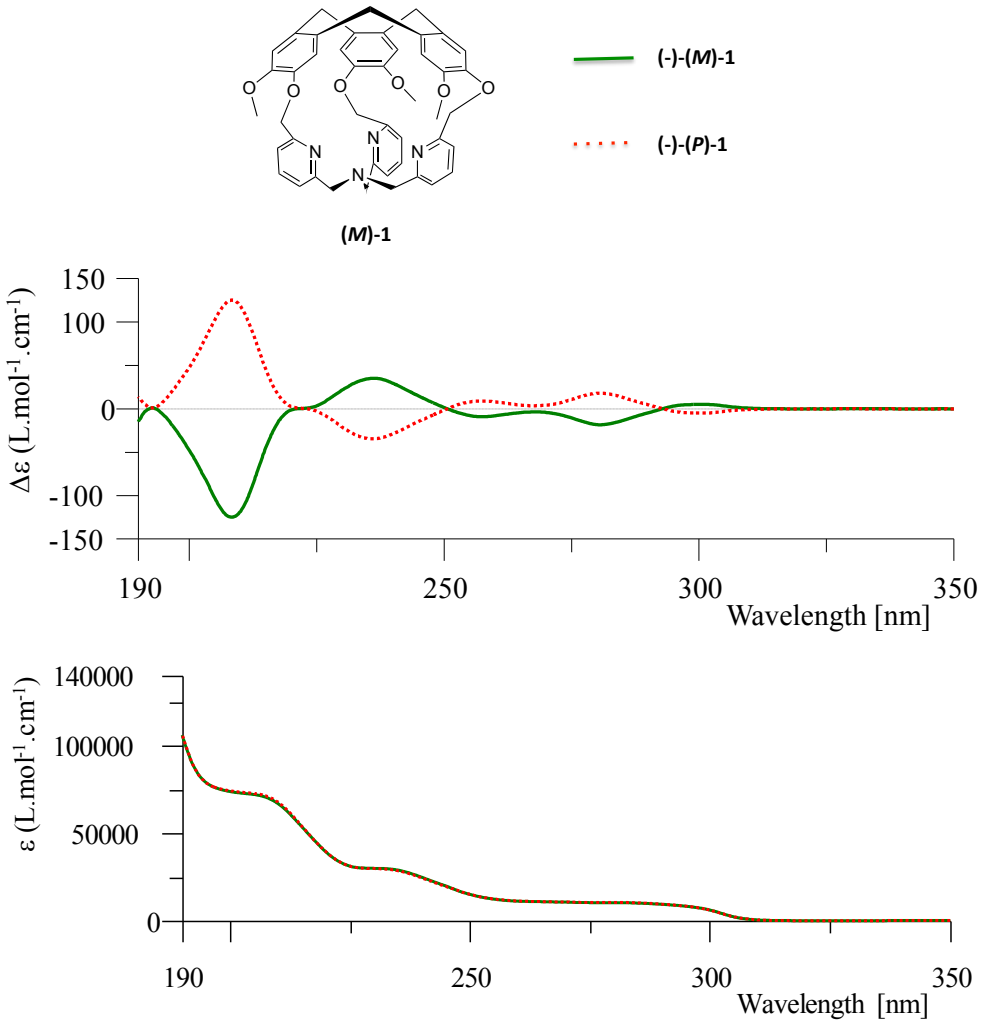

Figure S1. ECD (top) and UV (bottom) spectra of **(-)-1** and **(+)-1**. First eluted enantiomer **(-)-1** : green solid line (0.132 mM in CH_3CN). Second eluted enantiomer **(+)-1** : red dotted line, (0.148 mM in CH_3CN). Acquisition parameters: 0.1 nm as intervals, scanning speed 50 nm/min, band width 2 nm, and 3 accumulations per sample.

Absolute configuration assignement:

The spectra of the first eluted enantiomer exhibit a characteristic positive-negative bisignate curve from 230 to 250 nm corresponding to the *M*-configuration.[S6] A mirrored ECD signal is observed for the second eluted enantiomer attesting for its P-configuration. Indeed, according to Collet et al. the sign of the ^1L_a bands around 240nm can be used to assign the absolute configuration of the CTV unit because of its low sensitivity to the nature of substituents linked to the CTV part.[S6] The universal character of this assignment was confirmed by comparison with previsously reported *M* or *P* stereodescriptor of hemicryptophane analogues.[S7] Finally, the comparison between experimental and simulated ECD spectra of **(*M*)-1** (Figure S14 and S15) confirm this assignement. Therefore, according to both literature and ECD spectra calculations, the first eluted enantiomer on Chiralpak ID with $[\alpha]_D^{25}$ (CH_2Cl_2, c = 0.17) = -168, is the (*M*)-enantiomer.

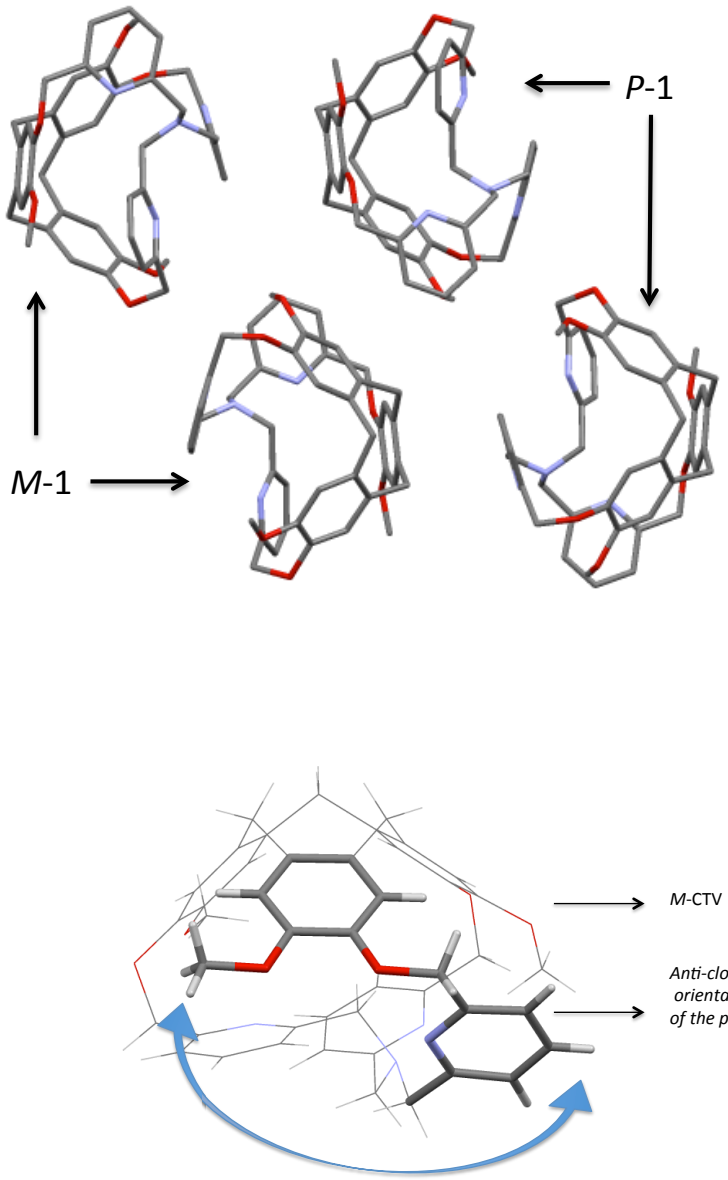

Figure S2. (Top) Crystal packing of **1** showing the presence of the two enantiomers **(*M*)-1** and **(*P*)-1**.
(Bottom) Diagram of the XRD structure of **(*M*)-1**, highlighting the rotation of the pyridines away from the closest CTV's -OMe group; resulting in they anti-clockwise orientation. The putative structure in which a clockwise arrangement of the pyridines is placed in the *M*-CTV environment (rotation of the pyridine toward -OMe group) can not be observed, probably because it will cause additional strain.

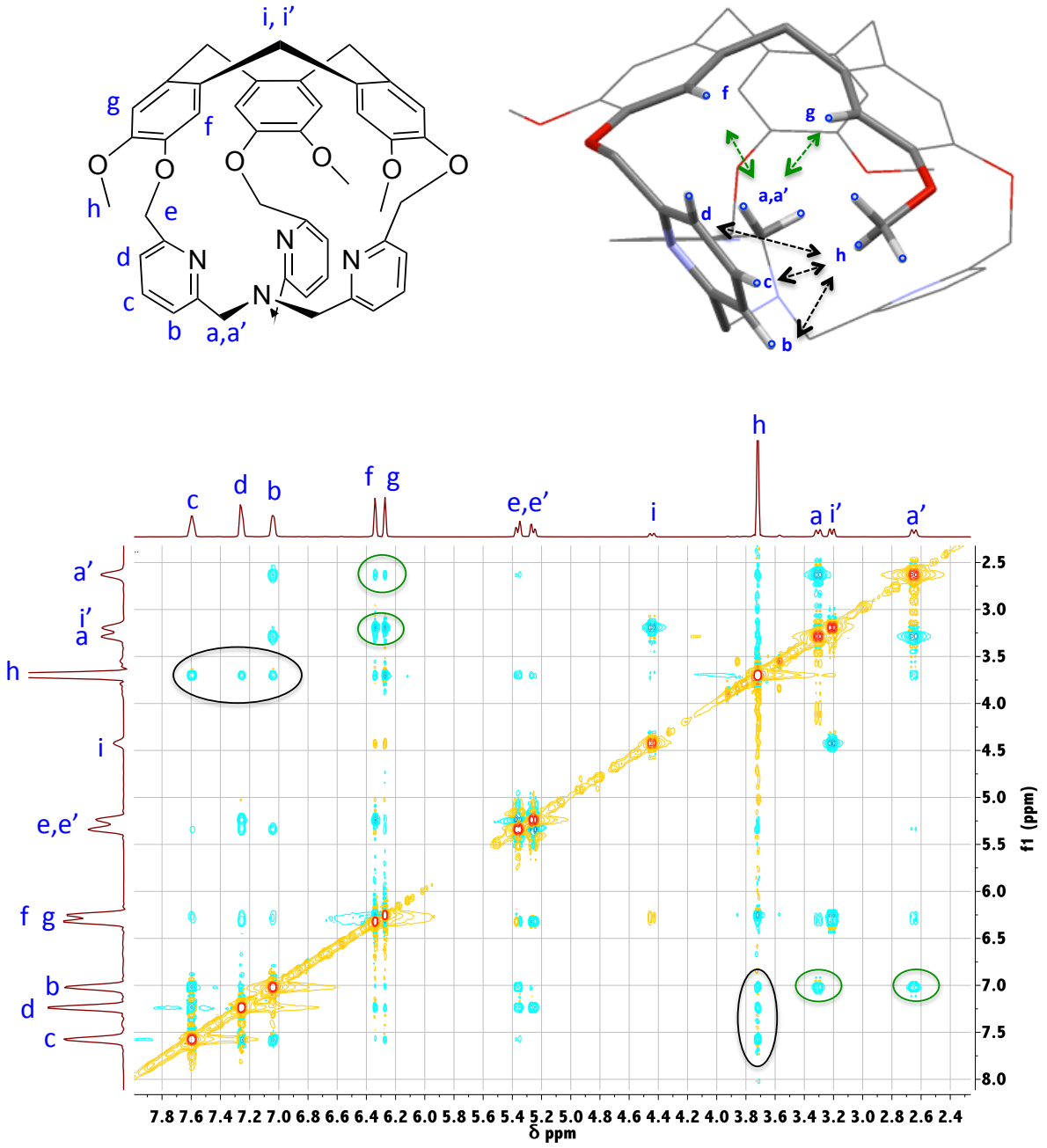

Figure S3. 2D NOESY spectrum (500MHz; mixing time of 500ms) of **1** in $CDCl_3$, at 298K. In the *C_1* symetrical conformation of **1** observed in solid state (top right), the imposed torsion and orientation of all pyridines give distances H_c(pyridine)…H_h(OMe) of 2.40 Å, 2.56 Å and 3.21 Å for the three pyridines (Fig. S4), which are consistent with the experimentally observed NOE (Same for H_a...H_f and $H_{a'}$..H_g which respectively display distances of 3.12 Å and 3.68 Å).
On the contrary, in the putative *C_3* symetrical conformation of **1** (top left), the methylene protons –**CH_2**-N ($H_{a,a'}$) are pointing outward (away from the CTV unit), excluding any through-space correlation with H_f and H_g protons.

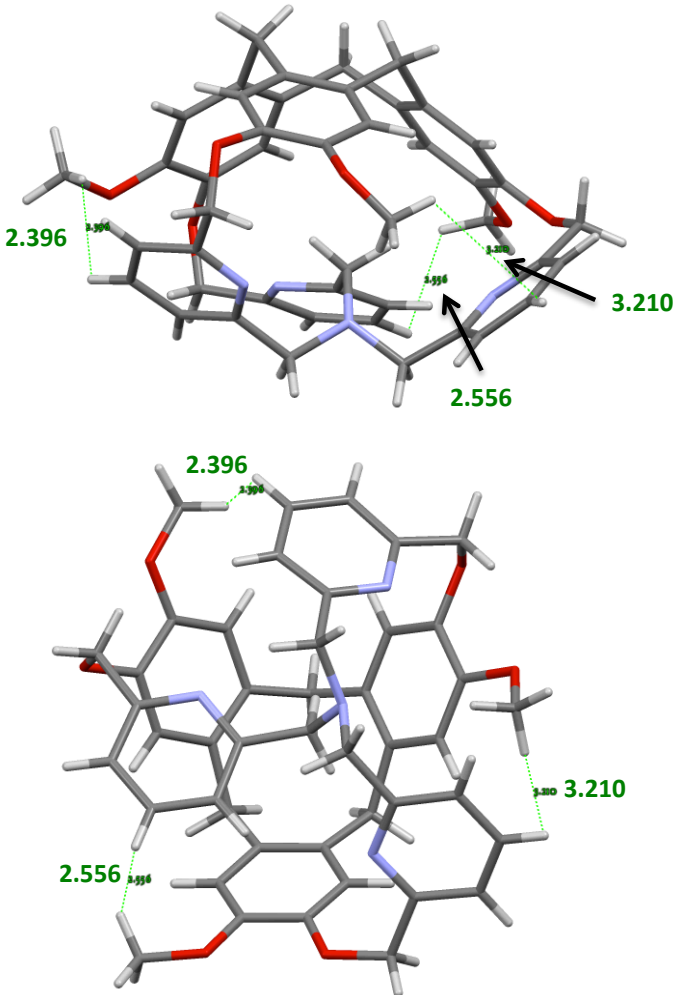

Figure S4. Side (top) and south views (bottom) of the XRD structure of ***P*-1**. Distances between H_c proton (Å) of the pyridines and the closest $-OCH_3$ proton of CTV unit are depicted in green.

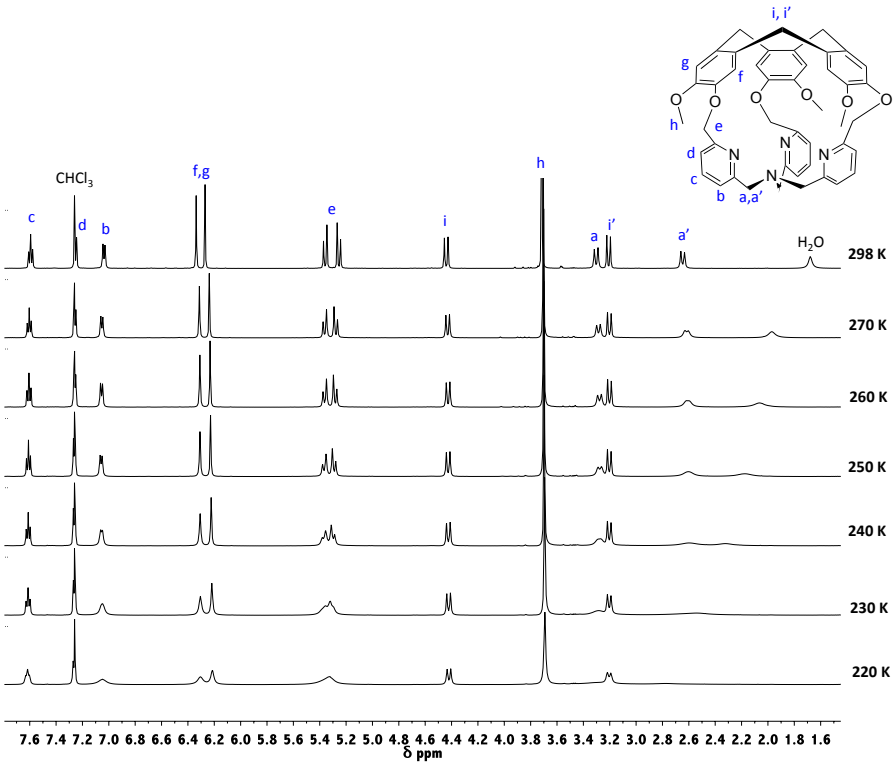

Figure S5. Temperature dependence of the ^{1}H-NMR spectra (500 MHz, $CDCl_3$) of **1** from 298 to 220K.

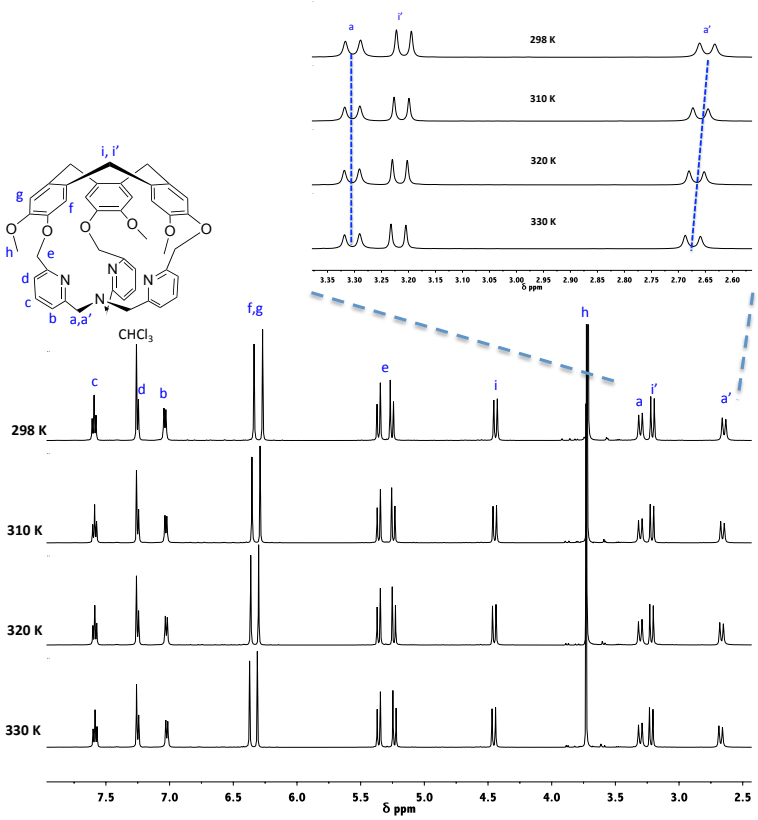

Figure S6. Temperature dependence of the ^{1}H-NMR spectra (500 MHz, $CDCl_3$) of **1** from 298 to 330K.

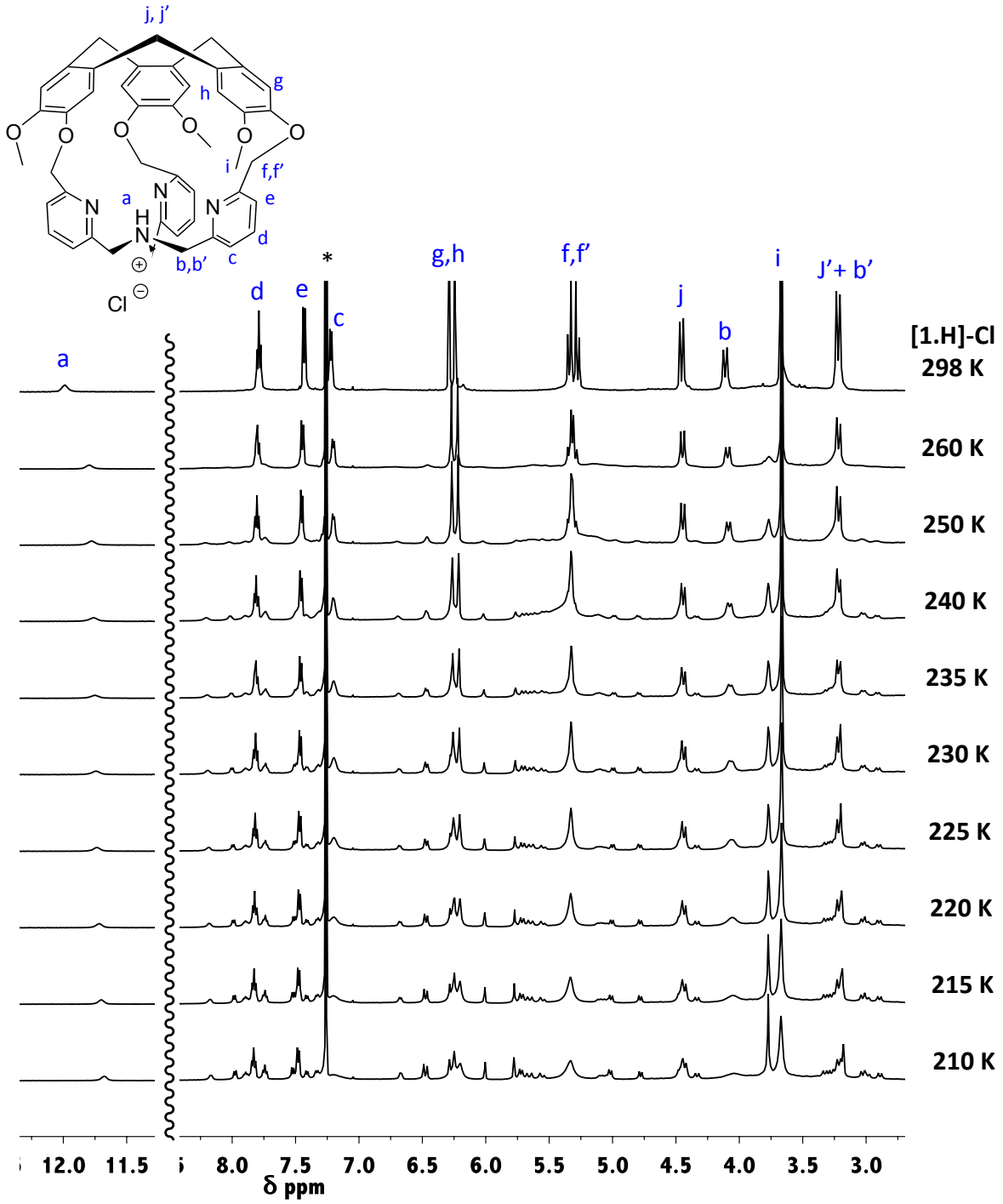

Figure S7. Temperature dependence of the ^{1}H-NMR spectra (500 MHz, $CDCl_3$) of **[1.H]-Cl** from 210 to 298K.

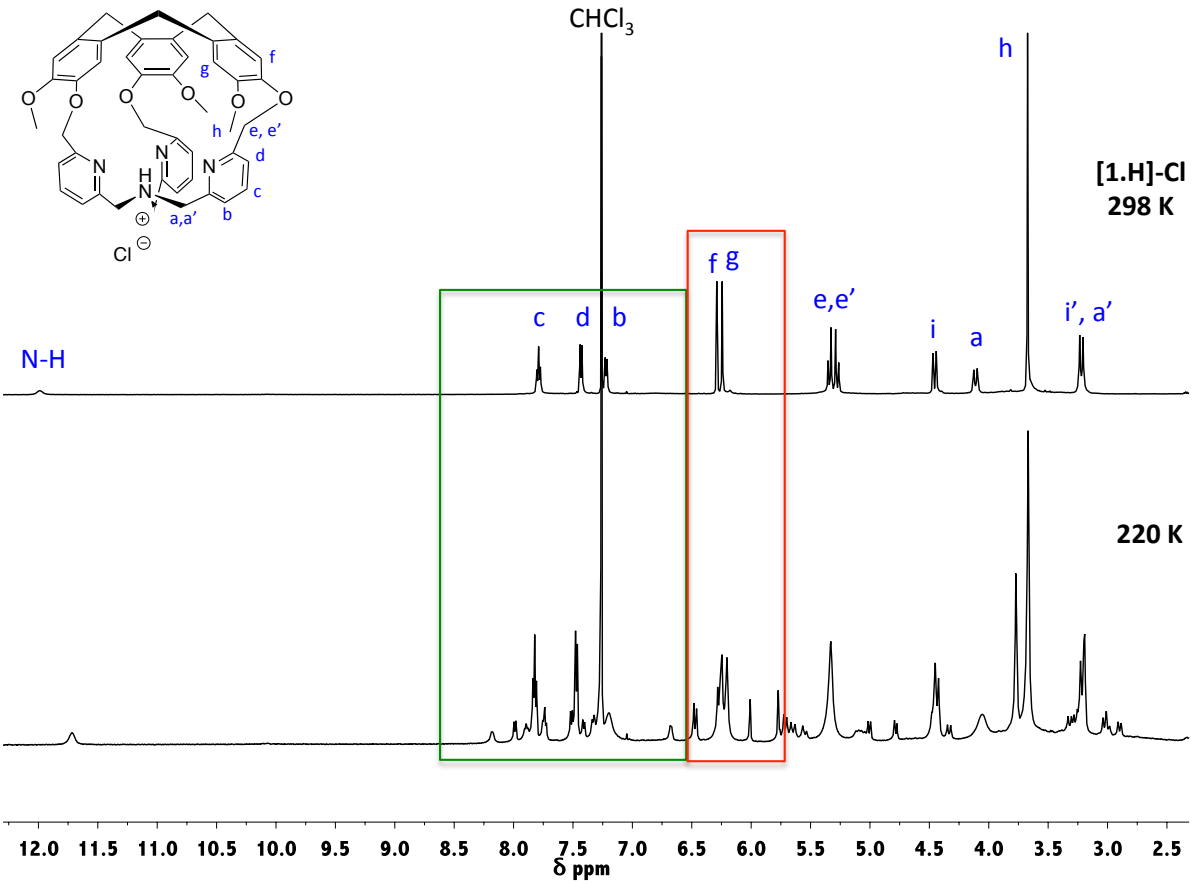

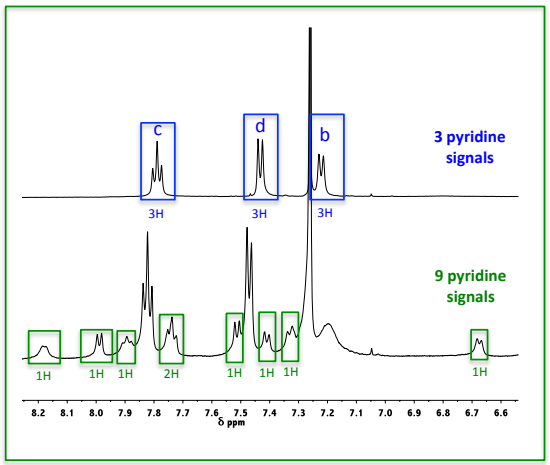

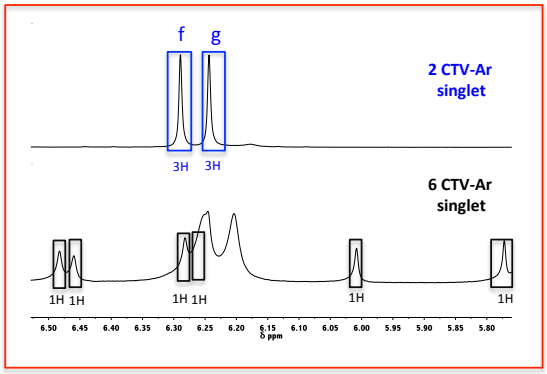

Figure S8. Comparison of the ^{1}H-NMR spectra ($CDCl_3$, 500 MHz) of **[1.H]-Cl** at 298K and 220K (top). Zoom on the region 6.6-8.2 ppm and 5.80-6.5 ppm showing the appearance of signal corresponding to the C_1 symmetrical form of **1** at lower temperature.

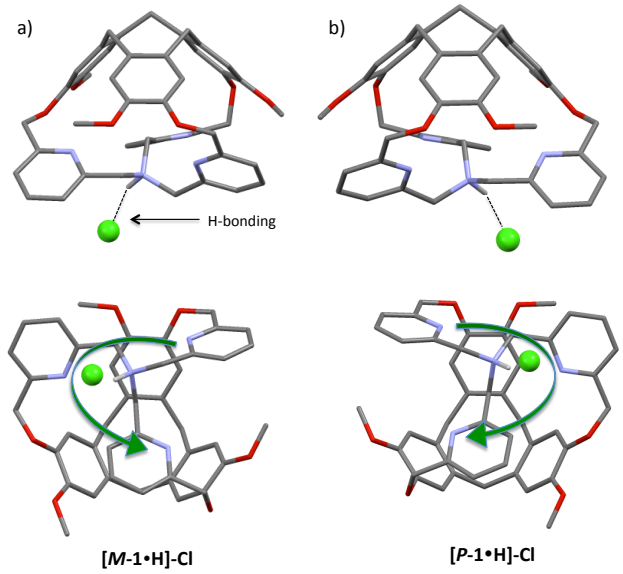

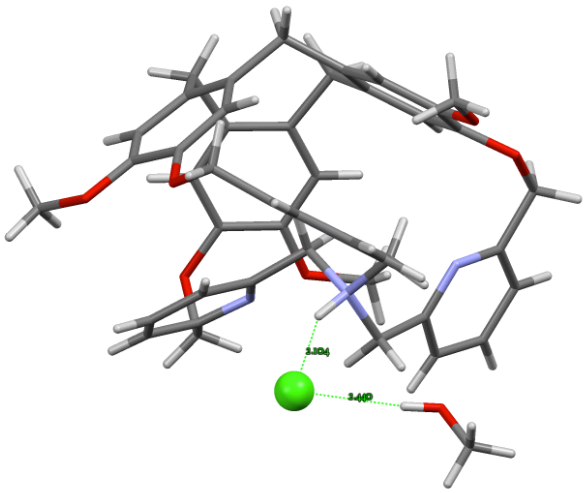

[*M*-1•H]-Cl

Figure S9. Top : Side and south views of the X-ray crystal structure of the protonated capsule **[1.H]-Cl** displaying **[*M*-1.H]-Cl** (a) and **[*P*-1.H]-Cl** (b) enantiomers. Only hydrogen atom belonging to the protonated tertiary amine has been included for clarity.

Bottom: Diagram of the X-ray crystal structure of **[1.H]-Cl**, only the *M* enantiomer is represented. The chlorine anion appear in close contact with both the protonated tertiary amine of **1** ($D_{N\text{-}H\text{--}Cl}$= 2.104 Å, $\Theta_{N\text{-}H\text{—}Cl}$ = 153.29°) and an exogeneous molecule of MeOH ($D_{O\text{-}H\text{--}Cl}$ = 2.440 Å, $\Theta_{O\text{-}H\text{—}Cl}$ = 159.47°).

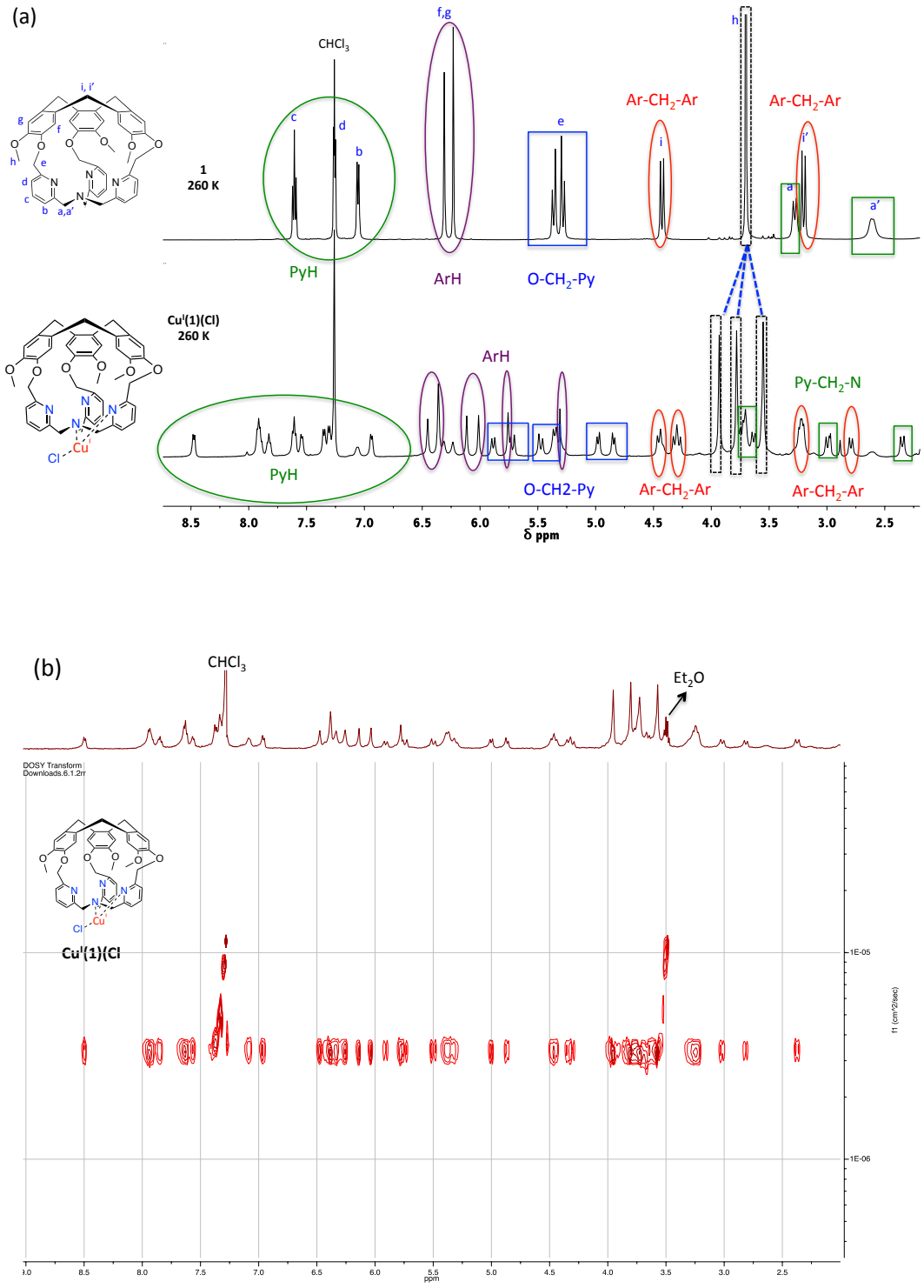

Figure S10. (a) Comparison of the ^{1}H NMR spectra (260K, $CDCl_3$, 500 MHz) of **1** (top) and **Cu^{I}(1)(Cl)** (bottom). Compared to **1** all proton signals belonging to **Cu^{I}(1)(Cl)** appear tripled attesting for the retention of the C_1 symmetrical structure observed in the DRX structure (see figure 7 main text). (b) 2D-DOSY NMR spectrum (500 MHz) of **Cu^{I}(1)(Cl** in $CDCl_3$ at 260K, all signals assigned to **Cu^{I}(1)(Cl** in the range 8.5-2.0 ppm have identical diffusion coefficient. The DOSY spectra of **Cu^{I}(1)(Cl** afford a diffusion coefficient of D= $3.74.10^{-10}$ m^2s^{-1} (fitted function f (x) = Io * exp (-D * x^2 * gamma^2 * littleDelta^2 (bigDelta-littleDelta/3)* 10^4 ; little delta= 0.003 s, big delta= 0.0754 s.

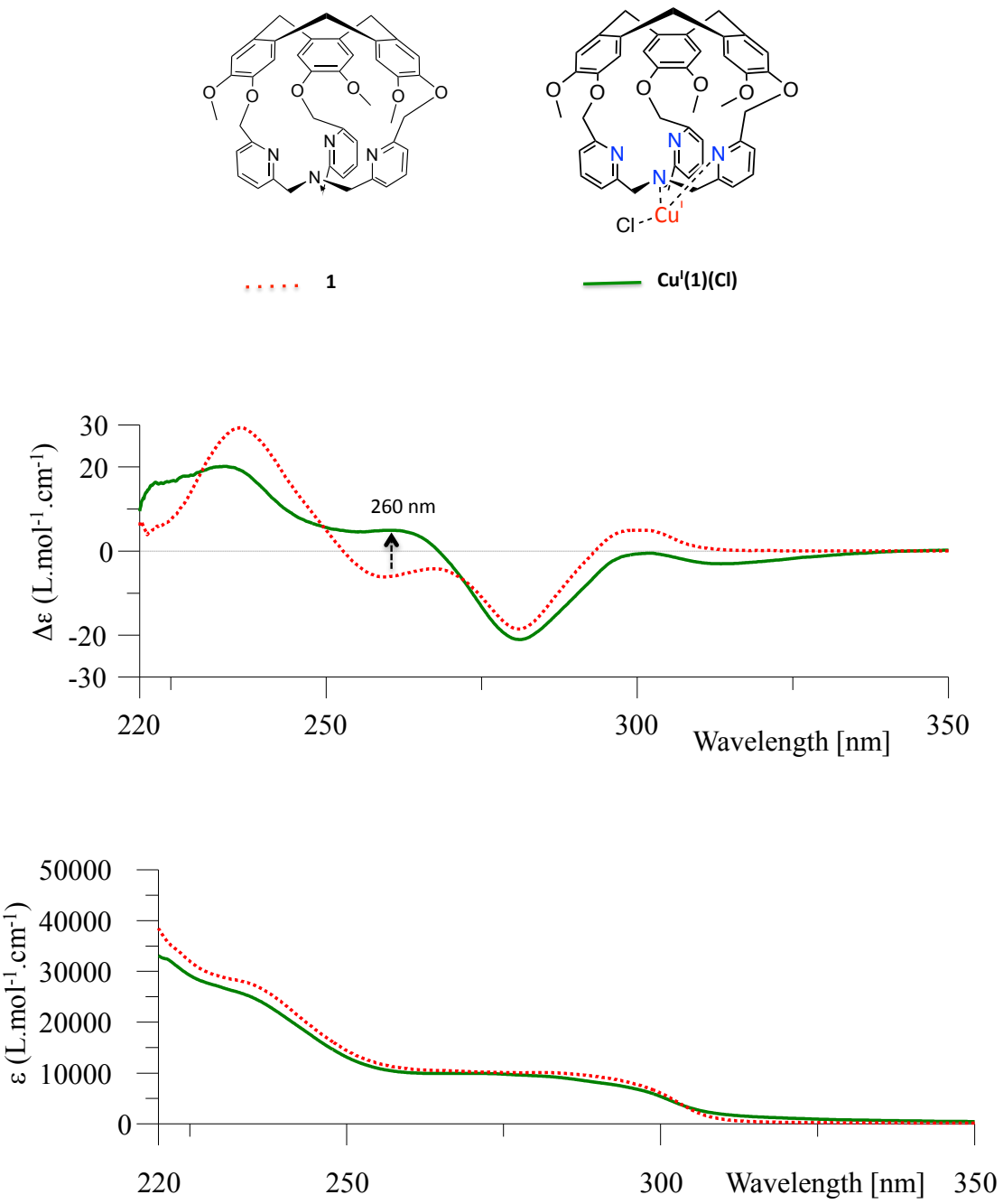

Figure S11. ECD (top) and UV (bottom) spectra of **(*M*)-Cu(1)Cl** (green solid line, 0,512mM in CH_2Cl_2), and **(*M*)-1** (red dotted line, 0,569mM in CH_2Cl_2).

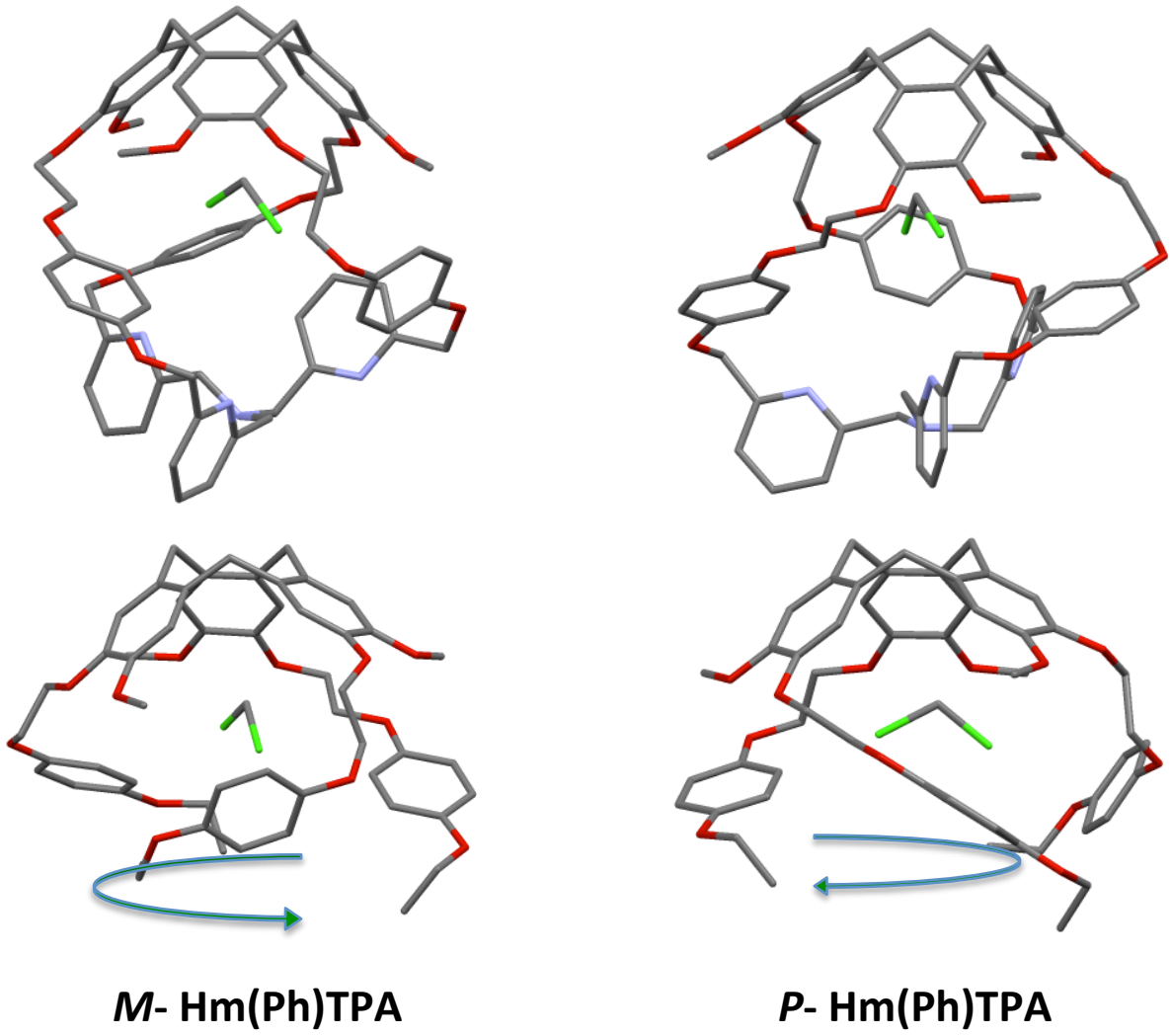

Figure S12. Representation of the XRD structure of **Hm(Ph)TPA** (top),[S8] same structure with omitted southern TPA unit for clarity (bottom). Structures of the (*M*-) and (*P*-) enantiomers of **Hm(Ph)TPA** are represented. A triple-stranded helical arrangement of the phenyl linkers is observed. No propeller orientation of the TPA moiety could be observed

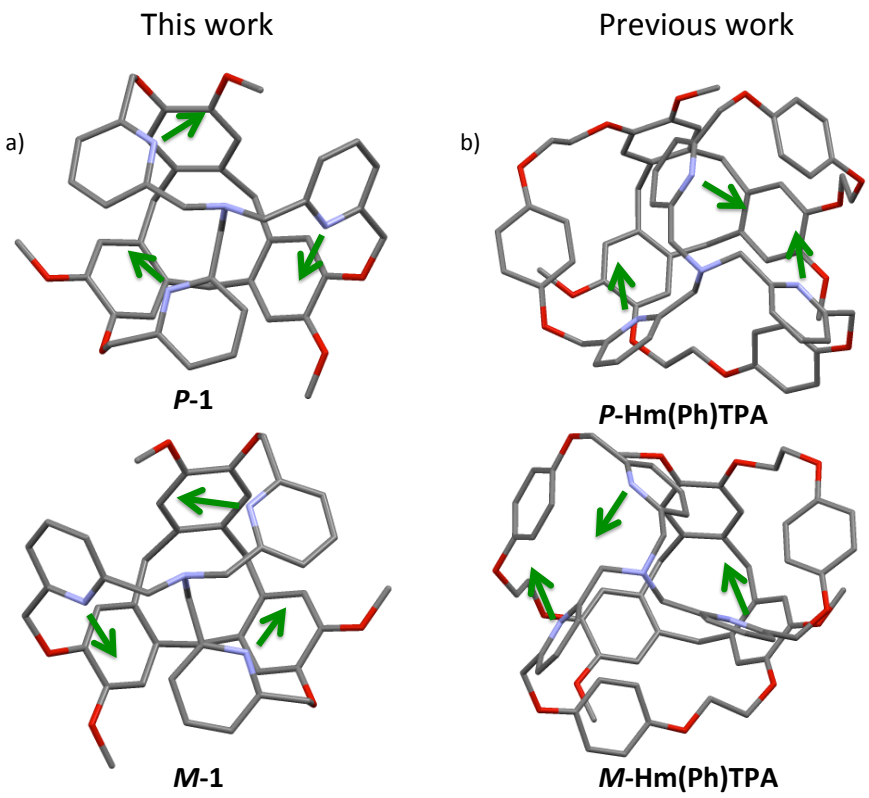

Figure S13. View from the south-north axis of the XRD structure of **1** (a) and **Hm-Ph-TPA,**[S8] (b). Both *P*- (top) and *M*- (bottom) enantiomers are depicted. Green arrows represent the orientation of the pyridine units. Unlike **1**, no propeller-like orientation of the pyridines could be observed in the case of **Hm-Ph-TPA**. Entrapped CH_2Cl_2 solvent molecule is omitted in the case of **Hm-Ph-TPA** for clarity.

4. Calculations

DFT and TD-DFT calculations were performed using Gaussian 16 package,[S9] with the default parameters for solvent used in SMD. Spectra were plotted with Specdis v. 1.71[S9] as sum of Gaussians with σ as half the bandwidth at $1/e$ peak height.
Calculations were done on the geometry obtained by X-ray analysis. The (*M*)-enantiomer was calculated.

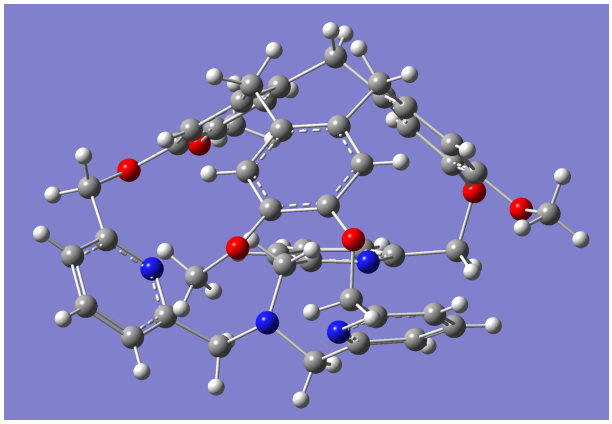

1) TD-DFT calculations at SMD(CH_3CN)/LC-ωhPBE/Def2SVPP level : 120 excited stated were computed.

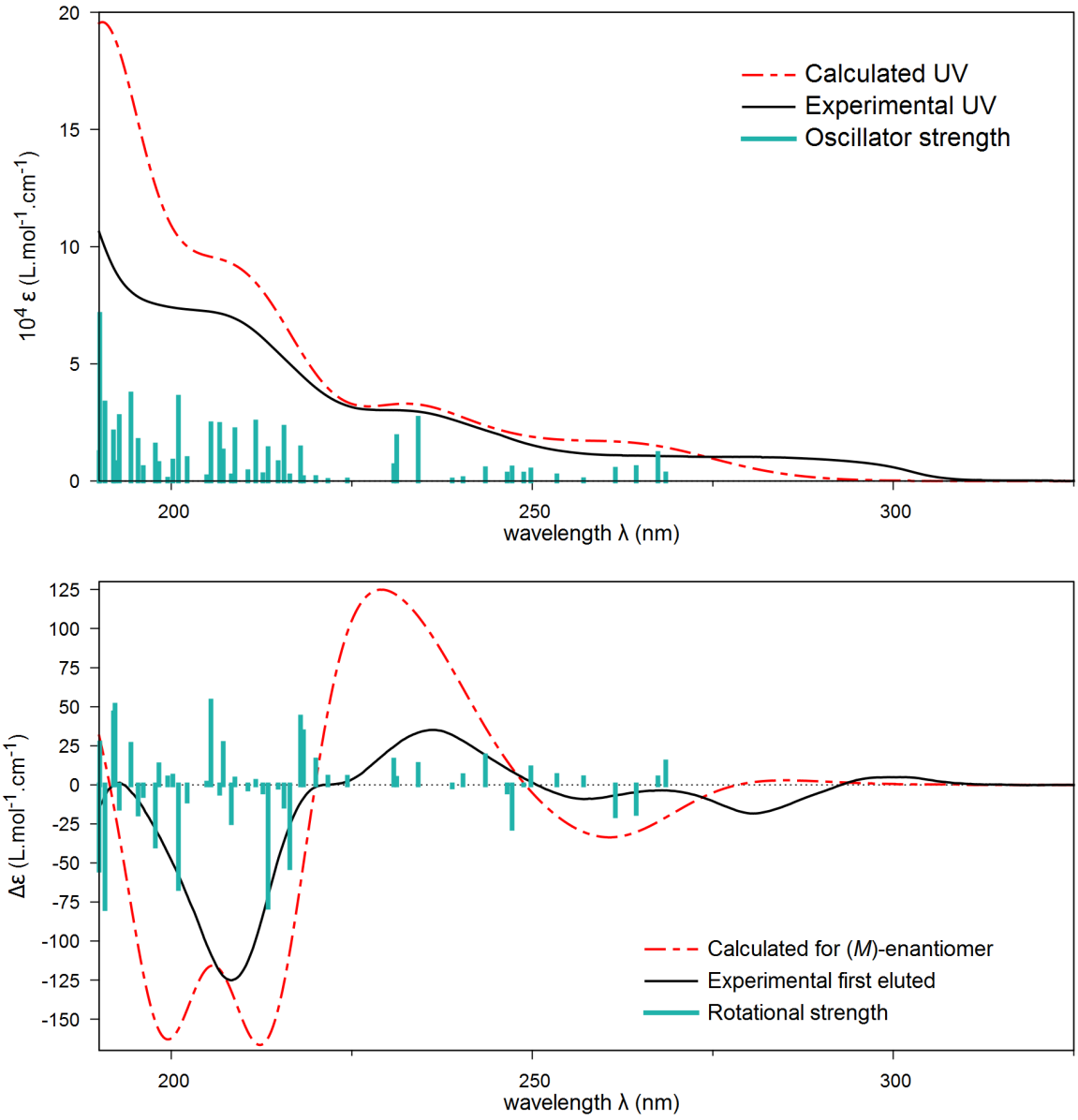

Figure S14. Comparison of UV (top) and ECD (bottom) experimental spectra in acetonitrile for the first eluted enantiomer on Chiralpak ID and TD-DFT calculated spectra (σ = 0.30 eV, shifted by 24 nm). Vertical bars are oscillator and rotational strengths calculated for the two conformers with arbitrary unit.

2) TD-DFT calculations at SMD(CH_3CN)/CAM-B3LYP/6-31++g(d, p) level : 180 excited stated were computed.

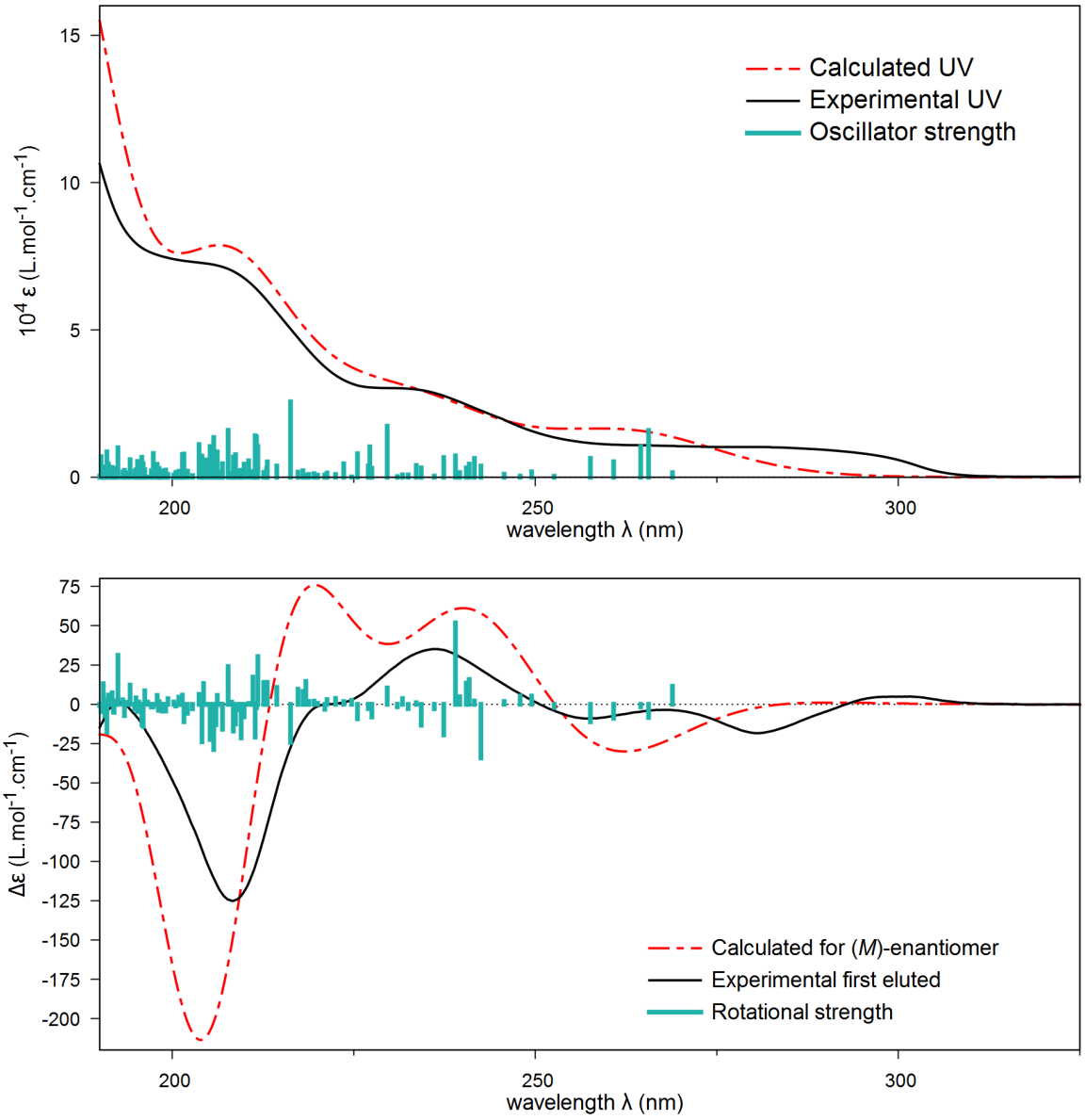

Figure S15. Comparison of UV (top) and ECD (bottom) experimental spectra in acetonitrile for the first eluted enantiomer on Chiralpak ID and TD-DFT calculated spectra (σ = 0.30 eV, shifted by 10 nm). Vertical bars are oscillator and rotational strengths calculated for the two conformers with arbitrary unit.

According to both above ECD spectra calculations, the first eluted enantiomer on Chiralpak ID with $[\alpha]_D^{25}$ (CH_2Cl_2, c = 0.17) = - 168, is the (*M*)-enantiomer.

5. Acknowledgements:

Calculations were supported by the computing facilities of the CRCMM, '*Centre Régional de Compétences en Modélisation Moléculaire de Marseille'*. We thank spectropole and Mme R. Rosas for NMR assistance.

6. Supplementary references.

[S1] D. Zhang, B. Bousquet, J. C. Mulatier, D. Pitrat, M. Jean, N. Vanthuyne, L. Guy, J. P. Dutasta and A. Martinez, *J. Org. Chem.*, 2017, 82, 6082- 6088

[S2] T.Brotin, V. Roy and J. P. Dutasta, *J. Org. Chem.*, 2005, **70**, 6187-6195

[S3] O. V. Dolomanov, L. J. Bourhis, R. J. Gildea, J. A. K. Howard, H. J. Puschmann, *Appl. Cryst.,* 2009, **42**, 339-341.

[S4] G. M. Sheldrick, *ActaCryst.*, 2015, **A71**, 3-8.

[S5] G. M. Sheldrick, *ActaCryst.* 2015, **C71**, 3-8.

[S6](a) A. Schmitt, O. Perraud, E. Payet, B. Chatelet, B. Bousquet, M. Valls, D. Padula, L. Di Bari, J. P. Dutasta, A. Martinez, *Org. Biomol. Chem.*, 2014, **12**, 4211. (b) O. Perraud, P. Dimitrov-Raytchev, A. Martinez, J. P. Dutasta, *Chirality*, 2010, **22,** 88. (c) J. R. Cochrane, A. Schmitt, U. Wille, C. A. Hutton, *Chem. Commun.*, 2013, **49**, 8504. (d) J. Canceill, A. Collet, J. Gabard, G. Gottarelli, G. P. Spada, *J. Am. Chem. Soc.*, 1985, **107**, 1299. (e) J. Canceill, A. Collet, G. Gottarelli, P. Palmieri, *J. Am. Chem. Soc.*, 1987, **109**, 6454.)

[S7] Ł. Szyszka, P. Cmoch, A. Butkiewicz, M. A. Potopnyk, S. Jarosz, *Org. Lett.* 2019, **21**, 6523−6528

[S8] S. A. Ikbal, C. Colomban, D. Zhang, M. Delecluse, T. Brotin, V. Dufaud, J. P. Dutasta, A. B. Sorokin and A. Martinez, *Inorg. Chem.*, 2019, **58**, 7220-7228

[S9] (a) Gaussian 16, Revision A.03, M. J. Frisch, G. W. Trucks, H. B. Schlegel, G. E. Scuseria, M. A. Robb, J. R. Cheeseman, G. Scalmani, V. Barone, G. A. Petersson, H. Nakatsuji, X. Li, M. Caricato, A. V. Marenich, J. Bloino, B. G. Janesko, R. Gomperts, B. Mennucci, H. P. Hratchian, J. V. Ortiz, A. F. Izmaylov, J. L. Sonnenberg, D. Williams-Young, F. Ding, F. Lipparini, F. Egidi, J. Goings, B. Peng, A. Petrone, T. Henderson, D. Ranasinghe, V. G. Zakrzewski, J. Gao, N. Rega, G. Zheng, W. Liang, M. Hada, M. Ehara, K. Toyota, R. Fukuda, J. Hasegawa, M. Ishida, T. Nakajima, Y. Honda, O. Kitao, H. Nakai, T. Vreven, K. Throssell, J. A. Montgomery, Jr., J. E. Peralta, F. Ogliaro, M. J. Bearpark, J. J. Heyd, E. N. Brothers, K. N. Kudin, V. N. Staroverov, T. A. Keith, R. Kobayashi, J. Normand, K. Raghavachari, A. P. Rendell, J. C. Burant, S. S. Iyengar, J. Tomasi, M. Cossi, J. M. Millam, M. Klene, C. Adamo, R. Cammi, J. W. Ochterski, R. L. Martin, K. Morokuma, O. Farkas, J. B. Foresman, and D. J. Fox, Gaussian, Inc., Wallingford CT, **2016**.
(b) Specdis version 1.71. T. Bruhn, A. Schaumlöffel, Y. Hemberger, G. Pescitelli. Berlin, Germany, **2017**, https://specdis-software.jimdo.com/.

II.3 Preliminar catalytic tests on copper-catalyzed asymmetric transformations using enantiopure 1-Cu^{I}(Cl) catalyst

The enantiopure complexes **(*M*)Cu^{I}(1)(Cl)** and **(*P*)Cu^{I}(1)(Cl)** have been prepared according to the procedure described in the previous section. With these new catalysts in hand, we first tried to perform selective conjugate addition of diethylzinc to unsaturated ketene. Indeed, this reaction has been previously achieved using copper-based catalysts owning enantiopure ligand with ee values of 96%.[30] The reaction 1 (Figure 2.5) was carried out by mixing the substrate **41** with 1.1 equivalents of diethylzinc in the presence of 1.0 mol % of CuCl and 1.2 mol % of the enantiopure cage **(*M*)1** in diethyl ether at 0 °C. After two hours, a reaction yield of 80% was observed but after chiral-HPLC analysis, it was found that both enantiomers of **42** were equally formed with no enantiomeric excess. Besides, this complex was also examined in an other potentially enantioselective reaction (Henry's reaction) by using benzaldehyde **43** as the substrate (reaction 2 in Figure 2.5).[31] The reaction 2 was performed by mixing with 1.4 equivalents of pyridine in the presence of 5.0 mol % of CuCl and 5.5 mol % of the **(*P*)1** ligand in EtOH at room temperature. After one night, the benzaldehyde was converted to the desired product in a 50% yield, but chiral-HPLC analysis of the product reveal that both R ans S product were formed with no enantiomeric excess.

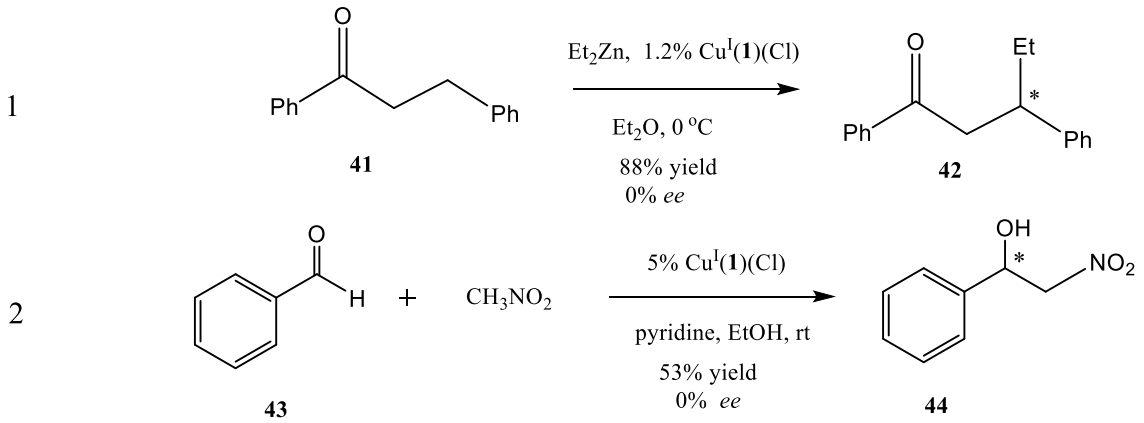

Figure 2.5 (1) **Cu^{I}(*M*-1)(Cl)**-catalyzed asymmetric conjugate addition of diethylzinc to chalcone, (2)Enantioselctive Henry reaction catalyzed by **Cu^{I}(*P*-1)(Cl)**.

These preliminary catalytic tests therefore indicate that our new enantiopure copper-based cage-ligand cannot induce enantioselectivy when applied to two classical reactions from the literature.

However, the two transformations that have been tested are usually performed by copper center displaying ligands that strongly differ from the TPA structure (for example chiral phosphines). Furthermore, considering that *i*) an enantioselective transformation controlled by a chirality transfert in a cage will represent a totally unprecedented report, and *ii*) the geometry at the copper center in **Cu^{I}(1)(Cl)** is also unprecedented for TPA-based ligands (and therefore not documented, which preclude any comparison with parent models devoid of the CTV cap), it is particularly difficult to find a good model reaction. We therefore believe that enantioselective transformation catalyzed by our complex need to be further study in depth. In previous reports, other enantiopure hemicryptophane-based metal complexes have rarely been used as chiral catalysts. Such catalysts therefore need to be optimized for a good application.

II.4 Computational calculations: explanation of the chirality transfer and molecular dynamic of cage 1

A computational treatment was performed to rationalize the experimental observations relative to the chirality transfer in **1**. This work aims to focus on the following aspects: understanding why *i*) the PM (corresponding to *P*-CTV and left-handed propeller orientation of the TPA), or MP (*M*-CTV and right-handed propeller arrangement of the TPA), structures are not obtained experimentally; and *ii*) why the ^{1}H-NMR experience suggests a C_3 symmetrical structure in solution for the neutral cage that does not correspond to the XRD structure, where a bottom CH_2 differs from the two others, as it is inside the cage. The question here is whether there is a possible mechanism that allows for fast conformation changes and that the ^{1}H-NMR signals are due to an averaging of the possible structures.

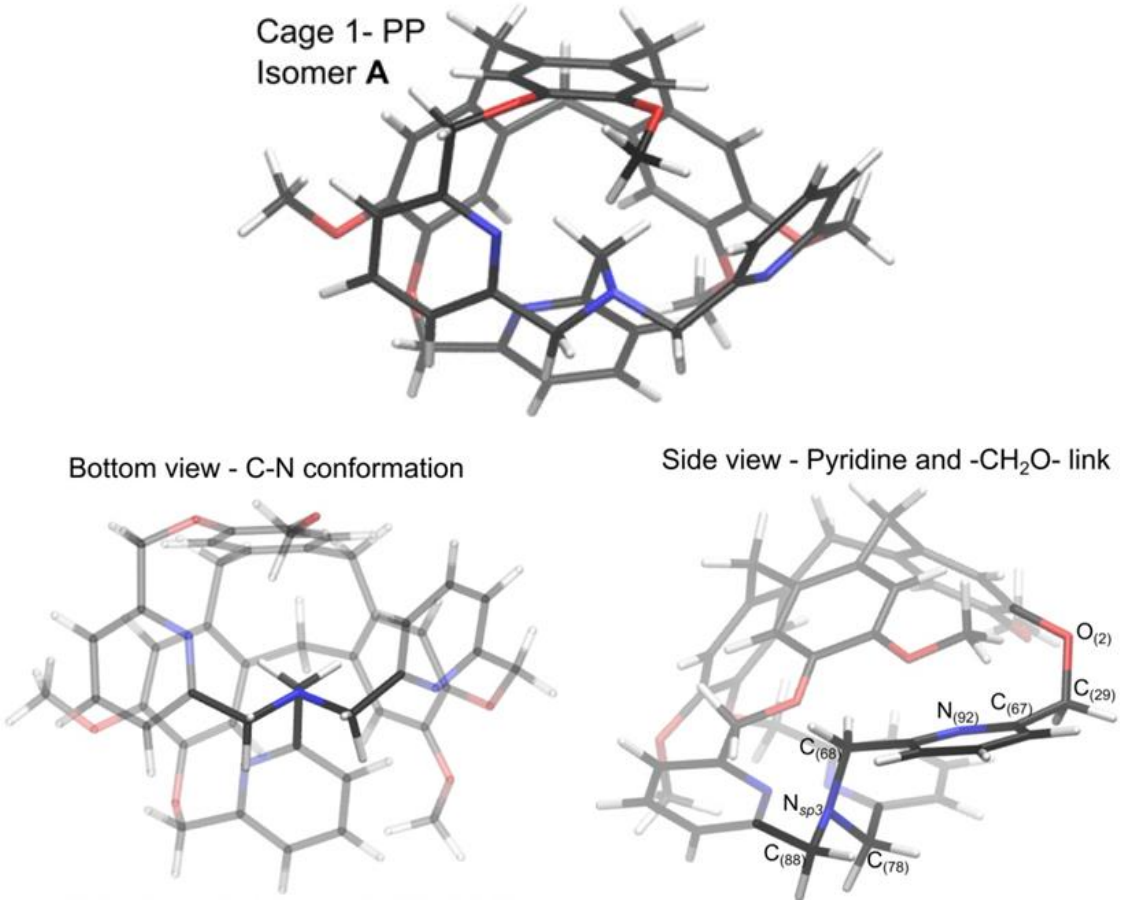

Figure 2.6 Structure of cage **1**, isomer PP. By observing the bottom part, we notice that the C(68)H_2 connected to the nitrogen atom Nsp3 has its hydrogen atoms pointing inside the cage (one-arm-inside conformation).

II.4.1 Computational details:

The computational treatment combines two approaches: molecular dynamics runs were performed to explore the potential energy surface of the neutral cage; Density Functional Theory calculations were performed to explore the potential energy surface of the neutral cage. Several minima and transition states, which are significant for the conformational analysis of the cage, were located and fully characterized. The functional PBE0 was used, in combination with the D3 dispersion empirical corrections (PBE0-D3).[32-37] Preliminary calculations were performed by employing the def2-SV(P) basis set, results were further checked by employing the def2-TZVP basis set.[38] The RI-J technique was employed to reduce the computational time.[39] The TURBOMOLE program package was user throughout. (TURBOMOLE V7.2 2017, a

development of University of Karlsruhe and Forschungszentrum Karlsruhe GmbH, 1989-2007, TURBOMOLE GmbH, since 2007; available from http://www.turbomole.com.)

II.4.2 Chirality transfer (issue 1):

The structure of the isomer PP（corresponding to *P*-CTV and right-handed propeller orientation of the TPA), optimized from the XRD data, is shown in Figure 2.6. The one-arm-inside conformation guarantees a staggered conformation of the three CH_2 links connecting the nitrogen atom Nsp3 to the pyridine moieties. By considering the inside-arm, the pyridine ring is nearly orthogonal to the C(68)- Nsp3 bond and the CH_2O link connecting the pyridine to the top CTV is oriented in such a way that the dihedral angle N(92)-C(67)-C(29)-O(2) is of 92.60 (computed structure), reducing the repulsion between the nitrogen and the oxygen lone pairs.

In the XRD structure, some disorder is observed concerning the position of the -OMe groups of the CTV. The enthalpy difference between two optimized structures differing by the positions of these groups is negligeable (1.3 kJ/mol ZPE energy corrected) and the conversion barrier between them is of only 24.4 kJ/mol (enthalpy value).

As already presented, only the PP (and MM) structure are experimentally observed. To better understand this remarkable chirality transfer, we optimized hypothetical conformations for the PM cage (P→ CTV; M→ left-handed TPA). Results from the DFT calculations are reported in Figure 2.7, where the structures are depicted from a top view, to underline the position of the aromatic rings. The optimized structure for the PP cage is also reported for comparison.

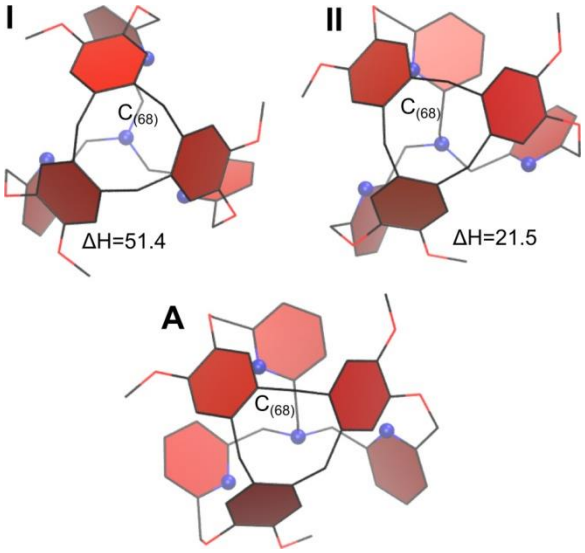

Figure 2.7 Optimized structures for hypothetical PM isomers of cage **1** (I) together with the structure of cage **1** where the TPA ligand does not show a propeller arrangement of its pyridine (II). The optimized structure for the PP cage is also reported for comparison (A). Blue spheres represent the nitrogen atoms. Enthalpy differences are indicated (kJ/mol).

The first structure I, is built by assuming a C_3 symmetrical arrangement of the cage (even if the optimization was conducted without imposing the symmetry constraint). This conformation is the all-arm-outside, with an evident PM pattern. The aromatic rings of the CTV are almost eclipsed with the pyridines of the bottom of the cage, whereas in the PP cage they are clearly alternating, without superposition. This aspect contributes to the higher energy of I with respect to the PP isomer.

These results therefore suggest that the preferential formation of PP (or MM) diastereomers compared to the PM (or MP) structures arises from the less stable eclipsed structure observed in the latter case.

II.4.3 Dynamic Aspects (issue 2) :

Cage **1** is formed by three arms, each connecting the bottom nitrogen to two top CH_2 units of the CTV. These arms are not equivalent: in Figure 2.8 three isoenergetic isomers are depicted, where the inside arm contains respectively C(68) (A, red arm inside), C(88) (B, green arm inside), and C(78) (C, cyan arm inside).

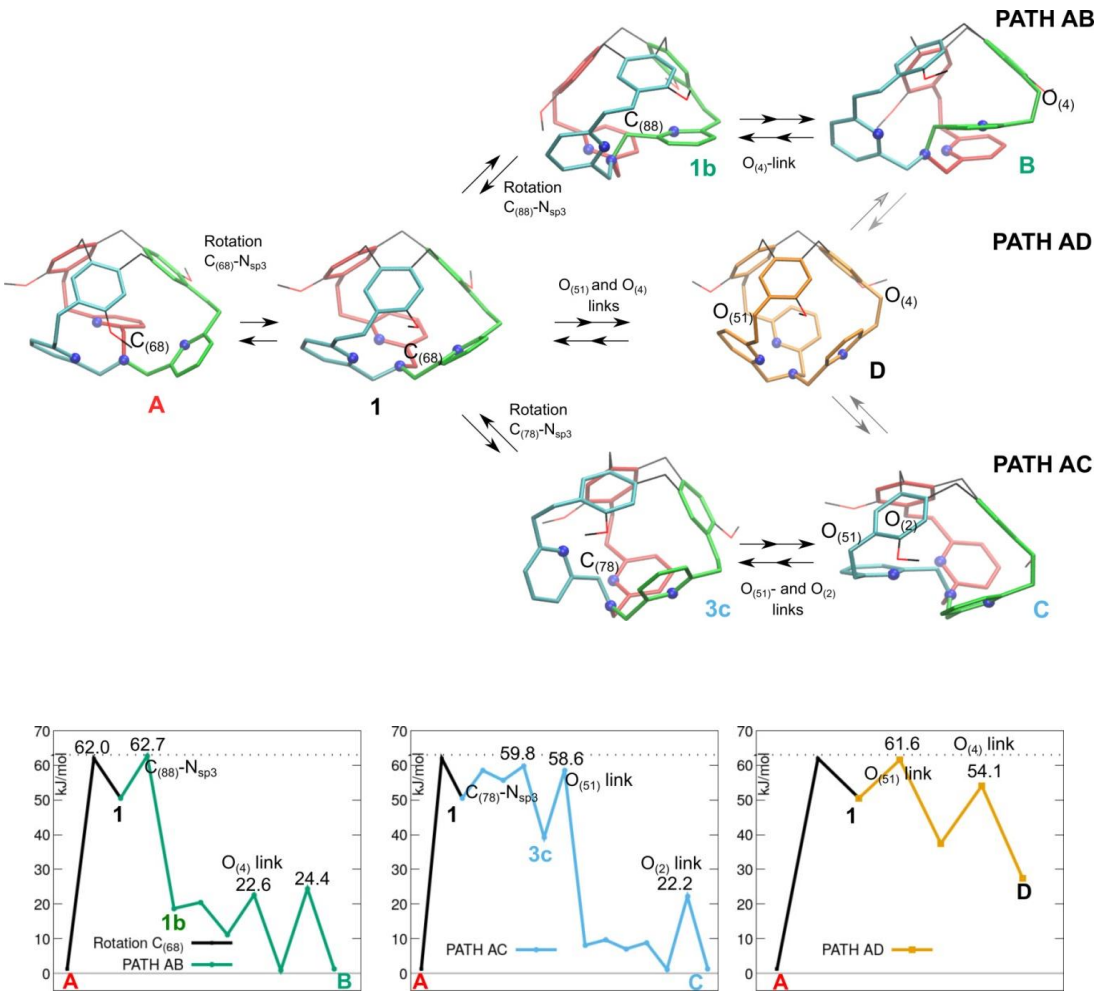

Figure 2.8 Interconversion pathways between isoenergetic structures of cage **1**: A (red arm inside), B (green arm inside), C (cyan arm inside). The atoms involved in the conformational changes (excluded the -OMe rotations) with respect to the depicted previous intermediate are indicated. The blue spheres represent the N atoms. The reaction enthalpy profiles are shown.

We present in Figure 2.8 three computed pathways for the conversion of A into B and/or C and their reaction enthalpy profiles. The conversions of A to B and to C are achieved by following respectively the AB and AC pathways. An alternative mechanism is proposed that implies an intermediate where the three bottom arms are equivalent and it can therefore evolves to either A, or B, or C (path AD). The three pathways share the first step, located at 62 kJ/mol, which is a rotation of the -C(68)H2- moiety leading to intermediate 1 in Figure 2.8. The AB pathway implies a step to rotate the arm containing C(88) into the cage, resulting in the intermediate 1b, where all the pyridines have already approximately the final conformation. The transition state corresponding to this transformation is located at 62.7 kJ/mol. The following steps are rearrangements to reorient the OMe groups and the oxygen link of the new inside-arm. The AC

pathway implies two successive steps to rotate the arm C(78) into the cage. In the resulting intermediate, 3c, the pyridine ring connected to C(78) is in an unfavorable position, with the nitrogen atom pointing inside the cage. In the next step a rotation occurs that adjust simultaneously the positions of the pyridine rings and the oxygen link of the new inside arm (O(51)). From there, the following steps are rearrangements to reorient the OMe groups and the oxygen link O(2). With the exception of the first step, the transitions states are all lower than 60 kJ/mol in reaction enthalpy.

Finally, in the AD path, two rotations implying the oxygen links O(51) (transition state located at 61.6 kJ/mol) and O(4) leads to intermediate D, which presents a '*C*3 symmetry' and it can therefore evolve to each of the three isoenergetic A, B and C structures.

All over, the barriers are small: the highest transition states are located at 60-62 kJ/mol above the computed energy of the crystal structure. This implies that there exist paths for fast conversions among A, B and C and that the NMR signal is averaged on these structures. The computed pathways do not differ significantly from an energetic point of view and possibly they all co-exist. The AC path appears slightly preferred in terms of enthalpy, however differences are tiny. We notice here that the D intermediate is lower in energy than 1, even if the two structures share a similar conformation of the bottom part of the cage (all-arm-outside conformation). The optimized structures of 1 and D are compared in Figure 2.9; it is indeed instructive to visualize some geometrical features that contribute to their relative stability, as this points out general structural parameters that might contribute to stabilize conformations. Differently than in A, the CH_2 links connected to the bottom Nsp3 have almost eclipsed conformations in 1 and D. Interestingly, D is significantly lower in energy than 1. The differences between 1 and D are related to the positions of the -CH_2O- links connecting the pyridines to the top CTV (O(4), O(51) and O(2)). In D, all these links are optimally oriented, as the relative positions of the oxygen atoms with respect to the nitrogen atoms allow for reducing the repulsion due to their lone pairs. This is not the case for O(4) and O(51) in 1; moreover, even if the O(2) atom is properly oriented with respect to the nitrogen atom, one hydrogen atom is eclipsed with the pyridine ring.

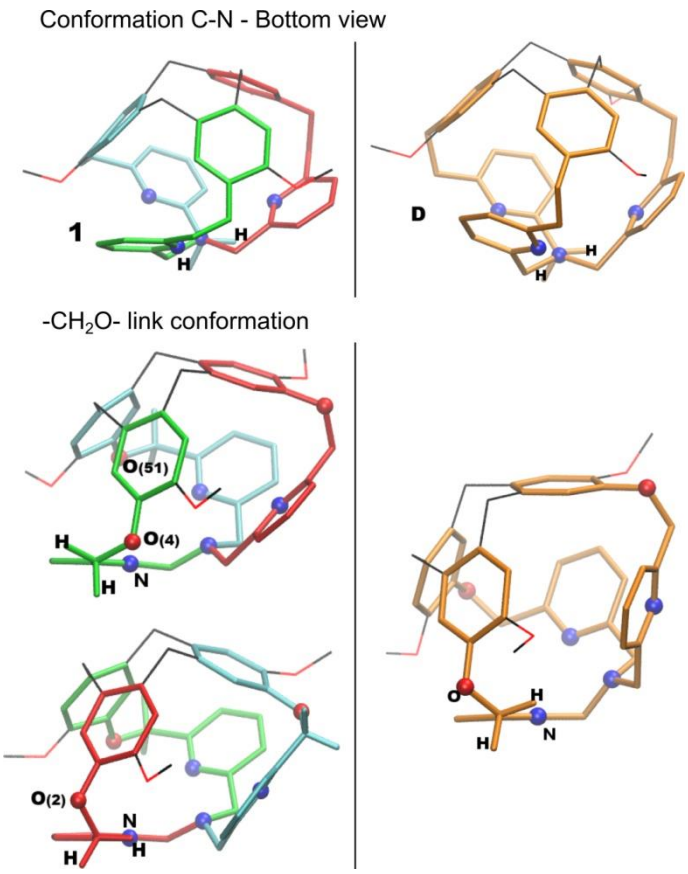

Figure 2.9 Optimized structures of 1 and D.

The PP (or MM) one-arm-inside structures (A, B and C) are the more stable among the computed ones as they possess optimal conformations, minimizing eclipsed bonds and showing a favorable orientation of the heteroatom lone pairs (nitrogen and oxygen atoms). Several conformations could be optimized and some pathways could be proposed for the conversion of one structure into the another, suggesting that equilibria are possible among A, B and C. As a consequence, the NMR signal is averaged on all the possible structures. The MP (or PM) isomers are less stable, however there exist some structures, as II, where the P or M descriptors are no more applicable for the bottom unit and that are only slightly higher in enthalpy than A.

II.5 Conclusions

We have demonstrated in this chapter that structurally contracted hemicryptophane cages (short linkers) could be used to induce and control the helical arrangement of a southern C_3 symmetrical ligand. This strategy has been employed to generate a new kind of copper(I) complexes with controlled helicity of the Cu-TPA core. We have then used the resulting enantiopure *M*- or *P*- **Cu^{I}(1)(Cl)** catalyst to try some initial test on asymmetric catalysis. However this new catalyst did not show good enantioselectivity when applied to classical copper-catalyzed reactions and additional studies are required to find more suitable model reactions. Finally, we have performed DFT calculations on the cage molecules to simulate its structural configuration and dynamic behavior, which, in particular, explained the reason why the chirality of the CTV part control the propeller arrangement of the TPA unit.

II.6 Reference

1. Lim, M.H., et al., *An FeIV=O complex of a tetradentate tripodal nonheme ligand.* Proceedings of the National Academy of Sciences of the United States of America, 2003. **100**(7): p. 3665-3670.
2. Borrell, M. and M. Costas, *Mechanistically Driven Development of an Iron Catalyst for Selective Syn-Dihydroxylation of Alkenes with Aqueous Hydrogen Peroxide.* Journal of the American Chemical Society, 2017. **139**(36): p. 12821-12829.
3. Borrell, M., et al., *Characterized cis-FeV(O)(OH) intermediate mimics enzymatic oxidations in the gas phase.* Nature Communications, 2019. **10**(1): p. 901.
4. Peterson, R.L., et al., *Cupric Superoxo-Mediated Intermolecular C−H Activation Chemistry.* Journal of the American Chemical Society, 2011. **133**(6): p. 1702-1705.
5. Garcia-Bosch, I. and M.A. Siegler, *Copper-Catalyzed Oxidation of Alkanes with H2O2 under a Fenton-like Regime.* Angewandte Chemie International Edition, 2016. **55**(41): p. 12873-12876.
6. Diaz, D.E., et al., *Impact of Intramolecular Hydrogen Bonding on the Reactivity of Cupric Superoxide Complexes with O−H and C−H Substrates.* Angewandte Chemie International Edition, 2019. **58**(49): p. 17572-17576.
7. Joyce, L.A., et al., *A Simple Method for the Determination of Enantiomeric Excess and Identity of Chiral Carboxylic Acids.* Journal of the American Chemical Society, 2011. **133**(34): p. 13746-13752.
8. You, L., J.S. Berman, and E.V. Anslyn, *Dynamic multi-component covalent assembly for the reversible binding of secondary alcohols and chirality sensing.* Nature Chemistry, 2011. **3**(12): p. 943-948.
9. Jo, H.H., et al., *Mechanistic studies on covalent assemblies of metal-mediated hemi-aminal ethers.* Chemical Science, 2015. **6**(1): p. 158-164.
10. Badetti, E., et al., *Multimetallic Architectures from the Self-assembly of Amino Acids and Tris(2-pyridylmethyl)amine Zinc(II) Complexes: Circular Dichroism Enhancement by Chromophores Organization.* Chemistry – A European Journal, 2016. **22**(19): p. 6515-6518.

11. Berardozzi, R., et al., *Co(ii)-induced giant vibrational CD provides a new design of methods for rapid and sensitive chirality recognition.* Chemical Communications, 2016. **52**(54): p. 8428-8431.

12. Zhiquan, L., et al., *A Stimuli-Responsive Molecular Capsule with Switchable Dynamics, Chirality, and Encapsulation Characteristics.* Journal of the American Chemical Society, 2018. **140**(35): p. 11091-11100.

13. Bravin, C., et al., *Triggering Assembly and Disassembly of a Supramolecular Cage.* Journal of the American Chemical Society, 2017. **139**(18): p. 6456-6460.

14. Le Poul, N., et al., *Gating the electron transfer at a monocopper centre through the supramolecular coordination of water molecules within a protein chamber mimic.* Chemical Science, 2018. **9**(43): p. 8282-8290.

15. Canary, J.W., et al., *Conformationally Driven, Propeller-like Chirality in Labile Coordination Complexes.* Journal of the American Chemical Society, 1995. **117**(32): p. 8484-8485.

16. Zhiquan, L., et al., *Russian Nesting Doll Complexes of Molecular Baskets and Zinc Containing TPA Ligands.* Journal of the American Chemical Society, 2016. **138**(26): p. 8253-8258.

17. Bravin, C., et al., *A Diastereodynamic Probe Transducing Molecular Length into Chiroptical Readout.* Journal of the American Chemical Society, 2019. **141**(30): p. 11963-11969.

18. Zhang, D., et al., *Synthesis, Resolution, and Absolute Configuration of Chiral Tris(2-pyridylmethyl)amine-Based Hemicryptophane Molecular Cages.* The Journal of Organic Chemistry, 2017. **82**(12): p. 6082-6088.

19. Ikbal, S.A., et al., *Bioinspired Oxidation of Methane in the Confined Spaces of Molecular Cages.* Inorganic Chemistry, 2019. **58**(11): p. 7220-7228.

20. Zhang, D., A. Martinez, and J.-P. Dutasta, *Emergence of Hemicryptophanes: From Synthesis to Applications for Recognition, Molecular Machines, and Supramolecular Catalysis.* Chemical Reviews, 2017. **117**(6): p. 4900-4942.

21. Colomban, C., B. Châtelet, and A. Martinez, *Different Strategies for Obtaining Enantiopure Hemicryptophanes.* Synthesis, 2019. **51**(10): p. 2081-2099.

22. Perraud, O., et al., *Resolution and absolute configuration assignment of a chiral hemicryptophane molecular cage.* Chirality, 2010. **22**(10): p. 885-888.

23. Szyszka, Ł., et al., *Synthesis of Cyclotriveratrylene-Sucrose-Based Capsules.* Organic Letters, 2019. **21**(16): p. 6523-6528.

24. Moore, C.M., et al., *A 3-Fold-Symmetric Ligand Based on 2-Hydroxypyridine: Regulation of Ligand Binding by Hydrogen Bonding.* Inorganic Chemistry, 2014. **53**(7): p. 3278-3280.

25. Dahl, E.W., H.T. Dong, and N.K. Szymczak, *Phenylamino derivatives of tris(2-pyridylmethyl)amine: hydrogen-bonded peroxodicopper complexes.* Chemical Communications, 2018. **54**(8): p. 892-895.

26. Eckenhoff, W.T. and T. Pintauer, *Atom Transfer Radical Addition in the Presence of Catalytic Amounts of Copper(I/II) Complexes with Tris(2-pyridylmethyl)amine.* Inorganic Chemistry, 2007. **46**(15): p. 5844-5846.

27. Eckenhoff, W.T., S.T. Garrity, and T. Pintauer, *Highly Efficient Copper-Mediated Atom-Transfer Radical Addition (ATRA) in the Presence of Reducing Agent.* European Journal of Inorganic Chemistry, 2008. **2008**(4): p. 563-571.

28. Bete, S.C., C. Würtele, and M. Otte, *A bio-inspired imidazole-functionalised copper cage complex.* Chemical Communications, 2019. **55**(30): p. 4427-4430.

29. You, L., et al., *An Exciton-Coupled Circular Dichroism Protocol for the Determination of Identity, Chirality, and Enantiomeric Excess of Chiral Secondary Alcohols.* Journal of the American Chemical Society, 2012. **134**(16): p. 7117-7125.

30. Takahashi, Y., et al., *P-Chiral o-Phosphinophenol as a P/O Hybrid Ligand: Preparation and Use in Cu-Catalyzed Asymmetric Conjugate Addition of Diethylzinc to Acyclic Enones.* The Journal of Organic Chemistry, 2005. **70**(22): p. 9009-9012.

31. Arai, T., et al., *Asymmetric Syn-Selective Henry Reaction Catalyzed by the Sulfonyldiamine−CuCl−Pyridine System.* The Journal of Organic Chemistry, 2008. **73**(13): p. 4903-4906.

32. Dirac, P.A.M. and R.H. Fowler, *Quantum mechanics of many-electron systems.* Proceedings of the Royal Society of London. Series A, Containing Papers of a Mathematical and Physical Character, 1929. **123**(792): p. 714-733.

33. Slater, J.C., *A Simplification of the Hartree-Fock Method.* Physical Review, 1951. **81**(3): p. 385-390.

34. Perdew, J.P. and Y. Wang, *Accurate and simple analytic representation of the electron-gas correlation energy.* Physical Review B, 1992. **45**(23): p. 13244-13249.

35. Perdew, J.P., K. Burke, and M. Ernzerhof, *Generalized Gradient Approximation Made Simple.* Physical Review Letters, 1996. **77**(18): p. 3865-3868.

36. Perdew, J.P., M. Ernzerhof, and K. Burke, *Rationale for mixing exact exchange with density functional approximations.* The Journal of Chemical Physics, 1996. **105**(22): p. 9982-9985.

37. Grimme, S., et al., *A consistent and accurate ab initio parametrization of density functional dispersion correction (DFT-D) for the 94 elements H-Pu.* The Journal of Chemical Physics, 2010. **132**(15): p. 154104.

38. Weigend, F. and R. Ahlrichs, *Balanced basis sets of split valence, triple zeta valence and quadruple zeta valence quality for H to Rn: Design and assessment of accuracy.* Physical Chemistry Chemical Physics, 2005. **7**(18): p. 3297-3305.

39. Eichkorn, K., et al., *Auxiliary basis sets for main row atoms and transition metals and their use to approximate Coulomb potentials.* Theor. chem. acc. 97 (1997) S. 119-124., 1997.

Chapter III: Design, preparation, and applications of novel tris-triazole based hemicryptophanes

III.1 Introduction

In this chapter, the design, preparation and initial application tests of two novel tris-triazole based hemicryptophanes were described. These cages were conceived to act as ligands to perform catalytic reactions in a confined space, upon coordination to a transition metal center. Our attention was directed to azide-alkyne cycloaddition reactions. The cycloaddition reaction between azides and alkynes to give triazoles[1] is one of the most important way to synthesize five-membered rings. However, the desired triazole-forming cycloaddition may require elevated temperatures and usually results in a mixture of the 1,4 and 1,5 regioisomers (**Figure 3.1**). [2]

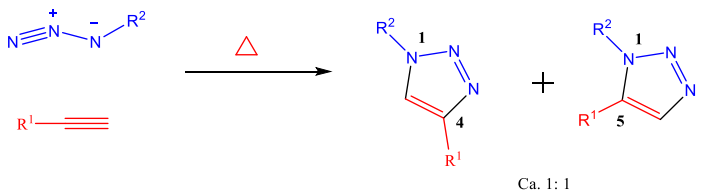

Figure 3.1 Cycloaddition between azides and alkynes

In the reaction depicted in Figure 3.2 azide **46** reacts neatly with alkyne **45** to afford the triazole products as a mixture of the 1,4-adduct (**47**) and 1,5-adduct (**48**) at 98 °C in 18 hours without catalysts. These two isomers exist in a 1: 1 ratio.

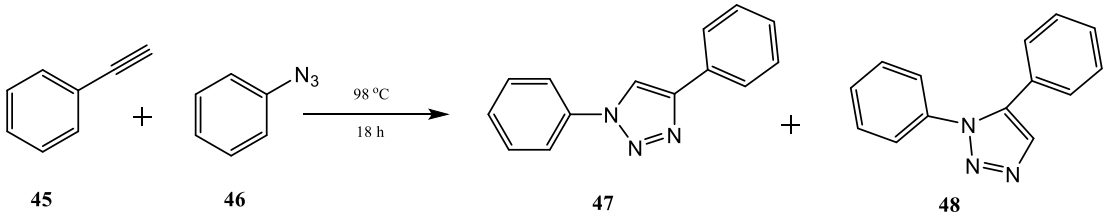

Figure 3.2 The cycloaddition reaction between the acetylene **45** and the azide **46** gives comparable amounts of the two triazole regioisomers.

However, the control of the selectivity in non-metal-catalyzed cycloadditions, has been achieve by performing the reactions in a self-assembled capsule.[3] J. Rebek and coworkers reported a synthetic chamber that accelerates the 1,3-dipolar cycloaddition. In this cylindrical cavity, the orientations of the two different aromatic substrates are constrained in such a way that only their peripheral substituents make contact, resulting in the 1,4-isomer.

Since its discovery in 2002, the copper(I)-catalyzed azide-alkyne cycloaddition (CuAAC) reaction, which regiospecifically combines azides and terminal acetylenes to give the 1,4-disubstituted 1,2,3-triazoles, has received a great deal of use in diverse fields such as chemical biology, materials science, medicinal chemistry, and polymers.[4, 5] Unlike the well-established thermal Huisgen cycloaddition reaction, the CuAAC reaction (i) allows for controlling the 1,4-stereoselectivity, (ii) is not limited to highly activated alkynes, and (iii) proceeds efficiently even in aqueous media. Although a number of copper(I) sources can be used directly, the catalyst is usually prepared from Cu(II) salts in combination with sodium ascorbate as the reductant, which are less costly and often more pure than Cu(I) salts.[6]

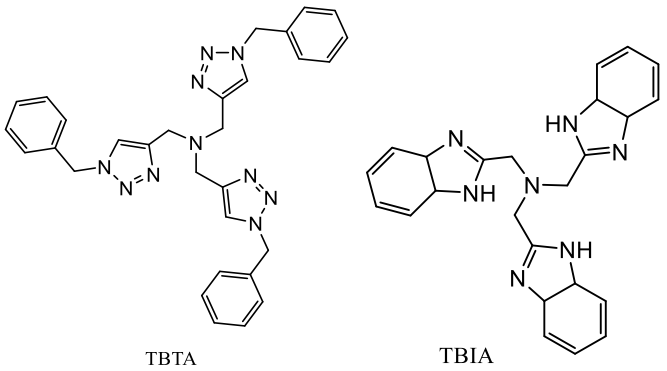

Figure 3.3 Structure of the TBTA (left) and TBIA (right) ligands that are able to coordinate and stabilize Cu(I), resulting in efficient catalyst for CuAAC reactions.

Moreover, due to the thermodynamic instability of Cu(I), which is easily oxidized to Cu(II) in the presence of O_2, the catalytic efficiency of Cu(I) salt alone is limited and the use of stabilizing ligand is often needed. The most commonly used accelerating

ligand is the tris(benzyltriazolylmethyl)amine (TBTA). This C_3-symmetric ligand, was discovered by the Sharpless laboratory in 2004 (Figure 3.3).[7] TBTA was found to be a powerful stabilizing ligand for copper(I), leading to a more reliable click cycloaddition reaction by reducing the oxidation of catalytic Cu(I) by dissolved oxygen, while enhancing its catalytic activity. Usually, in this reaction, the Cu(II) salt is pre-complexed with TBTA to form a blue complex. The resulting catalyst is then mixed with the alkyne and the azide substrates and a subsequent addition of the sodium ascorbate reductant initiate the CuAAC reaction (reduction of the Cu(II) into Cu(I)). The ligand promotes the stabilization of the copper(I) oxidation state, while allowing for the catalytic cycle of the CuAAC reaction to proceed (Figure 3.4). Although the reported structural analysis (XRD) of the $Cu^{II}(TBTA)(BF_4)_2$ complex reveals a binuclear structure (Figure 3.5), it was found that the CuAAC reaction catalyzed by the Cu^{I}(TBTA) complex proceeds with a first order dependence on copper(I) concentration[8]. Such behavior contrasts with the postulated mechanism for ligand free CuAAC reactions that usually involves two copper centers (Folkin's mechanism, Figure 3.4).[9]

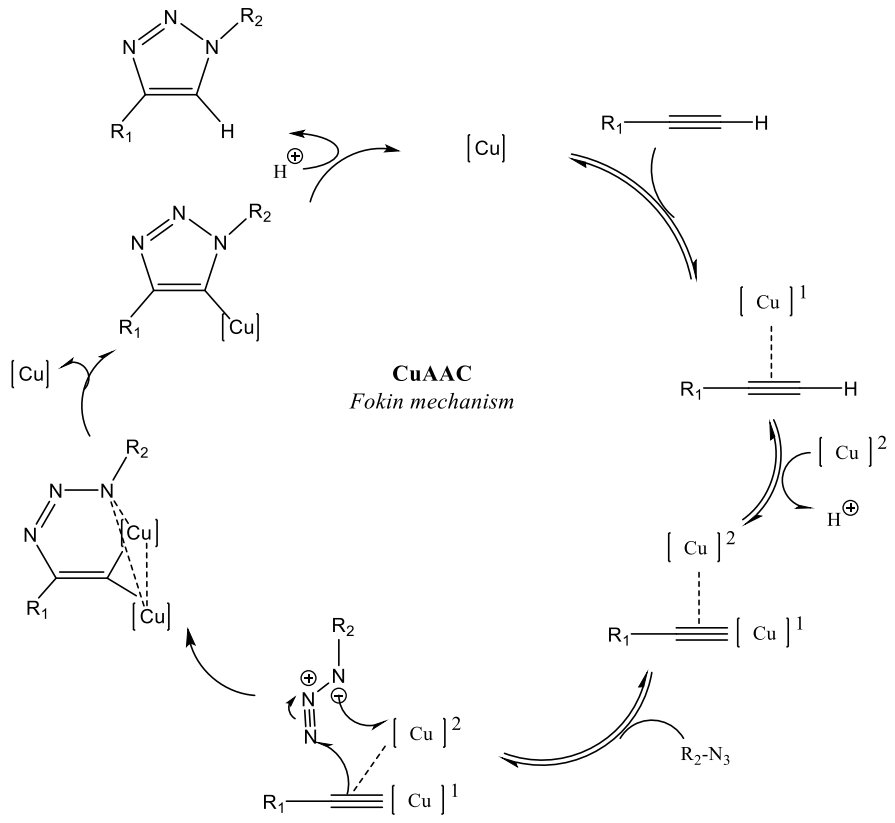

Figure 3.4 Fokin's mechanism of the CuAAC reaction

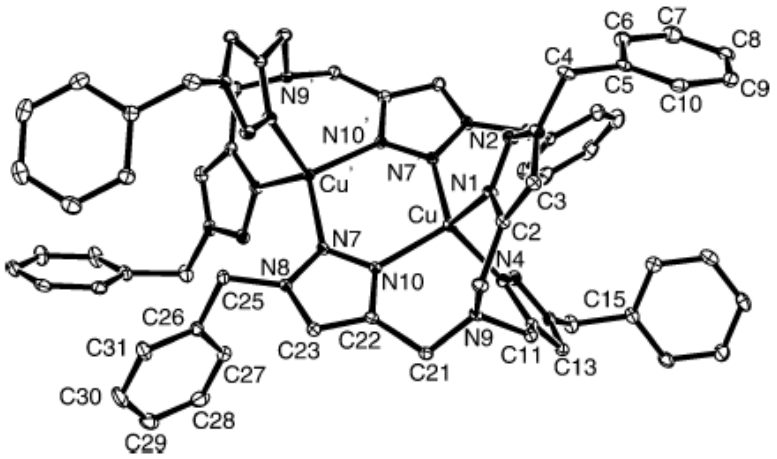

Figure 3.5 Representation of the XRD structure of the binuclear complex formed between two $Cu^{II}(TBTA)(BF_4)_2$ complexes [8]

Tris(2-benzimidazolylmethyl)amines (TBIA) (Figure 3.3), which contains three benzimidazoles, have also been found to be a superior accelerating ligands for the CuAAC reaction[10]. In addition, many ligands based on the triazole coordinating unit have been used to catalyze such reactions, because the nitrogen contained in triazole can coordinate to metals. For instance，the tris(1,2,3-triazol-4-yl)methanols ligand (TTM) and its derivatives (Figure 3.6) are constructed through regioselective, one-pot triple [3+2] cycloaddition of azides and alkynes. The TTM ligand shows a good acceleration effect in CuAAC reactions performed in aqueous media due to the fact that the TTM structure efficiently protects the metal centre against undesired oxidation or disproportionation leading to inactive Cu(II) species.[11]

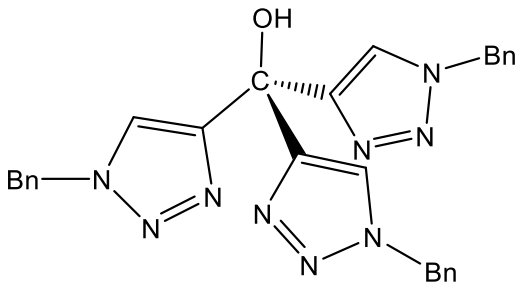

Figure 3.6 Structure of TTM ligand

III.1.1 Site selective and enantioselective CuAAC reaction.

Stereoselectivity and chemoselectivity have been key factors in the developments of organic synthesis. For instance, the site-selective and enantioselective CuAAC reaction has received much attention. Site-selective transformations, which allow for the selection of one site of reaction in a molecule, are particularly useful for example in the context of late stage functionalization reactions. The chemoselectivity of alkyne in copper-catalyzed azide-alkyne click reactions was studied and compared through competition experiments using one equivalent of the BnN_3 substrate, one equivalent of a first alkyne substrate and one equivalent of another alkyne substrate (Figure 3.7, the reactivity trend 49>50>51>52>53>54 was observed，and the rate-determining step depend on alkyne class and subtype. For the substrate 49，the Cu^{II} coordinate to the benzimidazole resulting in an increase in alkyne C-H acidity facilitating a rapid Cu acetylide formation). [9]

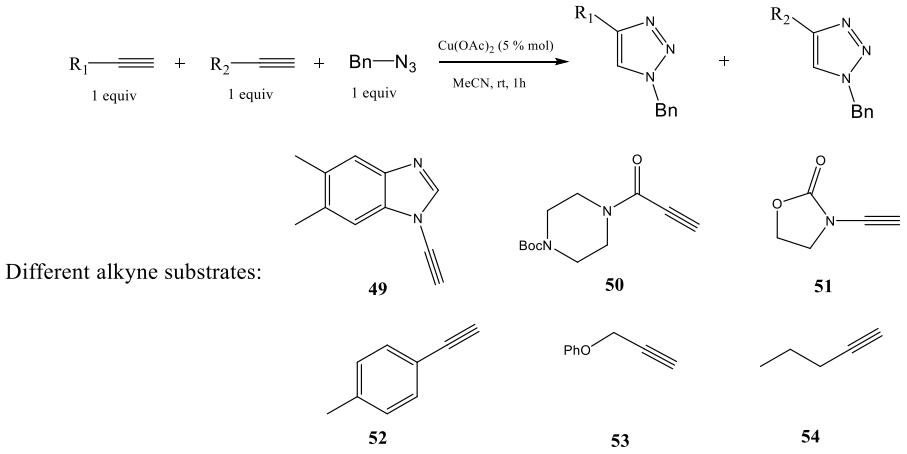

Figure 3.7 Competition CuAAC reaction with two alkynes (top) and representation of the different alkynes substrates tested in this study (bottom).

Over the last several years, there has been a huge increase in the development of new efficient organocatalysts for enantioselective pericyclic reactions. Among many processes of cycloaddition reactions (such as the [3+2]; [3+3]; [4+2]; vinylogous [4+2] and 1,3-dipolar cycloadditions), the enantioselective CuAAC reaction has attracted considerable attentions. Since Sharpless and colleagues proposed the concept of "click chemistry" in 2001,[12] the enantioselective catalytic Huisgen [3 + 2] cycloaddition reaction has been studied by many groups. For instance, new chiral

catalysts (as shown in Figure 3.8) used in copper-catalyzed azide-alkyne cycloaddition reactions have been reported. [13] The PYBOX ligand give chiral Cu(I) catalyst that affors the product **56** in 77% yield with 90% *ee*. This kind of chiral ligand therefore provides a powerful strategy for highly enantioselective intermolecular desymmetrization reactions.

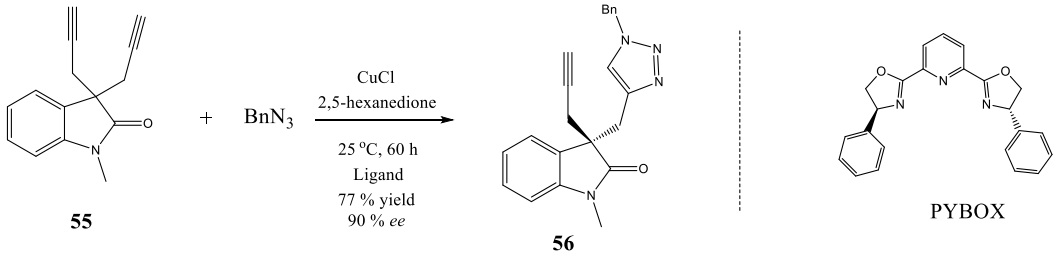

Figure 3.8 Example of one chiral ligand (right) used for asymetric CuAAC reaction on a bis-alkyne substrate (left).

In 2015, the group of Liwen Xu has developed a new type of chiral phosphine ligand (**59** in Figure 3.9) for catalytic asymmetric Huisgen [3+2] cycloaddition between azides and bis-alkynes substrate.[14] This new catalyst has shown high yield (up to 80%), and excellent enantioselectivity (ee up to 99%) on the desymmetrization of bis-alkynes. Some of their preliminary studies indicate that the ligand plays a crutial role in the formation of active binuclear or polynuclear catalysts in this asymmetric CuAAC, in which the phosphine center and the diol moiety are both important for achieving high yields and enantioselectivity.

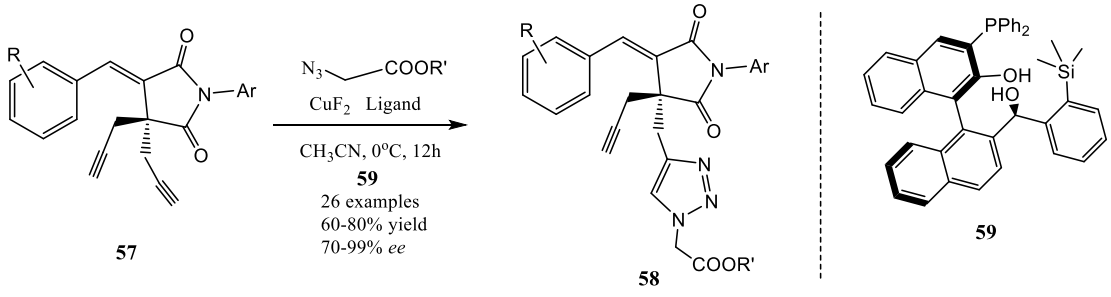

Figure 3.9 Catalytic asymmetric azide- bis-alkyne click cycloaddition (left), catalyzed by Cu^{I} complexes based on the chiral ligand **59** (right).

III.1.2 Construction of rotaxane and cages by mean of CuAAC reaction

The copper-catalyzed click cycloaddition reaction has recently found an interesting application for the preparation of supramolecular object such as rotaxanes or catenanes. These molecules, in which some of the components are connected mechanically rather than by covalent bonds, could potentially find applications for their peculiar physical and chemical properties. The use of hydrogen bonding, metal coordination, hydrophobic force, covalent bonding, or Coulomb interaction could be used to prepare interlocked structures. Leigh and colleagues have found an easy way to obtain rotaxanes, in which metal atoms catalyze the formation of covalent bonds and, at the same time, work as templates for assembling mechanically interlocked structures.[15] Because rotaxanes are mechanically combined, the size of the macrocycle is very important. Goldup's group uses the CuAAC active template reaction as a model to explore the effect of macrocycle size in the synthesis of rotaxanes.(Figure 3.10)[16] They found although sizes matters, larger macrocycles are not always better. In addition, they confirmed that the formation of rotaxane is promoted by: (*i*) a ratio of macrocycle to metal (Cu^{I}) is close to unity; (*ii*) non-coordinating solvent; (*iii*) higher reaction temperature.[17] They also designed a mechanically planar chiral rotaxane ligand, which can direct enantioselective catalysis for the Au^{I}-catalyzed Ohe-Uemura cyclopropanation of benzoate esters. This is the first time that a rotaxane ligand (**62** in Figure 3.10) has been applied in enantioselective transformations.[18]

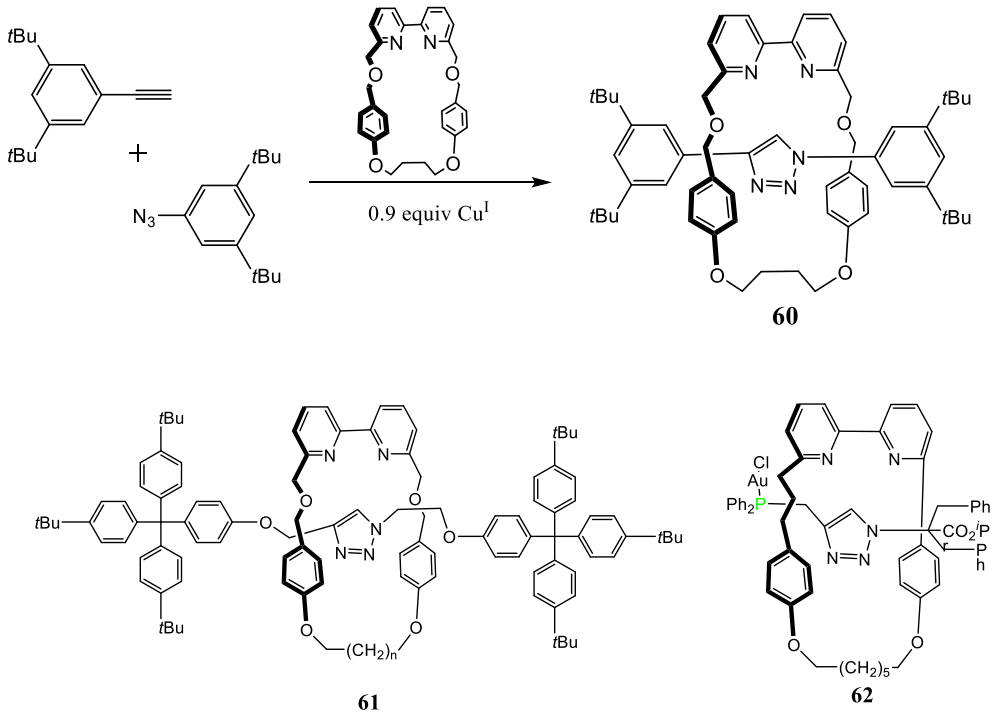

Figure 3.10 Structure of the rotaxane **60**, **61** and **62** developped by Goldup and coworkers.

Finally, very few examples of cages built from triazole-based structures have been reported. A first example of a tris(triazole) hemispherical cage, synthesized in a one-pot procedure, was reported in 2009 (**63** in Figure 3.11).[19] Recently, a new cage containing six 1,2,3-triazoles was reported (**64** in Figure 3.11). This cage, which can work as a chloride-selective receptor due to the strong C-H hydrogen bonding from the six triazoles, displays an exceptional affinity for this annion (up to 10^{17} M^{-1}). This receptor has been used for the liquid-liquid extractions of chloride from water into the non polar dichloromethane solvents).[20] Besides, another triazole-based cage, able to selectively recognize the Cl^- anion in water, was very recently synthesized via CuAAC.[21] However, to the best of our knowledge, no example of CuACC reaction performed in the confined space of molecular cages could be found in the literature. With the aim of running the CuAAC reaction in confined spaces, we wanted to introduce the (tris)triazole unit into an hemicryptophane cage. This kind of organic capsule has never been used before as ligand for CuAAC reaction. Hence, these new kind of hemicryptophane could be obtain through the covalent capping of the *C3* symmetrical (tris)triazole moiety by a CTV unit. Herein, we report two new

(tris)-triazole-based hemicryptophane cages called **cage 2** and **cage 3** (Figure 3.11). This part will be devoted to the synthesis, characterization, and use of these new cage-ligands for copper-catalyzed CuAAC reaction in confined space, as well as a first attempt to prepare hemicryptophane-based rotaxane.

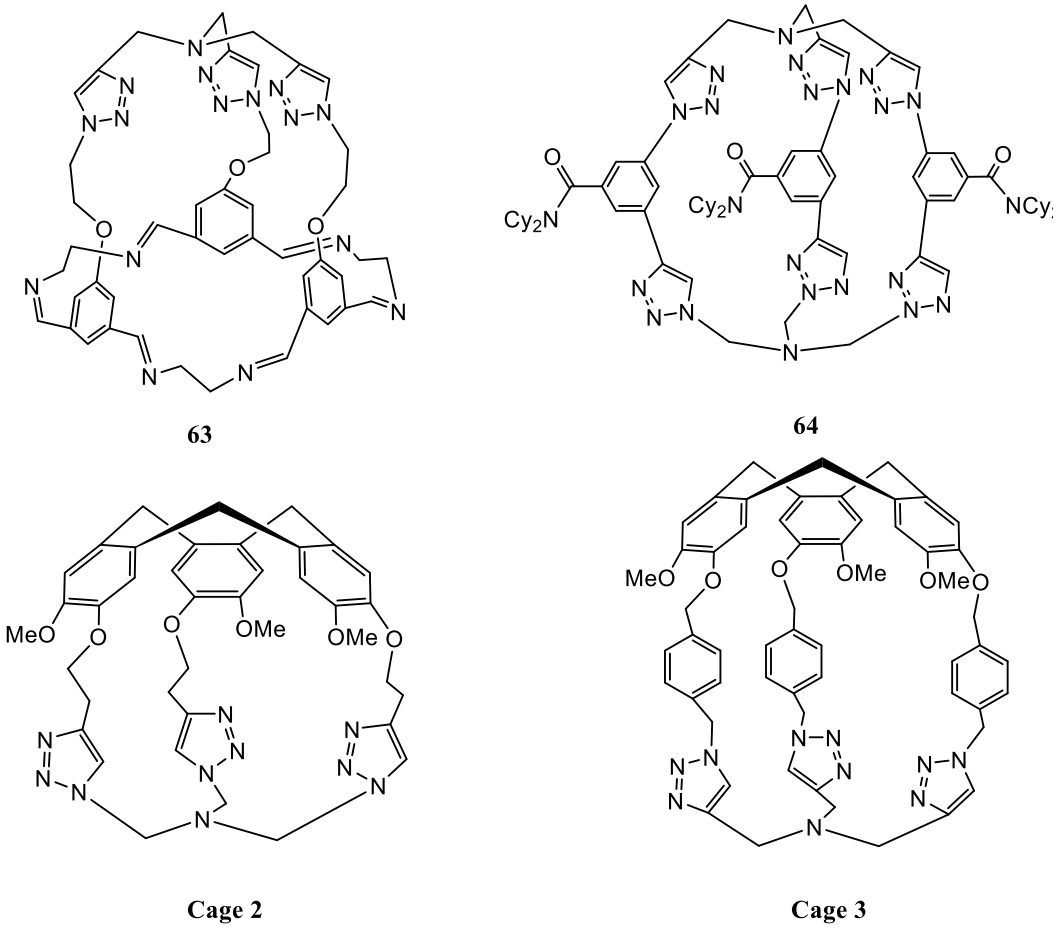

Figure 3.11 Structures of reported triazole-based cages **63** and **64** (top), and hemicryptophane cages targeted in this study (**cage 2** and **cage 3**, bottom).

III.2 Result and discussion

III.2.1 Synthesis

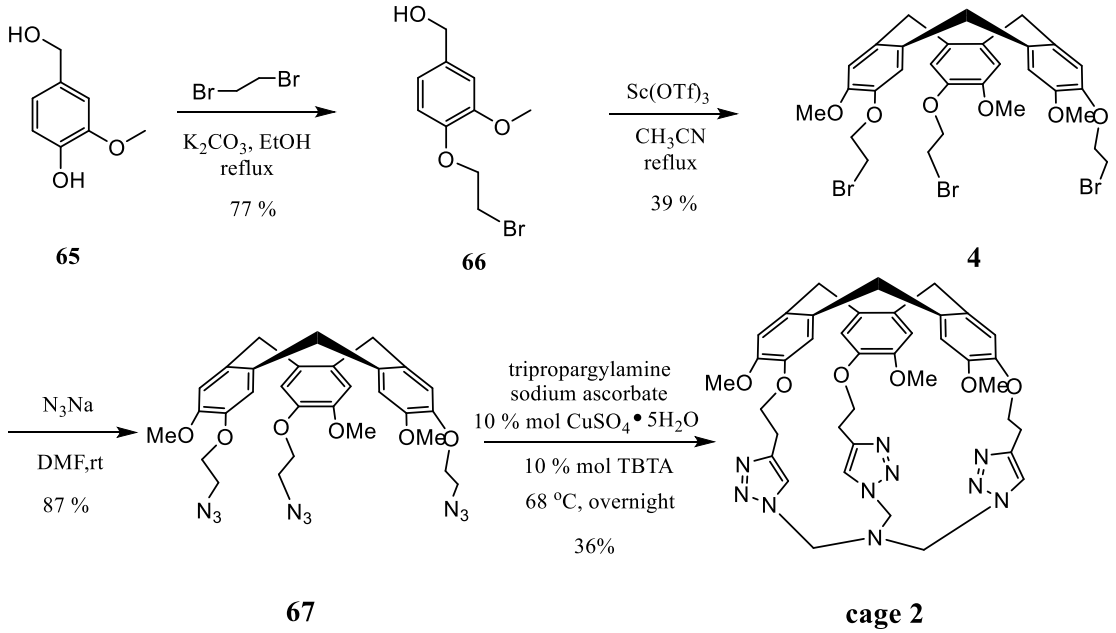

Figure 3.12 Synthetic route of the synthesis of **cage 2**

The **cage 2** was prepared following a 4 steps synthesis in an overall yield of 10 %. The synthesis started with the reaction between vanillyl alcohol and 1,2-dibromoethane to yield **66** (77% yield). The CTV derivative **4** was then obtained by the macrocyclisation reaction of **66** in CH_3CN, catalyzed by the Lewis-acid $Sc(OTf_3)$. The bromine substituents of **4** were then replaced by N_3 to generate the azide-based CTV **67**. Finally, the **cage 2** was obtained in 36% yield by a final cage-closure reaction involving three CuAAC reactions between **67** and the tripodal tripropargylamine unit, catalyzed by the Cu^I(TBTA) complex.

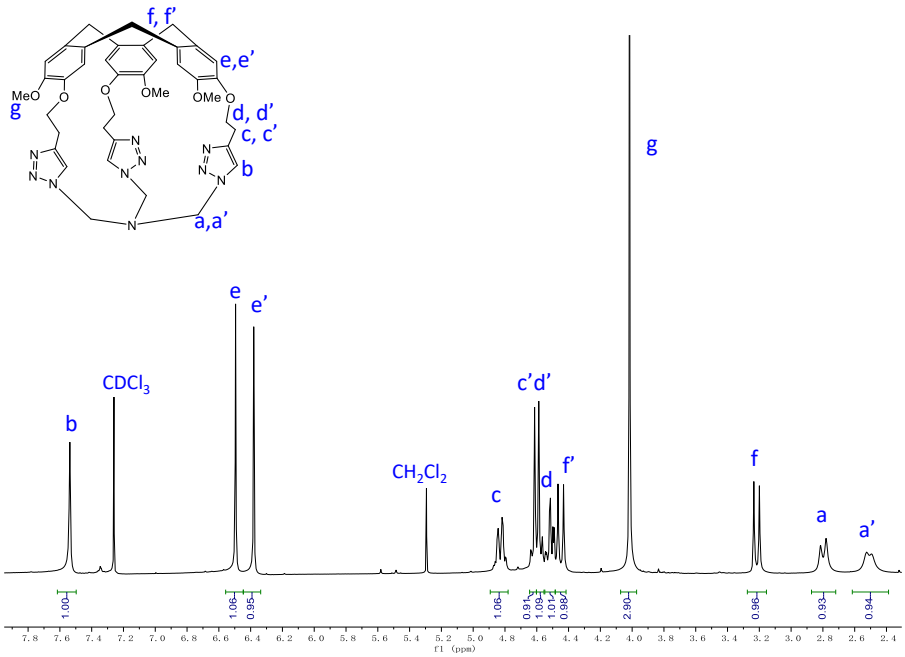

Figure 3.13 ^{1}H-NMR (400 MHz, $CDCl_3$, 298 K) of **cage 2**.

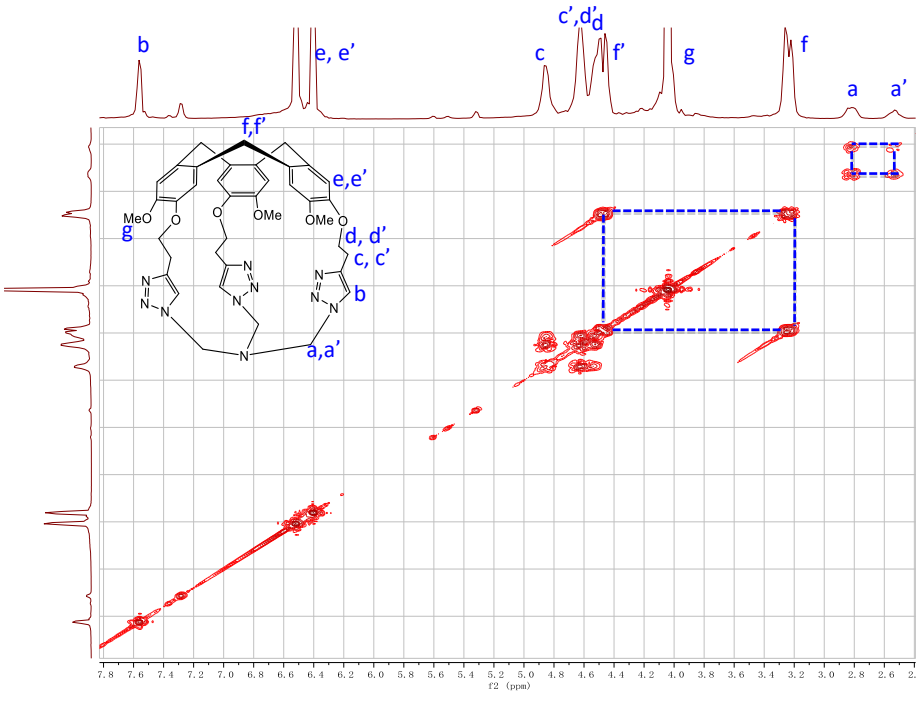

Figure 3.14 2D COSY-NMR spectra (400 MHz, $CDCl_3$, 298 K) of **cage 2** .

The ^{1}H NMR spectrum of **cage 2 (**Figure 3.13**)** shows that the structure has an average C_3 symmetry in solution. It shows the general characteristics of the CTV unit structure ($H_{f,f'}$, and $H_{e,e'}$), one singlet from the triazole C-H bond (H_b), and one singlet for the CTV's OCH_3 group (H_g). The attribution of the diastereotopic proton on the -CH_2N- of the (tris)triazole part, was confirmed by 2D COSY-NMR analysis (Figure 3.14).

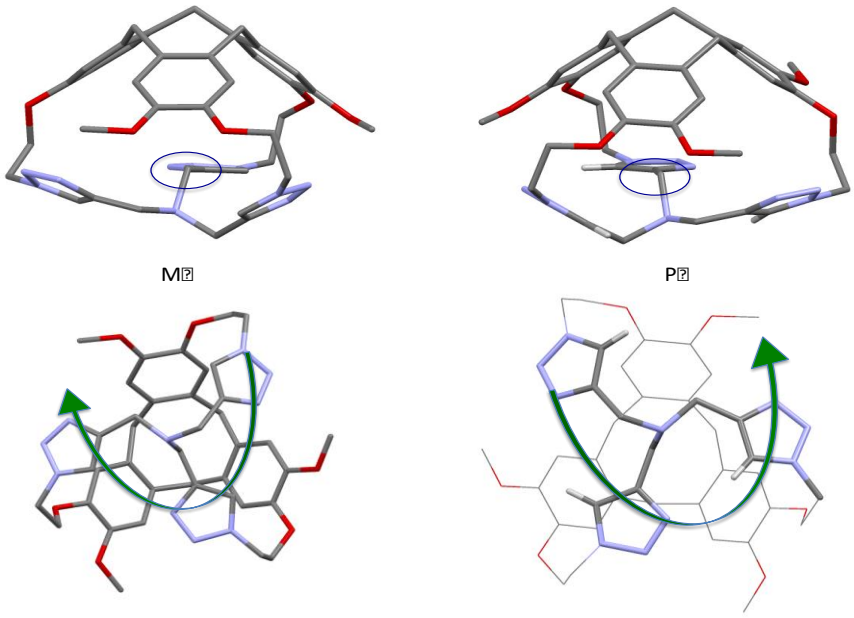

Figure 3.15 Representation of the X-ray structure of **cage 2**. Green arrow: orientation of the arrangement of the triazole depending on the nature of the CTV cap (*M*- or *P*-)

The X-ray crystal structure of **cage 2** was obtained by slow diffusion of diethyl ether into a solution of the cage in dichloromethane. Interestingly, we can see from the XRD structure of **cage 2** (Figure 3.15), that a chirality transfer phenomenon, identical to the one observed in the case of **cage 1** (chapter II), can be observed. Its southern structure (tris-triazole) indeed presents a propeller-like arrangement, with an orientation dictated by the chirality of CTV unit. By comparison with **cage 1**, which displays –CH_2- methylene linkers, the CTV and the (tris)triazole ligand in **cage 2** are connected by ethylene –C_2H_4- bridges. Therefore, this result interestingly demonstrate

that the transfer of chirality from the CTV unit to a southern ligand still occurs with slightly longer linkers. Like in **cage 1**, one CH_2-N of the southern part resides inside the cavity of the cage in the solid-state structure. However, from the ^{1}H-NMR we can see that **cage 2** has a C_3-symmetrical structure in solution, this may be due to the rapid exchange between the three –CH_2-N of the cage like in the case of **cage 1** (see chapter II, calculations).

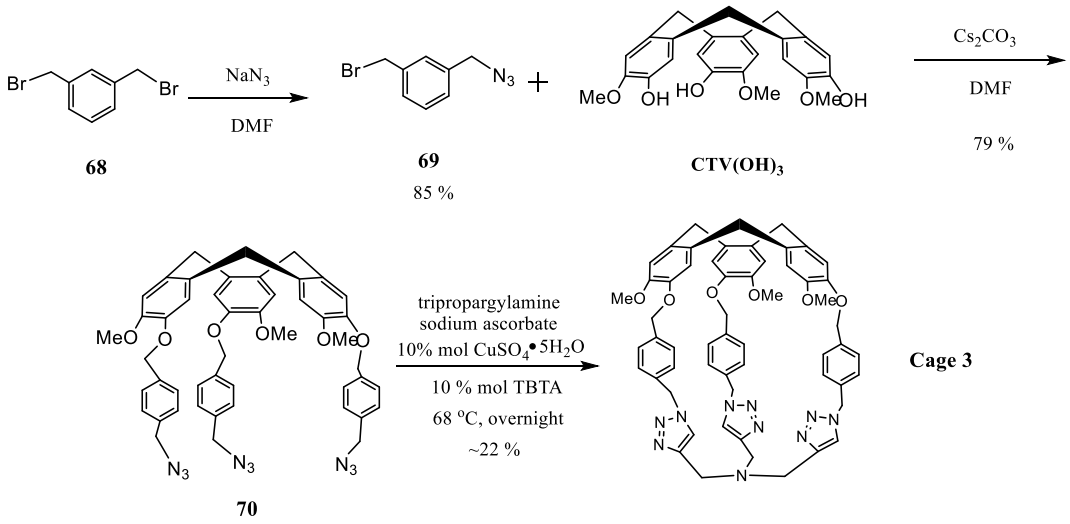

Figure 3.16 Synthetic route of the preparation of **cage 3**

The **cage 3** was prepared following a 2 steps synthesis starting form the **CTV(OH)3**, which has been prepared according to the synthesis shown in chapter II (see Annex N°1). Compound **69** was firstly obtained by the mono-substitution of 1,3-Bis(bromomethyl)benzene with NaN_3. Then, it reacted with **CTV(OH)3** in DMF using Cs_2CO_3 as base to provide CTV **70** in 79% yield. Finally, the Cu(I) catalyzed cycloaddition reaction between **79** and tripropargylamine form the **cage 3** in 22% yield. For this last step, TBTA was used as ligand, since it has been found to be a good ligand for the CuAAC reaction.

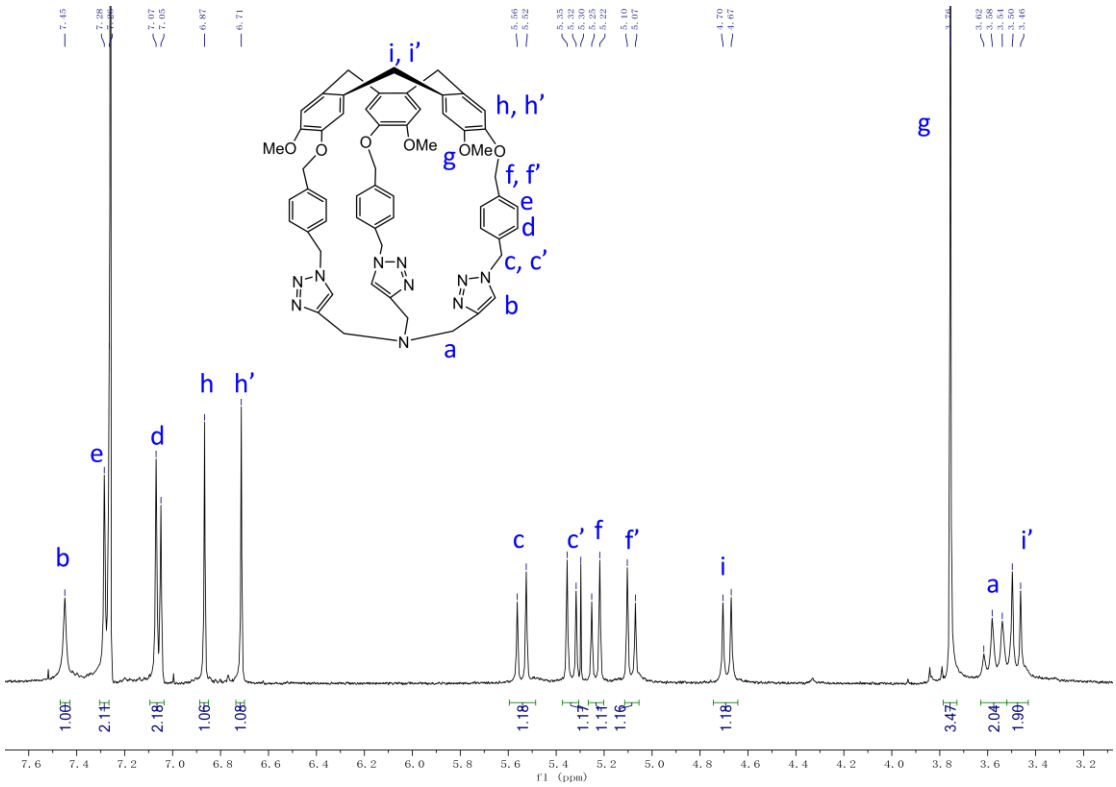

Figure 3.17 ^{1}H-NMR (400 MHz, $CDCl_3$, 298 K) of **cage 3** in $CDCl_3$

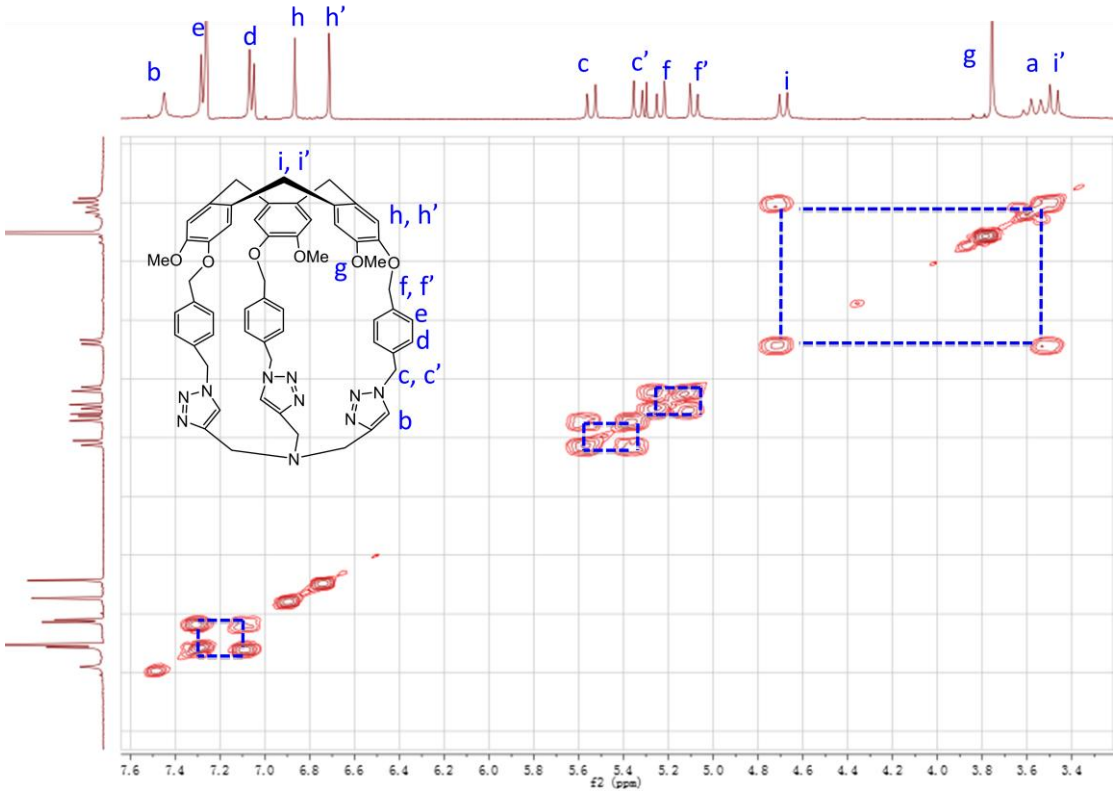

Figure 3.18 2D COSY-NMR (400 MHz, $CDCl_3$, 298 K) of **cage 3**.

Like **cage 2**, the ^{1}H NMR spectrum of **cage 3** (Figure 3.17), reveal a C_3 symmetry in solution on average. Beside, the general characteristics of the CTV unit aromatics ($H_{i,i'}$, $H_{h,h'}$) and OCH_3 group (H_g), and the singlet from the triazole's C-H (H_b), it is interesting to see that the signal of proton Ha (CH_2-N) are diastereotopic like in the case of **cage 2**.

III.2.2 CuAAC in confined space : first catalytic tests

We initially tried using the **cage 2** and **cage 3** as ligands for a common CuAAC reaction, and compared them with the TBTA ligand. Here we will discuss some preliminary data that have been obtained.

a) Catalytic tests using Cu(II) salt in an aqueous solvent mixture.

At the beginning, we first tried to use the copper(II) salt $CuSO_4 \cdot 5H_2O$ as the source of copper, and the sodium ascorbate salt as the reducing agent to carry out the reaction in an aqueous solvent system (THF/H_2O/^{t}BuOH solvent mixture) following a catalytic protocol reported by Sharpless et al.[6] CuAAC reactions between the two common substrates phenylacetylene and benzyl azide were monitored by ^{1}H-NMR using 2,4-dibromomesitylene as internal standard (Figure 3.19).

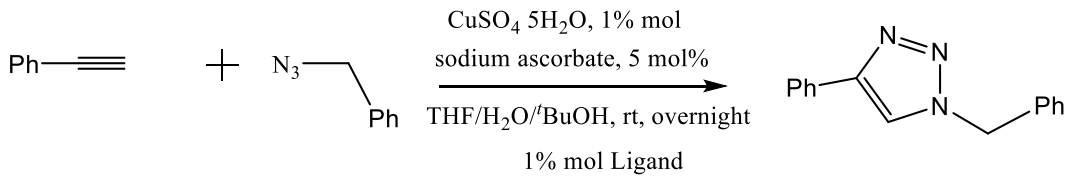

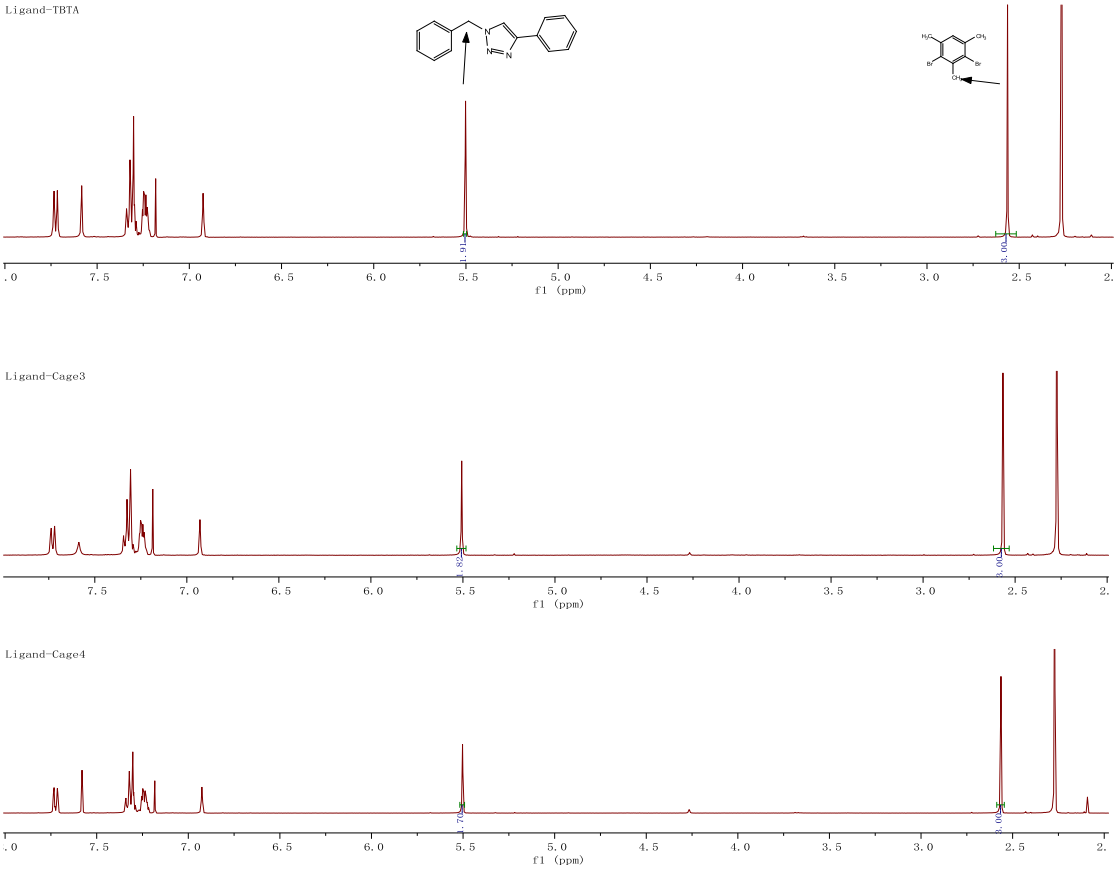

Figure 3.19 Representation of the CuAAC reaction studied together with the analysis of reaction at room temperature using ligands TBTA (top), **cage 2** (middle) and **cage 3** (bottom), after overnight.

We follow similar reaction conditions as the one used by Sharpless et al.:1 mol% of the three different ligands (TBTA, **cage 2** and **cage 3**), in a 2 : 1 : 1 THF/H_2O/^{t}BuOH solvent mixture. Yields for the different reactions between the benzyl azide and the phenylacetylene were determined by comparing integration of the triazole product (-CH_2- signal at 5.51 ppm) with the signal of the internal standard 2,4-dibromomesitylene. Reactions were also monitored after 30 minutes, one and two

hours of reaction (Figure 3.19). Different results were observed with TBTA , **cage 2** and **cage 3**. We observed that after one hour, the reaction with TBTA was almost 2 times faster (47 % yield), than with **cage 3** that displays a yield of 18 %. Furthermore, we observed that the reaction was faster with **cage 2** than with **cage 3** but still slower than in the case of TBTA with 30% yield (Figure 3.20). The TBTA ligand performs more efficiently, maybe due to its open structure, which allows for an easier access to both alkyne and azide substrates. According to *i*) the XRD structure of **cage 2**, and *ii*) the characterization of the Cu(I) complex of **cage 1** (see chapter II), it is reasonable to propose that the binding of one copper center to **cage 2** will occur outside of the cage. Therefore the CuAAC reaction probably occurs outside of the **cage 2**, explaining the fact that the reaction is more efficient with **cage 2** than with **cage 3** (easyier access to both substrates).

Because we wanted to compare the classical CuAAC reaction with the click reaction performed within the hemicryptophane cavity, we then chose to focus our attention on the comparison between **cage 3** and TBTA. In order to determine if the reaction really takes place inside the cavity of the hemicryptophane, identical reactions were performed using TBTA and **cage 3**, in the presence of tetramethyl ammonium picrate ($N(Me)_4^+Pic^-$). It is indeed reported that the amonium cation of $N(Me)_4^+Pic^-$ is effectively stabilized by the CTV unit of hemicryptophanes (inside the cavity) while the picrate anion (Pic^-) is too big to enter the hemicryptophane cavity.[22]

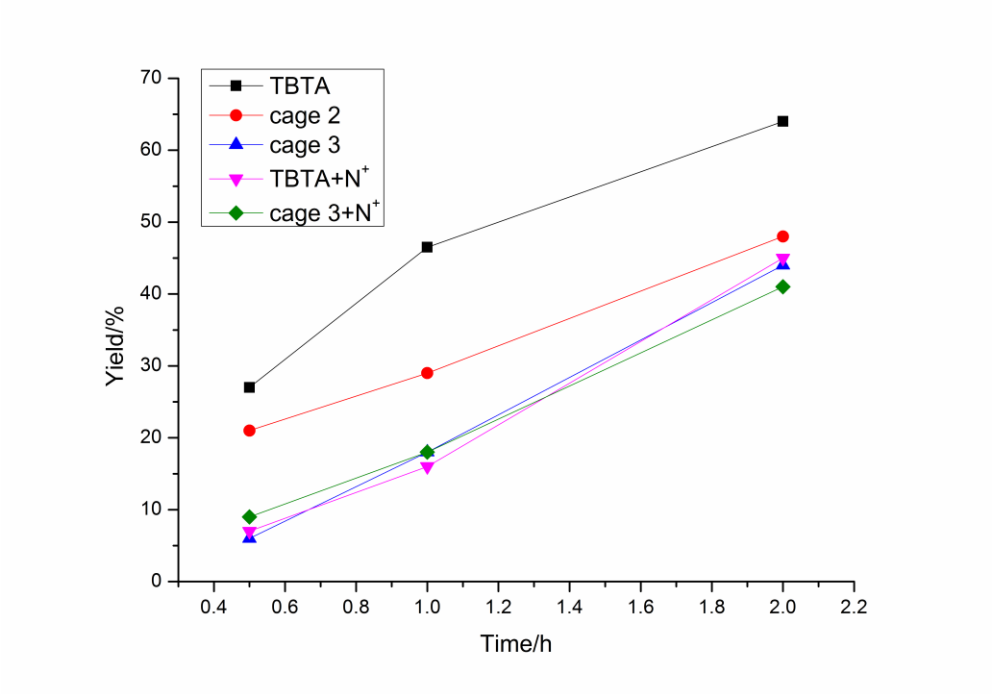

Figure 3.20 Time-dependent (0.5, 1 and 2 hours) catalytic efficiency (yield in triazole product) of the CuAAC reaction between phenylacetylene and benzyl azide (reaction in Figure 3.19), using different ligands in the absence or presence of 7 equivalent of the tetramethylammonium picrate $NMe_4^+Pic^-$ guest (**N)**. Black line : TBTA alone; red line: **cage 2** alone; blue line : **cage 3** alone; purple line: TBTA with $NMe_4^+Pic^-$; green line : **cage 3** with $NMe_4^+Pic^-$. (Reaction conditions: 1% mol $CuSO_4 \cdot 5H_2O$, sodium ascorbate, 5 mol% mol, 1% mol Ligand, THF/H2O/^{t}BuOH=2:1:1, rt, overnight)

Surprisingly, the reaction using **cage 3** as a ligand only reveal minor changes when performed in the presence of 7 equivalent of $NMe_4^+Pic^-$ (Figure 3.20 blue and green line). Conversely, when TBTA is used as a ligand, the efficiency of the reaction decreases significantly in the presence of NMe_4^+Pic: the yield drops from 47% to 16% after 1 hour and from 64 % to 45 % after 2 hours, as shown in Figure 3.20 black and purple line. Our hypothesis to explain this behavior is: because the reaction is performed in $H_2O/^t$BuOH/THF, we suppose that this aqueous solvent mixture prevents the encapsulation of the water-soluble NMe_4^+ guest within the cage, therefore no changes on the catalysis are observed. The repulsion between the positive charged Cu(I) and the $N(Me)_4^+$ can also account for the lack of complexation. On the other side, the TBTA-Cu^{II} system reveals a significant drop in the catalytic efficiency upon addition of $NH_4^+Pic^-$. In order to explain this observation we propose that the

picrate anion acts as an axial ligand to the Cu(II) center preventing the CuACC reaction. Interestingly, in the case of the **cage 3**, the picrate anion, which is too big to enter the cavity, do not reduce the catalytic efficiency. In order to confirm this hypothesis we then choose to turn our attention to CuACC reactions performed in organic solvent using Cu(I) sources.

b) Catalytic tests using Cu(I) salt in organic solvent.

The initial CuAAC results obtained combining the Cu(I)(PF_6) salt and ligand (TBTA or **cage 3**) in an organic solvent mixture (CH_2Cl_2:MeOH=10:1) and in the presence or absence of potatium picrate K^+Pic^- (7 equivalents compared to the copper) are shown in the following table. From table 1 we can see that after adding the K^+Pic^-, the efficiency of the CuAAC reaction with TBTA is decreased by almost a factor 2 (from 35% to 17%) after 2 hours. However, even after adding the K^+Pic^-, the reaction with **cage 3** shows almost identical catalytic efficiency. From these results, we infer that because the picrate group is relatively large, it cannot enter the molecular cage, but it can be coordinated to the copper center in the case of the open model ligand TBTA, leading to a reduction in the reaction efficiency. Importantly, this confirms that the reaction takes place inside the cavity of **cage 3**. Finally, these results strongly suggest that our cage-ligand could be use to avoid the inhibition of the CuAAC reactions observed in the case of open Cu-complexes in the presence of large ligands able to bind to the Cu-center (like the picrate anion).

Table 3.1 Catalytic efficiency (yield in desired triazole product) of the CuAAC reaction between phenylacetylene and benyl azide under different reaction conditions.

Conditions	Yield after 0.5h	Yield after 2h
TBTA+ Cu(I)(PF_6)	12%	35%
TBTA+ Cu(I)(PF_6)+K^+Pic^-	6%	17%
cage 3 + Cu(I)(PF_6)	6.5%	17%
cage 3 + Cu(I)(PF_6)+ K^+Pic^-	7%	18.5%

Reaction conditions: Phenylacetylene (0.25 mmol), Benzyl azide (0.25 mmol), 1% mol Cu(I)(PF_6), 1 mol% catalyst, 2 mL DCM, then 0.2 mL MeOH under argon for 2 hours. (7 equivalents of potatium picrate K^+Pic^- compared to the copper)

In order to take adavantage of the cage-structure of our hemicryptophane ligand, future work will focus on selective CuAAC using substrates of different size. The idea is to estimate if the cage-ligand could be used to discriminate between large and small substrates, aiming at achieving CuAAC reactions with original selectivity. We therefore intend to test more substrates, and will study the competitive reaction of different substrates in the presence of the cage as ligand.

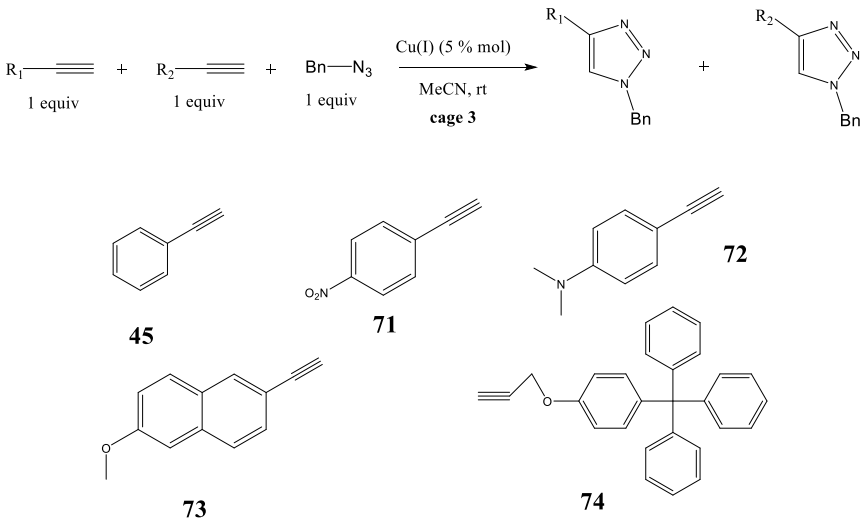

Figure 3.21 Competition CuAAC reaction with two alkynes (top) and representation of the different alkyne substrates will be tested in the future (bottom)

c) Preliminary results of the preparation of rotaxane within hemicryptophane cages

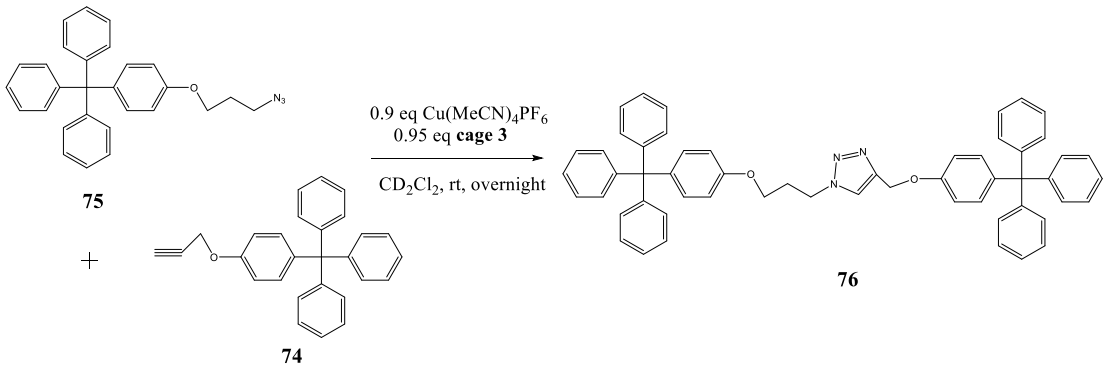

Figure 3.22 Representation of the CuAAC reaction that has been studied in the presence of **cage 3** to studied the possible formation of a rotaxane.

In order to access the possibility of constructing the first rotaxane based on a hemicryptophane cage we have tried to performed the CuAAC reaction between substrates **74** and **75** (in Figure 3.22) owning a large substituent that could act as stoppers to block the resulting triazole product within the cavity of **cage 3**. We performed this reaction with Cu(I) (0.9 eq) and **cage 3** (0.95 eq). We observed the formation of the product by ^{1}H-NMR and ESI-MS but we could not detect the presence of signal of the product inside the cage (no changes in the signal of the cage which remains C_3-symmetrical), maybe the reaction occurs in only one of the three windows of cage, then the product is ejected. Therefore, this result indicates that the construction of hemicryptophane-based rotaxanes by locking a triazole product displaying large stopper, is not an easy task. Probably the high flexibility of the hemicryptophane cages allows for an easy ejection of the CuAAC product.

III.3 Conclusions

In summary, we have designed and synthesized two new molecular cages, for the catalysis of copper-catalyzed cycloaddition reactions in a confined environment. Interestingly, we have demonstrated that the CuAAC reaction takes place inside the cavity of **cage 3** and that this cage-ligand could be used to prevent the inhibition of the CuAAC reaction resulting from a binding of large ligands (like the picrate annion) to the copper center. In the future, we will also test a series of competiton reactions between substrates of different size, using our molecular cage as a ligand, in order to achieve size-selective CuAAC reactions. Meanwhile, we also expect to construct a new rotaxane by improving the size and shape of the alkyne and azide substrates (such as increasing the length of the side chain and size of the stoppers).

III.4 References

1. Huisgen, R., *Kinetics and reaction mechanisms: selected examples from the experience of forty years.* Pure and Applied Chemistry, 1989. **61**(4): p. 613.
2. Clarke, D., R. W. Mares, and H. McNab, *Preparation and pyrolysis of 1-(pyrazol-5-yl)-1,2,3-triazoles and related compounds1.* Journal of the Chemical Society, Perkin Transactions 1, 1997(12): p. 1799-1804.
3. Chen, J. and J. Rebek, *Selectivity in an Encapsulated Cycloaddition Reaction.* Organic Letters, 2002. **4**(3): p. 327-329.
4. Tornøe, C.W., C. Christensen, and M. Meldal, *Peptidotriazoles on solid phase: [1,2,3]-triazoles by regiospecific copper(i)-catalyzed 1,3-dipolar cycloadditions of terminal alkynes to azides.* The Journal of organic chemistry, 2002. **67**(9): p. 3057-3064.
5. Finn, M.G. and V.V. Fokin, *Click chemistry: function follows form.* Chemical Society Reviews, 2010. **39**(4): p. 1231-1232.
6. Rostovtsev, V.V., et al., *A Stepwise Huisgen Cycloaddition Process: Copper(I)-Catalyzed Regioselective "Ligation" of Azides and Terminal Alkynes.* Angewandte Chemie International Edition, 2002. **41**(14): p. 2596-2599.
7. Chan, T.R., et al., *Polytriazoles as Copper(I)-Stabilizing Ligands in Catalysis.* Organic Letters, 2004. **6**(17): p. 2853-2855.
8. Donnelly, P.S., et al., *'Click' cycloaddition catalysts: copper(i) and copper(ii) tris(triazolylmethyl)amine complexes.* Chemical Communications, 2008(21): p. 2459-2461.
9. Seath, C.P., G.A. Burley, and A.J. Watson, *Determining the Origin of Rate-Independent Chemoselectivity in CuAAC Reactions: An Alkyne-Specific Shift in Rate-Determining Step.* Angew Chem Int Ed Engl, 2017. **56**(12): p. 3314-3318.

10. Rodionov, V.O., et al., *Benzimidazole and Related Ligands for Cu-Catalyzed Azide−Alkyne Cycloaddition.* Journal of the American Chemical Society, 2007. **129**(42): p. 12696-12704.

11. Etayo, P., C. Ayats, and M.A. Pericàs, *Synthesis and catalytic applications of C3-symmetric tris(triazolyl)methanol ligands and derivatives.* Chemical Communications, 2016. **52**(10): p. 1997-2010.

12. Kolb, H.C., M.G. Finn, and K.B. Sharpless, *Click Chemistry: Diverse Chemical Function from a Few Good Reactions.* Angewandte Chemie International Edition, 2001. **40**(11): p. 2004-2021.

13. Zhou, F., et al., *Asymmetric copper(I)-catalyzed azide-alkyne cycloaddition to quaternary oxindoles.* J Am Chem Soc, 2013. **135**(30): p. 10994-7.

14. Song, T., et al., *Enantioselective copper-catalyzed azide-alkyne click cycloaddition to desymmetrization of maleimide-based bis(alkynes).* Chemistry, 2015. **21**(2): p. 554-8.

15. Aucagne, V., et al., *Catalytic "Active-Metal" Template Synthesis of [2]Rotaxanes, [3]Rotaxanes, and Molecular Shuttles, and Some Observations on the Mechanism of the Cu(I)-Catalyzed Azide−Alkyne 1,3-Cycloaddition.* Journal of the American Chemical Society, 2007. **129**(39): p. 11950-11963.

16. Lahlali, H., et al., *Macrocycle Size Matters: "Small" Functionalized Rotaxanes in Excellent Yield Using the CuAAC Active Template Approach.* Angewandte Chemie International Edition, 2011. **50**(18): p. 4151-4155.

17. Neal, E.A. and S.M. Goldup, *Competitive formation of homocircuit [3]rotaxanes in synthetically useful yields in the bipyridine-mediated active template CuAAC reaction.* Chemical Science, 2015. **6**(4): p. 2398-2404.

18. Heard, A.W. and S.M. Goldup, *Synthesis of a Mechanically Planar Chiral Rotaxane Ligand for Enantioselective Catalysis.* Chem, 2020. **6**(4): p. 994-1006.

19. Steinmetz, V., F. Couty, and O.R.P. David, *One-step synthesis of chiral cages.* Chemical Communications, 2009(3): p. 343-345.

20. Liu, Y., et al., *Chloride capture using a C–H hydrogen-bonding cage.* Science, 2019. **365**(6449): p. 159.

21. Chen, Y., et al., *Selective Recognition of Chloride Anion in Water*. Organic Letters, 2020. **22**(12): p. 4878-4882.

22. Zhang, D., et al., *Tailored oxido-vanadium(V) cage complexes for selective sulfoxidation in confined spaces.* Chemical Science, 2017. **8**(1): p. 789-794.

Chapter IV: Design and preparation of a novel hemicryptophane cage with two different metal binding-site

IV.1 Introduction

The selective oxidation of unactivated C-H bonds is still a challenge in modern chemistry. The inert nature of this bond requires the use of highly reactive species, which poses major issues in terms of chemo-, regio- and stereoselectivity. It is therefore a major task to design a unique catalyst that can promote high reactivity, but at the same time act as a highly selective oxidant, which selectively mediates C–H oxidation reactions. For instance, in the case of the oxidation of methane CH_4, high temperature and pressure are often required to initiate the reaction, and the selective oxidation of CH_4 to CH_3OH is therefore difficult to control. Because the C-H bonds in the methane molecule are very strong (the highest C-H bond dissociation energies of about 104 kcal mol^{-1}), its oxidation requires a very strong oxidant or very harsh conditions, that often lead to overoxidation of the methanol into formic acid or even carbon dioxide.[1] The efficient and selective conversion of methane into methanol under mild conditions has always been desired because methanol, which is liquid under ambient conditions, has advantages in transportation, storage, and safety.

However, in nature, the enzymes called soluble and particulate methane monooxygenases (MMOs and MMOp respectively), can selectively hydroxylate methane into methanol under mild conditions.[2-4] Although the exact nature of the MMOp and MMOs active sites are still under debate, it is admitted that the activation of O_2 at the particulate methane monooxygenase involves a dinuclear copper active site, which is reported to play a crucial role in CH_4 hydroxylation.[5, 6] Such hypothesis has been supported by bioinspired studies using zeolite-supported dicopper active center with $[Cu_2O]^{2+}$ cores.[7, 8] The far superior efficiency of dinuclear copper complexes built from the TPA ligand, compared to the mononuclear counterpart have also been recently reported for the challenging water oxidation reaction.[9] Moreover, through the use of density functional theory (DFT) calculations, it was confirmed that some dicopper complexes have the catalytic performance to perform the hydroxylation of methane to methanol.[5] On the other side, it has been proposed that the soluble methane monooxygenase catalyses the selective oxidation of methane through the formation of highly reactive non-heme diiron oxo species (presumably $O=Fe^{IV}$-O-Fe^{IV}-OH) [10]. In order to mimic the reactivity of the MMOs, bio-inspired dinuclear iron catalysts have been developed. In

2009, the group of Lawrence Que have generated a novel diiron(IV) complex, and demonstrated that this catalyst can cleave strong C–H bonds with higher efficiency compared to the corresponding mononuclear Fe^{IV}=O complexes.[11] Another remarkable example have been reported in 2012 by Sorokin et al. with a binuclear heme complex displaying two iron active centers (N-bridged diiron porphyrin catalysts) that has been proved to oxidize methane with an unprecedented efficiency by an N-bridged high-valent diiron oxo-active species (L)Fe^{IV}=N-Fe^{IV}($L^{+\cdot}$)=O (L= heme ligand). [12]

Altogether theses examples highlight the importance of dinuclear copper or iron active centers to reach an efficient oxidation of CH_4 under mild conditions. In the previous work of our research group, hemicryptophanes have been used for the oxidation of methane into methanol, and the catalytic activity, selectivity and stability of the encaged complexes have been compared to those of the non-cage model ligands. The Fe(II)@hemicryptophane catalyst, bearing a TPA moiety as coordinating site, shows enhanced reactivity and selectivity compared to the model (Figure 4.1, **Hm-Ph-TPA** is the structure of the cage ligand used in this study).[13] However, the catalytic activity of this catalyst, that owns only one iron active site, remains low with turnover number below 10. In order to improve the reactivity and obtain both selective and efficient catalysts, one strategy might be to create cages that could incorporate two metal sites. Therefore, through the following works, our goal was to introduce two metallic active centers into one hemicryptophane. This chapter will describe the design, synthesis, and characterization of a new type of hemicryptophane cage displaying two potential metal-binding sites, as well as some preliminary results regarding the coordination of Zn(II) and Cu(II) metal ions.

IV.2 Result and discussion

We chose to design a new cage displaying one TPA ligand (first binding-site) that is surmounted by a tris-triazole crown (second binding site). The hemicryptophane **Cage 4** (also named **Hm-TriA-TPA**), is indeed build from a northern CTV unit connected to the tris(2-pyridylmethyl)amine (TPA) ligand, by three triazole spacers.

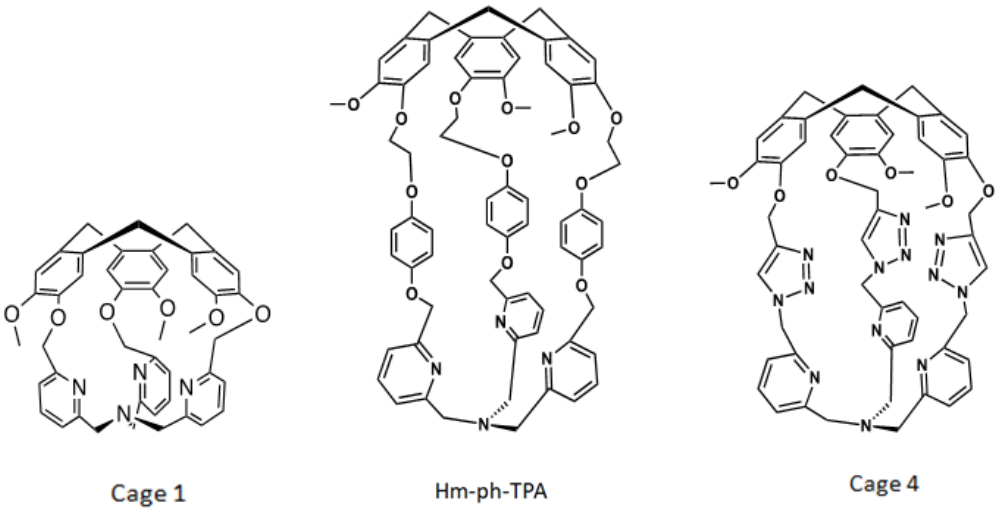

Figure 4.1 Schematic representation of the TPA-based hemicryptophanes displaying –CH_2- (left), phenyl (middle) and triazole (right, target of this chapter) linkers.

By comparison with the previousy reported TPA-based hemicryptophanes **Cage 1** and **Hm-Ph-TPA** (Figure 4.1), the triazole units in **cage 4** aims at (*i*) providing a second coordination site for the preparation of binuclear bioinspired complexes or (*ii*) taking advantage of the hydrogen bond donating properties of the triazole C-H bond to stabilize highly reactive mononuclear metal-based species (Figure 4.2b) or anion (Figure 4.2c).

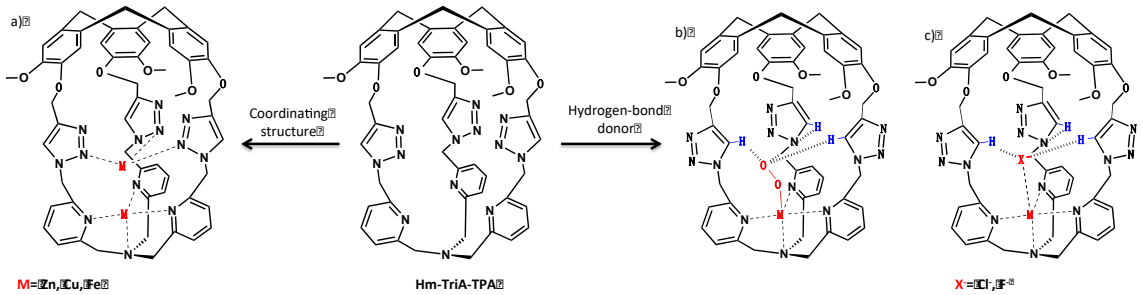

Figure 4.2 Representation of the two potential functionalities (coordinating structure or hydrogen-bond donor) of the triazole linkers of **cage 4** for (a) coordination of two metal centers, (b) stabilization of highly reactive metal-oxygen species and (c) recognition of anions

IV.2.1 Synthesis and characterization of cage 4

In the first chapter we introduced the two main synthetic methods for the preparation of hemicryptophanes ("[1 + 1] coupling" and "template method"). At first, for the synthesis of the new cage **4**, we adopted the first method aiming at connecting the CTV and the other unit with covalent bonds. As shown in Figure 4.3, we first synthesized the CTV compound **78** owning three alkynyl groups. Then we synthesized the precursor **79** (TPA-Cl) in the same way as it was done for the preparation of **cage 1** (chapter II), and we obtained compound **80** after replacing the chlorine group with azide. The 1+1 coupling reaction between **78** and **80**, by a CuAAC reaction, was then investigated (table 4.1). However, the results of many attempts through this route were not satisfactory. Indeed, after the reaction, only traces of the cage were detected by ESI-MS, and mostly polymers and oligomers were formed.

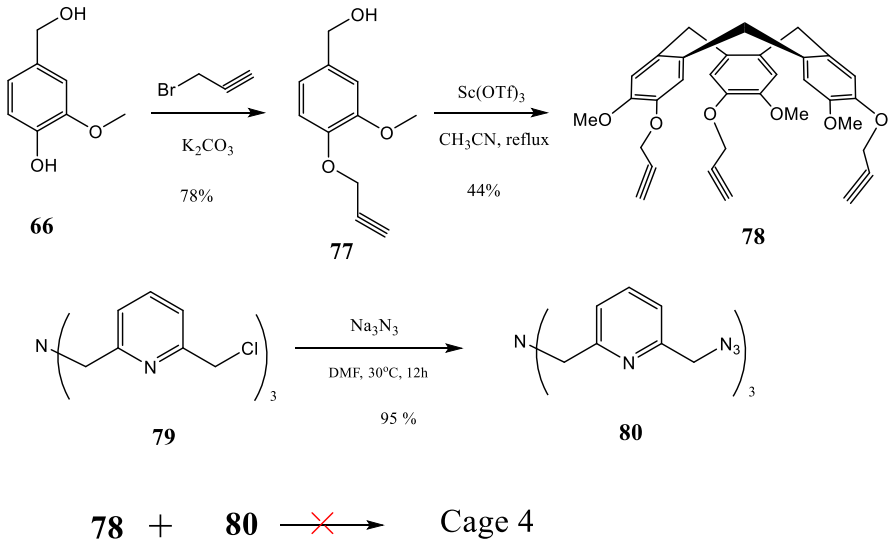

Figure 4.3 The first synthetic route proposed for the preparation of **cage 4** (pathway 1).

Table 4.1 Screening of different reaction conditions for the final step of the synthesis of the targeted cage by pathway 1 (in every case only trace of cage could be detected).

Catalyst	Base or reducing agent	Solvent	Temperature	Time	yield
CuI	DIPEA	$CHCl_3/CH_3CN$	rt	3 days	0
CuI	DIPEA	$CHCl_3/CH_3CN$	reflux	overnight	0
$Cu(CH_3CN)_4[PF_6]$	No	CH_3CN	reflux	overnight	trace
$Cu(CH_3CN)_4[PF_6]$	2,6-lutidine	CH_3CN	reflux	overnight	trace
$CuSO_4.5H_2O$	Ascorbic Acid	$H_2O/^tBuOH$,1:1	rt	3 days	0
$CuSO_4.5H_2O$	L-Ascorbic Acid Sodium Salt	CH_3CN	reflux	3 days	trace

So we tried another synthetic method, where the last step was to synthesize the CTV unit by an intramolecular macrocyclization reaction. As shown in Figure 4.4, firstly, we use the THP group to protect the benzyl alcohol group of the starting precursor **77**. Then we synthesized **85** (for the desired TPA part, the bottom part of the cage molecule), and we connected the two precursors **81** and **85** by the formation of a triazole link (CuAAC reaction) to achieve **86**. Then the TPA part was synthesized by using ammonia gas as the nitrogen source. Finally, the CTV part was synthesized using $Sc(OTf)_3$ as catalyst. This synthetic route looks longer than pathway 1, but the reaction of most steps were easy to perform, and all the yields were high, especially the yield of cage formation in the last step reached nearly 30%.

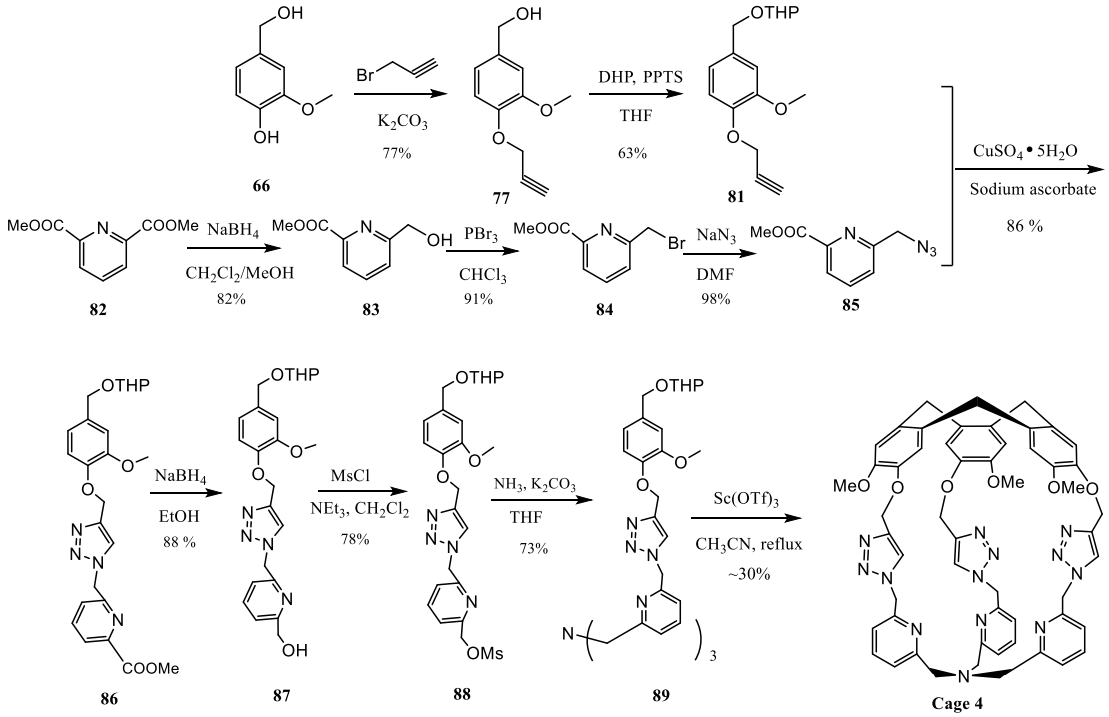

Figure 4.4 The second synthetic route that has been followed for the preparation of **cage 4** (pathway 2).

Molecular **cage 4** has been fully characterized by mean of ^{1}H-NMR(Figure 4.5) , as well as by high resolution mass spectrometry analysis. The ^{1}H NMR spectrum of **cage 4** shows that the capsule have an average C_3 symmetry in solution. It shows the general characteristics of the CTV unit structure, the 2 singlets of aromatic protons, the singlet from triazole and the singlet of OCH_3 group. The attribution of each protons has been confirmed by 2D NMR analysis of COSY and NOESY (Figure 4.6 and 4.7). spectrum.

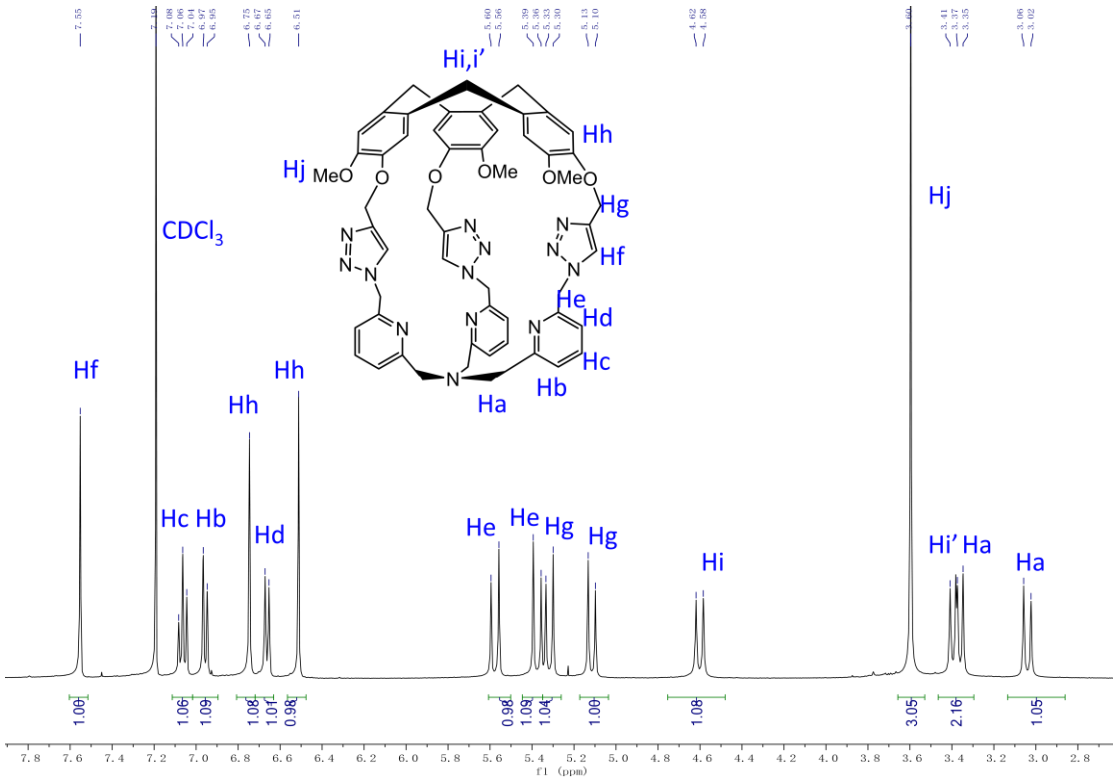

Figure 4.5 ^{1}H NMR spectrum ($CDCl_3$, 300 MHz, 298K) of **cage 4**

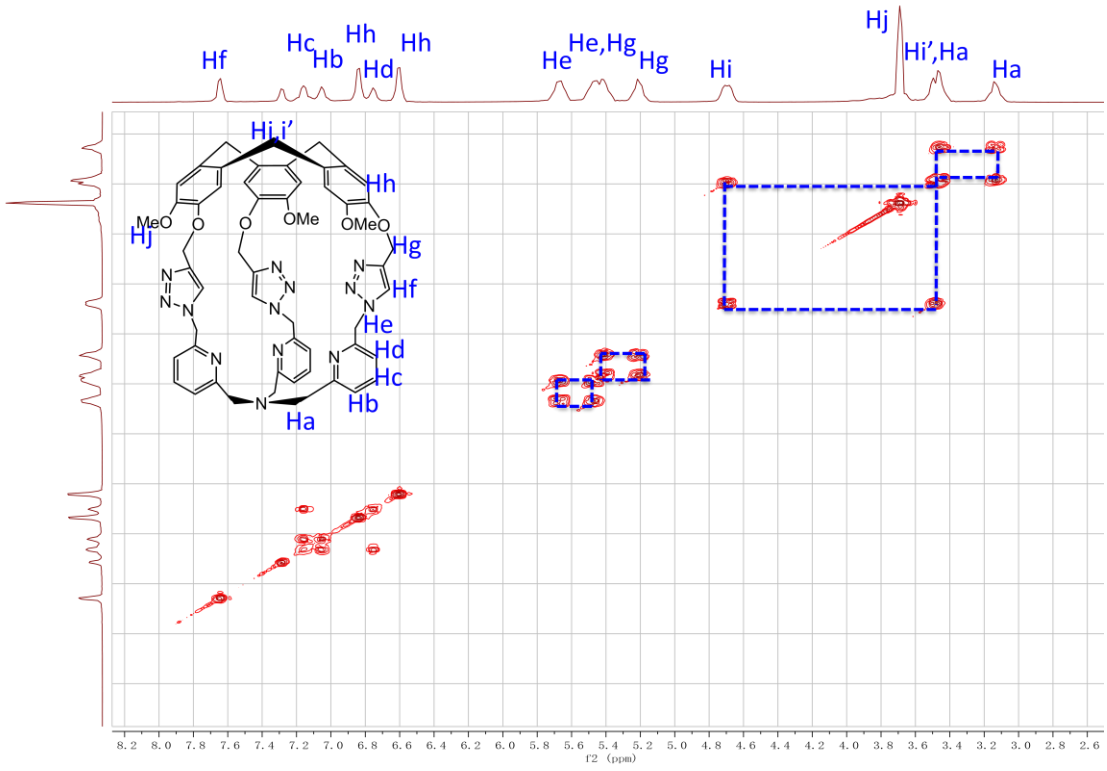

Figure 4.6 COSY spectrum ($CDCl_3$, 300 MHz, 298K) of **cage 4**

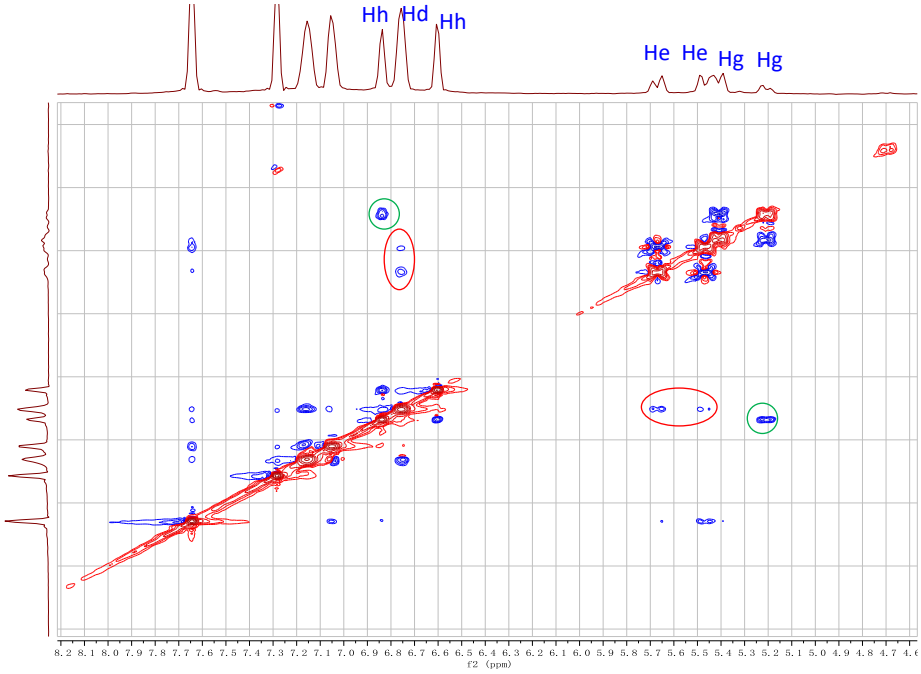

Figure 4.7 NOESY spectrum ($CDCl_3$, 300 MHz, 298K) of **cage 4.** The NOE cross-peaks between the -CH2 proton Hg and aromatic C-H bond on the CTV Hh (green circle in Figure 4.5) and between -CH2 proton He and the pyridine-Hd (red circle in Figure 4.5) have been observed.

Single crystals of **cage 4** have been obtained by slow diffusion of diethyl ether into a DCM solution. From its X-ray crystal structure, we can see that the structure of the cage in the solid-state differs than in solution as it is not C_3 symmetric (one linker is inside the CTV's cavity, Figure 4.8).

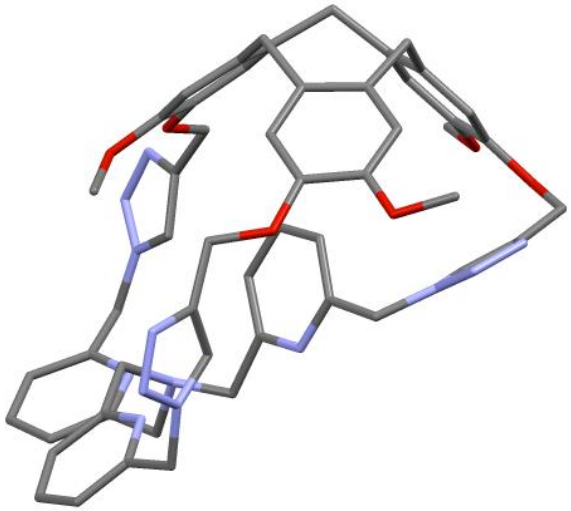

Figure 4.8 Diagram of the X-ray crystal structure of **cage 4**.

IV.2.2 Preparation and ^{1}H-NMR characterisation of the corresponding diamagnetic Zinc complex.

In order to evaluate the coordination properties of the cage **cage 4**, we first studied the ability of the cage-ligand to form metallo-complexes through Zn^{II} coordination at its TPA and tris-triazole units. The binding of the air stable zinc triflate salt $Zn^{II}(OTf)_2$ was investigated by ^{1}H-NMR. The mono-nuclear complex **Zn^{II}(cage 4)$(OTf)_2$** was prepared by reacting **cage 4** with one equivalent of $Zn^{II}(OTf)_2$ in acetonitrile. The metalation occured imediatly and the resulting complex was precipitated with diethyl ether, isolated, and characterized by ^{1}H-NMR (Figure 4.9). The ^{1}H NMR spectrum of complex **Zn^{II}(cage 4)$(OTf)_2$** shows that it still contains an average C_3 symmetric structure.

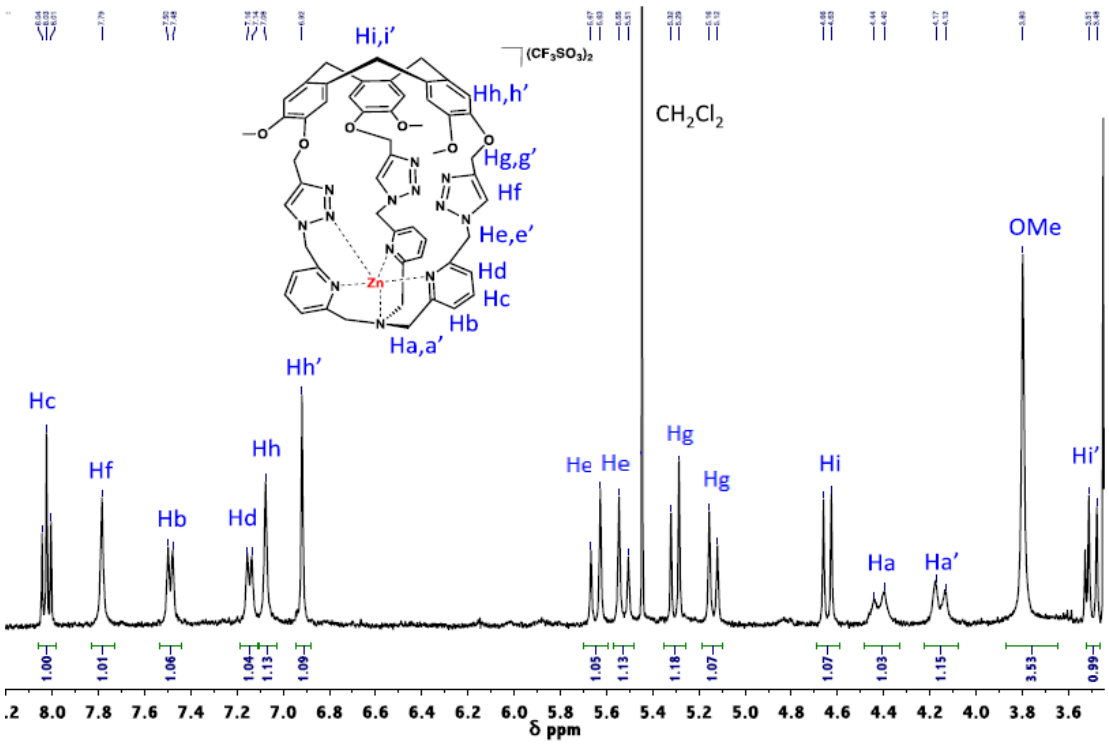

Figure 4.9 ^{1}H-NMR spectra (CD_3CN, 300 MHz, 298 K) of **Zn^{II}(cage 4)$(OTf)_2$** together with its protons assignement.

The ability of **cage 4** to accomodate a second equivalent of metal at its tris-triazole crown was then investigated through the ^{1}H-NMR monitoring of the additions of 0.5, 1.0 and 2.0 equivalents of $Zn^{II}(OTf)_2$ (Figure 4.10). The ^{1}H-NMR spectra of **cage 4** in the presence 0.5 equivalent of the Zn^{II} salt interestingly reveal two sets of signals that have been attributed (by comparison with the spectra of the authentic products) to the presence of the zinc complex and the empty cage in a 1 :1 ratio (Figure 4.10a). The ^{1}H-NMR spectra in the presence of 1.0 equivalent of $Zn^{II}(OTf)_2$ only display signal corresponding to the metal complex **Zn^{II}(cage 4)$(OTf)_2$** (Figure 4.10b). However, no change could be oberved upon addition of a second equivalent of the zinc salt (Figure 4.10c), evidencing that the hemicryptophane **cage 4** was not able to accomodate more than one equivalent of Zn(II) metal.

The preferential formation of metallo-complexes in a 1 :1 stoichiometry, using hemicryptophane **cage 4**, could be explained by a combinaison of two factors (*i*) electrostatic repulsion between the two positively charged metals and (*ii*) the coordination of one of the triazole linkers to the metal center, avoiding the

coordination of a second metal at the triazole rim. It should be noted that the ^{1}H-NMR spectra of **Zn^{II}(cage 4)$(OTf)_2$** at 298K (Figure 4.9) reveal a C_3 symmetrical structure on average. Therefore, if an axial coordination of the Zn^{II} by one of the triazole unit occurs (hypothesis *ii*), this NMR results implies that a fast exchange between the three triazoles might occur in solution at 298K. In order to confirmed this hypothesis, we then turned our attention to the elucidation of the solid state structure of (**cage 4**)-based metal complexes.

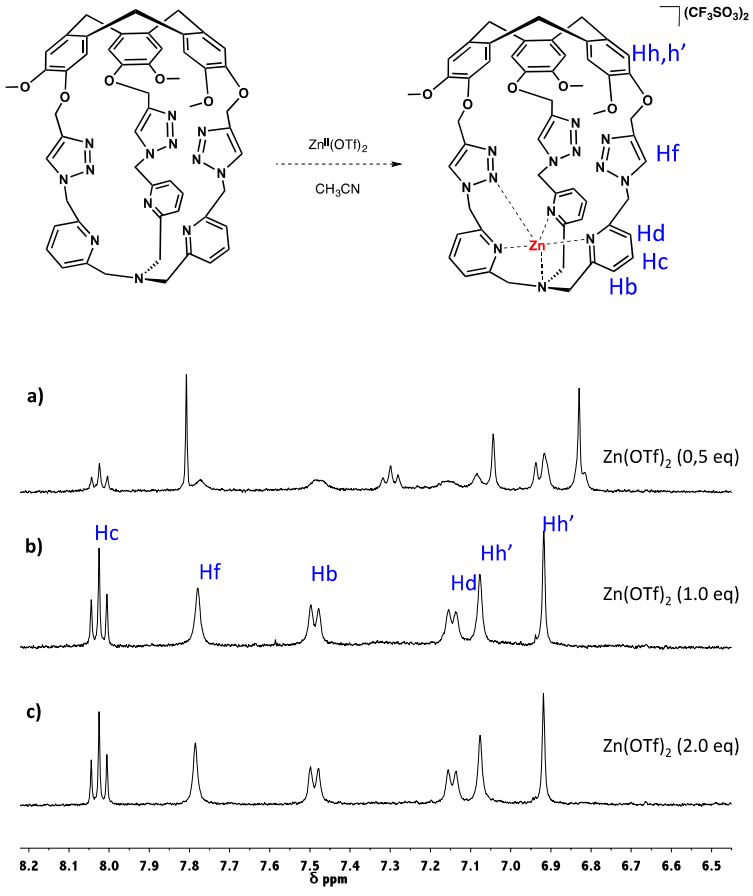

Figure 4.10 ^{1}H-NMR spectra (CD_3CN, 300 MHz, 298 K) of **(cage 4)** in the presence of 0.5 equivalent (a), 1.0 equivalent (b) and 2.0 equivalents (c) of $Zn^{II}(OTf)_2$ (Depicted region : 6.5 – 8.2 ppm). No changes could be observed between spectra b and c.

IV.2.3. Solid states studies

While no good quality crystals of **Zn^{II}(cage 4)$(OTf)_2$** were obtained, its Cu^{II} analogous **Cu^{II}(cage 4)$(OTf)_2$** afforded single crystals suitable for X-ray diffraction (Figure 4.11). The structure reveals one encaged copper center in a trigonal bipyramidal geometry, where the trigonal plane comprises the three nitrogen atoms of the TPA's pyridine (N2, N3 and N4). The axial positions are occupied by the tertiary amine nitrogen (N1) and, more interestingly, by the nitrogen of one of the three triazole linkers (N5). Such result therefore confirms our hypothesis that the axial binding of the metal center by one of the triazole linker prevents the complexation of a second metal. It should be further noted that a well-defined cavity, described by the CTV unit and the triazole rim, could be observed just above the Cu^{II} center. This cavity is occupied by one guest molecule of solvent (CH_3CN), highlighting the benefits of this cage-ligand (and its related complexes), for potential applications in recognition or supramolecular catalysis.

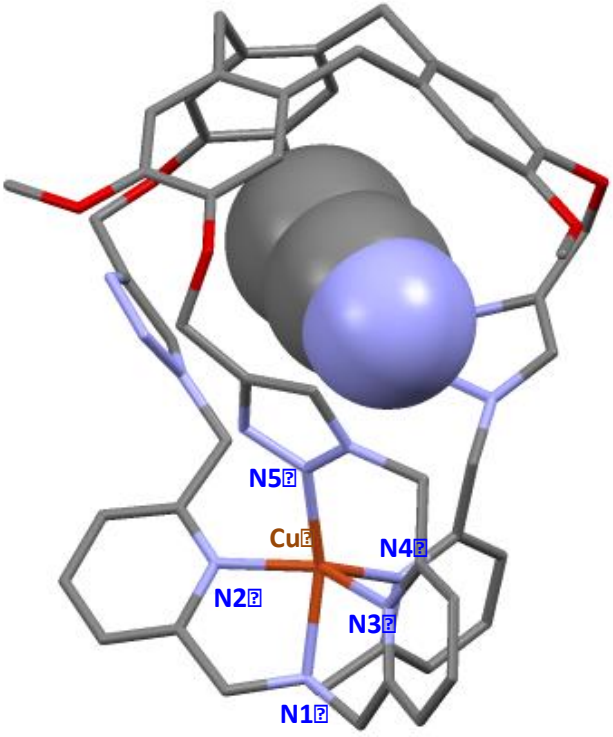

Figure 4.11 Diagram of the X-Ray crystal structure of **Cu^{II}(cage 4)$(OTf)_2$**. Triflate counterions have been omitted for clarity.

The formation of **Cu^{II}(cage 4)$(OTf)_2$** have also been characterized in the gas phase through ESI-HRMS analysis (Calcd for C54H51CuN13O6 1040.3381, found 1040.3396). Importantly, identical isotopic patterns, corresponding to the mono-nuclear **Cu^{II}(cage 4)$(OTf)_2$** (m/z = 520.7; 2+) was observed upon additions of two equivalents of $Cu^{II}(OTf)_2$ to a solution of **cage 4** in CH_3CN, confirming that the hemicryptophane ligand is not able to simultaneously bind two Cu^{II} centers, like in the case of the Zn^{II} metal.

IV.2.4 Study of the interaction of Cu^{II}(cage 4)$(OTf)_2$ with N_3.

We have seen that the axial binding of one of the triazole unit to the TPA-Cu^{II} center of **Cu^{II}(cage 4)$(OTf)_2$** prevents the use of the tris-triazole core as coordinating unit or hydrogen-bond donor. On this basis we ask themselves: could this triazole ligand be removed upon addition of an exogeneous axial ligand to the copper center ?

On this basis, the azide ligand (N_3^-) is particularly interesting as it is well-known as axial ligand for TPA-based Cu^{II} complexes. Furthermore, its way to bind to Cu^{II} complexes have been reported as a good electronic and structural model of cupric-superoxide centers $(Cu^{II}(O_2^{\cdot-})]^+$) that arise from O_2 activation at the Cu(I) centers of mono-oxygenases.[14] Therefore, the comprehension of the binding of N_3^- to a Cu^{II} complex is a convenient way to evaluate its potential application in the challenging activation of O_2 to form highly oxidizing Cu-superoxo active species $[Cu^{II}(O_2^{\cdot-})]^+$.

Interestingly, the addition of an excess of sodium azide NaN_3 (solid) to a 5 mM solution of **Cu^{II}(cage 4)$(OTf)_2$** in acetone results, within a few minutes, in a clear color change from a deep blue to a bright green solution (Figure 4.12a). The ability of **Cu^{II}(Cage 4)$(OTf)_2$** to bind N_3^- was further investigated by the time-dependent UV-vis monitoring of the addition of NaN_3 (3.2 equiv.) to an acetone solution of the complex (Figure 4.12b). The UV-vis results reveal the appearance of a new absorbance band at 420 nm characteristic of the formation of the $[Cu^{II}N_3^-]^+$ coordinating structure with TPA-based copper complexes[15]. Until now all the attempts to obtain single crystals of the resulting **Cu^{II}(cage 4)(OTf)(N_3)** have not been successful.

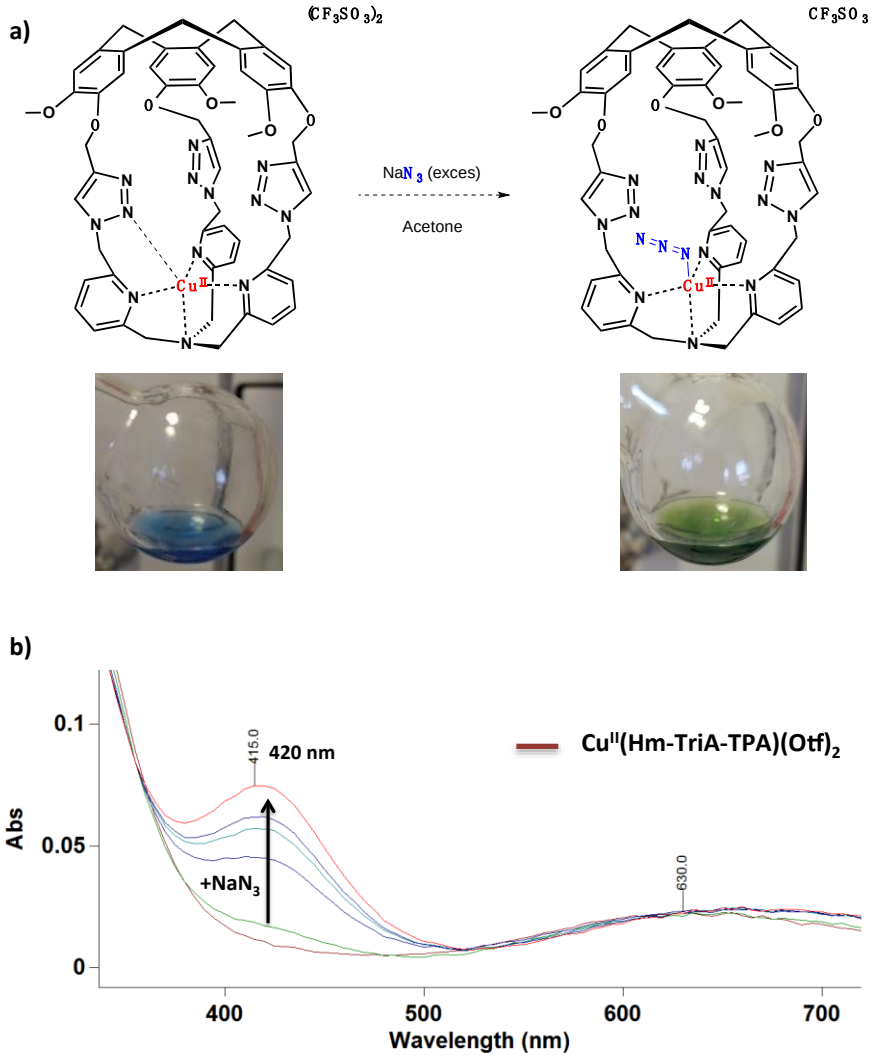

Figure 4.12 a) Schematic representation of the binding of N_3^- at the TPA-metal core of **Cu^{II}(cage 4)(OTf)$_2$**, along with pictures highlighting the change of color observed upon addition of an excess of NaN_3 to an acetone solution of the copper complex (turn bright green). b) Time-dependent changes of the UV-Vis spectra of **Cu^{II}(cage 4)(OTf)$_2$** in acetone (0,2 mM, brown line) upon addition of 3.2 equivlents of NaN_3 (green line), and after 3, 5, 7 and 17 minutes stirring. The final UV-vis spectra (red line) display a band at 420nm characteristic of the formation of the binding of the azide ligand ($[Cu^{II}N_3^-]^+$).

In order to assess if the axial binding of N_3 to **Cu^{II}(cage 4)(OTf)$_2$**, which liberates the triazole linker, allows for the coordination of a second metal, one equivalent of $Cu^{II}(OTf)_2$ was added to an acetone solution of **Cu^{II}(cage 4)(OTf)(N_3).** The addition results in a clear color change from a green to a blue solution. UV-vis analysis of the

resulting mixture indicated the disappearance of the band at 420 nm to the profit of the appearance of a band at 630 nm, which is similar to the signal of **Cu^{II}(cage 4)$(OTf)_2$** (Figure 4.13b). These results suggest that the addition of a second equivalent of copper promote the extraction of the N_3^- ligand from the cage (to form a $Cu^{II}N_3$ adduct outside of the structure) leading to the recovery of the initial **Cu^{II}(cage 4)$(OTf)_2$** complex (Figure 4.13a).

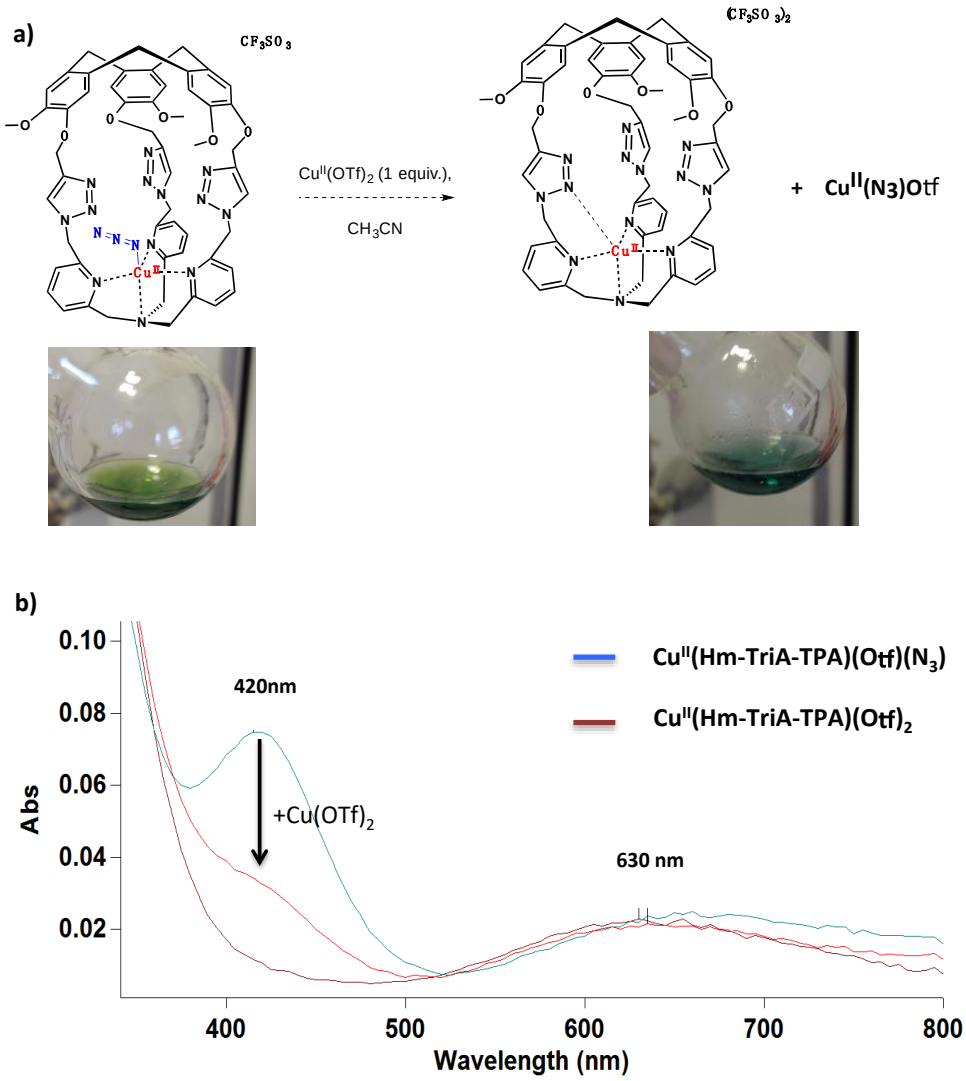

Figure 4.13 a) Schematic representation of the postulated reaction of **Cu^{II}(cage 4)(OTf)(N_3)** with a second equivalent of $Cu(OTf)_2$ resulting in the formation of **Cu^{II}(cage 4)$(OTf)_2$** along with pictures highlighting the observed change of color. b) UV-vis spectra of an acetone solution of **Cu^{II}(cage 4)(OTf)(N_3)** (0,2 mM, blue line) upon addition of 1 equivalent of $Cu^{II}(OTf)_2$ (red line), compared with the spectra of **Cu^{II}(cage 4)$(OTf)_2$** (brown line), identical absorbance feature at 630 nm could be observed

IV.3 Conclusion and perspectives.

Altogether these results indicate that the new hemicryptophane **cage 4** do not allow for the simultaneous binding of two Zn^{II} or Cu^{II} metals within its cavity. This behaviour could be explained by the electrostatic repulsion between the two metals combined with the axial binding of one of the triazole unit to the firstly coordinated metal, preventing the coordination of a second cation. However, UV-vis analysis indicates that the addition of the exogeneous ligand N_3^- to the mononuclear copper complex **Cu^{II}(cage 4)(OTf)$_2$** results in the formation of a $[Cu^{II}N_3^-]^+$ unit that releases the triazole unit. Therefore the tris-triazole core in **Cu^{II}(cage 4)(OTf)(N_3)** becomes free and could be used, for example, as an H-bond donor units. Furthermore the binding of N_3 at the axial position of **Cu^{II}(cage 4)** paves the way for future applications of **Cu^{I}(cage 4)** toward the activation of O_2 (**Figure 4.14**). Hydrogen bonding plays an important role in the kinetic stability of copper superoxide complexes. Copper complexes based on TPA derivatives owning hydrogen bond donor units have indeed been reported to enhance the stability of the corresponding copper superoxide specie.[16] Future work will consist in the ^{1}H-NMR characterization of Cu^I-complexes of the **cage 4** ligand, as well as their study as bioinspired catalyst for the activation of O_2 (formation of the highly reactive Cu^{II}-superoxo species $[Cu^{II}(O_2^{\cdot-})]^+$) for challenging oxidation reactions.

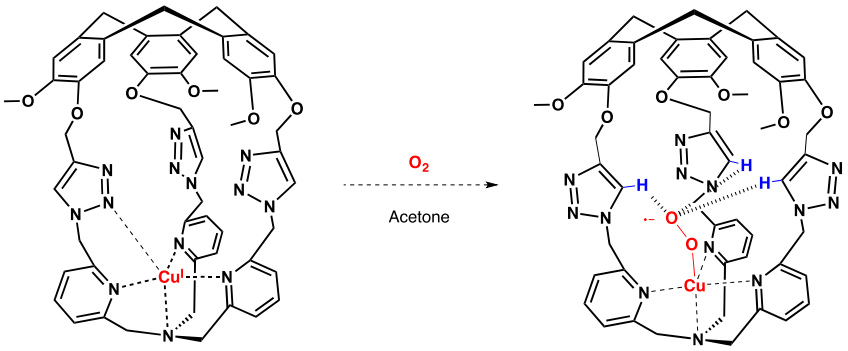

Figure 4.14. Schematic representation of the activation of O_2 at the Cu^I center of **Cu^{I}(cage 4)**. The H-bond donating properties of the triazole C-H bond is expected to stabilized the putative cupric-superoxo active species $[Cu(O_2^{\cdot-})]^+$

As a final remark, it is envisioned that complex **Zn^{II}(cage 4)**, which presents a southern TPA-metal core with a tris-triazole unit, could be particularly usefull for the recognition of anions such as Cl^- or F^-, through the combinaison of H-bonding and metal-coordination (**Figure 4.15a**). Preliminary ^{1}H-NMR tests have been performed using the TBAF guest, however only very small shifts of the host signal could be observed upon addition of 2 equivalents of TBAF (**Figure 4.15b**). The competition with the binding of one triazole at the axial position of the Zn^{II} might explain such limited response. Future work will aim at providing a better understanding of the behaviour of this system toward recognition of small anions.

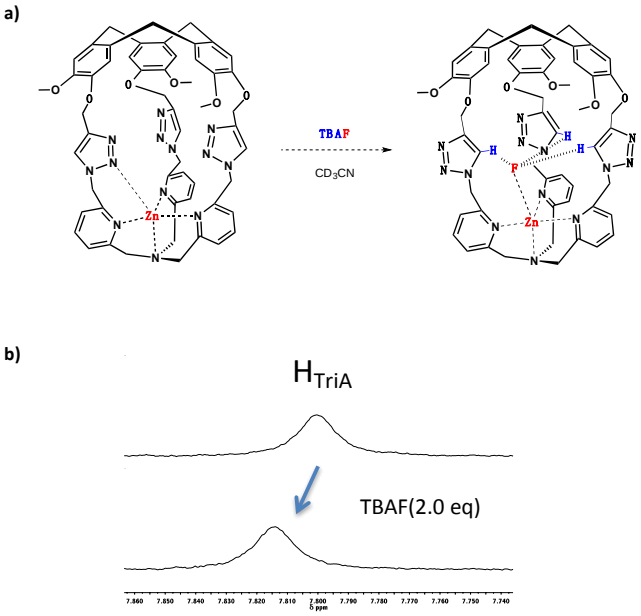

Figure 4.15 a) Schematic representation of the expected binding of F^- within the **Zn^{II}(cage 4)** cage. b) Partial ^{1}H-NMR spectra (300 MHz, CD_3CN) of the **Zn^{II}(cage 4)** complex **(top)** upon addition of 2 equivalent of the TBAF guest (bottom).

IV.4 References

1. Wang, V.C., et al., *Alkane Oxidation: Methane Monooxygenases, Related Enzymes, and Their Biomimetics.* Chem Rev, 2017. **117**(13): p. 8574-8621.
2. Merkx, M., et al., *Dioxygen Activation and Methane Hydroxylation by Soluble Methane Monooxygenase: A Tale of Two Irons and Three Proteins.* Angewandte Chemie (International ed. in English), 2001. **40**(15): p. 2782-2807.
3. Lippard, S.J., *Hydroxylation of C-H bonds at carboxylate-bridged diiron centres.* Philosophical Transactions of the Royal Society A: Mathematical, Physical and Engineering Sciences, 2005. **363**(1829): p. 861-877.
4. Baik, M.-H., et al., *Mechanistic Studies on the Hydroxylation of Methane by Methane Monooxygenase.* Chemical Reviews, 2003. **103**(6): p. 2385-2420.
5. Hori, Y., et al., *Catalytic Performance of a Dicopper–Oxo Complex for Methane Hydroxylation.* Inorganic Chemistry, 2018. **57**(1): p. 8-11.
6. Paul, M., et al., *Exceptional Substrate Diversity in Oxygenation Reactions Catalyzed by a Bis(μ-oxo) Copper Complex.* Chemistry – A European Journal, 2020. **26**(34): p. 7556-7562.
7. Woertink, J.S., et al., *A [Cu2O]2+ core in Cu-ZSM-5, the active site in the oxidation of methane to methanol.* Proceedings of the National Academy of Sciences, 2009. **106**(45): p. 18908-18913.
8. Tsai, M.-L., et al., *[Cu2O]2+ Active Site Formation in Cu–ZSM-5: Geometric and Electronic Structure Requirements for N2O Activation.* Journal of the American Chemical Society, 2014. **136**(9): p. 3522-3529.
9. Zhang, X., et al., *A Dinuclear Copper Complex Featuring a Flexible Linker as Water Oxidation Catalyst with an Activity Far Superior to Its Mononuclear Counterpart.* Inorganic Chemistry, 2020. **59**(8): p. 5424-5432.
10. Banerjee, S., et al., *Sc3+-Promoted O–O Bond Cleavage of a (μ-1,2-Peroxo)diiron(III) Species Formed from an Iron(II) Precursor and O2 to Generate a Complex with an FeIV2(μ-O)2 Core.* Journal of the American

Chemical Society, 2020. **142**(9): p. 4285-4297.

11. Wang, D., et al., *A diiron(iv) complex that cleaves strong C–H and O–H bonds.* Nature Chemistry, 2009. **1**(2): p. 145-150.
12. Kudrik, E.V., et al., *An N-bridged high-valent diiron–oxo species on a porphyrin platform that can oxidize methane.* Nature Chemistry, 2012. **4**(12): p. 1024-1029.
13. Ikbal, S.A., et al., *Bioinspired Oxidation of Methane in the Confined Spaces of Molecular Cages.* Inorganic Chemistry, 2019. **58**(11): p. 7220-7228.
14. Bhadra, M., et al., *Intramolecular Hydrogen Bonding Enhances Stability and Reactivity of Mononuclear Cupric Superoxide Complexes.* Journal of the American Chemical Society, 2018. **140**(29): p. 9042-9045.
15. Wada, A., et al., *Steric and Hydrogen-Bonding Effects on the Stability of Copper Complexes with Small Molecules.* Inorganic Chemistry, 2004. **43**(18): p. 5725-5735.
16. Diaz, D.E., et al., *Impact of Intramolecular Hydrogen Bonding on the Reactivity of Cupric Superoxide Complexes with O−H and C−H Substrates.* Angewandte Chemie International Edition, 2019. **58**(49): p. 17572-17576.

Chapter V: Synthesis of CTV-based self-assembled supramolecular cages

V.1 Introduction

Supramolecular chemistry focuses on weak and reversible non-covalent interactions between molecules.[1] These forces include hydrogen bonding, metal coordination, hydrophobic forces, van der Waals forces, π-π interactions, and electrostatic effects. [2] In particular, self-assembly driven by metal coordination is currently one of the most effective tool that could be used to build functional architectures based on non-covalent interactions. [3, 4] The strategy of self-assembly has been used to prepare capsules of various shapes and sizes that can recognize many different guests. Such self-assembled metal-organic cages have been interestingly applied in many ways, including molecular recognition, [5, 6], on-demand encapsulation/release of guest[7, 8], chiral sensing,[9] and catalysis.[10, 11]

By selecting specific building blocks, three-dimentional structures with predictable geometries can be constructed. In particular, aniline and pyridine-based tripodal building blocks have been efficiently used by the group of Nietschke to build tetrahedral cages that have found various applications such as selective anions recognition and extraction via hydrogen bonding and electrostatic interactions. [8, 12]. In this context, the C_3 symmetrical cyclotriveratrylene (CTV) appear as an interesting building block for self-assembly as its bowl-shaped structure could create molecular cavities in which guest molecules can be non-covalently bonded.[13] Using the metal-coordinated supramolecular assembly strategy, self-assembled cages structure based on the CTV structure have been constructed. The first example of self-assembled cryptophane was reported by Shinkai and colleagues, by connecting two equivalent of a pyridine-based CTV by its cis-coordination to a Pd(II) bridging complex (to form triangular double-cone capsules).[14] If the chiral resolution of the CTV precursor was performed in advance, then only the enantiopure cage was formed. In addition, by using the CTV-type of ligands, larger M_4L_4 and M_6L_8 metal supramolecular assemblies have been formed. Such assemblies have been reported by the group of Hardie, through the coordination of silver ions by the pyridine units linked to the CTV. [15] By changing the different functional groups attached to the CTV, different types of M_4L_4 assemblies can be achived. [16] Moreover, small changes to the system might result in completely different self-assembled products. For example, a different CTV derivative (from quinoline group to pyridine group) does not result in formation of a

M_3L_2 metallo-cryptophane but rather a M_2L_2 species. [15] The different shapes and binding modes formed by CTV-based ligands make them excellent ligands for the construction of metal-based supramolecules, and the internal binding sites of such structures can be used in nanoreactor applications.

Hence, this chapter focus on the preparation of three new pyridine-based tripodal CTVs and their use as ligand for the construction of original CTV-functionalized $Fe^{II}_4L_4$ tetrahedrons. This work is part of a collaborative project between our team (conception, synthesis and characterization of the CTV ligands) and the team of Professor Michaele Hardie (University of Leeds) which is a specialist of the preparation of self-assembled cages and catenanes based on the CTV moiety.[17, 18]

V.2 Result and discussion

V.2.1 Synthesis and characterization of pyridine-based CTV ligands

We designed these two pyridine-based CTV ligands. The CTV-CHO ligand **92**, contains aldehyde groups attached to pyridine, after reacting with another 3 equivalent of imines and complexing metals, it can form supramolecular metalla-cages through self-assembly. Similarly, the CTV-NH_2 ligand **95** can also work with another 3 equivalents of aldehydes.

The ligand **92,** displaying a CTV unit equiped with three pyridine carboxaldehyde units, was prepared following a 3 steps synthesis starting from compound **CTV(OH)$_3$** (Figure 5.1), which has been described in the second chapter of this manuscript. Under basic conditions (Cs_2CO_3), the Methyl-6-(bromomethyl)-2-pyridinecarboxylate was connected to the CTV to obtain compound **90.** Then **90** was reduced by sodium borohydride, to yield the hydroxyl compound **91**. The final step was to oxidize the hydroxy compound with manganese dioxide to obtain the targeted aldehyde-based compound **92**. It is important to point out here that manganese dioxide must be activated. The ^{1}H NMR spectrum of **92 (**Figure 5.2**)** shows that the structure has an average C_3 symmetry in solution. It shows the general characteristics of the CTV unit structure, one singlet from the group of -CHO (H_a), and one singlet for the CTV's OCH_3 group (H_d).

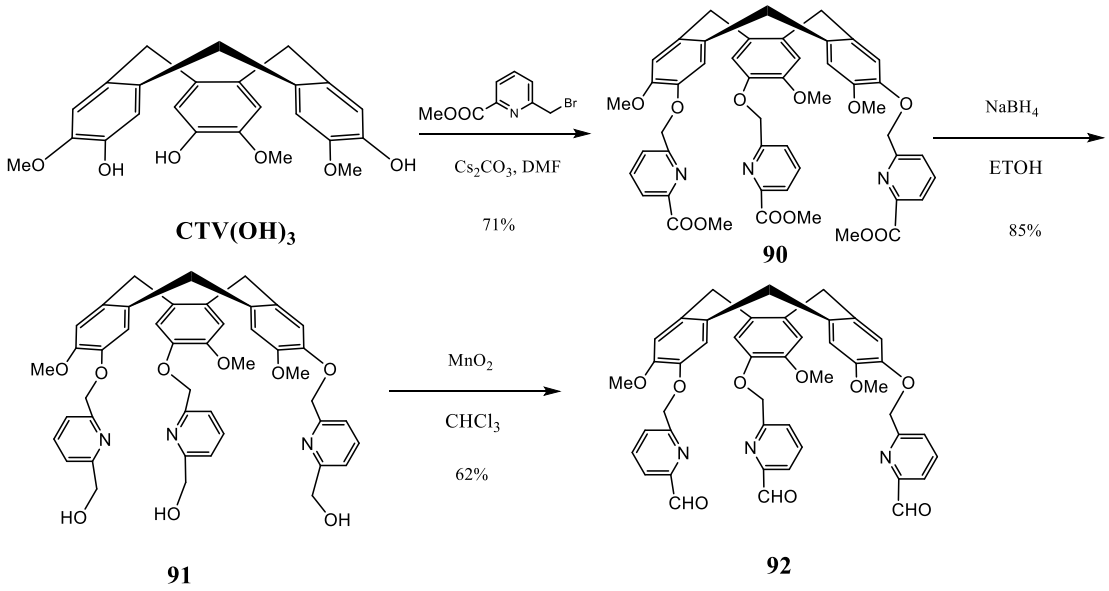

Figure 5.1 Synthetic route of the CTV-CHO ligand **92**.

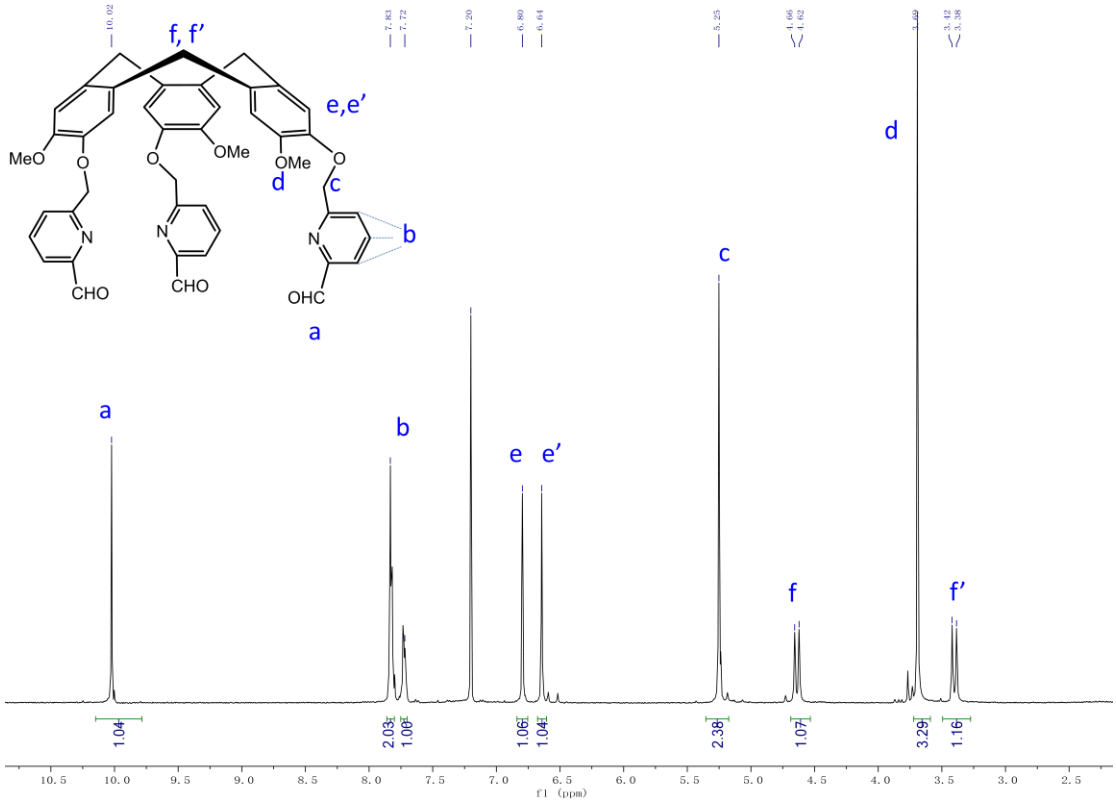

Figure 5.2 ^{1}H NMR spectra (400 MHz, $CDCl_3$, 298 K) of the CTV-CHO ligand **92**.

The ligand **95**, wich display CTV unit connected to a pyridine moiety substituted with a methyl amine group as prepared in a 3 steps synthesis starting from compound **91** which was prepared by the same method as described above. Then hydroxyl is replaced by chlorine under the conditions of $SOCl_2$, which work both as reactant and solvent. After four hours of reaction, compound **93** can be obtained. This compound is unstable at room temperature (usually stored at -18 degrees). The chlorine atom is then replaced by an azide group to afford compound **94**. Finally, the targeted product **95** was obtained by using triphenylphosphine to reduce compound **94**. Since this reaction will produce a large amount of triphenylphosphine oxide, its purification through chromatography column becomes difficult. However, after adding a certain amount of ether, the product precipitated due to its poor solubility in ether, but the triphenylphosphine oxide were still dissolved in ether. By this strategy, the pure product was then obtained after recrystallization in about 30 % yield. The ^1H NMR spectrum of **95 (**Figure 5.4**)** shows that the structure has an average C_3 symmetry in solution. It shows the general characteristics of the CTV unit structure($H_{h,h'}$), the singlet for the CTV's OCH_3 group (H_f).

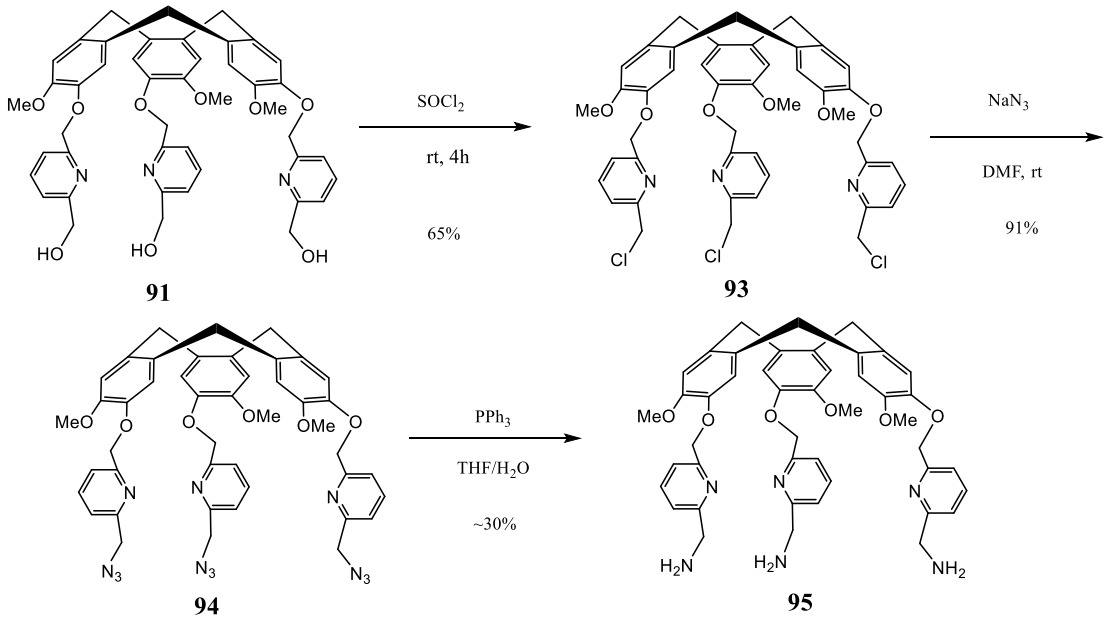

Figure 5.3 Synthetic route for the CTV-NH_2 ligand **95**.

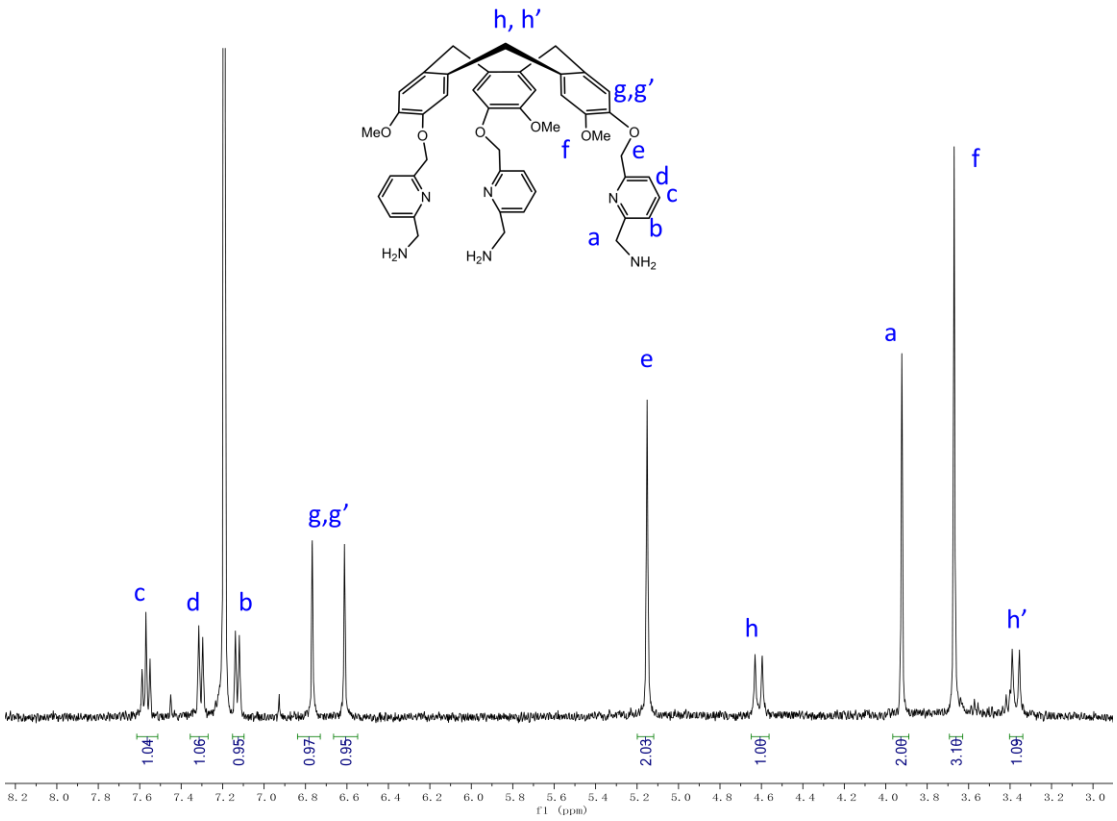

Figure 5.4 ^{1}H NMR spectra (400 MHz, CDCl3, 298 K) of the CTV-NH_2 ligand **95**.

Finally, the CTV ligand **96** that consist of a CTV unit surmounted by three bis-pyridines methyl amine groupments, was prepared following a known procedure with modification.[19] The unstable compound **93** reacted with three equivalents of [(Methylamino)methyl]pyridine in the presence of potassium carbonate and DIPEA to obtain the product **96** in the yield of 47%.

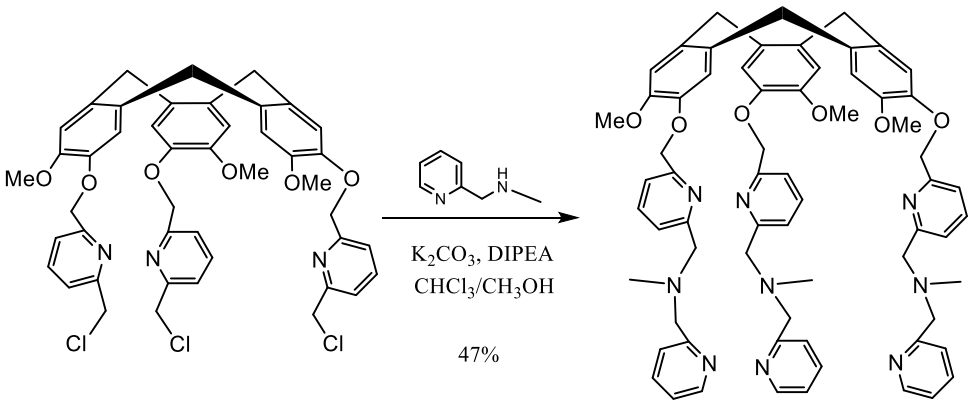

93 **96**

Figure 5.5 Synthesis of hemicryptophane –Py-N-Py **96**

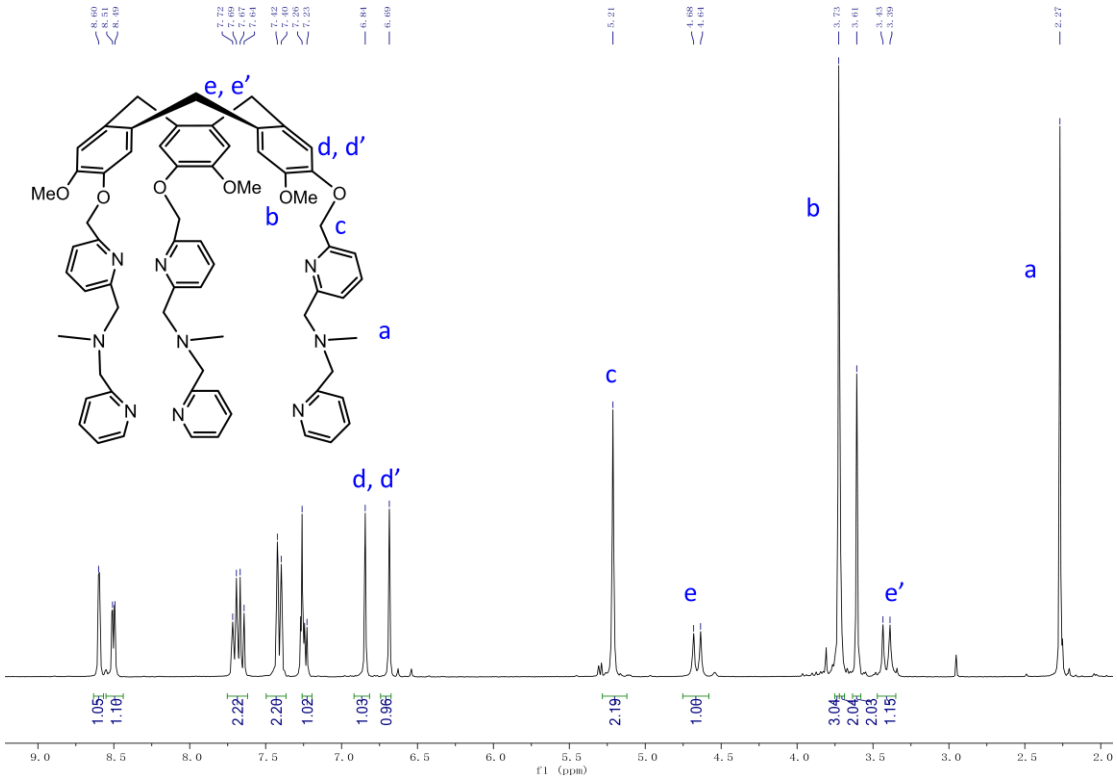

Figure 5.6 ^{1}H NMR spectra (400 MHz, $CDCl_3$, 298 K) the CTV ligand **96**, and patial characteristic peaks of **96**.

The successful generation of three products **92**, **95**, and **96** were all confirmed by ^{1}H NMR spectroscopic analysis (Figure 5.2, 5.4, and 5.6) and ESI-MS spectrometry.

V.2.2 First self-assembly results (group of M. Hardie)

The CTV ligands **92**, **95** and **96** have been send to the group of Prof. M. Hardie to engage the first self-assembly tests. We indeed believe that such CTV units might be used to build novel CTV-based self-assembled structures and that it could be a good opportunity to develop collaboration between our two research groups. A combination between **92** ($CTV(Py\text{-}CHO)_3$) or **95** ($CTV(Py\text{-}NH_2)_3$), iron(II) salt, and aniline or carboxaldehyde derivatives, might respectively result in new CTV-functionalized "Nitschke-like" self-assembled tetrahedrons (Figure 5.7 top and middle). Furthermore, if it works, the use of substituted anilines or carboxaldehydes might result in the formation of various capsules decorated with different functional groups. We also

think that a combination between two equivalents of **96** (CTV-Py-N-Py) and iron(II) salt (3 equiv.) could be of interest as it might result in the formation of new self-assembled cryptophanes (Figure 5.7, bottom), with a possible formation of interlocked structures. All these self-assembly tests are currently under investigation in the Hardie's group.

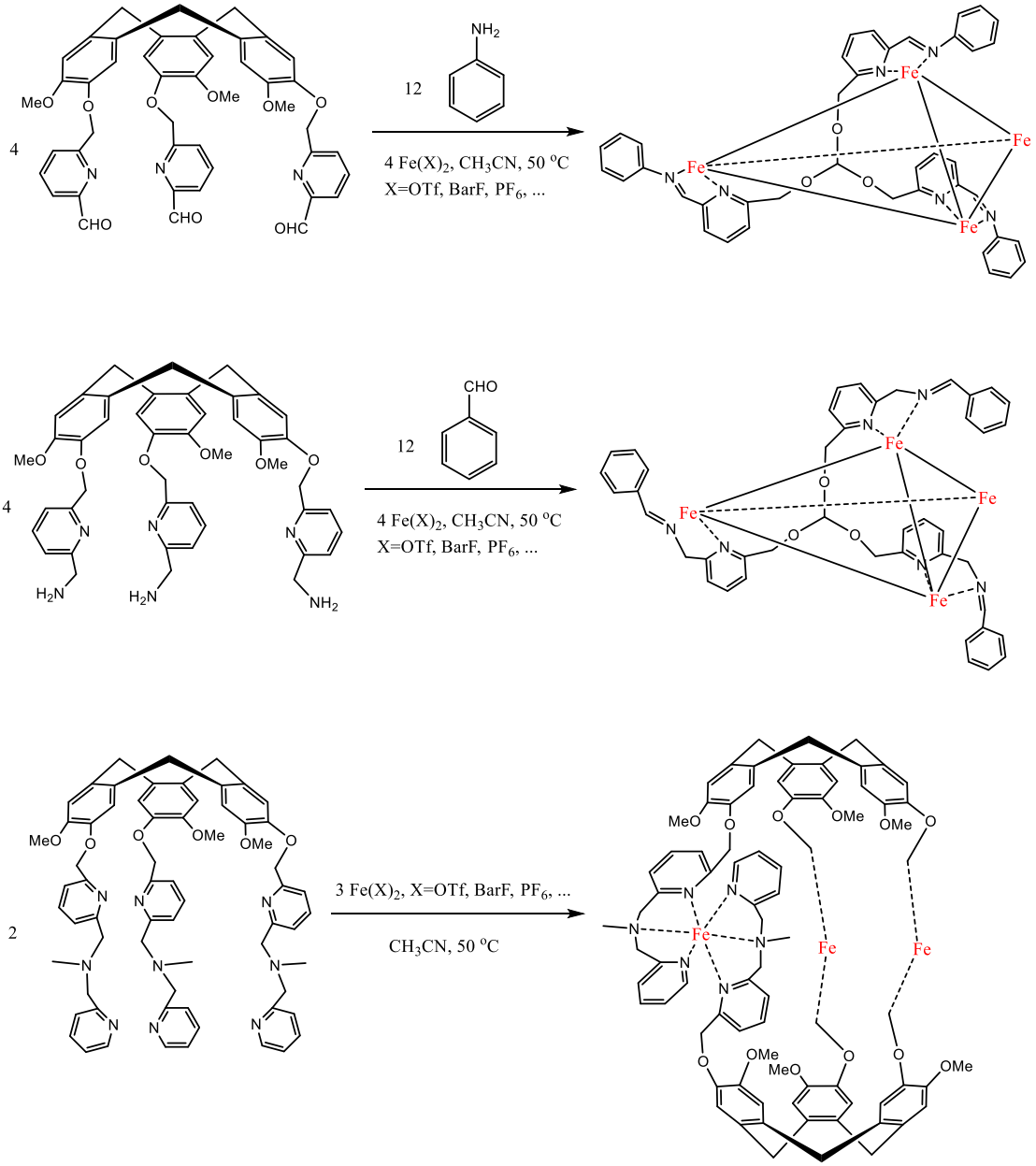

Figure 5.7 Three expected self-assembly products build from **92** (top), **95**(middle), and **96** (bottom).

V.3 Conclusions

We have designed and synthesized three novel CTV derivatives, which have the potential to form supramolecular metalla-cages through self-assembly. These CTV ligands have been send to the group of Prof. M. Hardie (University of Leeds) to engage the first self-assembly tests. And now we are waiting for the initial results.

V.4 References

1. Schneider, H.J., *Binding mechanisms in supramolecular complexes.* Angew Chem Int Ed Engl, 2009. **48**(22): p. 3924-77.
2. Biedermann, F. and H.-J. Schneider, *Experimental Binding Energies in Supramolecular Complexes.* Chemical Reviews, 2016. **116**(9): p. 5216-5300.
3. Wang, W., Y.-X. Wang, and H.-B. Yang, *Supramolecular transformations within discrete coordination-driven supramolecular architectures.* Chemical Society Reviews, 2016. **45**(9): p. 2656-2693.
4. Cook, T.R. and P.J. Stang, *Recent Developments in the Preparation and Chemistry of Metallacycles and Metallacages via Coordination.* Chemical Reviews, 2015. **115**(15): p. 7001-7045.
5. Bloch, W.M., et al., *Geometric Complementarity in Assembly and Guest Recognition of a Bent Heteroleptic cis-[Pd2LA2LB2] Coordination Cage.* Journal of the American Chemical Society, 2016. **138**(41): p. 13750-13755.
6. Bruns, C.J., et al., *Emergent Ion-Gated Binding of Cationic Host–Guest Complexes within Cationic M12L24 Molecular Flasks.* Journal of the American Chemical Society, 2014. **136**(34): p. 12027-12034.
7. Croué, V., et al., *Reversible Guest Uptake/Release by Redox-Controlled Assembly/Disassembly of a Coordination Cage.* Angewandte Chemie International Edition, 2016. **55**(5): p. 1746-1750.
8. Szalóki, G., et al., *Controlling the Host–Guest Interaction Mode through a Redox Stimulus.* Angewandte Chemie International Edition, 2017. **56**(51): p. 16272-16276.
9. You, L., J.S. Berman, and E.V. Anslyn, *Dynamic multi-component covalent assembly for the reversible binding of secondary alcohols and chirality sensing.* Nature chemistry, 2011. **3**(12): p. 943-948.
10. Yoshizawa, M., M. Tamura, and M. Fujita, *Diels-Alder in Aqueous Molecular Hosts: Unusual Regioselectivity and Efficient Catalysis.* Science, 2006. **312**(5771): p. 251.

11. Cakmak, Y., S. Erbas-Cakmak, and D.A. Leigh, *Asymmetric Catalysis with a Mechanically Point-Chiral Rotaxane.* Journal of the American Chemical Society, 2016. **138**(6): p. 1749-1751.

12. Zhang, D., et al., *Anion Binding in Water Drives Structural Adaptation in an Azaphosphatrane-Functionalized Fe(II)4L4 Tetrahedron.* J Am Chem Soc, 2017. **139**(19): p. 6574-6577.

13. Ahmad, R. and M.J. Hardie, *Building cyclotriveratrylene host molecules into network structures.* CrystEngComm, 2002. **4**(42): p. 227-231.

14. Zhong, Z., et al., *Creation of Novel Chiral Cryptophanes by a Self-Assembling Method Utilizing a Pyridyl−Pd(II) Interaction.* Organic Letters, 2001. **3**(7): p. 1085-1087.

15. Sumby, C.J., et al., *Tris(pyridylmethylamino)cyclotriguaiacylene cavitands: an investigation of the solution and solid-state behaviour of metallo-supramolecular cages and cavitand-based coordination polymers.* Chemistry, 2006. **12**(11): p. 2945-59.

16. Carruthers, C., et al., *The dimeric "hand-shake" motif in complexes and metallo-supramolecular assemblies of cyclotriveratrylene-based ligands.* Chemistry, 2008. **14**(33): p. 10286-96.

17. Hardie, M.J., *Self-assembled Cages and Capsules Using Cyclotriveratrylene-type Scaffolds.* Chemistry Letters, 2016. **45**(12): p. 1336-1346.

18. Thorp-Greenwood, F.L., A.N. Kulak, and M.J. Hardie, *An infinite chainmail of M6L6 metallacycles featuring multiple Borromean links.* Nature Chemistry, 2015. **7**(6): p. 526-531.

19. Maiti, D., et al., *Molecular oxygen and sulfur reactivity of a cyclotriveratrylene derived trinuclear copper(I) complex.* Inorg Chem, 2009. **48**(17): p. 8342-56.

General conclusions and perspectives

The objectives of this thesis were multiple:

1) Induce and control a helical arrangement in the tris(2-pyridylmethyl)amine (TPA) ligand by its covalent capping with a CTV unit: synthesis and applications of a small TPA-based hemicryptophane for chirality transfer.

2) Preparation of the two first tris-triazole-based hemicryptophanes and their application as supramolecular ligands for copper-catalyzed azide alkyne cycloaddition (CuAAC) reaction in confined space.

3) Pave the way to the preparation of systems where two metals could be coordinated in a single cavity by the design and preparation of a novel hemicryptophane cage displaying two different binding-site.

4) Open the door to the synthesis of new CTV-based self-assembled supramolecular cages by preparing new CTV precursors functionalized with different pyridine units.

In this thesis, we have first of all introduced the a brief history about the development of the hemicryptophanes organic cages. The synthetic methods for the preparation of hemicryptophanes have described, and some of their recent applications have been highlighted (host-guest chemistry, catalysis in confined space). Furthermore, the currents examples of control and transfer of chirality within tripodal cages have been described in a mini-review.

In Chapter II, we have decribed the synthesis of a new TPA-based hemicryptophane displaying short linkers, in which the chirality of the CTV unit is transferred to the southern unit yielding to a propeller-like arrangement of the TPA with an orientation (clockwise or anticlockwise) that is dictated by the nature (*M*- or *P*-) of the CTV). Interestingly, the predictable chiral arrangement of the TPA ligand was maintained

upon metallation of the hemicryptophane ligand. Chirality transfers in both the empty cage and the copper complex have been unambiguously demonstrated by XRD structures. In the future we will continue to study such kind of enantiopure metal-complexes as asymmetric catalysts. Besides, we will extend the length of the alkyl linker between the CTV and the TPA (from $-CH_2$ to $-C_2H_4$ or $-C_3H_6$) to see if the chirality will continue to be successfully transferred to the TPA part when slightly longer spacers are used.

The works in Chapter III mainly focus on the catalysis in confined space (in the cavity of hemicryptophanes). In this chapter, we have presented the design and synthesis of the two first examples of hemicryptophanes based on a tris-triazole coordinating unit (TBTA ligand). Such derivatives of the TBTA ligand (which is a very common ligand for copper-catalyzed cycloadditions reactions), have been applied for CuAAC reaction in a confined environment. Interestingly, we have demonstrated that the reaction occurs inside the cavity and that the hemicryptophane structure protects the active copper center against its deactivation by the complexation of an external ligands like picrate. In the future, we will also test a series of competiton reactions between substrates of different size, using our molecular cage as a ligand, in order to achieve size-selective CuAAC reaction. Meanwhile, we also expect to construct a new rotaxane by improving the size and shape of the alkyne and azide substrates.

As described in Chapter IV, the first hemicryptophane cage displaying two metal binding-sites in a single cavity have been designed and prepared aiming at reproducing the key structure of some methane monooxygenases enzymes. Unfortunately, this new hemicryptophane do not allow for the simultaneous binding of two Zn^{II} or Cu^{II} metals within its cavity. In the future, we will continue to look to the generation of a bimetallic complex by using two Cu^{I}. Compared to the Cu^{II}, two equivalents of Cu^{I} centers might be indeed more easy to coordinate to our cage due to (*i*) less repulsion between the metal ions and *ii*) the preferential formation of tetra-coordinated Cu^{I} complexes. Besides, we will try to take advantages of the C-H bond from the tris-triazole crown to increase the stability of Cu-oxygen adducts.

In Chapter V, we have presented the design and synthesis of three novel CTV derivatives, which have potential to form supramolecular metalla-cages through self-assembly. These CTV ligands have been send to the group of Prof. M. Hardie (University of Leeds) to engage the first self-assembly tests. Now we are still waiting the initial results from them.

In summary, we have designed and synthesized some new hemicryptophanes, displaying various coordinating units that have been used to prepare confined metal-complexes (Cu and Zn). In particular these supramolecular cage-ligands have been (and will be) used to (i) induce and control chirality at the metal core and (ii) obtain more stable, selective, and efficient catalysts. Although a lot of work remains to be completed, we believe that this work will bring a lot of new concepts into the fields of supramolecular catalysis and metal-coordination in confined spaces.

Experimental section

General information

All commercial reagents and starting materials were used directly as received without further purification, unless otherwise noted. All dry solvents were purified prior to use through standard procedures or obtained from a solvent drying system (MB-SPS-800). All the reactions were carried out under an atmosphere of argon, unless otherwise noted. Flash column chromatography was performed using silica gel 60 (230-400 mesh). Thin-layer chromatography was per-formed on aluminum-coated plates with silica gel 60 F_{254} and was visualized with a UV lamp or by staining with potassium permanganate. ^{1}H NMR spectra were recorded at either 300 or 400 MHz on BRUKER Avance III nanobay spectrometers. ^{13}C NMR spectra were recorded at either 101 or 126 MHz and reported in ppm relative to $CDCl_3$ (δ = 77.4 ppm), unless otherwise noted. Chemical shifts were referenced to tetramethyl silane, whose resonance was set to 0 ppm. High-resolution mass spectra (HRMS) were performed at Spectropole Analysis Service of Aix Marseille University.

Synthesis and characterization

Procedure for preparation of cage 2

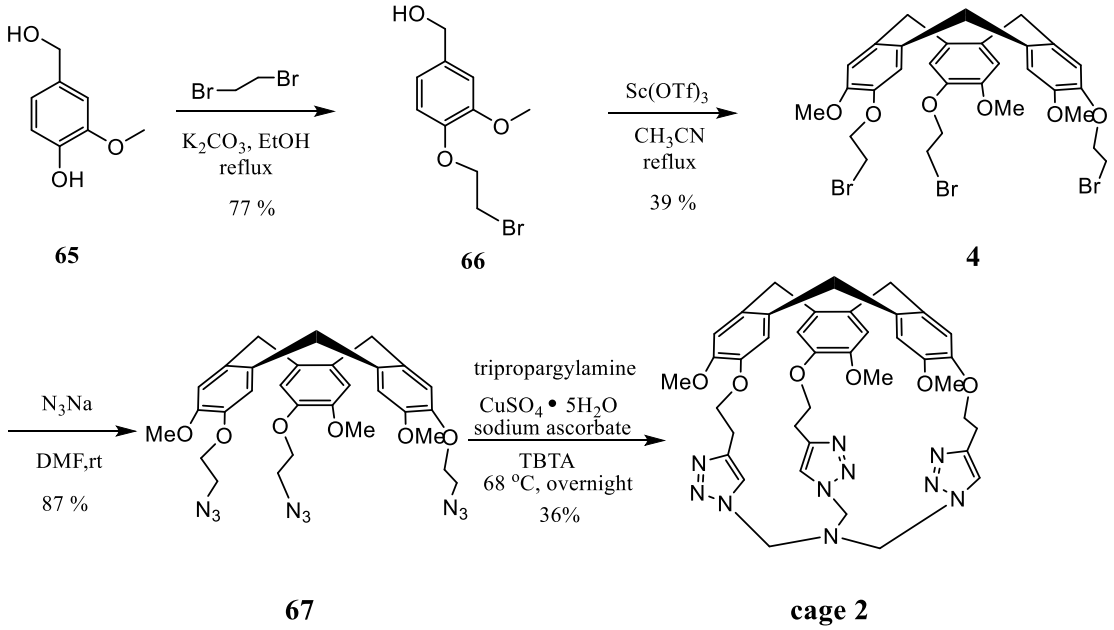

65 **66** **4**

67 **cage 2**

Synthetic route for preparation of **cage 2**

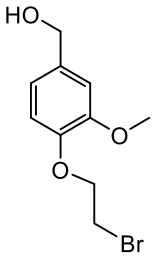

66

(4-(2-bromoethoxy)-3-methoxyphenyl)methanol (**66**) was prepared according to a known procedure.[1] To a 500 mL round-bottomed flask was added vanillyl alcohol (23.5 g), 1,2- dibromoethane (50.0 mL), potassium (24.0 g) and ethanol (200 mL) as solvent. The mixture was stirred and refluxed over night. The solution was cooled to room temperature, and the solvent was evaporated, then 200 mL of EtOAc and 150

mL of water were added and stirred for 3 hours. The mixture was filtered and was washed by EtOAc (100 mL) and water (100 mL) for 3 times. Then the organic layer was dried over by anhydrous Na_2SO_4. filtered, and concentrated under vacuum to give crude product, which was purified by recrystallization (dichloromethane and petroleum ether) to give theproduct **66** (77%). **^{1}H NMR** (300 MHz, $CDCl_3$) δ 6.94 (s, 1H), 6.91 – 6.83 (m, 2H), 4.61 (s, 2H), 4.31 (t, *J* = 6.7 Hz, 2H), 3.87 (s, 3H), 3.64 (t, *J* = 6.7 Hz, 2H); **^{13}C NMR** (75 MHz, $CDCl_3$) δ 150.09, 146.99, 135.29, 119.40, 115.07, 111.39, 69.50, 65.12, 56.03, 28.90.

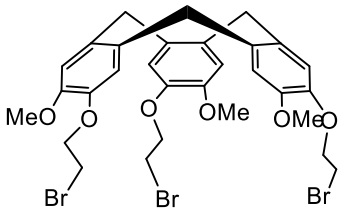

4

Cyclotriveratrylene (CTV) **4**. To a flame-dried 250 mL round-bottom flask was added **66** (10.0 g), $Sc(OTf)_3$ (800 mg) and CH_3CN (100 mL), the reaction mixture was refluxed at 90 °C overnight. The solvent was evaporated, then it was added H_2O (100 mL), and extracted by CH_2Cl_2 (2 × 100 mL), The organic phase was dried over anhydrous Na_2SO_4, filtered, and concentrated under vacuum to give crude product, which was purified on silica gel by flash chromatography (pure CH_2Cl_2) to give the title compound **4** as a white solid (3.8 g, 39 %). **^{1}H NMR** (300 MHz, $CDCl_3$) δ 6.93 (s, 3H), 6.85 (s, 3H), 4.73 (d, *J* = 13.7 Hz, 3H), 4.29 (t, *J* = 6.7 Hz, 6H), 3.85 (s, 9H), 3.62 – 3.50 (m, 9H); **^{13}C NMR** (75 MHz, $CDCl_3$) δ 149.04, 145.98, 133.86, 131.83, 117.95, 113.99, 69.97, 56.25, 36.40, 29.19. These data are consistent with literature.[1]

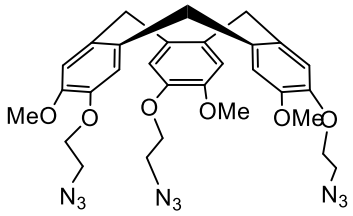

67

Compound **67**. A solution of **4** (1.23 g, 1.70 mmol) and NaN_3 (1 g, 16.0 mmol) in DMF (40 mL) was stirred at rt for 12 h and then concentrated. The resulting residue was extracted with CH_2Cl_2 (30 mL). The organic phase was washed with water (2 x 50 mL) and brine (30 mL), then dried over $MgSO_4$. After concentrated under vacuum, the crude product was recrystallized from EtOAc to yield **67** as a yellow solid (1.08 g, 88 %). **^{1}H NMR** (400 MHz, $CDCl_3$): δ 6.93 (s, 3H), 6.84 (s, 3H), 4.75 (d, J = 14.0 Hz, 3H), 4.15-4.13 (m, 6H), 3.83 (s, 9H), 3.57-3.54 (m, 9H). **^{13}C NMR** (100 MHz, $CDCl_3$): δ 149.1, 146.4, 133.8, 131.8, 118.0, 114.1, 69.2, 56.2, 50.3, 36.4. HRMS (ESI): Calcd for $C_{30}H_{33}N_9Na_1O_6$ $[M + Na]^+$: 638.2446. Found: 638.2445.

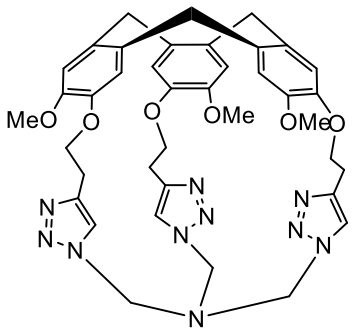

cage 2

Cage 2. In a 500 ml round-bottom flask, **67** (615 mg, 1 mmol) and tripropargylamine (131 mg, 1 mmol) were suspended in a mixture of MeCN (300 ml) and tert-butyl alcohol (50 mL). Sodium ascorbate (0.2 mmol, 40 mg) was added, followed by $CuSO_4 \cdot 5H_2O$ (12.5 mg, 0.05 mmol, in 30 mL of water) and TBTA (26.5 mg, 0.05 mol). The reaction was stirred at 70 ^oC for 24h. Then after concentration under reduced pressure, the residue was triturated with $CHCl_3$ (300 mL) and the solution was washed with water (2 x100 mL) and brine (50 mL), then dried over Na_2SO_4. Upon removal of the solvent, the crude product was purified by column

chromatography (CH_2Cl_2/MeOH from 50:1 to 20 :1) to give **cage 2** as a white solid (260 mg, 36%). **^{1}H NMR** (400 MHz, $CDCl_3$) δ 7.54（s, 3H）, 6.49 (s, 3H), 6.38 (s, 3H), 4.85 (m, 3H) , 4.61(m, 3H), 4.52(m, 6H), 4.43(d, 3H), 4.02 (s, 9H), 3.23(d, 3H), 2.81(d, 3H), 2.52(d, 3H). **^{13}C NMR** (101 MHz, $CDCl_3$) δ 147.83, 145.69, 142.93, 132.24, 130.88, 125.24, 113.44, 113.12, 77.33, 77.02, 76.70, 67.12, 56.10, 51.13, 36.46, 30.88. HRMS (ESI): Calcd for $C_{39}H_{42}N_{10}O_6$ $[M + H]^+$: 747.3289. Found: 747.3274.

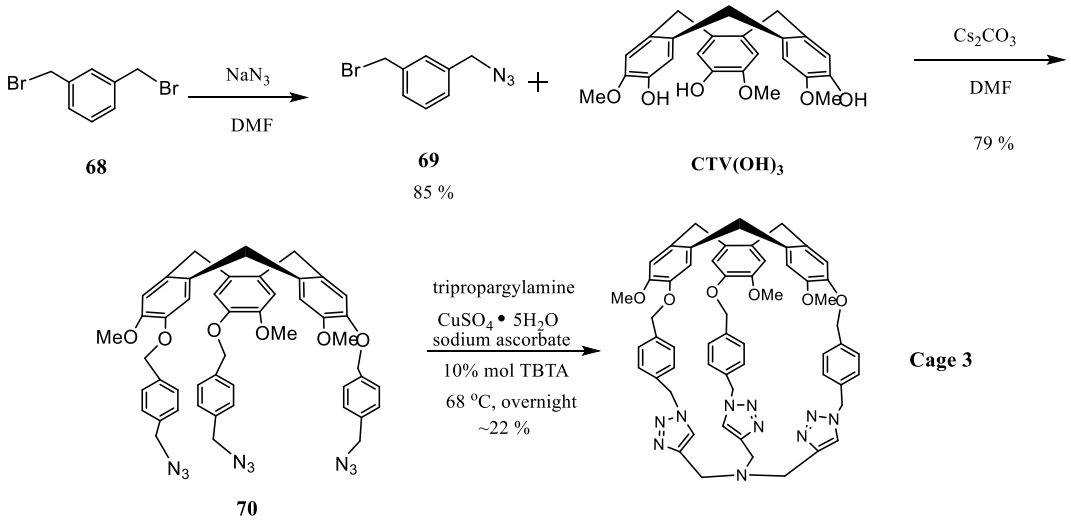

Synthetic route of **cage 3**

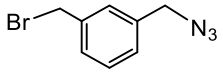

69

Compound **69** was was prepared following a known procedure with modification. Sodium azide (325 mg, 5 mmol) was added to a stirred solution of the appropriate a, a'-dibromoxylene(1.12 g, 5 mmol) in 50 mL anhydrous DMF under N_2, and the reaction was stirred at room temperature overnight. The reaction mixture was diluted with ethyl acetate (100 mL) and the organic layer washed with saturated brine (2 x 50 mL), dried with $MgSO_4$ and concentrated. The crude products were then used without further purification. **^{1}H NMR** (300 MHz, $CDCl_3$) δ 7.43- 7.28(4H, benzyl), 4.50(s, 2H), 4.34(s, 2H). **^{13}C NMR** (75 MHz, $CDCl_3$) δ 129.54, 128.59, 77.44, 77.02, 76.59, 54.38, 32.84.

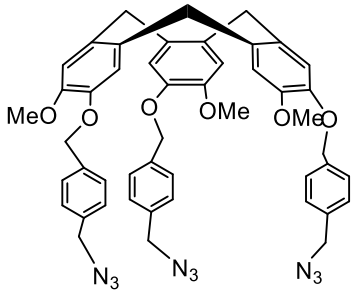

70

Compound **70**. To a solution of **CTV(OH)$_3$** (408 mg, 1 mmol) and **69** (230 mg, 1.03 mmol) in DMF(50 mL), Cs_2CO_3 (500 mg) was added in one portion. Then the solution was stirred overnight at 90°C under argon. The mixture was then allowed to return to room temperature, evaporated and water was added (200 mL). The aqueous mixture was extracted with CH_2Cl_2 (3x 100 mL). The combined organic phases were washed with 1M aqueous NaOH (100 mL), washed with brine (100 mL), dried over Na_2SO_4, filtered and evaporated to dryness. The residue was purified purified by column chromatography on silica (eluent : CH_2Cl_2 / EtOAc; 2:1) to afford a white solid. Yield: 92%. **^{1}H NMR** (300 MHz, $CDCl_3$) δ 7.45(s, 3H), 7.32(s, 3H), 7.30(s, 3H), 7.26(s, 3H), 6.85(s, 3H), 6.72(s, 3H), 5.09(s, 6H), 4.73 (d, 3H), 4.34(s, 6H), 3.75(s, 9H), 3.49(d, 3H). **^{13}C NMR** (75 MHz, $CDCl_3$) δ 147.5, 137.5, 133.4, 131.5, 129.2, 127.0, 116.8, 113.3, 71.1, 56.2, 55.4, 33.8.

Cage 3. In a 500 ml round-bottom flask, **70** (422 mg, 0.5 mmol) and tripropargylamine (66 mg, 0.5 mmol) were suspended in a mixture of MeCN (300 ml) and tert-butyl alcohol (50 mL). Sodium ascorbate (0.1 mmol, 20 mg) was added, followed by $CuSO_4 \cdot 5H_2O$ (6.25 mg, 0.025 mmol, in 20 mL of water) and TBTA (26.5 mg, 0.05 mol). The reaction was stirred at 68 ^oC for 24h. Then after concentration under reduced pressure, the residue was triturated with $CHCl_3$ (300 mL) and the solution was washed with water (2 x100 mL) and brine (50 mL), then dried over Na_2SO_4. After removal of the solvent, the crude product was purified by column chromatography (CH_2Cl_2/MeOH from 50:1 to 20 :1) to give **cage 3** as a white solid (260 mg, 22%). **^{1}H NMR** (400 MHz, $CDCl_3$) δ 7.45(s, 3H), 7.28(d, 6H), 7.07(d, 6H), 6.87(s, 3H), 6.71(s, 3H), 5.56(d, 3H), 5.35(d, 3H), 5.30(d, 3H), 5.22(d, 3H), 5.10(d, 3H), 4.67(d, 3H), 3.76(s, 9H), 3.58(d, 6H), 3.50(d, 3H). HRMS (ESI): Calcd for $C_{57}H_{54}N_{10}O_6$ $[M + H]^+$: 975.4228. Found: 975.4305.

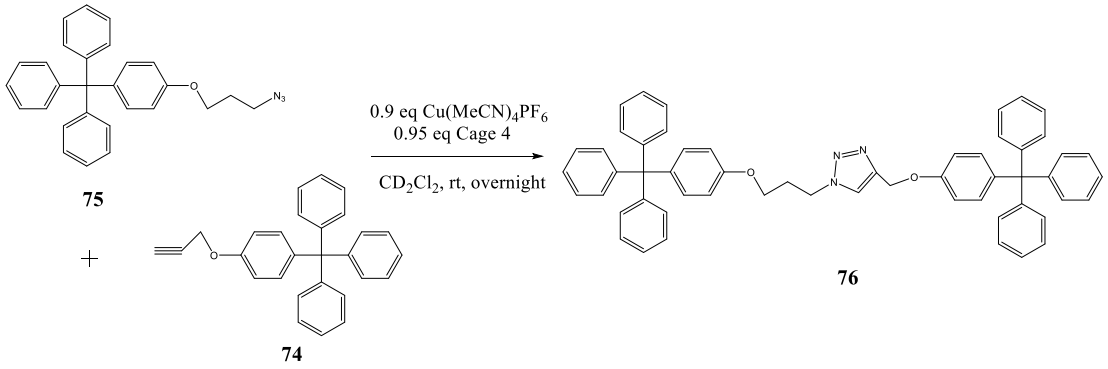

Synthetic route of **76**

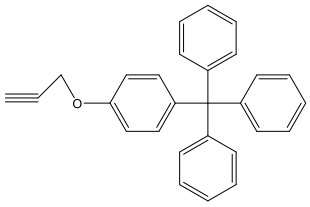

74

Compound **74**. ((4-(3-azidopropoxy)phenyl)methanetriyl)tribenzene To a solution of 4-tritylphenol (1.0 g, 3 mmol) and 4-bromobut-1-yne (80 % solution in toluene, 0.49 mL, 4.5 mmol) in DMF (30 mL) was added potassium carbonate (2.08 g, 15 mmol). The suspension was heated at 80°C for 18 h under an atmosphere of nitrogen. After cooling, the solution was concentrated under reduced pressure then diluted with water (30 mL) and extracted with EtOAc (3 x 20 mL). The resulting yellow solid was recrystallized from 5% $CHCl_3$ in CH_3CN to give the expected alkyne as a colorless solid. (1.6 g, yield = 95%). **^{1}H NMR** (400 MHz, $CDCl_3$, 298 K): δ =7.23 (d, 6H), 7.11 (d, 2H), 7.07 (d, 6H), 6.84 (d, 2H), 4.71 (d, 2H), 2.52 (t, 1H); **^{13}C NMR** (101 MHz, $CDCl_3$) δ 206.86, 155.65, 146.94, 139.93, 132.23, 131.13, 127.42, 125.89, 113.64, 78.70, 77.35, 77.03, 76.71, 75.42, 64.35, 55.81, 30.88. HRMS (ESI): Calcd for $C_{28}H_{22}O$ $[M + H]^+$: 375.1671. Found: 375.1669.

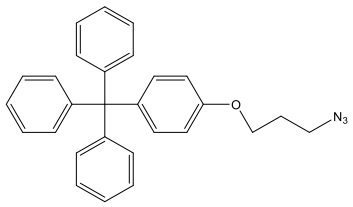

75

Compound **75**. To a solution of 1-(3-bromopropoxy)-4-(triphenylmethyl)benzene (400 mg, 0.876 mmol) in N,N-dimethylformamide (10 mL), sodium azide (68.4 mg, 1.05 mmol) was added. The reaction mixture was heated at 50 ^oC for 5 h, cooled to room temperature and added to ethyl acetate. The solution was washed with water, and dried (Na_2SO_4). After evaporation of the solvent, the residue was purified by column chromatography (silica gel; hexane: ethyl acetate = 9 : 1) to give a white solid **75**(340 mg, 0.810 mmol, Yield: 92%).**^{1}HNMR** ($CDCl_3$, 500 MHz, ppm): δ 7.16-7.25 (m, 15H, phenyl), 7.10 (d, J = 7.4 Hz, 2H, phenyl), 6.77 (d, J = 7.4 Hz, 2H, phenyl),

4.06 (t, J = 5.8 Hz, 2H, methylene), 3.53 (t, J = 6.9 Hz, 2H, methylene), 2.06 (q, J = 6.3 Hz, 2H, methylene). **^{13}C NMR** ($CDCl_3$, 125 MHz, ppm): δ 156.6, 147.0, 139.3, 132.2, 131.1, 127.4, 125.4, 113.2 (C of phenyl), 68.8, 64.3 (sp3 carbon of triryl), 48.3, 28.8 (C of methylene). HRMS (ESI): Calcd for $C_{28}H_{26}N_3O$ $[M+H]^+$: 420.2076, found 420.2068.

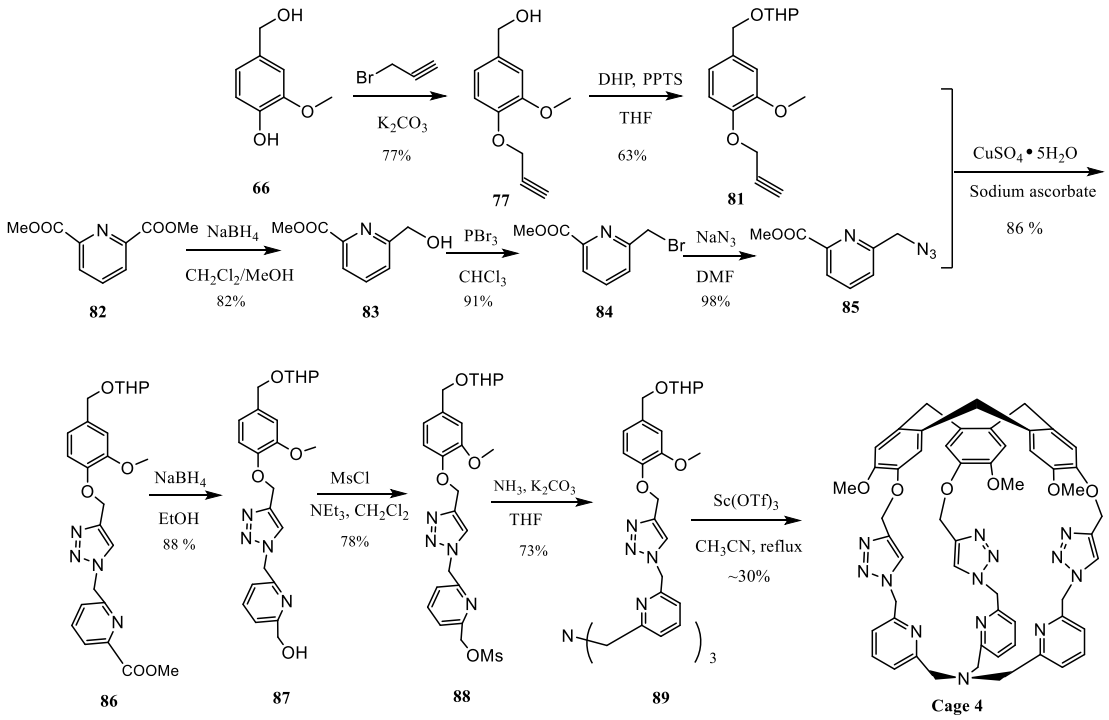

The synthetic route of **cage 4**.

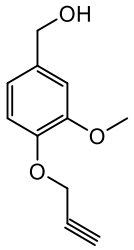

77

Compound **77**. A solution of PPTS (0.64 g, 0.026 mol) dissolved in CH_2Cl_2 (10 mL) was added in one portion to a stirred solution of **66** (6.9 g, 0.026 mol) and DHP (3.22 g, 0.038 mol) in THF (100 mL) at room temperature. The solution was stirred overnight at room temperature. The solvent was then evaporated under reduced pressure, and the residue was extracted with diethyl ether. The organic layer was washed twice with brine and then dried over sodium sulfate. The solvent was evaporated under reduced pressure to leave a residue, which was purified by chromatography (Et_2O/pentane: 50/50). Evaporation of the solvent gave white crystals of compound **77** (7.74 g, 84%): **^{1}H NMR** (400 MHz, $CDCl_3$) δ 7.02(d, 2H), 6.95(s, 1H), 6.89(d, 2H), 4.76(s, 2H), 4.62(s, 2H), 3.88(s, 3H), 2.49(t, 1H); **^{13}C NMR** (400 MHz,$CDCl_3$) 150.6, 148.2, 121.3, 117.7, 114.5, 112.3, 78.7, 76.4, 65.8, 57.6, 56.1. HRMS (ESI): Calcd for $C_{11}H_{12}O_3$ $[M+H]^+$: 193.0786, found 193.0781.

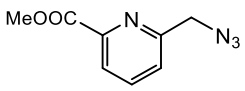

85

Compound **85.** Starting from the compound **84** (228 mg), which was disolved in 20ml DMF. Then 1.3 equivalent NaN_3 was added slowly. The reaction was kept at room temperature over night. Then the solution was washed twice with brine and then dried over sodium sulfate. The solvent was evaporated under reduced pressure to leave a residue, which was purified by chromatography. (180 mg, 98%) **^{1}H NMR** (400 MHz, $CDCl_3$) δ 8.07(d, 1H), 7.88(t, 1H), 7.70 (d, 2H), 4.64(s, 2H), 4.01(s, 3H). **^{13}C NMR** (400 MHz,$CDCl_3$) 165.65, 158.42, 147.83, 138.17, 125.56, 121.53, 55.7, 51.4. HRMS (ESI): Calcd for $C_{11}H_{12}O_3$ $[M+H]^+$: 193.0647, found 193.0651.

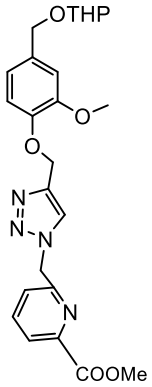

86

Compound **86**. A suspension of **81** (276 mg, 1 mmol) and **85** (192 mg, 1.02 mmol), $CuSO_4 \cdot 5H_2O$(22.5 mg, 0.09 mmol), and sodium ascorbate (30 mg, 0.1 mmol) in a mixture of $CHCl_3$ (15 mL) and MeCN (15 mL) was stirred for 24 h. The solid was filtrated and the filtrate concentrated under reduced pressure. The resulting residue was triturated with $CHCl_3$ (40 mL) and the solution was washed with water (2 X 20 mL) and brine (20 mL), then dried by Na_2SO_4. After removal of the solvent, the crude product was purified by column chromatography (CH_2Cl_2/MeOH=50:1) to give **86** as a white solid (390 mg, 86%). **^{1}H NMR** ($CDCl_3$, 400 MHz): δ 7.77(s, 1H), 7.68(t, 1H), 7.26(d, 1H), 7.07(d, 1H), 7.01(d, 1H), 6.92(s, 1H), 6.89(d, 1H), 5.65(s, 2H), 5.30(s, 2H), 4.77-4.62(m, 4H), 4.46(d, 1H), 3.92(m, 1H), 3.90(s, 3H), 3.86(s, 3H), 3.60(m, 1H), 1.92-1.57(m, 6H). **^{13}C NMR** (75 MHz, $CDCl_3$): δ 165.1, 157.0, 149.7, 148.7,147.7, 142.3, 138.1, 130.8, 125.8, 122.5, 121.6, 114.6, 112.1, 72.7, 71.4, 63.3, 56.0, 51.5, 30.7, 25.5, 19.5 ppm.

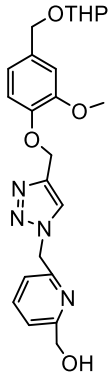

87

Compound **87.** $NaBH_4$ (360 mg, 9.52 mmol) was added to a suspension of **86** (230 mg, 0.495 mmol) in anhydrous EtOH(8 mL) at 0 ^oC. The reaction mixture was refluxed for 2 h and the solvent was removed under reduced pressure. The resulting crude residue was dissolved in CH_2Cl_2 (10 mL), washed with brine (2X10 mL), and with an aqueous saturated Na_2CO_3 solution (2 mL). The organic layer was dried with Na_2SO_4 and concentrated. Recrystallization from CH_2Cl_2/Et_2O (1:1) yielded pure **87** (154 mg, 82%) as a white solid. **^{1}H NMR** (300 MHz, $CDCl_3$) δ 7.77(s, 1H), 7.68(t, 1H), 7.26(d, 1H), 7.07(d, 1H), 7.01(d, 1H), 6.92(s, 1H), 6.89(d, 1H), 5.65(s, 2H), 5.30(s, 2H), 4.77-4.62(m, 4H), 4.46(d, 1H), 3.92(m, 1H), 3.86(s, 3H), 3.60(m, 1H), 1.92-1.57(m, 6H). **^{13}C NMR** (75 MHz, $CDCl_3$) δ 159.61, 153.30, 149.62, 147.02, 144.85, 138.02, 131.93, 123.52, 120.87, 120.49, 120.18, 114.24, 111.82, 97.77, 77.48, 77.05, 76.63, 68.78, 64.02, 63.33, 62.37, 55.89, 55.42, 30.62, 25.46, 19.52. HRMS (ESI): Calcd for $C_{23}H_{28}N_4O_5$ $[M+H]^+$: 441.2060, found 441.2058.

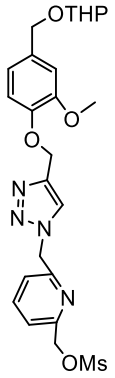

88

Compound **88.** A solution of MsCl (233 mg, 2.1mmol) dissolved in CH_2Cl_2 (10 mL) was added slowly at 0 °C to a stirred solution of **87** (850 mg, 2 mmol) and Et_3N 3 ml in CH_2Cl_2 (100 mL). The solution was stirred overnight at room temperature. The solvent was then evaporated under reduced pressure, and the residue was extracted with DCM. The organic layer was washed twice with brine and then dried over sodium sulfate. The solvent was evaporated under reduced pressure to leave a residue, which was purified by chromatography (Et_2O/pentane: 50/50). **^{1}H NMR** (300 MHz, $CDCl_3$) δ 7.77(s, 1H), 7.68(t, 1H), 7.26(d, 1H), 7.07(d, 1H), 7.01(d, 1H), 6.92(s, 1H), 6.89(d, 1H), 5.65(s, 2H), 5.30(d, 4H), 4.77-4.62(m, 2H), 4.46(d, 1H), 3.92(m, 1H), 3.86(s, 3H), 3.60(m, 1H), 1.92-1.57(m, 6H). **^{13}C NMR** (75 MHz, CDCl3) δ 154.38, 154.00, 149.59, 147.05, 144.85, 138.50, 131.98, 123.64, 122.25, 122.02, 120.48, 114.12, 111.82, 97.78, 77.48, 77.06, 76.64, 71.01, 68.77, 63.26, 62.36, 55.88, 55.30, 38.06, 30.63, 25.47, 19.52. HRMS (ESI): Calcd for $C_{24}H_{30}N_4O_7S$ $[M+H]^+$: 519.1835, found 519.1910.

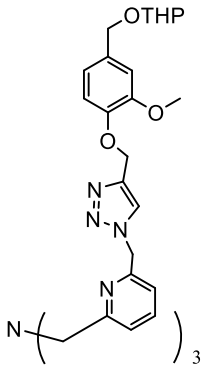

89

Compound **89**. In a 100 mL round-bottom flask, **88** (267 mg, 0.516 mmol) was dissolved in THF (22 mL). Then the NH_3 gas was bubbled slowly for more than half an hour.Then Cs_2CO_3 (757 mg, 2.32 mmol) was added in one portion. The reaction was stirred at 90 °C for 3 days. Then the mixture was cooled to rt, and THF was removed under vacuum. Then 300 mL CH_2Cl_2 and 300 mL H_2O were added. After thoroughly mixing, the organic layer was separated, and the aqueous phase was extracted with CH_2Cl_2 (2 × 100 mL). The combined organic layers were dried over Na_2SO_4, and the organic solvent was removed under vacuum. The crude product was purified by column chromatography on silica gel with a 25:1 mixture of CH_2Cl_2:MeOH as eluent to give hemicryptophane precursor **89** as a white oil (493 mg, 73 % yield). **^{1}H NMR** (300 MHz, $CDCl_3$) δ 7.75(s, 1H), 7.67(t, 1H), 7.24(d, 1H), 7.06(d, 1H), 6.97(d, 1H), 6.91(s, 1H), 6.85(d, 1H), 5.64(s, 2H), 5.29(s, 2H), 4.74(d, 2H), 4.69(m, 2H), 4.44(d, 1H), 3.92(m, 1H), 3.85(s, 3H), 3.53(m, 1H), 1.63(m, 6 H). **^{13}C NMR** (75 MHz, $CDCl_3$) δ 159.49, 153.31, 149.63, 147.03, 144.90, 138.02, 131.93, 123.48, 120.89, 120.50, 120.17, 114.24, 111.82, 97.77, 77.45, 77.03, 76.60, 68.79, 63.97, 63.35, 62.37, 55.90, 55.44, 30.62, 25.47, 19.52. HRMS (ESI): Calcd for $C_{69}H_{81}N_{13}O_{12}$ $[M+Na]^+$: 1306.6128, found 1306.6012.

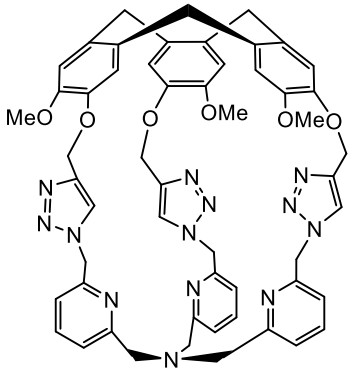

Cage 4

Cage 4. A solution of hemicryptophane precursor **89** (257 mg, 0.2 mol) in CH_3CN (18 mL) was added dropwise (4 h) under argon at 68 °C to a solution of $Sc(OTf)_3$ (125 mg, 0.28 mol) in CH_3CN (50 mL). The mixture was stirred under argon at 68 °C for 24 h. The solvent was then evaporated. The crude product was purified by column chromatography on silica gel with 25:1 mixture of CH_2Cl_2:MeOH (with 3 drops of triethylamine) as eluent to give **cage 4** as a white solid (57 mg, 29% yield). **^{1}H NMR** (300 MHz, $CDCl_3$) δ 7.62(s, 3H), 7.14(t, 3H), 7.04(d, 3H), 6.81(s, 3H), 6.74(d, 3H), 6.58(s, 3H), 5.67(d, 3H), 5.46(d, 3H), 5.37(d, 3H), 5.20(d, 3H), 4.69(d, 3H), 3.66(s, 9H), 3.47(d, 3H), 3.45(d, 3H) 3.12(d, 3H). **^{13}C NMR** (75 MHz, CDCl3) δ 159.20, 153.01, 147.85, 146.06, 145.28, 137.35, 132.78, 131.85, 123.45, 123.27, 120.28, 114.85, 113.60, 77.33, 77.01, 76.69, 63.24, 58.61, 56.37, 55.34, 36.57. HRMS (ESI): Calcd for $C_{54}H_{51}N_{13}O_6$ $[M+H]^+$: 978.4085, found 978.4160.

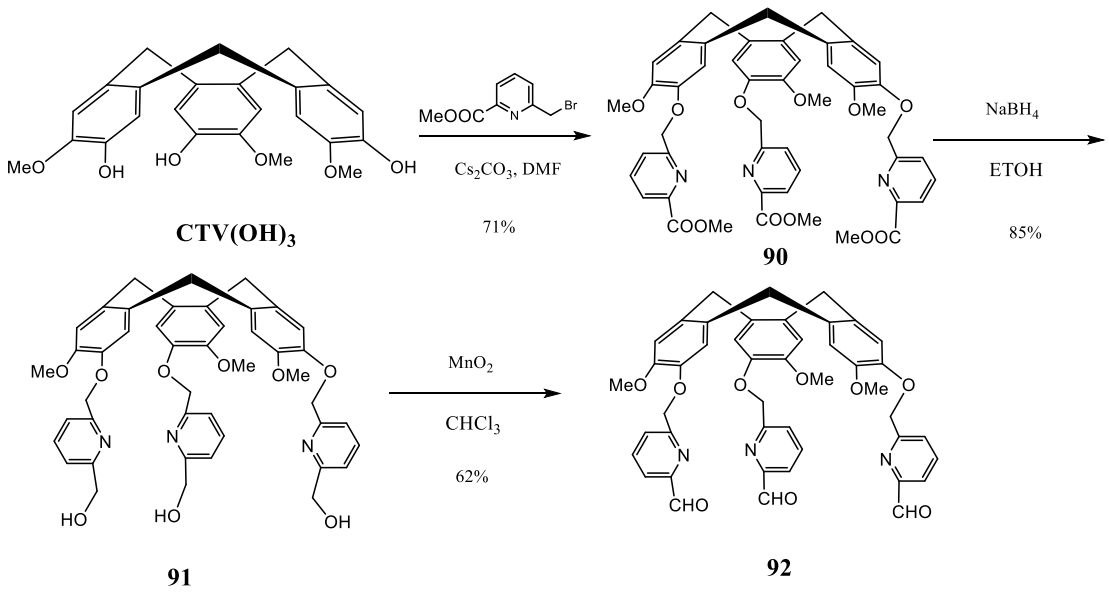

CTV(OH)$_3$

90

91

92

The synthetic route of **92**

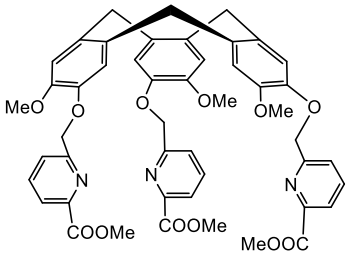

90

Compound **90**. Starting from compound **CTV(OH)$_3$** (1.63g, 4 mmol), methyl 6-(bromomethyl)picolinate (980mg, 4.3mmol) were dissolved in DMF 120ml. Then excess Cs_2CO_3 was added in one portion. The reaction was stirred at room temperature overnight. The solvent was removed under vacuum. Then 200 mL CH_2Cl_2 and 200 mL H_2O were added. After thoroughly mixing, the organic layer was separated, and the aqueous phase was extracted with CH_2Cl_2 (2×100 mL). The combined organic layers were dried over Na_2SO_4, and the organic solvent was removed under vacuum. The crude product was purified by column chromatography on silica gel with a 5:1 mixture of CH_2Cl_2:EtOAc as eluent to give **90** as a white solid.(71%). **^{1}H NMR** (300 MHz, $CDCl_3$) δ 8.04(t, 1H), 7.86(d.1H), 7.75(d, 1H), 6.84(s, 1H), 6.68(s, 1H), 5.34(s, 2H), 4.71(d, 1H), 4.03(s, 3H, COOMe), 3.73(s, 3H, OMe), 3.46(d, 1H). **^{13}C NMR** (75 MHz, $CDCl_3$) δ 165.58, 158.51, 148.21, 147.35, 146.48, 137.95, 132.75, 131.76, 124.52, 124.09, 115.24, 113.89, 77.43, 77.01, 76.58, 71.49, 56.36, 52.97, 36.52, 22.31, 14.02.

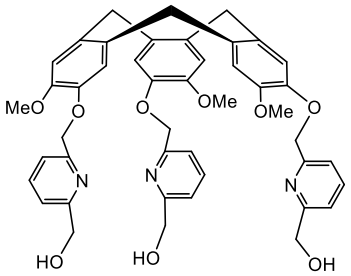

91

Compound **91.** $NaBH_4$ (360 mg, 9.52 mmol) was added to a suspension of **90** (420 mg, 0.495 mmol) in anhydrous EtOH(20 mL) at 0 ^oC. The reaction mixture was refluxed for 2 h and the solvent was removed under reduced pressure. The resulting crude residue was dissolved in CH_2Cl_2 (10 mL), washed with brine (2X10 mL), and with an aqueous saturated Na_2CO_3 solution (2 mL). The organic layer was dried with Na_2SO_4 and concentrated. Recrystallization from CH_2Cl_2/Et_2O (1:1) yielded pure **91** (327 mg, 85%) as a white solid. **^{1}H NMR** (400 MHz, $CDCl_3$) δ 7.67(t, 1H), 7.42(d, 1H), 7.17(d, 1H), 6.81(d, 1H), 6.67(d, 1H), 5.23(s, 2H), 4.78(s, 2H), 4.70(d, 1H), 3.74(s, 3H), 3.47(d, 1H). **^{13}C NMR** (101 MHz, $CDCl_3$) δ 158.39, 156.64, 148.21, 146.69, 137.61, 132.69, 131.80, 119.75, 119.26, 115.44, 113.91, 77.34, 77.02, 76.71, 71.72, 63.97, 56.33, 36.47. HRMS (ESI): Calcd for $C_{45}H_{45}N_3O_9$ $[M+H]^+$: 772.3156, found 772.3221.

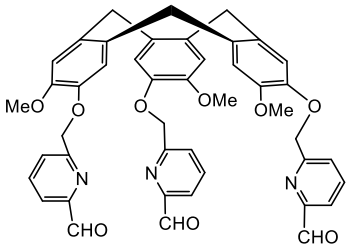

92

Compound **92**. MnO_2(1.29g , 15 mmol) was added in one portion into the solution of **91** (771 mg, 1mmol) in 150 ml $CHCl_3$. Then the reaction was stirred at 68 ^oC overnight. After the solution cooled down to rt, the black solid (MnO_2) was remove by filtering. Then the organic solution was washed with brine (2X50 mL), and with an aqueous saturated Na_2CO_3 solution (2 mL). The organic layer was dried with Na_2SO_4 and concentrated. Recrystallization from CH_2Cl_2/Et_2O (1:1) yielded pure **92** (473 mg, 62%) as a white solid. **^{1}H NMR** (400 MHz, $CDCl_3$) δ10.08(s, 1H,CHO), 7.89(t, 1H), 7.88(d, 1H), 7.78(d, 1H), 6.86(s, 1H), 6.70(s, 1H), 5.31(s, 2H), 4.72(d, 1H), 3.75(s, 3H), 3.48(d, 1H). **^{13}C NMR** (101 MHz, $CDCl_3$) δ 193.04, 158.71, 152.16, 148.33, 146.51, 138.00, 132.97, 131.79, 125.59, 120.89, 115.66, 113.91, 77.34, 77.02, 76.70, 71.57, 56.32, 36.49. HRMS (ESI): Calcd for $C_{45}H_{39}N_3O_9$ $[M+H]^+$: 766.2686, found 766.2744.

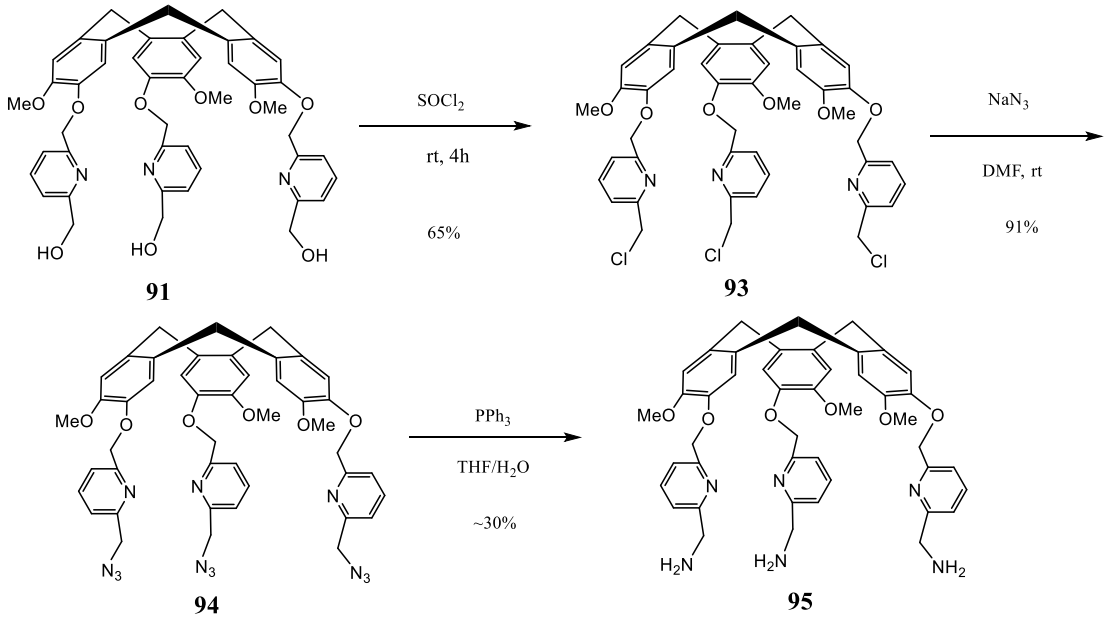

91 **93** **94** **95**

The synthetic route of **95**

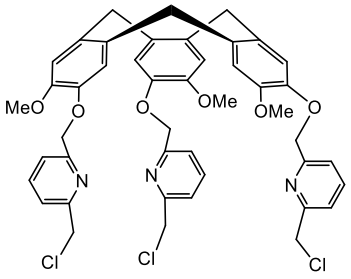

93

Compound **93**. $SOCl_2$ (22.0 mL, 302 mmol) was added dropwise to compound **91** (2.3 g, 3 mmol) at 0 ^oC. The resulting suspension was stirred for 5.5 h at room temperature and the excess of $SOCl_2$ was removed under reduced pressure. The residue was dissolved in CH_2Cl_2 (200 mL) and an aqueous solution of NaOH (1M) was added slowly at 0 ^oC until the mixture became basic (pH > 12). The organic layer was separated and the aqueous layer was extracted with CH_2Cl_2 (2X200 mL). The combined organic layers were washed with water (3X100 mL), dried over Na_2SO_4, and evaporated to dryness. Compound **93** was obtained as a pure colorless solid without other proccesing (2.77 g, 76%).

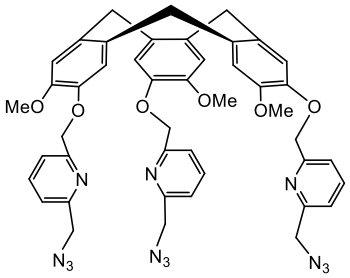

94

Compound **94**. Starting from the compound **93** (827 mg, 1 mmol), that was disolved in DMF 30 ml. Then 1.3 equivalent NaN_3 was added slowly. The reaction was stirred at room temperature over night. Then the solution was washed twice with brine and then dried over sodium sulfate. The solvent was evaporated under reduced pressure to leave a residue, which was purified by recrystallation.(DCM:EtO_2=1:10) (760 mg, 91 %) **^{1}H NMR** (400 MHz, $CDCl_3$) δ 7.67(t, 1H), 7.43(d, 1H), 7.18(d, 1H), 6.88(d, 1H), 6.47(d, 1H), 5.13(d, 2H), 4.48(d, 2H), 4.70(d, 1H), 3.74(s, 3H), 2.90 (d, 1H). **^{13}C NMR** (101 MHz, $CDCl_3$) δ 158.40, 156.55, 148.27, 146.66, 137.65, 132.66, 131.70, 119.65, 119.36, 114.44, 113.81, 77.64, 77.12, 76.61, 71.72, 63.67, 56.43, 36.57.

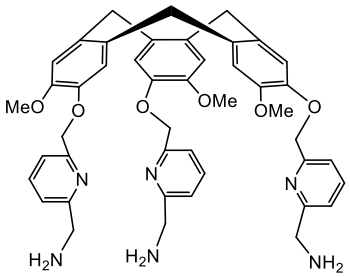

95

Compound **95**. In a 50 mL round-bottom flask, **94** (673 mg, 0.796 mmol), PPh_3 (3.75 g, 14.3 mmol), H_2O (0.5 mL), and THF (15 mL) were mixed and stirred at rt under argon overnight. The solvents were removed under vacuum. CH_2CL_2 (200 mL) and H_2O (100 mL) were then added. After thoroughly mixing, the organic layer was separated, and the aqueous phase was extracted with CH_2Cl_2 (2 × 100 mL). The combined organic layers were dried over Na_2SO_4, and the organic solvent was removed under vacuum. The crude product was added 100 ml Et_2O, and the solution

was stirred overnight. After filtration the compound **95** was obtained as a white solid (yield~30%). **^{1}H NMR** (400 MHz, $CDCl_3$) δ 7.66(t, 1H), 7.38(d, 1H), 7.21(d, 1H), 6.84(s, 1H), 6.68(s, 1H), 5.22(s, 2H), 4.70(d, 1H), 3.99(s, 2H), 3.74(s, 3H), 3.46(d, 1H). **^{13}C NMR** (101 MHz, $CDCl_3$) δ 158.71, 155.16, 148.33, 146.51, 138.00, 132.97, 131.79, 125.59, 120.89, 115.66, 113.91, 77.34, 77.02, 76.70, 71.57, 56.32, 47.55 36.49. HRMS (ESI): Calcd for $C_{45}H_{48}N_6O_6$ $[M+H]^+$: 769.3635, found 769.3744.

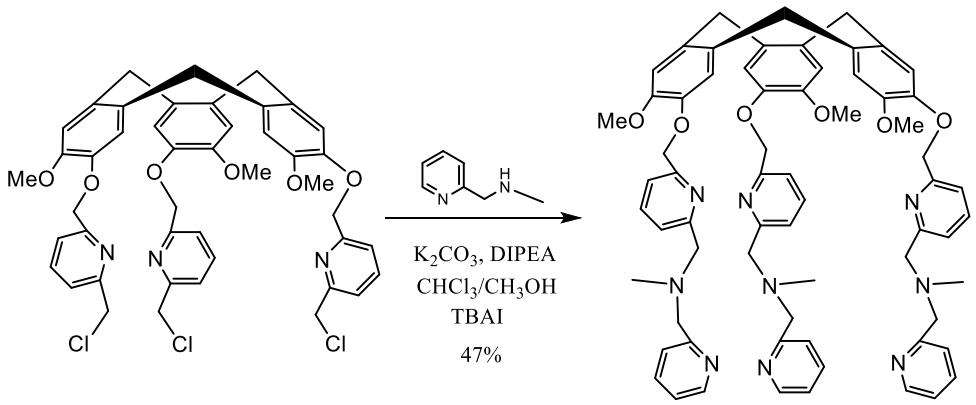

93 **96**

Compound **96**. To a flame-dried 2-neck 250 mL round-bottom flask equipped with a stir bar was added in the following order under argon: K_2CO_3 (5.0 g, 36.1 mmol), tetrabutylammmonium iodide (TBAI, 2.5 g, 6.78 mmol), N-methyl-1-(pyridin-2-yl)methanamine (1.53 g, 12.6 mmol), 125 mL of $CHCl_3$, 25 ml CH_3OH, diisopropylethylamine (2.5 mL, 14.4 mmol), and **93** (1.2 g, 1.45 mmol). The reaction mixture was heated to 35 ^{o}C and allowed to stir at room temperature under argon overnight. Then, the solvent was removed under evaporation and the yellow-brown oil was dissolved in 300 mL of dichloromethane, washed with water (2X300 mL), brine (200 mL), dried over Na_2SO_4 and filtered. The crude product was purified by column chromatography on silica gel with a 100:5 mixture of CH_2Cl_2:CH_3OH as eluent to give **96** (900 mg, 0.68 mmol) as an off-white solid in 47 % yield. **^{1}H NMR** (CDCl3): δ 8.53 (d, 6H), 7.2-7.68 (m, 15H), 6.80 (s, 3H), 6.63 (s, 3H), 5.22 (s, 6H,OCH2), 4.67(d, 3H), 3.74(s, 9H), 3.73(s, 6H), 3.63(s, 6H), 3.43(d, 3H), 2.27(s, 9H). **^{13}C NMR** (75 MHz, $CDCl_3$) δ 158.70, 157.05, 150.42, 148.69, 148.17, 146.81, 137.40, 136.52, 134.27, 132.49, 131.75, 123.33, 121.71, 119.52, 115.33, 113.81, 77.46, 77.04, 76.61, 71.96, 63.37, 59.28, 56.34, 42.55, 36.50. HRMS (ESI): Calcd for $C_{66}H_{69}N_9O_6$ $[M+H]^+$: 1084.5371, found 1084.5744.

1. Raytchev, P.D., et al., *A New Class of C3-Symmetrical Hemicryptophane Hosts: Triamide- and Tren-hemicryptophanes.* The Journal of Organic Chemistry, 2010. **75**(6): p. 2099-2102.

RESUME

Ces travaux de thèse ont consisté en la conception, la préparation et l'utilisation de nouvelles cages hémicyptophanes en tant que ligands supramoléculaires pour la coordination de métaux en milieu confiné. En particulier, nous nous sommes intéressés au développement de nouvelles méthodes pour l'obtention (i) de complexes énantiopures présentant une hélicité controllée et (ii) de nouveaux catalyseurs confinés plus efficaces et sélectifs. La première partie de ce travail consiste en une étude bibliographique sur (i) la synthèse et les applications des hémicryptophanes en reconnaissance et catalyse et (ii) les examples récents de transfert de chiralitéau sein de cages tripodes. Ensuite nos résultats sur le transfert de chiralité au sein d'un nouvel hémicryptophane permettant de contrôler l'hélicité du ligand TPA (et des complexes de cuivre correspondant), seront décrits. Nous avons ensuite étudié un nouvel hémicryptophane basé sur le ligand TBTA pour la catalyse de réactions de cycloadditions catalysée au cuivre, en milieu confiné. Enfin, nous avons préparéune nouvelle cage présentant deux sites de coordination au sein d'une cavité unique dans le but de mimer la structure du site actif des enzymes methane monooxygenases.

MOTS-CLES:

Chimie supramoléculaire, Hémicryptophanes, catalyse en milieu confiné, complexes énantiopures, contrôle de la chiralité

ABSTRACT

The main goal of this thesis was to design, prepare and applied new hemicryptophane cages as supramolecular ligand for metal coordination in confined space. In particular, this work aimed at developping new method for the obtention of (i) enantiopures complexes with controlled helicity and (ii) new confined catalyst with enhanced efficiency and selectivity. The first part consist in a comprehensive literrature review about (i) history of the development of such cage compounds, as well as their applications in recognition and catalysis and (ii) recent examples of control and transfer of chirality within tripodal cages. Then, results about how chirality transfer in a new hemicryptophane can controls the propeller arrangement of the tris(2-pyridylmethyl)amine ligand and its corresponding copper-complex will be discussed. We then studied new TBTA-based hemicryptophane cages as new ligands for copper-catalyzed alkyne-azide cycloaddition (CuAAC) in confined space. Finally, new hemicryptophane cages displaying two metal binding-sites in a single cavity have been developed aiming at reproducing the key structure of methane monooxygenases enzymes.

KEYWORDS:

Supramolecular chemistry, Hemicryptophanes, catalysis in confined space, enantiopures complexes, chirality control